THE UNIVERSITY
of EDINBURGH

THE UNIVERSITY of EDINBURGH

Investigating the Role of IQGAP1 in Intracellular Life of *Burkholderia pseudomallei*

Niramol Jitprasutwit

Submitted for the degree of

PhD (Immunology and Infection Research)

Royal (Dick) School of Veterinary Studies

Roslin Institute

University of Edinburgh

2017

Lay Summary

Burkholderia pseudomallei is an intracellular bacterium that causes melioidosis, a severe disease in humans and animals that is endemic in Southeast Asia and Northern Australia. Particularly in Northeast Thailand, melioidosis is an emerging infectious disease and is the third most common cause of death from infectious diseases after HIV/AIDS and tuberculosis. This bacterium is the second most common cause of community-acquired bacteraemia with an average mortality rate of around 40%. Due to the wide range of clinical presentations associated with this disease, the lack of rapid diagnostic tests, the resistance of *B. pseudomallei* to common antibiotics and the absence of a suitable vaccine, research aimed at understanding *B. pseudomallei* pathogenesis is of key importance.

This pathogen is able to invade cells and exploit host cellular actin, which is an abundant host cell protein that plays an important role in cell movement and shape. The bacteria make a protein on its surface called BimA. BimA mimics a host cell protein and assembles actin to form a rocket-like actin tail which it uses to propel itself within and between the host cells. This study aims to better understand how BimA harnesses the host actin-assembly machinery. It revealed that a cellular protein known as IQGAP1 is recruited to *B. pseudomallei* actin tails. IQGAP1 was removed from a human cell line by a genetic technique. Surprisingly, the bacteria could still form actin tails in these cells, but the tail length was significantly shorter. Moreover, the number of intracellular bacteria and the efficiency of *B. pseudomallei* spread to neighbouring cells decreased in the cells lacking IQGAP1. This indicates that IQGAP1 plays an important role in actin tail formation and intracellular life of *B. pseudomallei*. This study provides a better understanding of *B. pseudomallei* intracellular life and is of importance for the design of future novel therapeutic approaches for melioidosis.

Abstract

Burkholderia pseudomallei is a Gram-negative intracellular bacterium that causes melioidosis, a serious disease of humans and animals in tropical countries. This pathogen can subvert the host cell actin machinery by a process known as actin-based motility, for promoting its movement both within and between cells. The bacterial factor required for this process is known as BimA (Burkholderia intracellular motility A). Intracytoplasmic bacterial pathogens use distinct mechanisms for actin-based motility, hijacking host cytoskeletal proteins for their benefit. However, the molecular mechanism by which BimA subverts the cellular actin machinery is ill-defined. From an affinity approach coupled with mass spectrometry to identify cellular proteins recruited to BimA-expressing bacteria under conditions that promote actin polymerisation, a group of cellular proteins that are recruited to the *B. pseudomallei* surface in a BimA-dependent manner was identified. A subset of these proteins was independently validated with specific antisera including IQ motif containing GTPase activating protein 1 (IQGAP1). IQGAP1 is a ubiquitous scaffold protein that integrates several key cellular signalling pathways including those involved in actin dynamics. Previous studies demonstrated IQGAP1 was targeted by pathogens to regulate the actin cytoskeleton, for example promoting *Salmonella* invasion into epithelial cells or supporting cell attachment and pedestal formation of Enteropathogenic *Escherichia coli*. The aim of this study is to explore the roles of IQGAP1 in the intracellular life of *B. pseudomallei.*

This present study revealed that IQGAP1 was recruited to *B. pseudomallei* actin tails in infected HeLa cells. This protein has not previously been associated with actin-based motility of other intracellular pathogens. To examine the effect on actin-based motility of *B. pseudomallei*, siRNA was utilised to knockdown IQGAP1 in HeLa cells. After optimisation of siRNA transfection, IQGAP1 expression in HeLa cells was suppressed by approximately 70% as assessed by IQGAP1 immunoblotting. The siIQGAP1 knockdown cells were infected with *B. pseudomallei*. The bacteria could still form actin tails in the knockdown cells, however, the data showed a statistically significant increase in overall tail length with a concomitant decrease in actin density, compared with the tails formed by *B. pseudomallei* in control cells.

Actin-based motility is essential in the life cycle of several cytoplasmic bacterial pathogens, particularly in cell-to- cell spread. After entry into the host cell cytosol, *B. pseudomallei* polymerises actin in a BimA-dependent manner and propels itself within and between cells. This is accompanied by cell fusion which generates multi-nucleated giant cells (MNGCs), a process mediated by a Type 6 Secretion System that is co-regulated with BimA. To gain an understanding of the impact of IQGAP1 on the intracellular life of *B. pseudomallei*, IQGAP1 was successfully knocked-out from HeLa cells using CRISPR-Cas9 technique. Interestingly, *Burkholderia* invasion was not affected in HeLa cells lacking IQGAP1. However, the bacteria showed a defect in intracellular survival in IQGAP1 knockout cells that was revealed after 6 hours post-infection. Moreover, there was no difference in the proportion of bacteria associated with actin in the control and knockout cells at 16 hours post-infection, although the bacteria formed longer actin tails in control cells with similar actin density. Consequently, the number of MNGCs decreased dramatically in the cells lacking IQGAP1, which was indicated by the absence of plaque formation.

Another element of this study was to determine whether BimA and IQGAP1 are direct interacting partners. Using either an *in vitro* pulldown assay or *in vivo* yeast two-hybrid system, a direct interaction between these proteins could not be detected. It is, therefore, likely that IQGAP1 is recruited to *B. pseudomallei* actin tails through its intrinsic ability to interact with F-actin. Despite the lack of a direct interaction between these two proteins, an N-terminal IQGAP1 fragment significantly augmented BimA-mediated actin polymerisation *in vitro*.

Taken together, this study provides the first evidence of the presence of IQGAP1 in *B. pseudomallei* actin tails and presents the importance of IQGAP1 in actin-based motility and intracellular life of this bacterium. Understanding the mechanism of *B. pseudomallei* actin-based motility is useful to gain insights into host cell actin dynamics and its role in pathogenesis. Targeting host cellular proteins that are required for the intracellular life of pathogens are a topical area of research, with the potential to be useful alternatives to classic antibiotic therapy. Indeed, IQGAP1 could be a potential novel therapeutic target to develop drugs for treating *B. pseudomallei* infection.

Declarations

I, Niramol Jitprasutwit, have read and understood The University of Edinburgh guidelines on plagiarism and declare that the work presented in this thesis is the result of my own original research, except where I indicate otherwise by proper use of quotes and references.

I confirm that:

(a) The thesis has been composed by myself, and

(b) Either that the work is the my own, or, if I have been a member of a research group, that I have made a substantial contribution to the work, such contribution being clearly indicated, and

(c) That the work has not been submitted for any other degree or professional qualification except as specified, and

(d) That any included publications are my own work, except where indicated throughout the thesis and summarised and clearly identified on the declarations page of the thesis.

Signed:  Date: 31 May 2018

Acknowledgements

This work would be impossible without my supervisor, Dr. Jo Stevens who is the most important for my PhD life. I would like to heartfelt thanks for her patience, genuine caring and concern, positive attitude and believe in me. I have learnt so much from Jo. She is not only expertise in fields of scientific work, also my (PhD) life-coach. She has shown me a good leader, mentor, researcher, safety officer, and friend can be all in one person. I cannot thank her enough. I owe everything to her.

I was a luckiest student to be a member of MMBP group under Dr. Jo supervision. I had a wonderful experience during working on my thesis project. I would like to thank Chas who never refused me when I asked for his help. A very special thanks to Hamimah who is not only my best labmate, and also my best friend. I could not imagine how hard my life in Edinburgh would be without her. It was an enjoyable time to spend with Seb and Kate in and outside the lab. It was very lovely to have Imogen as a member in the group too.

I am very gladfully to be a part in Stevens group under Prof. Mark Stevens who is also my external advisor. I was really appreciated to receive his highly perceptive comments and valuable feedbacks for developing my research skills. I had a great time to share lab with Robin, who helped me to troubleshoot and discussed with me about some strange results, Prerna who gave many good advice and suggestions, Cosmin for helping me some experiments. Thanks to Seema, Christina, Andrew, and Kay for a good memory in the lab. I am also grateful to the other research groups in Roslin Institute. With a special mention to Iain MacArthur who helped me to purify invisible proteins to be visible enabled me to finish my final chapter of my thesis. I also thank Bob, Mr. Robert Fleming who gave me a hand with the microscopy work. I wish to thank my thesis committee chair, Dr. Ian Dunn and my secondary supervisor, Dr. Pip Beard too. Also, I would like to take this opportunity to thank Professor Rick Titball – my external examiner and Dr Christine Tait-Burkard – my internal examiner for their very useful discussions and very helpful suggestions. As well as to those many people that I have not mentioned here, I owe my thankfulness to all of you.

I would like to acknowledge the financial support of Siriraj Development Scholarship, Bangkok, Thailand to provide me a fantastic opportunity to study at

University of Edinburgh and the Roslin Institute Studentship under Dr. Jo supervision to allow me to stay in the UK longer.

Finally, last but not least, I owe a lot to my parents and my sisters who encourage me at every stages of my life and longed to see this achievement. It might be too long until it comes true. I deeply miss my mother who is not with me to share this joy. She supported me unconditionally until the second year of my PhD study. I wish to thank her for everything that was of inestimable value, even she could not see me graduate. I am deeply indebted to my husband, Dr. Siroj Jitprasutwit who supported me in every possible way to see the completion of this work.

Contents

Contents **Page No.**

Contents **Page No.**

Contents **Page No.**

List of Figures

List of Tables

Chapter 1
Introduction

1.1 *Burkholderia pseudomallei*

B. pseudomallei is a Gram-negative motile rod-shaped bacterium that causes melioidosis, a serious infectious disease in humans and animals. Mature colonies of *B. pseudomallei* display a wrinkled appearance on Ashdown's selective agar (Inglis and Sagripanti, 2006). *B. pseudomallei* is an environmental saprophyte, which is endemic in 17 countries in Southeast Asia and Northern Australia with evidence of acquisition of the disease from the environment, specifically from contaminated soil and water (Limmathurotsakul et al., 2013). Recently, the whole genome sequencing data from *B. pseudomallei* isolates from 30 countries collected over 79 years indicated geographic spread of this bacterium from Australia and then to Southeast Asia (Chewapreecha et al., 2017). The reference genome of *B. pseudomallei* strain K96243, which was isolated from a case of human melioidosis in 1996, consists of two chromosomes, comprising a total of 7.25 megabase pairs (Mb) with a G+C content of 68% (Holden et al., 2004). The large chromosome (4.07 Mb) encodes many core functions associated with central metabolism and bacterial growth and the small chromosome (3.17 Mb) contains a greater proportion of accessory genes associated with adaptation and survival in different niches (Holden et al., 2004).

B. pseudomallei is classified as a Hazard Group 3 agent by the Health and Safety Executive (HSE) in the UK; an agent that can cause severe human disease and may spread to the community, but there is no effective treatment available. Additionally, *B. pseudomallei* is listed as a pathogenic agent that may be targeted or used by terrorists under Schedule 5 of the Anti-Terrorism Crime and Security Act 2001 (ATCSA) in the UK. In the US, *B. pseudomallei* is a Tier 1 select agent, which is categorised by the ability to cause a mass casualty event, being easily transmitted with a low infectious dose, and potential use as a weaponised agent (Wagar, 2016). It is also listed as a US category B bioterrorism agent because of its aerosol infectivity and lack of vaccine, despite many studies that have attempted to develop effective vaccines against melioidosis (Patel et al., 2011, Choh et al., 2013). Detailed understanding of the mechanisms of host-pathogen interactions is essential to enhance vaccine research and development of anti-infectives in the future.

1.1.1 Melioidosis

Melioidosis, also called Whitmore's disease, can affect humans and animals and is caused by the facultative intracellular pathogen, *B. pseudomallei*. In humans, melioidosis is an important cause of community-acquired sepsis in Southeast Asia and Northern Australia. In north-east Thailand, melioidosis has a reported mortality rate of 40% which is comparable to that for deaths from tuberculosis in this region. Melioidosis is the third most common cause of death from infectious diseases (Limmathurotsakul et al., 2010) and was the second most common cause of community-acquired bacteraemia in 2010 (Kanoksil et al., 2013). Recent computer modelling predicts that humans are infected with *B. pseudomallei* with an estimated 165,000 cases and global mortality of melioidosis of 89,000 per year (Limmathurotsakul et al., 2016).

Routes of infection are percutaneous inoculation via an open wound, ingestion from the contaminated water or food, or infection from inhalation (Reviewed in Wiersinga et al., 2012). Clinical presentation of melioidosis can mimic tuberculosis or cancer with a variety of severity from an acute septic illness to a chronic infection. A prospective database of 624 patients with culture-confirmed melioidosis in the top end of the Northern Territory, Australia showed that 51% of cases presented with pneumonia as the primary diagnosis (Meumann et al., 2012), whereas fever was the most common presentation with localised infection in the majority of melioidosis patients in Thailand (Churuangsuk et al., 2016, Limmathurotsakul et al., 2006). Additionally, patients may present with bacteraemia, internal organ abscesses and septic shock. A number of risk factors for developing melioidosis, such as diabetes and excessive alcohol use have been defined. Despite this, melioidosis is considered an opportunistic infection because it is unlikely to have a fatal outcome in a healthy person who is diagnosed early and treated with appropriate antibiotics. However, bacterial eradication is still challenging and requires a prolonged course of antibiotic treatment. Moreover, recurrent disease is common with the longest period of latency of up to 62 years being recorded (Reviewed in Wiersinga et al., 2012). Based on clinical presentation, patients take antimicrobial therapy in two separate phases, an intensive and an eradication phase of 6 months (Currie, 2015). However, infections caused by *B. pseudomallei* are

difficult to treat because of the inherent antibiotic resistance of *B. pseudomallei* to many antibacterial agents (Reviewed in Schweizer, 2012).

Melioidosis also affects a range of different animal species, both pets and livestock, with a variability in susceptibility between species. Sheep and goats are the most susceptible, compared with pigs and cattle (Choy et al., 2000, Limmathurotsakul et al., 2012). *B. pseudomallei* infection in birds, crocodiles and kangaroos was also reported (Choy et al., 2000). The incidence of fatal melioidosis in zoo animals showed an area and a seasonal correlation with the highest incidence of melioidosis in the rainy season in the north-east Thailand (Kasantikul et al., 2016). *B. pseudomallei* infected animals may display abscesses in many organs and acute illness, in a similar manner to the disease presentation of humans (Reviewed in Sprague and Neubauer, 2004, Limmathurotsakul et al., 2013).

1.1.2 The closely related species

From the large diversity of the *Burkholderia* genus (more than 70 species), *Burkholderia mallei* is the only member that is restricted to mammalian host cells, including humans, but it cannot persist in the environment outside its host. Different from *B. pseudomallei*, *B. mallei* is a non-motile bacterium because of the absence of flagella (Reviewed in Hatcher et al., 2015). *B. pseudomallei* and *B. mallei* share more than 90% genetic homology. The smaller genome size of *B. mallei* (5.8 Mb) is thought to underlie the adaptation of *B. mallei* to equine hosts and why it does not survive well outside the host (Nierman et al., 2004). A whole-genome comparative analysis of *B. mallei* strains compared with *B. pseudomallei* strains suggested that *B. mallei* is a clone of *B. pseudomallei* (Losada et al., 2010).

B. mallei causes the zoonotic disease glanders in solipeds such as horses, donkeys and mules. Glanders is characterised by ulcerating lesions of the skin and mucous membranes (Reviewed in Khan et al., 2013). This disease has been eradicated from developed countries, but it still remains in parts of Africa, Asia, South America and the Middle East. Glanders can be transmitted to humans and may present with similar symptoms to melioidosis. The mortality rate in humans without treatment is 95% and up to 40% with treatment. Additionally, it has been documented that *B. mallei* was used as a biological warfare agent during the World Wars (Reviewed in Van Zandt et al., 2013). Because of the lack of a vaccine, effective

treatment and diagnostic tools and its weaponisation potential, *B. mallei* is also listed in Schedule 5 of the ATCSA in the UK and as a Tier 1 select agent in the USA.

Whilst *B. pseudomallei* and *B. mallei* are the causative agents for melioidosis and glanders, respectively, *B. thailandensis* was later described with over 95% of 16S rDNA identity with *B. pseudomallei* (Brett et al., 1998). *B. thailandensis* is generally considered as relatively avirulent because a significantly higher infectious dose is required to cause disease in animal models (Brett et al., 1997). It is also avirulent because it is not associated with human disease, despite being present at very high titres in soil and water (Smith et al., 1997). Both *B. pseudomallei* and *B. thailandesis* are found in soil in Thailand but the ability of *B. thailandensis* to assimilate L-arabinose (Ara^+) differentiates the species (Smith et al., 1997). Although *B. thailandensis* can invade cells, escape the endocytic compartment, form actin tails and spread from cell-to-cell in cultured human epithelial cells, it is less efficient than the pathogenic *B. pseudomallei* (Kespichayawattana et al., 2004).

1.1.3 Intracellular lifestyle of *B. pseudomallei*

In common with many other intracellular bacteria, after internalisation, *B. pseudomallei* has evolved to escape from the vacuole and survive in the cytosol of host cells. A key virulence factor for the early stages of *B. pseudomallei* infection, which is known to be important for escaping from endocytic vesicle and intracellular survival, is the Type III Secretion System (T3SS) (Reviewed in Vander Broek and Stevens, 2017). T3SS-3 (also known as *Burkholderia* secretion apparatus; Bsa), which is one of three of T3SS encoded by *B. pseudomallei*, is the best characterised and is required for the efficient escape into the cytosol (Stevens et al., 2003, Stevens et al., 2002). Inside the cytoplasm, *B. pseudomallei* is able to induce actin polymerisation to propel itself for intra- and inter-cellular movement, which is mediated by BimA (*Burkholderia* intracellular motility A) (Stevens et al., 2005a). Uniquely, this pathogen spreads from cell-to-cell by cell fusion leading to multinucleated giant cell (MNGC) formation. Figure 1.1 shows the main stages of *B. pseudomallei* intracellular life. Numerous bacterial factors involved in its life cycle have been reviewed in Allwood et al (2011). Numerous bacterial factors involved in the life cycle of *B. pseudomallei* have been reviewed in Allwood et al. (2011) and recently reported in Willcocks et al. (2016).

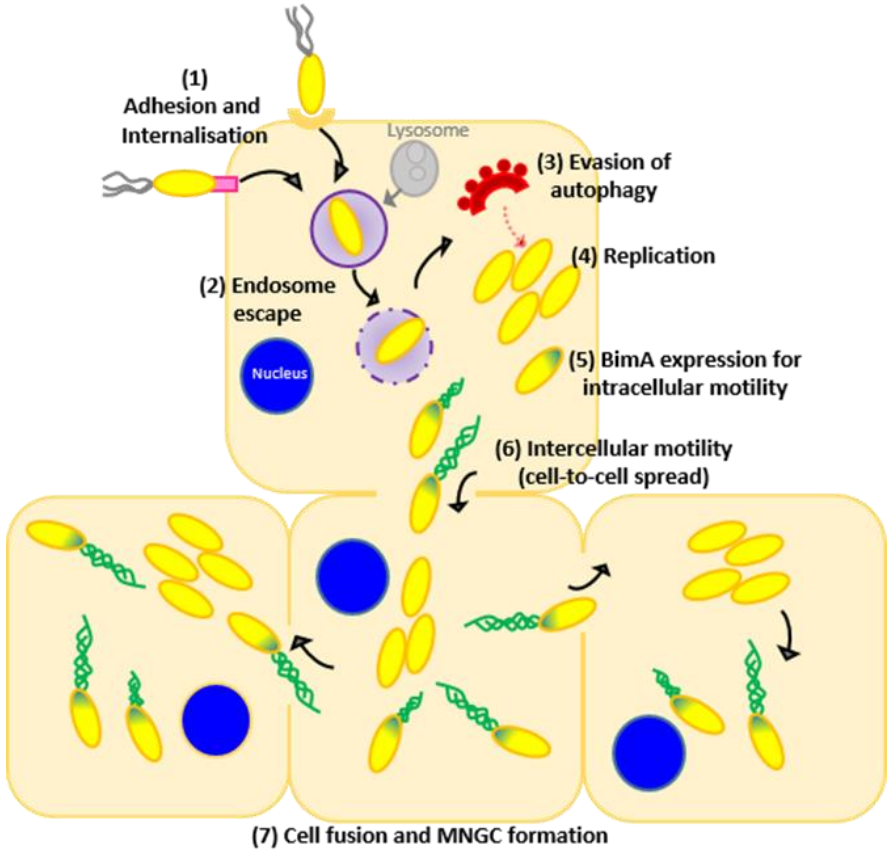

Figure 1.1: Intracellular lifestyle of *B. pseudomallei.*
Schematic representation of intracellular lifestyle of *B. pseudomallei* involves:
(1) Adhesion and internalisation: The bacterium is able to invade both phagocytic and non-phagocytic cells. Flagella facilitate both adhesion and invasion. The *bsa*-T3SS system (pink) encodes proteins that are required for invasion.
(2) Endosome escape: *B. pseudomallei* can rapidly escape from endocytic vacuoles into the cytoplasm
(3) Evasion of autophagy: The cytoplasmic *B. pseudomallei* is able to evade autophagy interfere with host defense mechanisms using unknown mechanism.
(4) Replication: *B. pseudomallei* can multiply intracellularly.
(5) BimA expression for intracellular motility: In the cytosol, *B. pseudomallei* requires BimA (as shown in green) expressed at one pole of the bacterial cell to polymerise the cellular actin and form an actin tail for protrusion within cells.
(6) Intercellular motility (cell-to-cell spread): The bacteria use actin-based motility to spread and between cells.
(7) Cell fusion and MNGC formation: *B. pseudomallei* can stimulate cell fusion with neighbouring cells and form multinucleated giant cells (MNGCs), which are a unique pathogenic feature of *B. pseudomallei*.

The first step of *B. pseudomallei* infection is cell adherence to the host cells. The attachment of *B. pseudomallei* to pharyngeal epithelial cells is facilitated by a thin capsular polysaccharide layer on the surface of *B. pseudomallei* (Ahmed et al., 1999). A previous study showed Type IV pili (fimbriae) is required for *B. pseudomallei* adherence (Essex-Lopresti et al., 2005). A *pilA* mutant demonstrated a decreased adherence to cell cultures and a delayed time to death of *C. elegans* nematodes (Essex-Lopresti et al., 2005). Adhesins also play a role in promoting the contact of *B. pseudomallei* with the host cells. BoaA and BoaB (*Burkholderia* Oca-like adhesin) share similarity with *Yersinia enterocolitica* autotransporter adhesin (YadA), a member of the oligomeric coiled-coil adhesin (Oca) family (Balder et al., 2010). The *boaA* and *boaB* mutants were impaired in their ability to bind to human respiratory epithelial cell lines, Hep2 and A549 cells (Balder et al., 2010).

To enter host cells, *B. pseudomallei* is able to invade phagocytic cells passively or it is taken up actively into non-phagocytic cells (Harley et al., 1998, Jones et al., 1996). Similar to other intracellular bacterial pathogens, *B. pseudomallei* exploits the arrangement of the host actin cytoskeleton to support its invasion. This is supported by the finding that bacterial invasion into A549 cells treated with cytochalasin D (a mucotoxin that binds actin filaments specifically and inhibits polymerisation) was greatly reduced (Jones et al., 1996). Additionally, a Bsa T3SS-secreted effector protein BopE, which is required for efficient invasion of *B. pseudomallei* into epithelial cells, exhibited guanine nucleotide exchange factor (GEF) activity for Rho GTPase that regulate the actin network promoting membrane ruffling (Stevens et al., 2003).

Shortly after invasion, *B. pseudomallei* is observed in membrane-bound vacuoles of infected HeLa cells at 4 hours post-infection (Jones et al., 1996). Before phagosome-lysosome fusion, the bacteria escape this degradation compartment by lysis of the endosome which is mediated by several Bsa T3SS proteins. For example, BsaZ and BipD that encode a structural component and needle tip protein of the T3SS apparatus respectively are involved in efficient endocytic escape (Stevens et al., 2002). Approximately 90% of *bsaZ* and *bipD* mutants in J774.2 cells were observed to co-localise with LAMP-1 (lysosome-associated membrane protein-1), a marker of lysosomes, indicating that the proteins are required for vacuole lysis leading to the escape of the bacteria into the host cell cytoplasm (Stevens et al., 2002). After escape

from the endosome, *B. pseudomallei* expresses a number of biosynthetic pathway genes to replicate and survive inside host cells (Pilatz et al., 2006). In the cytosol, *B. pseudomallei* is able to propel itself through the cytoplasm by hijacking the cellular actin to generate the actin polymerisation force known as actin-based motility. *B. pseudomallei* forms actin-rich tails at one pole of the bacterium after infection of both phagocytic and non-phagocytic cells to facilitate its movement and cell-to-cell spread (Kespichayawattana et al., 2000, Breitbach et al., 2003, Stevens et al., 2002). This process requires BimA expression at the pole of the bacterial cells where actin polymerisation occurs (Stevens et al., 2005a). A *bimA* mutant was unable to form actin tails in infected cells and actin tail formation could be restored by *trans*-complementation, indicated that BimA was sufficient for actin-based motility of *B. pseudomallei* (Stevens et al., 2005a) (Figure 1.2).

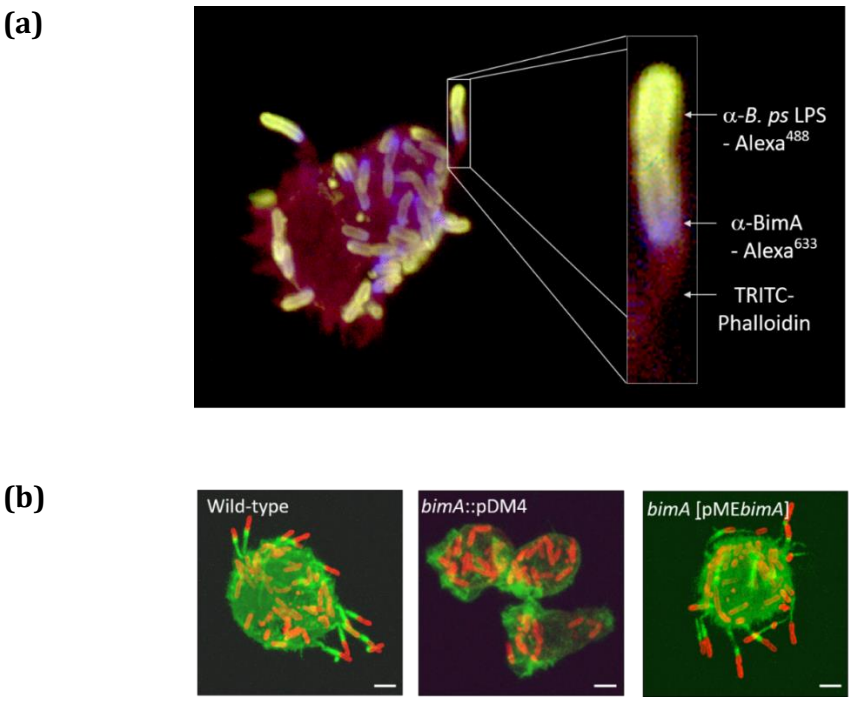

Figure 1.2: BimA is required for *B. pseudomallei* actin-based motility

(a) BimA is located at the bacterial pole where actin assembly takes place. *B. pseudomallei* infected J774.2 cell. Bacteria were stained green, F-actin was stained red and BimA was stained blue.

(b) Mutation of *bimA* abolishes actin-based motility of *B. pseudomallei* in J774.2 cells. Representative confocal micrographs of J774.2 cells infected with wild-type *B. pseudomallei* 10276, the 10276 *bimA*::pDM4 mutant, or the *trans*-complemented BimA mutant. Bacteria were stained red and F-actin was stained green. Scale bar = 5 μM.

(Figure taken with permission from Stevens et al., 2005a).

Whilst most of the *B. pseudomallei* is free in the cytosol, a proportion of the escaped bacteria have been described to be co-localised with microtubule-associated protein light chain (LC3), the autophagy marker protein, in both non-phagocytic and phagocytic cells indicating the *B. pseudomallei* infection induces autophagy (Cullinane et al., 2008). Intracellular survival of *B. pseudomallei* is reduced in cells that were treated with rapamycin, a pharmacological autophagy inducer (Cullinane et al., 2008). However, the majority of bacteria is able to evade autophagy using the Bsa T3SS effector, BopA for efficient escape (Cullinane et al., 2008, Gong et al., 2011).

In order to replicate intracellularly and move from cell-to-cell by avoiding extracellular immune responses, *B. pseudomallei* has a unique characteristic to induce cell-cell fusion leading to MNGCs. This feature is the result of direct cell-to-cell fusion that can be assessed by plaque assay. MNGC and plaque formation were observed in *B. pseudomallei*-infected HeLa cells and J774A.1, non-phagocytic epithelial cells and macrophage cells respectively (Kespichayawattana et al., 2000). *bimA* mutants were not able to form plaques in A549 monolayer because of the defect in actin tail formation (Sitthidet et al., 2011). In a study on HEK293 cells, it was demonstrated that plaque formation represents cell death which is a consequence of cell lysis following MNGC formation (French et al., 2011). Taken together, the motility of *B. pseudomallei* facilitates the efficiency of cell fusion (Sitthidet et al., 2011, French et al., 2011, Benanti et al., 2015). In addition to intracellular motility, it was proposed that contact between *B. pseudomallei* and host cell membrane is a prerequisite for membrane fusion through a process facilitated by Type Six Secretion System (T6SS) (Schwarz et al., 2014, Toesca et al., 2014). A mutation of a core gene on T6SS cluster 5, *vgrG5* (valine-glycine repeat protein), impaired the ability of the bacterium to induce MNGCs in HEK293 cells, despite it being able to escape from endosome and form an actin tail (Toesca et al., 2014).

1.2 Actin-based motility

Actin-based motility is a complex dynamic cellular process to organise directed movement, change cell shape or extend protrusions in response to environmental signals. The process is driven by the assembly and disassembly of actin filaments. Pathogens hijack host actin for propulsion by inducing actin polymerisation at the pole of a bacterial or viral pathogen in the cytosol. Many studies have been published on other intracellular bacterial pathogens that display actin-based motility and demonstrated that the mechanism of bacterial-induced actin-based motility differs between bacterial species.

1.2.1 Actin polymerisation

Actin is a 43-kDa abundant protein and highly conserved in eukaryotic cells. It exists in two forms, monomeric globular actin (G-actin) and filamentous actin (F-actin). Actin filaments are polar polymers with a right-handed helical twist and with different dynamic ends called barbed or plus (+) and pointed or minus (-) ends. G-actin is an ATPase, the ATP monomers add faster at the barbed end. As the filament grows, the ATPase actin hydrolyses the bound ATP and releases the phosphate moiety. The ADP-actin monomers remain in the filament and mainly dissociate from the pointed end. The dynamic process of cellular motility is driven by assembly and disassembly of the actin filaments.

Actin filament assembly can be triggered by spontaneous (*de novo*) actin nucleation from monomeric actin. However, this step is rate-limiting in actin polymerisation because the formation of dimers and trimers of monomeric actin are unstable. Also, most of the monomeric actin in the cytoplasm is sequestered by actin-monomer-binding proteins such as profilin. Once an F-actin nucleus, which usually consists of three actin monomers in complex, forms, the elongation process is initiated by further monomer addition onto the nucleus trimer on both of its ends to produce a filament. The barbed end elongates 10 times faster than the pointed end. The concentration of G-actin monomers decreases as actin filaments grow until an equilibrium is reached at the steady state where the amount of actin filament is balanced with G-monomer actin addition and polymer disassembly (Reviewed in Carlier et al., 2015).

Spontaneous nucleation is an inefficient process. In cells, there are three major classes of actin-nucleating factors; the actin-related protein 2/3 (Arp2/3) complex, formins, and tandem-monomer-binding proteins (Reviewed in Firat-Karalar and Welch, 2011). Although they form distinctive actin filament networks, they all contain WASP-homology 2 (WH2) domains (Reviewed in Dominguez, 2016). Also, most actin nucleators contain proline-rich domains to deliver actin monomers for actin polymerisation by interaction with an associated protein such as profilin (Reviewed in Holt and Koffer, 2001). The first actin nucleator that was discovered is the Arp2/3 complex, consisting of seven subunits; Arp2, Arp3 and ARPC1-5. Arp2 and Arp3 have a similar homology to monomeric actin that mimics the actin dimer and trimer resulting in initiation of actin polymerisation, generating filaments that grow at their barbed ends.

However, the Arp2/3 complex by itself is a weak nucleator, and nucleation-promoting factors (NPFs) are required for activation. The largest group of NPFs include Wiskott-Aldrich syndrome protein (WASP), neural WASP (N-WASP), WASP family verprolin-homologous proteins or also known as SCAR (WAVE/SCAR), and WASP and SCAR homologue (WASH). A common characteristic of these proteins is that they contain a C-terminal WCA domain. This domain (also called VCA) consists of three conserved motifs; W: one or more WASP homology (WH2) domains (also known as verprolin-homology domain), C: the cofilin-homology domain (also called central domain), and A: the acidic domain. For activation, actin monomers bind to the WH2 domain and the Arp2/3 complex is recruited to the CA domain (Reviewed in Campellone and Welch, 2010). The WASP family proteins are inactive in an auto-inhibited state. The upstream Rho-family GTPases, which are small GTP-binding proteins; such as Cdc42 and Rac1, regulate and activate the WASP and N-WASP by opening the WCA domain allowing the Arp2/3 to bind (Reviewed in Spiering and Hodgson, 2011).

In addition to the NPFs, the Arp2/3 complex requires the side of an existing actin filament to bind by joining at a 70° Y-branch angle. Thus, the Arp2/3 complex is a key mediator of actin polymerisation in cells, playing roles in the nucleation step as well as cross-linking actin filaments to form characteristic Y-branched actin filaments (Reviewed in Goley and Welch, 2006, Rotty et al., 2013).

The second group of actin nucleator includes the multidomain formin proteins, which initiate *de novo* polymerisation of actin. In contrast to the Arp2/3 complex and its NPFs, formin-mediated actin polymerisation leads to cross-linking of linear (unbranched) actin filaments in parallel arrays. Formin consists of formin homology 1 and 2 (FH1 and FH2) domains. The FH1 domain acts as a lasso to rope in profilin-actin molecules while the FH2 domain forms a doughnut- or ring-shaped homodimer that interacts with two actin monomers nucleating a filament at the barbed ends as well as protecting the filament from capping (Reviewed in Goode and Eck, 2007). The tandem-monomer-binding proteins such as Spire, Cordon-Bleu (Cobl), Leiomodin (Lmod) and Junction-mediating and regulatory protein (JMY) are the third group identified as an actin nucleator because of the presence of multiple repeating WH2 domains. The multiple WH2 domains bind monomeric actin and tether the molecules to form an F-actin nucleus. These tandem-monomer-binding proteins nucleate both branched and unbranched actin filaments. Differences in the number of WH2 domains and the length between them result in distinct structural arrangement of the resulting actin network (Reviewed in Qualmann and Kessels, 2009, Siton-Mendelson and Bernheim-Groswasser, 2017).

In addition to actin nucleators, actin elongators also promote actin polymerisation. Once nucleated, actin filament elongation provides the driving force for cellular movement. Elongation is rapid and can be enhanced by formin and Enabled/vasodilator-stimulated phosphoprotein (Ena/VASP) proteins. Formins not only nucleate unbranched actin filaments but remain bound to the elongating barbed end of the filament to promote F-actin polymerisation (Reviewed in Paul and Pollard, 2009). Ena/VASP recruits both actin monomer and actin filament, as well as actin-profilin complex, but reduces stability of branched actin filaments generated by the Arp2/3 complex (Reviewed in Krause et al., 2003). A recent study shows Ena/VASP are required for the formation of parallel actin filaments bundled by fascin (Winkelman et al., 2014).

For cell motility, actin filaments are formed in different patterns with specific factors for force generation. Lamellipodia and filopodia actin networks are the beginning step for migration. At the leading edge of lamellipodia, a sheet-like protrusion of plasma membrane is driven by a branched actin filament network. On

the other hand, filopodia formed by unbranched actin filaments bundles produce finger-like plasma membrane protrusions. Then the cell form adhesions connected to the extracellular matrix. Finally, the cell moves forward with concomitant disassembly of the anchor site. Apart from the functions of the actin-binding proteins to nucleate and elongate actin polymerisation as described above, other actin-binding proteins are also importance factors required for different organisation of actin filaments with distinct dynamic properties (Reviewed in Carlier et al., 2015, Pollard, 2016). Actin-monomer-binding proteins such as profilin, which is an abundant protein, binds monomeric globular actin to inhibit spontaneous actin nucleation and elongation at the pointed ends. Moreover, profilin competes with capping protein, which is an actin-binding protein to control the free barbed ends in cells by blocking the addition of actin (Reviewed in Edwards et al., 2014). The actin filaments can also be depolymerised by actin depolymerising factor (ADF), also known as cofilin, which binds to actin filaments and distort the helical twist of F-actin or severs actin filaments. However, the actin filaments can be protected from severing by cofilin with tropomyosin which is a filaments-binding protein. Bundles of actin filaments are connected together by actin cross-linking proteins, for example fascin and filamin that are present in either bundles or networks to control cell shape, and α-actinin that plays role in the rate of assembly of actin networks (Courson and Rock, 2010). When increasing the rate of actin assembly, the formation of actin bundles was abolished (Falzone et al., 2012).

To understand the process for generating the force for cell motility, two new models have been proposed. One model describes competition for actin monomers in which actin monomer availability is limiting (Suarez and Kovar, 2016), the second describes a global treadmilling process in which a steady-state amount of polymerisable actin monomers (Carlier and Shekhar, 2017) impacts actin cytoskeleton dynamics. Studies on actin-based motility of bacterial pathogens explore the molecular components necessary for this process, providing a better understanding of both cell biology and pathogenesis.

1.2.2 Actin-based motility of bacterial pathogens

With a range of different mechanisms of actin filament organisation, cells can migrate by a multistep process that produces force to drive motility. Pathogens hijack this process for their movement within and between host cells. Bacterial factors have similar function as the actin-binding proteins to nucleate and assemble actin filaments at one pole of the bacterium. The barbed ends of actin filaments are towards the pole of the bacterium that propel itself forward within and between cells by the asymmetric actin polymerisation forming comet- or rocket-actin tail behind it (Gouin et al., 1999).

Bacterial pathogens have evolved different mechanisms to manipulate the host actin cytoskeleton. Arp2/3 complex is a common target for pathogens to hijack actin for motility during infection (Reviewed in Welch and Way, 2013). ActA from *L. monocytogenes*, BimA from *B. thailandensis* and RickA from *Rickettsia* species of the spotted fever group (SFG) mimic a cellular NPF to activate the Arp2/3 complex. On the other hand, IcsA from *S. flexneri* recruits the host NPF N-WASP to the bacterial surface to promote their Arp2/3-mediated motility by activating upstream small GTPases (Reviewed in Stevens et al., 2006). Moreover, virulence proteins from Gram-negative bacteria; BimA from *B. pseudomallei* and *B. mallei* and Sca2 from SFG *Rickettsia* species, act as actin nucleators which are able to nucleate actin directly (Reviewed in Bugalhao et al., 2015). This diversity of bacterial proteins that regulate cellular actin dynamics demonstrates that the bacteria hijack the host cellular actin regulatory machinery by distinct molecular mechanisms. This results in different organisation of actin filaments formed by these bacteria impact on the efficiency of motility (Reviewed in Lamason and Welch, 2017).

1) *Listeria monocytogenes*

L. monocytogenes is a Gram-positive food-borne pathogen that causes listeriosis as well as meningitis and abortions. It is a facultative intracellular bacterium that can invade both non-phagocytic and phagocytic host cells, and then replicate within the cytosol where actin is recruited and polymerised to create the driving force for its movement and protrusion to the neighbouring cell. Initially, the bacteria are surrounded with actin forming an ″actin cloud″ around the bacterial cell,

before displaying trails of actin ″comet tails″ used for propulsion through the cytoplasm (Tilney and Portnoy, 1989). The length of *Listeria* comet tails in HEp2 cells was shown to vary from 4-12 μm (Gouin et al., 1999). In different cell lines, the bacteria moved in a straight line leaving a long F-actin tails up to 40 μm in length, moving at speeds in the cytoplasm between 0.25-1.46 μm/sec in J774 cells and from 0.12-0.35 μm/sec in PtK2 cells (Dabiri et al., 1990). Similarly, the movement rate of *L. monocytogenes* in Vero cells was recorded as 22 μm/min (Gouin et al., 1999). The force generated by actin-based motility supports bacterial movement until reaching the peripheral cell membrane, where the bacteria spread to the adjacent cells within a ″finger-like″ membrane protrusion containing the bacterium at the tip (Reviewed in Kuehl et al., 2015). The morphology of actin filaments formed by *Listeria* was observed by electron microscopy and showed that the filaments within the cytoplasm are short and randomly oriented with higher density at the vicinity of the bacterium (Gouin et al., 1999, Tilney and Portnoy, 1989). On the other hand, most of the actin filaments within the protrusion were long and bundled in a parallel array, although near the bacterial body the filament were less tightly bundled (Sechi et al., 1997).

The actin-based motility of *L. monocytogenes* requires the surface bacterial factor ActA, which was identified using mutants that were unable to accumulate actin or spread from cell-to-cell (Domann et al., 1992, Kocks et al., 1992). ActA was expressed and concentrated at one pole of the bacterium where actin assembly took place (Kocks et al., 1993, Dabiri et al., 1990). To initiate ActA-dependent actin polymerisation, *Listeria* hijacks the host Arp2/3 complex to mediate actin tail formation and motility (Welch et al., 1997). The N-terminal region of ActA contains a WCA domain that binds and activates the Arp2/3 complex to initiate nucleation of branched actin filaments (Welch et al., 1998, Boujemaa-Paterski et al., 2001, Welch et al., 1997). This demonstrated that ActA acts as a structural and functional mimic of NPF N-WASP to recruit Arp2/3 complex to the bacterial surface (Lommel et al., 2001, Boujemaa-Paterski et al., 2001). Moreover, the proline-rich repeats on the central domain of ActA also recruit profilin by interaction with Ena/VASP to promote actin-based motility (Smith et al., 1996). It has been shown that Ena/VASP in *L. monocytogenes* movement is involved in controlling speed and directionality of movement (Auerbuch et al., 2003). At the later stage of infection, the time-lapse live-

cell imaging showed that VASP was not recruited to the actin tail of *L. monocytogenes* but it interacted with the host cell protein lamellipodin (Lpd) which is an Ena/VASP binding protein (Wang et al., 2015). In *L. monocytogenes*-infected HeLa cell, Lpd accumulated at the interface between the bacteria and the developing actin tail (Wang et al., 2015). *L. monocytogenes* infected Lpd-depleted cells showed significantly fewer and smaller plaques than control cells implying a role of Lpd in cell-to-cell spread (Wang et al., 2015). The activity of ActA is also regulated by host cell phosphorylation. A study demonstrated that casein kinase 2 (CK2)-mediates phosphorylation of the Arp2/3-binding domain (Chong et al., 2009). This ActA modification regulates the affinity of ActA for the Arp2/3 complex and is required for proper actin tail formation and cell-to-cell spread (Chong et al., 2009).

The use of *in vitro* reconstitution experiments uncovered a core set of host cell proteins that acts as the minimal requirements for actin assembly and disassembly, which are necessary for actin-based motility, consisting of actin, Arp2/3, capping protein and ADF/cofilin (Loisel et al., 1999). Consistently, in the *Listeria*-actin comet tail, the Arp2/3 complex, capping protein and cofilin have been detected (David et al., 1998). Despite this, a large number of host proteins participating in tail formation of *L. monocytogenes* was isolated from cell extracts *in vitro*, including actin-binding proteins and components of upstream signalling cascades (Van Troys et al., 2008). This suggested that actin tail formation was regulated by specific multicomponent regulatory complexes (Van Troys et al., 2008). Studies on numerous protein components localised in *Listeria*-comet tails demonstrated that the dynamic interaction of host cell proteins was exploited and involved in the characteristic actin filaments formed by this bacterium. Only actin and the Arp2/3 complex are essential for actin tail formation containing highly branched filaments (Brieher et al., 2004). Recently, a collapsin response mediator protein-1 (CRMP-1), which binds to both ActA and F-actin, was identified as a novel host cellular factor facilitating actin network formation by increasing Arp2/3-dependent actin filament branching (Yu-Kemp and Brieher, 2016). Nexilin, an actin-associated protein that localises to the leading edge and focal adhesion in motile cells, was identified as a crucial component for efficient comet tail formation of *L. monocytogenes* (Law et al., 2012). This protein accumulated at the point of comet tail

formation origin with less co-localisation along the length of the actin tail (Law et al., 2012). This implied that nexilin stabilised the actin-rich structure (Law et al., 2012).

The difference in actin filament networks between the bacteria within the cytoplasm and in the protrusion, implies certain host factors contribute to these actin polymerisation process. The Arp subunit p34 was enriched along with the comet tail in the cytosol but reduced levels of this protein were found in the *Listeria*-induced protrusion (Fattouh et al., 2015). Whereas α-actinin was contained in the *Listeria*-actin tail in the cytosol but it was not in the protrusions (Dabiri et al., 1990), and ezrin was detected in the *Listeria*-induced protrusion but not in the comet tail (Sechi et al., 1997, Fattouh et al., 2015).

Apart from the Arp2/3-dependent actin assembly, ActA also induced actin polymerisation *in vitro* in a VASP-dependent manner, but independent of the Arp2/3 complex, similar to the host zyxin-mediated actin polymerisation (Fradelizi et al., 2001). Interestingly, bundling proteins including fascin, fimbrin, and filamin, which were localised to the comet tail, were required for *Listeria* motility in the Arp2/3-independent elongation phase (Brieher et al., 2004). In the absence of Arp2/3 complex, the bacteria move faster with fascin-mediated propulsion (Brieher et al., 2004). The comet tail organisation that was generated in this stage was bundled parallel to the bacterial direction movement, differing from the branched filament of Arp2/3 nucleation (Brieher et al., 2004).

2) *Shigella flexneri*

S. flexneri is a Gram-negative enteropathogenic bacterium that causes bacillary dysentery, an intestinal disease in humans. After invasion, the bacterium is contained in a membrane-bound vacuole within the infected cells. Then, the vacuole is lysed and the pathogen is free in the cytosol where actin is recruited to the bacteria before forming an actin tail at one pole of the bacterium (Bernardini et al., 1989). The length of comet tail formed by *S. flexneri* in HEp2 cells varied from 5 to 15 μm with an average length of 7 μm (Gouin et al., 1999). Comparing movement rate with *L. monocytogenes*, *S. flexneri* moves faster with the highest speed recorded in Vero cells at 26 μm/min (Gouin et al., 1999). The force generated by actin polymerisation propels the bacteria within the cytosol until they eventually reach the peripheral membrane forming a large and long membrane protrusion (Monack and Theriot,

2001). This structure (5-30 μm in length and 0.5 μm width) contains the bacterium at the tip which is engulfed by adjacent cells leading to cell-to-cell spreading (Bishai et al., 2013).

The ultrastructure of the *S. flexneri* comet tail was observed by electron microscopy and showed that the actin filments were oriented with the barded ends towards the pole of the bacterium (Gouin et al., 1999). Similar to *L. monocytogenes*, the density of the filaments was higher in the vicinity of the bacterium, compared to the rest of the tails (Gouin et al., 1999). The actin filaments were cross-linked and formed a branching network which is a characteristics of Arp 2/3 complex nucleated filaments (Gouin et al., 1999, Tilney and Portnoy, 1989), but the filament along the sides of *S. flexneri* tails was shorter than those in *L. monocytogenes* tails (Gouin et al., 1999). Actin filament organisation formed by *S. flexneri* in membrane protrusions were more bundled towards the end of the tails, compared to those in the comet tail presented in the cytosol (Gouin et al., 1999).

The bacterial factor required for actin-based motility of *S. flexneri* is IcsA (also called VirG) (Makino et al., 1986). Expression of IcsA on the surface of *Escherichia coli* is sufficient to allow the bacterial actin-dependent movement in cytoplasmic extracts, with the same rate of *S. flexneri* in infected cells (Goldberg and Theriot, 1995, Kocks et al., 1995). IcsA is a member of the type V autotransporter family which are secreted across the cytoplasmic membrane to be presented on the outer membrane of *S. flexneri* (Brandon et al., 2003). IcsA is targeted at the pole of the bacteria before being secreted (Charles et al., 2001, Goldberg et al., 1993) and recruiting N-WASP (Suzuki et al., 1998).

Whilst ActA acts as an NPF mimic and directly activates Arp2/3 complex, the host NPF N-WASP is recruited to the *Shigella* pole and in turn activates Arp2/3 complex for initiation of actin nucleation and polymerisation (Egile et al., 1999). IcsA specifically interacts with N-WASP but it does not interact with other WASP family proteins (Suzuki et al., 2002). In N-WASP-defective fibroblasts, *Listeria* was able to form an actin tail but S*higella* failed to induce actin tail formation (Lommel et al., 2001). Consistently, overexpression of a dominant-negative N-WASP mutant inhibits actin assembly on *Shigella* but has no effect on the formation of actin tail by *Listeria* (Suzuki et al., 1998). Without significant sequence similarity to ActA, a glycine-rich repeat domain on IcsA is required for recruitment of N-WASP (Suzuki et al., 1998).

The interaction between IcsA and N-WASP activates an auto-inhibited conformation of N-WASP opening up the WCA domain to recruit the Arp2/3 complex and initiate actin assembly (Egile et al., 1999, Mauricio et al., 2017). This ability is similar to the cellular signalling molecules (Cdc42 or PIP2), suggesting that IcsA is a functional mimic of these molecules that recruit and activate N-WASP. This could explain why this pathogen was able to form actin tail in Cdc42-deficient cells (Shibata et al., 2002).

However, both Cdc42 and PIP2-induced actin polymerisation require Toca-1 (Transducer of Cdc42-dependent actin assembly) to interact with N-WASP to promote actin nucleation (Ho et al., 2004). Toca-1 was transiently recruited to the surface of *S. flexneri* at the stationary phase and dissociated from the bacteria when the bacteria begin to move (Leung et al., 2008). In Toca-1 depleted cells with expression of a constitutively open N-WASP, *S. flexneri* was able to assemble an actin tail, demonstrating that Toca-1 acts as a cellular cofactor for relief of N-WASP autoinhibition and efficient actin tail formation by *S. flexneri* (Ho et al., 2004, Leung et al., 2008). N-WASP-dependent actin polymerisation is also regulated by phosphorylation. In fibroblast cells, the Abl tyrosine kinase phosphorylates N-WASP (Burton et al., 2005). *S. flexneri* was able to restore the length of actin tail and the size of plaques in cells lacking Abl kinase when an activated N-WASP mutant was introduced, suggesting that Abl kinase was required for elongation of the *Shigella* actin tail as well as cell-to-cell spread (Burton et al., 2005). Similarly, in intestinal cells, Bruton's tyrosine kinase (Btk) played a role in actin tail formation and dissemination of *S. flexneri* by regulation of N-WASP phosphorylation (Dragoi et al., 2013).

Several cytoskeleton proteins found in the *Listeria*-actin tail are also present in the *Shigella*-actin tail (Gouin et al., 1999). Actin, Arp2/3 complex, actin depolymerisation factor and capping protein were the minimal requirement for *Shigella* movement *in vitro*, the same as for *Listeria in vitro* actin-based motility (Loisel et al., 1999). To fine-tune actin assembly dynamics, pathogens evolved their specific strategies to manipulate the host cell proteins differently. For example, VASP was present in both actin tail of *L. monocytogenes* and *S. flexneri* (Gouin et al., 1999) but this protein was essentail for motility rate of *L. monocytogenes* (Geese et al., 2002), but not in *S. flexneri* (Ally et al., 2004). Whilst a cytoskeleton protein, spectrin

was not recruited to *L. monocytogenes* actin tail, this protein was localised within comet tail of *S. flexneri* (Ruetz et al., 2011, Ruetz et al., 2012).

3) *Rickettsia*

Rickettsia are Gram-negative obligate intracellular bacteria that cause diseases such as typhus and spotted fever, transmitted to their mammalian host by arthropod vectors including ticks, lice and fleas. Whilst the spotted fever group (SFG) rickettsiae, such as *R. conorii*, *R. parkeri* and *R. rickettsia,* display long actin tails, the typhus group rickettsiae including *R. typhi* forms a very short actin tail with a hook shape, and no actin tail formation is displayed by *R. prowazekii* in infected Vero cells (Van Kirk et al., 2000, Heinzen et al., 1993). Different from the branched actin tails-mediated by Arp2/3 complex formed by *Listeria* and *Shigella* (Gouin et al., 1999), *R. conorii* actin tails are long and composed of helical bundles of actin filaments (Gouin et al., 1999). Similarly, the ultrastructure of *R. rickettsia* actin tails was observed by transmission electron microscopy and showed that the individual F-actin filaments are long and oriented with the fast-growing barded end towards the bacterial pole (Van Kirk et al., 2000). Using laser scanning confocal microscopy revealed that the SFG *R. rickettsia* actin tail is formed of bundles of actin filaments twisted around each other (Heinzen et al., 1999, Van Kirk et al., 2000). Despite a longer actin tail length with an average length of 16.7 μm of *R. rickettsia* (Van Kirk et al., 2000), the motility rate of SFG rickettsia in the cytoplasm of Vero cells was 2.5-3 times slower than that of *L. monocytogenes* (Heinzen et al., 1999, Van Kirk et al., 2000, Gouin et al., 1999). On the other hand, *Rickettsia* protrusions were shorter than those in *Listeria* infected cells (Gouin et al., 1999, Van Kirk et al., 2000).

Whilst *L. monocytogenes* and *S. flexneri* express a single surface protein to activate the Arp2/3 complex to exploit the host cell actin polymerisation pathway to drive actin-based motility, *Rickettsia* requires two bacterial factors function as an actin nucleator to initiate actin polymerisation in distinct phases. The early phase of motility within an hour after infection requires an Arp2/3 complex-activating protein called RickA and at 24 hours later requires a bacterial surface protein, Sca2 (Surface Cell Antigen 2) to facilitate cell-to-cell spread (Reed et al., 2014). The bacterial surface RickA was discovered through the similarity region with the WCA region of WASP protein in the SFG *Rickettsia* (Jeng et al. 2004). In contrast, RickA was

absent in the typhus group *R. prowazekii* that did not display actin-based motility (Gouin et al., 2004, Jeng et al., 2004). Interestingly, *R. typhi* was able to form a short actin tail despite lacking RickA (Heinzen et al., 1993). RickA stimulates Arp2/3-dependent actin polymerisation *in vitro* which generated branched actin networks (Gouin et al., 2004, Jeng et al., 2004). Despite this, the Arp2/3 complex was not detected in the actin tail and was not required for actin tail formation of the SFG *R. rickettsia* (Gouin et al., 2004, Serio et al., 2010). This led to the identification of the autotransporter protein Sca2 using transposon mutagenesis (Kleba et al., 2010). A Sca2 mutant of SFG *R. rickettsia* was unable to induce actin tail formation and displayed a small-plaque phenotype indicating that Sca2 was required for actin tail formation and cell-to-cell spread (Kleba et al., 2010). The N-terminal domain of Sca2 shares secondary structure similarity with the FH2 domains of formins (Haglund et al., 2010, Madasu et al., 2013).

Morphology of *Rickettsia* actin tail generated at different times during infection was also observed. After invasion, short and curved actin tails with slow movement were found in the early phase when the bacteria expressed RickA and the Arp2/3 complex as well as cofilin were recruited into the actin tail (Reed et al., 2014). Instead, the formin mimic, Sca2 was later expressed and the bacteria displayed long and straight actin tails leading to a faster motility (Reed et al., 2014). The molecular mechanism of *Rickettsia* actin-based motility in the early and late phase is also distinguishable. Early actin tail formation by SFG *R. parkeri* was impaired in the cells treated with an Arp2/3 inhibitor but there was no effect in the late actin tail formation (Reed et al., 2014). Indeed, a core set of host factors for SFG *R. parkeri* actin-based motility was identified as profilin, fimbrin/T-plastin, capping protein and cofilin (Serio et al., 2010). These proteins were localised throughout the actin tails and played a role in controlling actin tail length, morphology of the actin tail and motility rate (Serio et al., 2010).

4) *Mycobacterium marinum*

Mycobacterium tuberculosis causes the human disease tuberculosis. *M. marinum* is a waterborne pathogen of macrophages that causes a systemic tuberculosis-like disease in its natural hosts, e.g. fish and frogs, and in immunocompromised humans. *M. marinum* is closely related to *M. tuberculosis* with

a similar mode of pathogenesis and genetics (Stamm and Brown, 2004, Tobin and Ramakrishnan, 2008). However, *M. marinum* is the only mycobacterial species that displays actin tail formation (Stamm et al., 2003). The bacterium is able to escape from the *Mycobacterium*-containing vacuole (MCV) and enter the cytoplasm of the infected macrophage where it induces actin polymerisation to facilitate direct cell-to-cell spread. A number of *M. marinum* were motile within bone-marrow-derived macrophages (BMDM) at an average rate of 11 μm/min (Stamm et al., 2003). Additionally, *M. marinum* was able to form actin tails in the free-living amoeba, *Acanthamoeba castellanii* (Kennedy et al., 2012). *M. marinum* actin tails were also found in murine and fish macrophage cell lines, as well as in cell-free extract when using the bacterium isolated from the infected BMDM (Stamm et al., 2003). Electron microscopy showed that the actin filaments behind *M. marinum* were polymerised in a branched pattern (Stamm et al., 2003). A few of *M. marinum* formed the actin tail at the side of a bacterium, whereas most of them formed actin tails at the pole (Stamm et al., 2003). Phase contrast time-lapse microscopy showed that *M. marinum* moved beyound the cell membrane to the adjacent cell directly (Stamm et al., 2003). Focal growth of intracellular GFP-labeled *M. marinum* in the presence of antibiotics was also detected, indicating that the role of actin-based motility was in direct cell-to-cell spread (Stamm et al., 2003).

Actin filaments formed by *M. marinum* were in a branched pattern which is a characteristic of the Arp2/3 complex-mediated actin polymerisation (Stamm et al., 2003). Consistently, subunits of the Arp2/3 complex was detected in the *M. marinum* actin tail (Stamm et al., 2003). Whilst VASP was also found throughout the actin tail, WASP and N-WASP localised specifically to the bacterial pole (Stamm et al., 2003). *M. marinum* motility was shown to require only WASP and N-WASP from the WASP/WAVE family because the bacteria restored actin tail formation in fibroblasts lacking N-WASP with transient expression of either WASP and N-WASP but not WAVE2 proteins (Stamm et al., 2005). The mechanism of actin polymerisation of *M. marinum* is similar to *Shigella* which hijacks signalling for Arp2/3 complex-dependent actin polymerisation through activation of the WASP family proteins (Stamm et al., 2005).

Until now, the bacterial factor involved in *M. marinum* actin-based motility has not been defined. It has been reported that mutations in the type VII secretion

system ESX-1 impaired plaque formation in an A549 cell monolayer by *M. marinum* (Gao et al., 2004). This system was important for the *M. marinum* to escape from the vacuole, in turn, ESX-1 was required for actin tail formation because the bacterium initiated actin polymerisation only when it entered the cytosol (Smith et al., 2008). Similarly, ESX-1-deficient bacteria were not able to form actin tails in amoebae (Kennedy et al., 2012).

5) *B. pseudomallei*

B. pseudomallei is another intracellular pathogen that can invade host cells and replicate inside the cytosol where it can move inside and between cells using actin-based motility. Actin is polymerised at one pole of the bacterial cells (Breitbach et al., 2003, Kespichayawattana et al., 2000, Stevens et al., 2005a). Among the *Burkholderia* species, *B. mallei* and *B. thailandensis* also showed this feature (Stevens et al., 2005b). From genome sequence analysis, *bpss1492* encoding BimA was identified as a proline-rich autosecreted protein, which is a key feature of IcsA that is required for actin-based motility of *S. flexneri* (Breitbach et al., 2003, Kespichayawattana et al., 2000, Stevens et al., 2005a). BimA belongs to the family of Type V autotransporter proteins which is a large and diverse family of secreted and outer membrane proteins that play role in pathogenesis and immunity (Reviewed in Lazar Adler et al., 2011). Localisation of BimA was present at the polar of one daughter cell during cell division (Stevens et al., 2005a).

Similarly, to other intracellular pathogens that exploit the Arp2/3 complex, the components of this complex were recruited to *B. pseudomallei*-actin tails in infected cells (Breitbach et al., 2003). However, *in vitro* studies showed that BimA directly interacts with actin and stimulates actin polymerisation in an Arp2/3-independent manner (Stevens et al., 2005a, Benanti et al., 2015). Over-expression of a dominant negative domain of the cellular NPF Scar1, which inhibits *Listeria*, *Shigella* and SFG *R. conorii* motility, did not block *B. pseudomallei* tail formation, implying that Arp2/3 complex was not functionally required for *B. pseudomallei* actin-based motility (Breitbach et al., 2003). Furthermore, N-WASP and Ena/VASP proteins were not required for actin-based motility of *B. pseudomallei* (Breitbach et al., 2003).

BimA homologues from related *Burkholderia* species can compensate for the actin tail formation defect of the *B. pseudomallei bimA* mutant, suggesting that actin assembly is a common function among these proteins (Stevens et al., 2005b). Comparison of the *B. pseudomallei* BimA with BimA from *B. mallei* and *B. thailandensis* demonstrates that the carboxyl-terminal regions are conserved but the amino-terminal regions are different. *B. thailandensis* BimA differs greatly in primary amino acid sequence to the *B. pseudomallei* BimA with the inclusion of an amphipathic central and acidic (CA) domain between the amino-terminal WH2 domain and the proline-rich region as shown figure 1.3 (Stevens et al., 2005b). Interestingly, all BimA homologues bind directly with actin but only *B. thailandensis* BimA interacts with the Arp2/3 complex (Stevens et al., 2005b). Consistently, a recent study using Arp3 knockdown cells showed that *B. pseudomallei* and *B. mallei* were able to form actin tails in contrast to *B. thailandensis* which failed to form any actin tails in the knockdown cells (Lu et al., 2015a). Moreover, *B. thailandensis* BimA displays Arp2/3-dependent actin polymerisation *in vitro* (Stevens et al., 2005b, Sitthidet et al., 2010, Benanti et al. 2015). This indicated that *B. thailandensis* has a distinct mechanism for actin-based motility from *B. pseudomallei* and *B. mallei*.

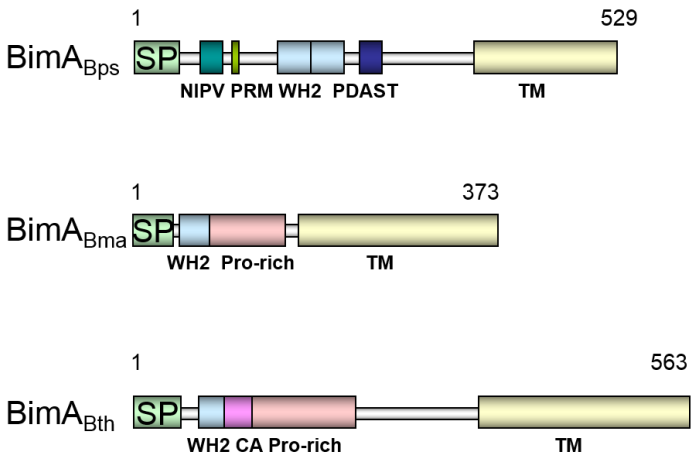

Figure 1.3: Domain organisation of the BimA proteins from *Burkholderia pseudomallei*, *B. mallei* and *B. thailandensis*
The putative domains are shown drawn to scale where: SP, predicted signal peptide; NIPV, repeat sequence in *B. pseudomallei* BimA with homology to human diaphanous 1 (hDia1); PRM, proline-rich motif 1 (IP7) with similarity to that found in hDia1, mouse formin and zyxin; WH2, WASP homology domain-2; PDAST, repeat sequence in *B. pseudomallei* BimA; TM, transmembrane anchor; Pro-rich, proline-rich regions; CA, central and acidic domains. (Figure taken with permission from Stevens et al., 2005b).

Studies on the functional regions of *B. pseudomallei* BimA demonstrated that the WH2 domains, but not a 13-amino acid repeat or proline-rich motif (PRM) domain, were required for actin binding, actin assembly, and plaque formation (Sitthidet et al., 2011). The predicted casein kinase II phosphorylation site (PDASX) domain was not required for actin binding, but deletion of PDASX repeats reduced the rate of actin polymerisation *in vitro* (Sitthidet et al., 2011). However, in-frame motif deletion mutants that lacked WH2 domains or a 13-amino acid repeat or PRM or PDASX domains did not impair BimA expression at the bacterial pole (Sitthidet et al., 2011). Expression of BimC was required for BimA-mediated *B. thailandensis* actin-tail formation as well as in *B. pseudomallei* and *B. mallei* (Lu et al., 2015a). In the same way, *B. mallei bimA, bimB, bimC, bimE* mutants could not form actin tails in infected cells (Schell et al., 2007). Similarly, a *B. mallei virG* mutant was unable to induce actin polymerisation (Schell et al., 2007). Overexpression of the *B. mallei* VirAG two-component regulatory system, encoded adjacent to the *bimA-E* genes on chromosome 2, up-regulated transcription of the *bimA*-containing gene cluster suggesting that *virAG* was essential for transcription of *bim* genes (Schell et al., 2007).

The unique mechanism of actin-based motility for *Burkholderia* species was revealed later and showed that *B. pseudomallei* BimA mimics host Ena/VASP proteins that can nucleate actin and promote actin filament elongation and bundling, generating a long and loosely bundled F-actin filament (Benanti et al., 2015) which agreed with our finding (Jitprasutwit et al., 2016). This actin filament organisation resulted in a long actin tail with straight paths of motility (Benanti et al., 2015). Similarly, BimA from *B. mallei* also mimics Ena/VASP showing the same actin tail morphology (Benanti et al., 2015). On the other hand, *B. thailandensis* BimA interacted and activated the Arp2/3 complex (Sitthidet et al., 2010, Stevens et al., 2005b), generated branched actin filaments displaying curved and dense actin tails with a shorter length compared to *B. pseudomallei*- and *B. mallei*-actin tails (Benanti et al., 2015). This characteristic suggested that *B. thailandensis* BimA was an NPF (Benanti et al., 2015).

B. pseudomallei uses a unique strategy to induce actin tail formation independently of the Arp2/3 complex. Our laboratory has previously performed a proteomic analysis similar to the previous studies that found new actin-binding proteins in the comet tails of *L. monocytogenes* (David et al., 1998, Van Troys et al.,

2008). From the list of host cell proteins recruited to bacteria expressing BimA, the minimal requirements for actin polymerisation *in vitro* including actin, Arp2/3 complex, actin-depolymerising factors and capping proteins were detected (Jitprasutwit et al. 2016) in agreement with the previous study (Loisel et al., 1999). Localisation of the Arp2/3 complex in the *B. pseudomallei* actin tail was previously described (Breitbach et al., 2003). Similarly, vinculin and α-actinin that were detected in actin tail of *B. pseudomallei* and also found in those of *L. monocytogenes* and *S. flexneri* (Breitbach et al., 2003), but not in *R. rickettsia* (Van Kirk et al., 2000), were also isolated from our *in vitro* system (Jitprasutwit et al., 2016). Interestingly, the host proteins that were identified in our previous work did not include microtubule components, intermediate filaments and myosins, which were previously detected in the actin tails of *L. monocytogenes* (Van Troys et al., 2008). Additionally, VASP and profilin that were recruited into *Rickettsia* actin tails (Van Kirk et al., 2000) were not found in our experiment (Jitprasutwit et al., 2016). While the molecular mechanism of the Arp2/3-mediated actin-based motility by *L. monocytogenes* and *S. flexneri* are well known (Reviewed in Welch and Way, 2013), the mechanism of actin-based motility displayed by *B. pseudomallei* and *B. mallei* are poorly characterised. Discovery of host factors that are involved in this process would be important in the further understanding of how pathogens exploit the actin cytoskeleton during infection.

1.3 BimA plays roles in intracellular survival and virulence

Actin-based motility impacts intracellular life cycle of several bacterial pathogens, particularly in cell-to-cell spread (Reviewed in Lamason and Welch, 2017). The force generated from actin-based motility is sufficient for the bacterium to create a membrane protrusion into the adjacent cell (Monack and Theriot, 2001). Dissemination defects are observed by mutants that cannot form actin tails. A *S. flexneri icsA* transposon mutant lacking an F-actin tail did not spread between host cells (Bernardini et al., 1989). Similarly, a transposon insertion in the *actA* gene of *L. monocytogenes* could not form plaques on a fibroblast monolayer (Kocks et al., 1992). In the same way, the Sca2 *R. rickettsii* mutant that did not produce an actin tail formed a smaller plaque phenotype than the wild-type (Kleba et al., 2010).

In addition to cell-to-cell spread, bacterial pathogens induce actin-based motility to manipulate autophagy or avoid lysosomal killing (Reviewed in Mostowy and Shenoy, 2015). In *L. monocytogenes*, ActA recruits Arp2/3 complex to the bacterial surface in order to escape autophagic recognition (Yoshikawa et al., 2009). Alternatively, IcsA from *S. flexneri* recruits N-WASP and then activates Arp2/3 complex for actin polymerisation, but at the same time, IcsA also binds to an autophagy protein forming septin cage-like structures to prevent actin tail formation (Mostowy et al., 2010). For evasion of autophagy recognition by *S. flexneri*, the type 3 secretion system effector IcsB is expressed to prevent the recruitment of autophagy proteins to the bacterial surface (Ogawa et al., 2005) (Reviewed in Krokowski and Mostowy, 2016).

Moreover, actin-based motility influences the virulence of bacterial pathogens (Reviewed in Choe and Welch, 2016). For example, the *actA* deletion mutant of *L. monocytogenes* that was defective to induce actin tail formation in tissue culture cells showed a decrease in virulence in mice (Brundage et al., 1993). Similarly, the *R. rickettsia sca2* mutant displayed reduced virulence in a guinea pig model of infection (Kleba et al., 2010).

Studying BimA explores the importance of actin-based motility in intracellular life of *B. pseudomallei*. A *bimA* mutant showed a reduction of net intracellular replication in J774.2 macrophage-like cells (Lazar Adler et al., 2015). BimA mutants with a defect in actin tail formation could not induce plaque formation (Benanti et

al., 2015, French et al., 2011, Sitthidet et al., 2011). Similarly, *B. oklahomensis*, an avirulent related species, which was not able to display actin tail formation during infection despite the presence of a gene encoding a 'BimA-like' protein with 40% identity to the *B. pseudomallei* BimA, showed a low virulence in *Galleria mellonella* larvae. (Wand et al., 2011). BimA is also required for full virulence in a murine model of infection. A *bimA* mutant showed a 10-fold increase in median lethal dose, compared to the isogenic parent strain *B. pseudomallei* in BALB/c mice, demonstrating attenuated virulence (Lazar Adler et al., 2015). This finding agreed with the result in our laboratory, a *bimA* mutant had a defect in intracellular survival, plaque formation and virulence in mice (Figure 1.4; Stevens, unpublished data). Immunisation with either recombinant *B. mallei* BimA increased survival percentage of mice after challenging with *B. mallei* and *B. pseudomallei* (Whitlock et al., 2010). Virulence of *B. pseudomallei*, and the requirement of the *bimA* gene in virulence, in the *Galleria mellonella* model was also observed by Vander Broek and Stevens (Unpublished observations).

The impact of BimA was also studied in human cases of melioidosis and animal models of infection and showed that it is a potent B-cell antigen (Felgner et al., 2009) and is recognised by T-cells in recovering melioidosis patients (Suwannasaen et al., 2011). A survey in the endemic area showed the *bimA* gene was present in 99 *B. pseudomallei* isolates having a high degree of conservation, 12% showed a geographically restricted subset of *B. pseudomallei* isolates from the Australian Northern Territory harbouring a *B. mallei*-like *bimA* allele (Sitthidet et al., 2008). This *bimA* variant had a significant association with neurological melioidosis (Sarovich et al., 2014).

Collectively, these evidences point to a role of BimA in intracellular life and virulence of *B. pseudomallei*.

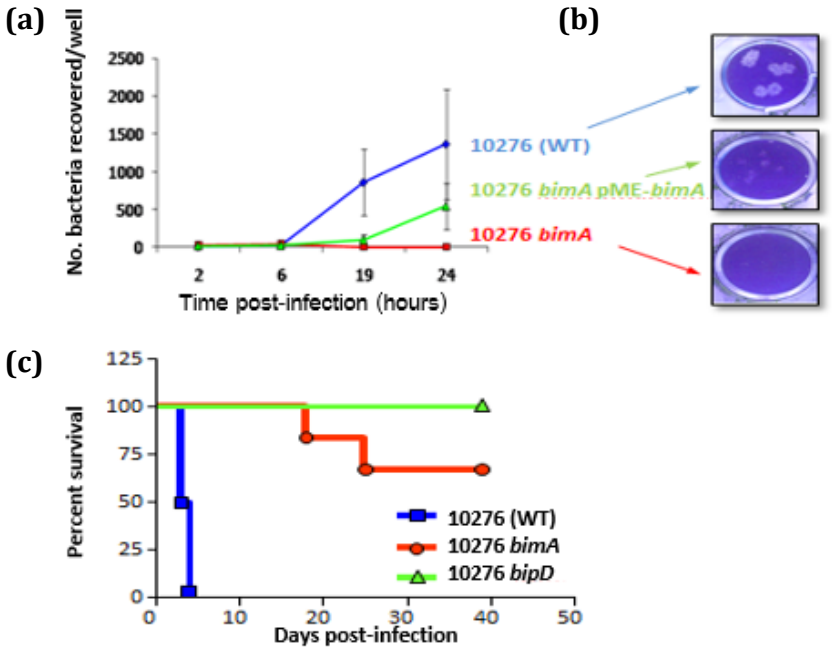

Figure 1.4: BimA is required for intracellular survival, cell-to-cell spread and virulence in mice (Unpublished data from Jo Stevens and Mark Stevens (UoE), and Greg Bancroft (LSTHM))

(a) Intracellular survival of *B. pseudomallei* 10276 WT (blue line), *bimA* mutant (red line) and *bimA* mutant *trans*-complemented with *bimA* (green line) in A549 cells.

(b) Plaque formation in A549 cell monolayers by *B. pseudomallei* 10276 WT, *bimA* mutant and *bimA* mutant *trans*-complemented with *bimA* (green line) at 24 hours post-infection.

(c) Percentage of survival of mice challenged with *B. pseudomallei* 10276 WT (blue line), *bimA* mutant (red line) and *bipD* mutant (a T3SS mutant used as an avirulent control) in an intranasal model of infection.

1.4 IQGAP1

IQ motif containing GTPase activating protein 1 (IQGAP1) is a member of the IQGAP family which is conserved in eukaryotes. This cytoplasmic scaffold protein contains an N-terminal calponin homology domain (CHD), a polyproline binding region (WW), an IQ domain (IQ), a Ras GTPase-activating protein-related domain (GRD) and Ras GAP C-terminus (RGCT). The 190-kDa *Homo sapiens* IQGAP1 is well-studied, performing an array of biological functions by binding and regulating several interacting proteins (Reviewed in Hedman et al., 2015). It is established as a regulator of the cytoskeleton playing roles in the organisation of the actin cytoskeleton (Reviewed in Watanabe et al., 2015). Several proteins associated with the cytoskeleton have been demonstrated to bind to IQGAP1. Figure 1.5 illustrates some partners that bind to a specific domain of IQGAP1. For instance, IQGAP1 binds F-actin directly and crosslinks the filaments (Bashour et al., 1997). The actin filaments are cross-linked by oligomerisation of IQGAP1 (Fukata et al., 1997). Regulation of IQGAP1 depends on free intracellular Ca^{2+} that promotes binding of calmodulin to IQGAP1, which in turn inhibits IQGAP1 binding actin of filaments (Mateer et al., 2002). IQGAP1 also plays a role in cell motility and invasion in a Cdc42- and Rac1-dependent manner (Mataraza et al., 2003). In addition, IQGAP1 enhances actin polymerisation *in vitro* and mediates actin assembly by forming complexes with N-WASP and Arp2/3 complex (Bensenor et al., 2007, Le Clainche et al., 2007). In migrating cells, IQGAP1 was identified as a binding partner of the Diaphanous-related formin (Dia1) which nucleates actin polymerisation to regulate cell motility and is required for the localisation of Dia1 for phagocytic cup formation (Brandt et al., 2007).

IQGAP1 is also a key regulator of cell adhesion and directional migration, which is controlled by these small Rho-family GTPases (Reviewed in Noritake et al., 2005). Cadherins comprise a major group of cell-cell adhesion molecules that mediate intercellular adhesion by engaging in Ca^{2+}-dependent manner (Takeichi, 1995). By forming *cis* homodimers, cadherins are clustered with their intracellular domains anchored to the actin cytoskeleton through α-catenin and β-catenin. Anchorage of cadherins to the actin cytoskeleton and their clustering are pivotal for the strong and rigid adhesion (Kuroda et al., 1998). The inhibition of IQGAP1 by RNAi

reduces the accumulation of actin filaments, E-cadherin and β-catenin at sites of cell-cell contact that leads to weak cell adhesion, indicating the important of IQGAP1 for cell-cell adhesion (Noritake et al. 2004).

IQGAP1 is also important in type I IFN production through the interaction with NLRC3, which is a nucleotide binding domain, leucine rich repeat CARD (caspase activation and recruitment domain) containing protein 3 (also known as CLR16.2 or NOD3), is a member of the NLR family of proteins. The nucleotide-binding domain and leucine-rich repeat containing (NLR) family is one of major familied of pattern recognition receptors (PRRs) that are an essential component of the host immune system (Tocker et al., 2017, Davis et al., 2017). NLRC3 is a negative regulator in response to bacterial and viral infection and expressed at high levels in various immune cell lines, but only at low levels in epithelial cell lines. NLRC3 regulates the type I IFN pathway by inhibiting subcellular redistribution and effective signalling of stimulator of IFN genes (STING), thus blunting the transcription of type I IFNs. A yeast two-hybrid screen using an amino terminal fragment of NLRC3 suggests that IQGAP1 associates with NLRC3 and can disrupt the NLRC3–STING interaction in the cytosol of human epithelial cells. A stable knockdown of IQGAP1 in THP1 human monocytic cell line and epithelial HeLa cell causes significantly more IFN-β production in response to cytosolic nucleic acids suggested a role of IQGAP1 in inhibition of production of type 1 IFN (Tocker et al., 2017). Localisation of NLRC3 and IQGAP1 to the cell cortex in human epithelial cells, possibly via interactions with RGCT domain on IQGAP1, was also shown in the previous study (Tocker et al., 2017). Also, in the absence of IQGAP1, human monocytic cells are hyperactive in response to cytosolic nucleotides (Davis et al., 2017).

In mammals, there are three IQGAP isoforms with a high level of amino acid sequence homology to IQGAP1, 62% and 59% for IQGAP2 and IQGAP3, respectively. They contain the same domain structure and each domain on IQGAP2 and IQGAP3 exhibits more than 70% similarity to IQGAP1 as shown in Figure 1.5. Since the domains found among the IQGAP family are highly conserved, they share some binding partners. Both IQGAP2 and IQGAP3 are involved in cytoskeleton interactions with F-actin (Schmidt et al., 2003, Wang et al., 2007).

In addition to binding partners, IQGAPs display specific expression patterns and different subcellular localisation in mammalian tissues. IQGAP1 is ubiquitously expressed in most cell types and distributed throughout the cytoplasm and cell membrane accumulating at cell-cell junctions and express. IQGAP2 is expressed predominantly in the liver (Wang et al., 2007) and IQGAP2 in rabbit gastric glands in primary culture localised in the nucleus and at sites of cell-cell contact (White et al., 2009). IQGAP3 is reported to be expressed mainly in lung, brain, testis, small intestine and colon (Wang et al., 2007). In rat adrenal gland phaeochromocytoma cells, IQGAP3 is diffusely distributed in the cytoplasm and it is also found at cell-cell junctions in mouse epithelial cells (White et al., 2009).

Intensive studies showed the importance of IQGAP1 in an array of biological functions. The finding of the role of IQGAP2 and IQGAP3 also have been accumulating and growing continuously. However, understanding the molecular mechanism of their functions is still poor. To gain insight into the involvement of IQGAPs in physiology and disease, further studies are required.

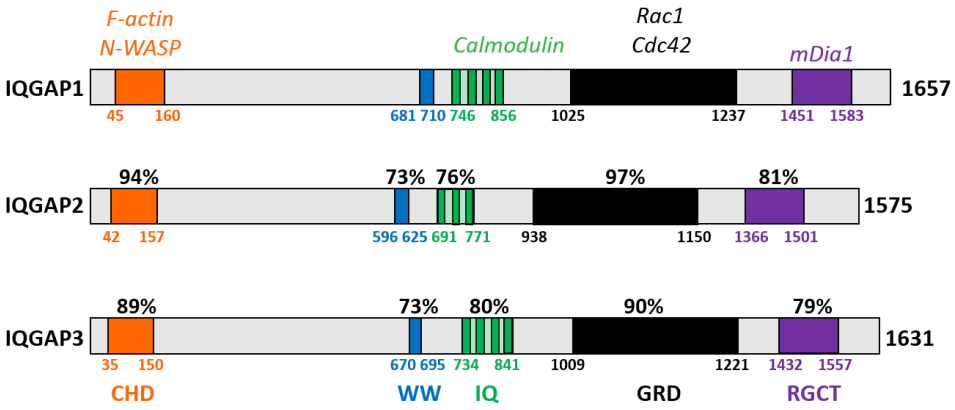

Figure 1.5: Domain structure of IQGAP isoforms and binding partners of IQGAP1 that associate with the actin cytoskeleton
Schematic presentation of domain organisation of IQGAP1 with 1657 amino acid, IQGAP2 with 1575 amino acid and IQGAP3 with 1631 amino acid length. The domain structures are indicated: CHD; calponin homology domain, WW; polyproline binding region, IQ; calmodulin-binding IQ motifs, GRD; Ras GTPase-activating protein-related domain, RGCT; Ras GAP C-terminus. The binding regions of IQGAP1 showing the regions of the interaction with its binding partners. Each domain of IQGAP2 and IQGAP3 was marked with the percentage of similarity with IQGAP1 analysed using pairwise sequence alignment (LALIGN). Italic shows the binding partners of IQGAP1.

1.4.1 IQGAP1 and bacterial pathogenesis

A number of pathogen-derived IQGAP1 interaction partners have been discovered, indicating that IQGAP1 may be a common target for pathogens to regulate the actin cytoskeleton during attachment or invasion of host cells (Reviewed in Kim et al., 2011b). IQGAP1 was identified as a component of *Salmonell*a invasion. It co-localised with the SopE and SopE2 effector proteins, and interacts with Rac, Cdc42 and actin to form phagocytic cups (Brown et al., 2007). Another *Salmonella* protein Ssel has been identified as an IQGAP1 binding partner that binds directly to IQGAP1 *in vitro* and co-localises with IQGAP1 during infection of macrophages (McLaughlin et al., 2009). Enteropathogenic *E. coli* (EPEC) also targets IQGAP1 through the bacterial Tir protein, an injected protein which manipulates the actin cytoskeleton by associating with calmodulin to induce actin pedestal formation (Brown et al., 2008). Moreover, Ibe is a novel bacterial effector of *E. coli* that interacts with IQGAP1 to induce pedestals and actin-rich membrane ruffles (Buss et al., 2009). IQGAP1 is also required for innate immune defence against pathogens. It interacts with $YopM^{KIM}$, an outer protein of *Yersinia pestis* KIM, and regulates inflammasome function in macrophages (Chung et al., 2014). Recently, OspB, a *Shigella* effector protein was identified as a binding protein of IQGAP1. During early *Shigella* infection, OspB triggers cell proliferation by activation of mTORC1. IQGAP1 interacts with both OspB and mTORC1 leading to restriction of the area of spread of *S. flexneri* (Lu et al., 2015b).

The interaction of IQGAP1 and selected bacterial proteins is not only utilised by the pathogens to support the infection but also exploited for manipulating other binding partners of IQGAP1. For example, in *S. enterica* serovar Typhimurium that usurps Rac1 and MAPK signalling to facilitate its internalisation, IQGAP1 is used as a scaffold to integrate these two different pathways to achieve invasion into mouse embryonic fibroblasts (Kim et al., 2011a). When IQGAP1 lacking Rac1 or MEK and ERK binding site, the percentage of *Salmonella* invasion reduced by 45%. Whilst IQGAP1-null MEFs reconstituted with the IQGAP1 without a Rac1 binding site into the cells pre-treated with MEK1 inhibitor, the invasion efficiency decreased by 75% (Kim et al., 2011a). However, Rac1 was not required for non-invasive EPEC to promote actin pedestal and bacterial adherence (Brown et al., 2008) Similarly,

invasion of *E.coli* K1 into human brain microvascular endothelial cells (HBMEC), requires IQGAP1 interaction with β-catenin, but not Rac1, to support its dissociation from the adherence junction causing actin rearrangement showing co-localisation of IQGAP1 with polymerised actin beneath the bacterial binding site (Krishnan et al., 2012). IQGAP1 also plays a role in promoting vascular smooth muscle cell adhesion and migration after *Chlamydia pneumoniae* infection-induced atherosclerosis (Zhang et al., 2012).

Moreover, IQGAP1 was identified as an essential component in the communication between bacteria and human epithelial cells causing changes in the cytoskeleton network. A quorum-sensing molecule N–acylhomoserine lactone produced by *Pseudomonas aeruginosa* interacts and co-localises with IQGAP1 which functions as an integrator of Rac1 and Cdc42 to trigger cytoskeleton organisation (Karlsson et al., 2012). Also, IQGAP1 is required with Cdc42 to inhibit cell migration of the opportunistic pathogenic bacterium *Legionella pneumophil*a infected cells (Simon et al., 2015). When A549 cells were treated with LAI-1 (3-hydroxypentadecane-4-one), a quorum sensing compound employed by this bacterium, Cdc42 was inactivated and IQGAP1 re-localised from the cytoplasm to accumulate at the cell cortex (Simon et al., 2015).

The current literature shows the role of IQGAP1 binding partners seems to be specific for different pathogens. However, there is no publication that demonstrates the role of IQGAP1 in bacterial actin-based motility. For this reason, the role of IQGAP1 as a novel protein involved in this process was investigated in this study.

1.5 Aims and Objectives

Aims

To explore the mode of action and functional significance of IQGAP1 in the intracellular life of *Burkholderia pseudomallei*.

Objectives

1) To determine the localisation of IQGAP1 in *B. pseudomallei*-infected cells and study the role of IQGAP1 in actin-based motility of *B. pseudomallei* in siRNA-mediated IQGAP1 knockdown cells.
2) To generate IQGAP1 knockout cells by CRISPR-Cas9 genetic engineering to examine the importance of IQGAP1 in the intracellular life of *B. pseudomallei*.
3) To determine whether IQGAP1 and BimA interact directly using an *in vitro* pull-down assay and *in vivo* yeast two-hybrid system and test the effect of IQGAP1 on the kinetics of actin assembly mediated by BimA.

Chapter 2
Materials and Methods

2.1 Maintenance of cell line, bacteria, and yeast

2.1.1 Cell maintenance

HeLa cells were maintained in a modified Dulbecco's Modified Eagles Medium containing high glucose, L-glutamine and sodium pyruvates (Gibco) and supplemented with 10% v/v heat-inactivated foetal calf serum (10% DMEM). Additionally, penicillin and streptomycin (P/S) were added at a concentration of 100 units/ml and 100 µg/ml respectively. To passage, cells were washed with Dulbecco's phosphate-buffered saline (D-PBS; Gibco) and detached with 1X Trypsin-EDTA (0.025% trypsin and 0.01% EDTA) (Gibco).

To store cells, the number of cells and viability were determined using 0.4% w/v Trypan Blue (Lonza). A final concentration of viable cells of 1 x 10^6 cells/ml in Recovery™ Cell Culture Freezing Medium (Gibco) was aliquoted into cryovials and kept in an ultra-low temperature freezer (~-140 °C).

2.1.2 Preparation of bacterial glycerol stock

Bacteria were cultured at 37°C on LB agar or LB broth (10 g/L Tryptone, 10 g/L NaCl and 5 g/L g yeast extract with or without 15 g/L bacto-agar, pH 7.4). An overnight culture from a single colony of bacteria in LB broth containing appropriate antibiotics was harvested by centrifugation. The cell pellet was re-suspended in LB broth and then mixed with 50% v/v glycerol in LB broth in a ratio of 1:1. The bacterial glycerol stock tubes were frozen at -80 °C.

2.1.3 Preparation of yeast glycerol stock

For long-term storage of *Saccharomyces cerevisiae*, a fresh colony of *S. cerevisiae* was scraped from either a yeast extract peptone dextrose (YPD) agar (10 g/L yeast extract, 20 g/L peptone, 2% w/v glucose, 20 g/L agar, pH 6.5) or synthetic defined (SD) plate (6.7 g/L yeast nitrogen base without amino acids, 20 g/L agar (Invitrogen), 2% w/v glucose, with amino acid supplements (Clontech), pH 5.8). The amino acids were added at the concentrations of 20 mg/L L-adenine hemisulfate salt, 20 mg/L L-arginine HCl, 20 mg/L L-histidine HCl monohydrate, 30 mg/L L-isoleucine, L-leucine 100mg/L, 30 mg/L L-lysine HCl, 20 mg/L L-methionine, 50

mg/L L-phenylalanine, 200 mg/L L-threonine, 20 mg/L L-tryptophan, 30 mg/L L-tyrosine, 20 mg/L L-uracil, 150 mg/L L-valine. Tryptophan, adenine and histidine were excluded from SD media where appropriate. The yeast colony was suspended in 200 µl of sterile water using a vortex. Next, the cell suspension was mixed with 200 µl of sterile 50% v/v glycerol in Phosphate-buffered saline (PBS). For *Pichia* cells, a single colony was cultured in 5 ml of YPD overnight. Then the cells were harvested and re-suspended in 1 ml of YPD containing 15% v/v glycerol. The stocks were stored at –80 °C.

2.2 SDS-Polyacrylamide gel electrophoresis (SDS-PAGE)

Proteins were separated by sodium dodecyl sulphate polyacrylamide gel electrophoresis (SDS-PAGE). Protein samples were mixed in 2X SDS-PAGE loading buffer (100 mM Tris-HCl pH 6.8, 4% w/v SDS, 0.2% w/v bromophenol blue and 20% v/v glycerol and supplemented with 2% v/v β-mercaptoethanol). For analysis under non-reducing conditions, the β-mercaptoethanol was omitted. After that, samples were heated at 99 °C for 5 minutes, loaded onto suitable SDS-polyacrylamide gels, submerged in running buffer (25 mM Tris base, 192 mM glycine, and 0.1% w/v SDS) or Tris Glycine SDS PAGE Buffer (National Diagnostics) and subjected to electrophoresis to the proteins. The following solutions were used for preparing gels:

Table 2.1: Volumes of components for preparing acrylamide resolving gel

Solution Components	% v/v acrylamide resolving gel		
	6%	8%	10%
ProtoGel 30% w/v (National Diagnostics)	2 ml	2.67 ml	3.33 ml
1.5 M Tris-HCl, pH 8.8	2.5 ml	2.5 ml	2.5 ml
10% w/v SDS	0.1 ml	0.1 ml	0.1 ml
Deionised water	5.29 ml	4.62 ml	3.96 ml
10% w/v ammonium persulphate	0.1 ml	1.0 ml	1.0 ml
TEMED	0.01 ml	0.01 ml	0.01 ml

Table 2.2: Volumes of components for preparing acrylamide stacking gel

Solution Components	5% v/v acrylamide stacking gel (10 ml)
ProtoGel 30% w/v (National Diagnostics)	2.4 ml
1.5 M Tris-HCl, pH 6.8	1.26 ml
10% w/v SDS	0.1 ml
Deionised water	6.3 ml
10% w/v ammonium persulphate	0.025 ml
TEMED	0.05 ml

A protein dual colour standard (Bio-Rad) or a three-color protein standard (Abcam) that was used as a molecular weight marker was also included.

2.2.1 Preparation of HeLa cell lysate for SDS-PAGE

HeLa cells were grown to confluency in a 24-well plate. Cells were washed with PBS before lysing with 100 µl of BugBuster® Master Mix (Novagen). Protein concentration was determined using a Direct detect spectrophotometer (EMD Millipore). The same amount of total protein was then suspended in 2X SDS-PAGE loading buffer containing 2% v/v β-mercaptoethanol. Occasionally, cells were harvested using 1X Trypsin-EDTA.

2.2.2 Preparation of *E. coli* cell lysates for SDS-PAGE

Total protein from *E. coli* cells were prepared using BugBuster Master Mix reagent. For small scale extractions, cells were harvested by centrifugation at 1,811 x g for 10 minutes. The pellet was re-suspended with 200 µl of BugBuster Master Mix per 1 ml of culture and then incubated at room temperature on a rocker for 10 minutes. Total cell lysate was subjected to SDS-PAGE as described above.

2.2.3 Preparation of yeast cell lysates for SDS-PAGE

For a rapid method to examine protein expression in *P. pastoris* or *S. cerevisiae*, cell lysates were prepared following a protocol described previously (Matsuo et al., 2006). Briefly, the optical density (OD) of an overnight culture was adjusted to 0.5 at OD600 and 1 ml pelleted by centrifugation at 16,060 x g for 1 minute. The cell pellet was washed with 1 ml of water and centrifuged. The washed pellet was re-suspended with 150 µl of water. Then 150 µl of 0.6 M NaOH was added to the cell suspension and incubated for 10 minutes at room temperature. The treated cells were harvested by centrifugation and the pellet was re-suspended with 30 µl of yeast sample buffer (60 mM Tris-HCl pH 6.8, 4% v/v β-mercaptoethanol, 4% w/v SDS, 0.01% w/v bromophenol blue, and 5% v/v glycerol), heated at 99 °C for 5 minutes and subjected to SDS-PAGE.

2.3 Coomassie blue staining

After proteins were separated by SDS-PAGE, protein bands were visualised by Coomassie blue staining. Gels were rinsed in water and then submerged in Coomassie staining solution (0.25 g/L Coomassie Blue G–250, 45% v/v methanol,

10% v/v acetic acid) for 1 hour at room temperature. After that, gels were washed twice in de-staining solution (45% v/v methanol, 10% v/v acetic acid) for 15 minutes each. Next, gels were further de-stained in water overnight. Occasionally, gels were stained with Bio-Safe Coomassie Brilliant Blue G-250 stain (Bio-rad) or InstantBlue Protein Stain (Expedeon) following manufacturer's instruction.

2.4 Silver staining

To detect proteins in low amounts after SDS-PAGE, silver staining was performed using a Pierce™ Silver Stain Kit (Thermo Fisher Scientific) and following manufacturer's instruction. Briefly, the gel was washed in ultrapure water and fixed in fixing solution (30% v/v ethanol, 10% v/v acetic acid). Next, the gel was washed in ethanol wash (10% v/v ethanol) and then in ultrapure water. After that, the gel was incubated in sensitiser working solution and then in stain working solution. The gel was rinsed with ultrapure water. Then developer working solution was added immediately and incubated until protein bands appeared. Finally, the gel was incubated with stop solution (5% v/v acetic acid) for 10 minutes.

2.5 Western blotting

After SDS-PAGE, proteins were transferred to a nitrocellulose membrane using Trans-Blot Turbo Transfer System (Bio-Rad) with a condition of 25 V and 1.0 A for 60 minutes in transfer buffer containing 1X transfer buffer (BioRad) and 20% v/v methanol followed by standard western blotting techniques. In brief, the membrane was washed with PBS (137 mM NaCl, 2.7 mM KCl, 4.3 mM Na_2HPO_4, 1.47 mM KH_2PO, pH 7.4) or Tris-buffered saline (TBS) containing 150 mM NaCl,20 mM Tris-HCl, pH 7.5, and then incubated with blocking buffer (5% w/v non-fat milk in PBS or TBS) for 30 minutes at room temperature. To detect specific proteins, primary antibodies were diluted in PBS or TBS supplemented with 0.1% v/v Tween-20 (PBST or TBST). The membrane was probed with primary antibodies at 4 °C overnight using a concentration described in table 7.4. After that, species specific secondary antibodies were added at an appropriate dilution and incubated for 45 minutes at room temperature. The membrane was washed with PBST or TBST and then washed with PBS or TBS before scanning on an Odyssey infrared imager (LI-COR Biosciences).

2.5.1 Quantitative Fluorescent Western Blotting

After blots were imaged using an infrared imager, fluorescent signals were quantified using ImageStudio software (LI-COR Biosciences). In each lane, the signal of each protein band of interest, for example IQGAP1, was divided by the signal of the internal loading protein control (either actin or GAPDH). The ratio of IQGAP1/actin or IQGAP1/GAPDH was compared to the ratio obtained from control cells, which was taken as 100%.

2.6 IQGAP1 siRNA knockdown

2.6.1 Cell preparation

One day before transfection, HeLa cells were detached by trypsinisation and then cells were harvested by centrifugation at 500 × g for 5 minutes. The media was removed and cell pellet was re-suspended in 10%DMEM (antibiotic-free). The number of cells was counted and then diluted to a concentration 6 x 10^4 cells/ml. Next, HeLa cells were plated in a 24-well plate using 500 µl of cell suspension to obtain 3 x 10^4 cells per well.

2.6.2 IQGAP1 siRNA transfection

HeLa cells were transfected using the optimised condition following method to achieve the lowest level of IQGAP1 expression. First, RNAi duplex (siRNA IQGAP1, ID S16837; Silencer Select, Ambion) and Lipofectamine RNAiMAX (Invitrogen) were diluted with Opti-MEM™ I reduced serum medium (Gibco) in a separate micro-centrifuge tube. To prepare RNAi duplex, 0.3 µl of 20 µM siRNA working stock was mixed with 99.7 µl of Opti-MEM. For Lipofectamine, 2 µl of RNAiMAX was diluted with 98 µl of Opti-MEM. Then the reagents were combined and incubated for 15 minutes at room temperature. HeLa cells were transfected with 200 µl containing 6 pmol of siRNA to obtain a final concentration of RNAi duplex at 30 nM. Transfected cells were incubated in a CO_2 incubator at 37 °C for 48 hours before infection.

2.7 Double nickase plasmid transfection

2.7.1 Cell preparation

One day before transfection, the number of HeLa cells were counted and diluted in 10%DMEM (antibiotic-free) to a concentration of 1.6 x 10^5 cells/ml. Then

3 ml of cell suspension were seeded in a 6-well plate to obtain 4.8 x 10^5 cells per well. HeLa cells were approximately 80% confluent at transfection.

2.7.2 Cell transfection with double nickase plasmid

IQGAP1 double nickase plasmid (sc-400597-NIC; Santa Cruz Biotechnology) was utilised to knockout IQGAP1 in HeLa cells. The mixture containing 3.5 μg of plasmid diluted in 175 μl of Opti-MEM and 12 μl of Lipofectamine 2000 (Invitrogen) diluted in 175 μl of Opti-MEM was prepared. The plasmid-Lipofectamine complex was incubated at room temperature for 5 minutes. Next, HeLa cells were transfected with 2.5 μg of plasmid by adding 250 μl of the complex into each well. The transfected cells were incubated in a CO_2 incubator at 37 °C for 24 hours. To determine transfection efficiency, transfected cells on a cover slip were washed with PBS and fixed with 4% w/v PFA in PBS for 1 hour at room temperature before staining nuclei with DAPI. GFP-expressing cells were observed under a Leica DMBL fluorescent microscope (Leica Biosystems).

2.7.3 Selection of transfected cells

At 24 hours post transfection the media was removed and replaced with 10%DMEM containing P/S and supplemented with 3 μg/ml of puromycin dihydrochloride (Sigma-Aldrich). Cells were incubated at 37 °C for 48 hours with the antibiotic selection. After that, the media was removed and replaced with the fresh medium supplemented with 3 μg/ml of puromycin and incubated further for 24 hours. After puromycin selection, the medium was removed and replaced with 10%DMEM containing P/S without puromycin and incubated for 4 days to allow expansion of the cells.

2.7.4 Isolation of clonal cell lines by dilution

The viable cells after transfection and selection were dissociated with 1X Trypsin-EDTA. The number of cells was counted and calculated to obtain the cell concentration as 1 cell/100 μl by making a serial dilution in 10%DMEM containing P/S. Then, 200 μl of cell suspension was plated into each well of five 96-well plates. On the 8^{th} day after isolation, cells were inspected for a clonal appearance with cells radiating from a central point. Wells with multiple colonies or without any live cells were labelled with an X and not monitored thereafter. In the remaining wells, the

media was replaced every 2-3 days until cells were more than 60% confluent. The cells were dissociated with 1X Trypsin-EDTA and replica-plated. Cells were passaged until the number of cells was enough for storage and validation by immunoblotting using anti-IQGAP1.

2.7.5 Detection of mutations by PCR

Genomic DNA (gDNA) was extracted from control and selected clonal cell lines followed a protocol by Strauss (2001). In brief, HeLa cells were harvested by centrifugation at 500 × g for 5 minutes. The supernatant was discarded. Cells were washed with ice-cold PBS twice. Then the cell pellet was re-suspended in 0.5 ml of digestion buffer (100 mM NaCl, 10 mM Tris-HCl pH 8, 25 mM EDTA pH 8, 0.5% w/v SDS and 0.1 mg/ml proteinase K (Sigma-Aldrich) and incubated with shaking at 50 °C. Next, the samples were extracted with an equal volume of phenol/chloroform/isoamyl alcohol (Sigma-Aldrich) and centrifuged at 1,700 × g for 10 minutes. The top (aqueous) layer was transferred to a new tube and a ½ volume of 7.5 M ammonium acetate and 2 volumes of absolute ethanol were added. DNA was recovered by centrifugation at 1,700 × g for 2 minutes and the pellet was washed with 70% v/v ethanol before air-drying. The DNA pellet was re-suspended in TE buffer (100 mM Tris-HCl pH 8.0, 10 mM EDTA pH 8.0).

To detect mutation within exon 13 of human IQGAP1, 200 ng of gDNA was used as template for amplification of a flanking region of exon 13 by Q5® High-Fidelity DNA Polymerase (New England Biolab) using the oligonucleotides described in Table7.3. Conditions of PCR were as follows: 98 °C for 1 minute and 35 cycles of 95 °C for 10 seconds, 67 °C for 20 seconds and 72 °C for 30 seconds, with a final extension step at 72 °C for 2 minutes. The PCR products were visualised by agarose gel electrophoresis before DNA purification and DNA sequencing (Source BioScience) using the same primers used for amplification. The nucleotide sequence of the control or wild-type (WT) HeLa cell line was analysed using *Homo sapiens* (human) Nucleotide BLAST (https://blast.ncbi.nlm.nih.gov/Blast.cgi) for verification. To detect mutations in the clonal cell lines, the DNA sequences of selected clones was aligned with WT using Clustal Omega (http://www.ebi.ac.uk/Tools/msa/clustalo/). The amino acid sequences of the mutated IQGAP1 sequences were then predicted using the 'Translate' web tool (http://web.expasy.org/translate/).

2.7.6 Immunoprecipitation

Approximately 10^8 HeLa cells were dissociated from a tissue culture flask using 1X Trypsin-EDTA. Cells were centrifuged at 500 × g for 5 minutes and washed with PBS twice. The pellet was lysed with 1 ml of lysis buffer (50 mM Tris-HCl pH 7.5, 150 mM NaCl, 1% v/v Triton X-100, 1 mM PMSF, 50 mM NaF, 1 mM Na_2VO_3, 1 mM EGTA) and the suspension was incubated on a tube rotator at 4 °C for 2 hours. Cell lysates were centrifuged at 14,000 × g for 15 minutes. The supernatant was pre-cleared by adding 100 µl of 50% v/v Protein A agarose bead slurry (Sigma-Aldrich) and incubated at 4 °C for 2 hours. Protein A agarose beads were removed by centrifugation. Total protein concentration in supernatant was determined using a direct detect spectrophotometer. 1.2 mg total protein was mixed with 4 µg of anti-IQGAP1 and incubated at 4 °C overnight. Next, the immune-complex was captured by adding 100 µl Protein A agarose bead slurry and gently rocking for 4 hours at 4 °C. The agarose beads were collected by pulse centrifugation and washed extensively with ice-cold lysis buffer. After removing the supernatant, the agarose beads were re-suspended in 30 µl of 2X SDS-PAGE loading buffer omitting β-mercaptoethanol to avoid breaking di-sulphide bond of the antibodies and heated at 70 °C for 10 minutes. The supernatant was subjected to SDS-PAGE in non-reducing condition followed by Coomassie blue staining and Western blot analysis.

2.8 *In vitro* cell infection

2.8.1 HeLa cells infection with *B. pseudomallei*

HeLa cells were infected with *B. pseudomallei* as described previously (Sitthidet et al., 2011). Briefly, a single colony of *B. pseudomallei* 10276 was inoculated into LB broth and incubated at 37 °C overnight with shaking. The bacterial culture was harvested by centrifugation at 1,811 x g for 10 minutes, washed with PBS twice and diluted in 10%DMEM. HeLa cells in a 24-well plate were washed with pre-warmed PBS before infected with *B. pseudomallei* at multiplicity of infection (MOI) of approximately 100. The bacteria were brought into contact with the cells by centrifugation at 300 × g for 5 minutes and then incubated at 37 °C for 30 minutes. Then, the medium was removed and replaced with fresh media containing 250 µg/ml of kanamycin to kill the remaining extracellular bacteria. At the specific time points,

the infected HeLa cells were washed twice with PBS before either fixation, preparation of cell lysates or enumeration of intracellular bacteria.

2.8.2 Infection of HeLa cells with *Salmonella*

HeLa cells were infected with *Salmonella enterica* serovar Typhimurium 4/74, a nalidixic acid-resistant (Nal^R) strain described by Brown et al., (2007). An overnight bacterial culture was harvested by centrifugation. HeLa cells (2×10^5 cells) were infected with the bacterium at MOI of approximately 20 and centrifuged at 500 × g for 5 minutes. The infected cells were incubated at 37 °C for 40 minutes. The media containing extracellular bacteria was removed and replaced with 10%DMEM containing 50 μg/ml gentamycin and incubated until the specified time point.

2.8.3 Invasion and intracellular survival assay

For invasion assay, the internalised bacteria were observed at 2 hours post-infection. Infected cells were washed with PBS twice before lysis with 500 μl of 0.1% v/v Triton X-100 in PBS. The suspension was transferred into a new micro-centrifuge tube containing 500 μl of PBS. Then, 100 μl of bacterial suspension was plated onto 3 separate LB plates. Plates were incubated at 37 °C and the number of bacteria was counted when the colonies appeared.

To determine intracellular survival over a time course of up to 48 hours post-infection, the intracellular bacteria were harvested at specific time points as described above. The bacterial suspension was serially diluted in PBS and plated on LB agar plates and incubated at 37 °C for 24-48 hours until the colonies appeared.

2.8.4 Plaque assay

At 24, 48 and 72 hours post-infection, the media in the wells of the infected cells was removed. Cells were washed gently with PBS. The wells were filled with crystal violet stain (1% w/v crystal violet, 20% v/v methanol) and incubated at room temperature for 1 hour before aspirating the staining solution. The fixed monolayers were washed with distilled water until plaques could be observed. The plates were air-dried and plaques counted upon visual inspection.

2.9 Immunofluorescence staining and confocal microscopy

At the specified time points, cells were washed twice with PBS before fixing with 4% w/v paraformaldehyde in PBS. Cells infected with *B. pseudomallei* were

fixed at 4 °C for at least 24 hours. Otherwise, uninfected cells were fixed at room temperature for 1 hour. After that, cells were washed with PBS and then permeabilised with 0.5% v/v Triton X-100 for 15 minutes. Then, primary antibodies were diluted in BSA/PBS (0.5% w/v bovine serum albumin (BSA) in PBS with 0.02% w/v sodium azide and filtered through a 0.2 μm filter) at a concentration described in table 7.4. Coverslips were covered with the primary antibodies and incubated at 4 °C overnight. After washing, secondary antibodies were added to the coverslips and incubated at 37 °C for 1 hour. Cells were washed, and then filamentous actin was stained using Alexa Fluor488 or Alexa Fluor568 phalloidin (Molecular Probes). Occasionally, 0.66 μg/ml of DAPI (Sigma-Aldrich) was used for nuclei staining. Coverslips were washed with PBS followed by water and then mounted with Prolong Gold (Molecular Probes) prior to microscopy. The samples were imaged using an LSM710 laser confocal microscope and images captured using Zen software (Zeiss).

2.9.1 Image analysis

The images captured by confocal scanning microscopy and Zen 2011 software (Zeiss) were analysed for actin density and actin tail length using ImageJ software (http://imagej/nih.gov/ij/). For each sample set, each tail was randomly selected by choosing a tail that did not overlap with another. Actin density was calculated from the corrected total cell fluorescence (CTCF) using the formula: CTCF = Integrated Density – (Area of selected cell x Mean fluorescence of background readings). To measure the length of a straight actin tail, Feret's Diameter parameter was used to obtain the value of the longest distance between any two points along the selection boundary (caliper length), as shown in figure 2.1a. For curved tails, the length of the tail was measured by drawing a segmented line along the tail with spline fit option (Figure 2.1b). The line was measured as the length of actin tail.

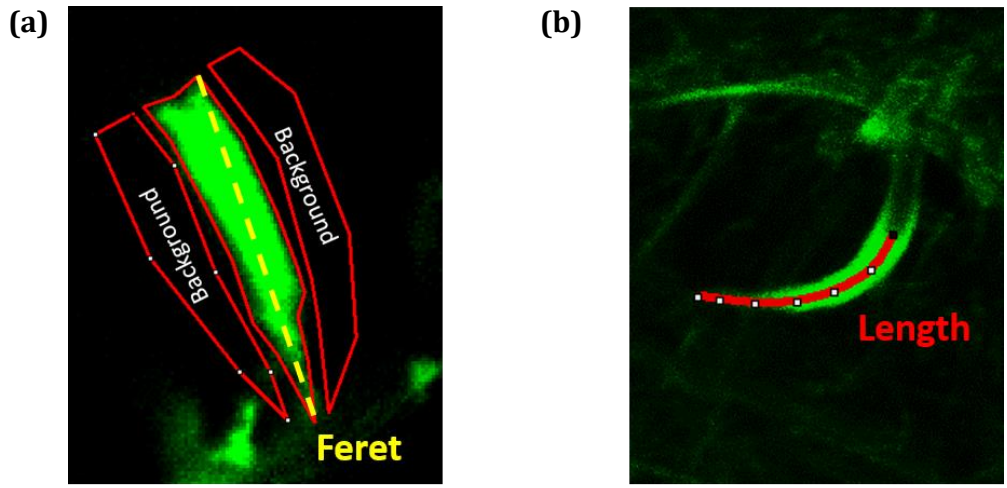

Figure 2.1: Actin tail analysis using ImageJ
Fluorescent images on green channel showing actin tail formation by *B. pseudomallei* were analysed for actin density and actin tail length using ImageJ software.

(a) Actin density was measured by corrected total cell fluorescence (CTCF) using the value of integrated density at the area of actin tail and subtracted from the average fluorescent signal of two regions next to the tail (background). For actin tail length, a straight tail can be measured using Feret's measurements that is the longest distance between any two points along the selection boundary (yellow dash line).

(b) For a curve tail, a segmented line (red) was drawn along the tail and then measured the length.

2.10 Cell cytotoxicity assay

At a specific time after transfection or infection, samples of the media overlaying the cells were collected to assess LDH release using CytoTox 96 Non-Radioactive cytotoxicity assay kit (Promega), following manufacturer's instruction. Briefly, 25 µl media was transferred to a 96-well assay plate. Next, 25 µl of reconstituted substrate mix was added into each well. The plate was covered to protect it from light and incubated for 30 minutes before adding 25 µl of the stop solution and reading absorbance at 490 nm using a FLUOstar OPTIMA (BMG Labtechnologies). Untreated medium was used as a blank control. Percentage of cytotoxicity was calculated by comparing values with maximum LDH release from non-transfected HeLa cells lysed with 0.1% v/v of Triton X-100, which was set as 100%.

2.11 DNA manipulation

2.11.1 Agarose gel electrophoresis

UltraPure™ agarose (Invitrogen) was used at 0.8% w/v or 1% w/v in TAE buffer (40 mM Tris, 20 mM acetic acid, 1 mM EDTA) supplemented with 1X SYBR™ Safe DNA Gel Stain (Invitrogen) for resolution of DNA fragment larger than 1 kb, or 2% for smaller fragments. DNA samples were mixed with 1/6th volume of 6X agarose loading dye buffer (0.25% w/v Bromophenol blue, 40% w/v sucrose). For small fragments (less than 1 kb), DNA samples were diluted with 5X Orange G loading dye (0.2% w/v Orange G Dye, 1.5% v/v glycerol in 0.6 M EDTA pH 8.0). Electrophoresis was performed at a constant voltage (150 V) for 30 minutes to 1 hour. DNA was visualised by exposure to ultraviolet light on a transilluminator using the G:BOX image capture system (Syngene) or FluorChem™ HD2 system (ProteinSimple).

2.12 Polymerase chain reaction (PCR) procedures

2.12.1 Polymerase chain reaction

Polymerase chain reactions (PCR) were performed in 25 µl volume, containing variable amounts of DNA template, 0.5 µM oligonucleotide primers, each deoxynucleotide (dNTPs) at 200 µM and 0.5 units of polymerase. The buffer provided with the enzyme was added to a final concentration of 1X. Occasionally, 3% v/v DMSO was included for amplification of *bimA* because of its GC-rich sequence.

Conditions for amplification were set as described in each of the relevant method section.

2.12.2 Colony PCR

To screen *E. coli* colonies for the presence of plasmids, a single colony was patched on a fresh LB agar plate supplemented with appropriate antibiotics using a sterilised pipette tip. After patching, the remaining cells on the tip was suspended directly into a PCR mixture containing all relevant reaction components. The thermo-cycling conditions were specific for amplification of each individual gene.

For screening of *Pichia pastoris* harbouring a plasmid, a sterile tip was use to pick up individual colonies and re-suspended in 20 µl of 20 mM NaOH. The cell suspension was boiled at 99 °C for 10 minutes. The sample was briefly centrifuged to pellet the cell debris and the supernatant (1 µl) was subjected to PCR amplification.

2.13 Plasmid construction

In this study, PCR amplification was performed using high-fidelity DNA polymerases. To amplify full-length, N-terminal and C-terminal of IQGAP1 and β-actin, HeLa cell cDNA (BioChain) was used as a template by Advantage 2 PCR Kit (Clontech). The fragments were cloned into pGEM-T Easy vector (Promega) using T4 DNA ligase (Promega) following the manufacturer's instructions. The ligation mixture was then transformed into *E. coli* XL-1 Blue by heat shock method. Transformants were selected by plating on LB agar plates containing ampicillin at 100 µg/ml and incubating at 37 °C overnight. Then the insertion was screened by colony PCR. Clones showing the expected sized of PCR product were cultured for plasmid extraction using a MiniPrep Kit (Qiagen). Restriction enzyme digestion was performed to confirm the presence of the desired insert before sequencing. After that the insertions were sub-cloned into pMAL-p2X vector (New England Biolabs) for expression in *E. coli.* In addition, full-length IQGAP1 was sub-cloned into pPICZ for expression in *P. pastoris* and into pGADT7 for yeast two-hybrid assay. Also, β-actin was sub-cloned into pGADT7 for expression in yeast. The fragments were purified by gel extraction kit (Qiagen) and then ligated into the plasmids with T4 DNA ligase (Promega). The ligation reaction mixture was cleaned up before taking the supernatant to transform into *E. coli* XL-1 blue by heat shock method. Clones containing the engineered plasmid were selected on LB agar plates containing

appropriate antibiotics. The inserts were confirmed by restriction enzyme digestion and DNA sequencing.

To express *B. pseudomallei* 10276 BimA (from amino acid residues 54 to 470), pME6032-BimA (Stevens et al., 2005) was used as a template for PCR amplification using two-step cycling. The resulting DNA fragment was cloned into pET-21b(+) via *Bam*HI (Promega) and *Sac*I (Promega) sites incorporated in the primers and then transformed into *E. coli* XL-1 blue competent cells using heat shock method. Transformants that grew on LB agar supplemented with 100 μg/ml ampicillin were screened for the *bimA* gene by colony PCR. A selected clone was cultured for plasmid extraction and then subjected to DNA sequencing. The sequencing result verified that the *bimA* gene fragment encoding amino acids 54-470 was inserted into the vector in the correct reading frame and in the correct orientation. To construct pMAL-p2X expressing $BimA_{54-470}$, $BimA_{54-470}$ was sub-cloned from pET-21b(+)$BimA_{54-470}$ into pMAL-p2X via *Bam*HI (Promega) and *Hind*III (Promega) sites. As above, the ligation reaction was transformed into *E. coli* XL-1 blue competent cells. Then, the plasmid was extracted for DNA sequencing to confirm the presence of the *bimA* gene in-frame with the gene encoding maltose-binding protein in pMAL-p2X.

2.14 Site directed mutagenesis

The sequencing result of the full-length IQGAP1 gene cloned into pGEM-T Easy vector showed 3 substitutions (A602C, T2130C and A3731G) when aligned against the human IQGAP1 sequence (NCBI Reference Sequence: NP_003861.1). These mutations that encode 2 different amino acids, K201T (lysine is changed to threonine) and D1244G (aspartic Acid is changed to glycine). In order to correct these mutations, QuikChange lightning site-directed mutagenesis kit (Agilent Technologies) was utilised, following the manufacture's instruction. This technique is based on PCR allows mutagenesis at a single site using two synthetic oligonucleotide primers that contain the desired mutation. IQGAP1 mutagenesis was performed in two rounds where A602C was mutagenized first and then A3731G. Briefly, pGEM-T-FL3D-IQGAP1, was used as a template with using primers described in table 7.3. PCR mutagenesis was performed using control primers and cycling condition following the manufacturer's instructions. Then *Dpn*I was added directly to the amplification reaction and immediately incubated at 37 °C for 5 minutes. The

*Dpn*I-treated DNA sample was transformed into *E. coli* XL10-gold ultracompetent cells by heat-pulse at 42 °C. Then preheated (42 °C) NZY$^+$ broth (10 g/L of NZ amine (casein hydrolysate), 5 g/L of yeast extract, 5 g/L of NaCl, pH 7.5 After autoclaving, added the filter-sterilised supplements, 12.5 ml of 1 M $MgCl_2$, 12.5 ml of 1 M $MgSO_4$, 20 ml of 20% w/v glucose) was added into the reaction and the tubes incubated at 37 °C for 1 hour before plating on LB agar plates supplemented with 100 μg/ml ampicillin. A transformant was cultured and plasmid extracted for sequencing using M13F, M13R, F802 R-IQ-N F2201 F-IQ-C and F3323 primers to cover the full-length of IQGAP1. The plasmid from the first round of mutagenesis was used as a template for the second round. The plasmid (pGEM-T-IQGAP1) that was generated from the second round of mutagenesis showed 100% identity with the database sequence. This plasmid was used as a template for IQGAP1 amplification by PCR to generate pPICZ B-IQGAP1 and pGADT7-IQGAP1.

2.15 Transformation of *E. coli*

2.15.1 Preparation of electrocompetent cells

Electrocompetent cells were prepared according to the protocol from Choi and colleagues (Choi et al., 2006). Briefly, 3 ml of *E. coli* overnight culture was pelleted and washed twice with 1 ml of 300 mM sucrose. And then, the pellet was re-suspended with 100 μl of 300 mM sucrose. For transformation, 50 μl of electrocompetent cells was mixed with 2 μl of plasmid and transferred to a pre-chilled cuvette gap with a gap width of 1 mm for electroporation.

2.15.2 Transformation of plasmid DNA into *E. coli* by electroporation

E. coli were electroporated with a single pulse of 25 μF, 1.8 kV and 200 Ω. After electroporation, 1 ml of LB broth was added immediately into the cuvette and then the contents were transferred to a new culture tube. The transformed cells were incubated at 37 °C with shaking for 1 hour. Clones were selected on LB agar plate containing relevant antibiotic selection and incubated at 37 °C overnight.

2.15.3 Transformation of plasmid DNA using heat shock method

A commercial competent cell, *E. coli* XL-1 Blue (Agilent Technologies) was used in some instances following the manufacturer's protocol. Ligation reactions were cleaned up with StrataClean resin (Agilent Technologies) and then the supernatant

was subjected to transformation. 10 µl of the reaction was mixed with thawed *E. coli* cells on ice for 30 minutes. The mixture was then heat-pulsed in a 42 °C water bath for 45 seconds. After that, the tube was placed on ice for 2 minutes and 0.45 ml of preheated SOC medium (2% w/v tryptone, 0.5% w/v yeast extract, 10 mM NaCl, 2.5 mM KCl, 10 mM $MgCl_2$, 10 mM $MgSO_4$, and 20 mM glucose) added. The cells were transferred into a new 15-ml tube and incubated at 37 °C for 1 hour with shaking. Transformation mixture was plated on appropriate LB agar and incubated at 37 °C overnight. For transformation control, pUC18 was used in every transformation experiment.

2.16 Transformation of *Pichia*

2.16.1 Preparation of *Pichia* for electroporation

Pichia transformation by electroporation was performed following the manufacturer's instructions of the EasySelect™ *Pichia* Expression Kit (Invitrogen). In brief, a single colony of *Pichia pastoris* GS115 or KM71H was inoculated into 10 ml of YPD and incubated at 30 °C with shaking. 100 µl of the overnight culture was inoculated into 125 ml of fresh medium and incubated at 30 °C with shaking to an OD600 ~ 1.3 to 1.5. Cells were pelleted at 1,500 × g for 5 minutes and re-suspended with 125 ml of ice-cold sterile water. Next, cells were centrifuged and re-suspended with 62.5 ml of ice-cold sterile water. Then, cells were harvested by centrifugation and re-suspended in 5 ml of ice-cold 1 M sorbitol. Finally, the cells were centrifuged and the pellet was re-suspended in 250 µl of ice-cold 1 M sorbitol. These competent cells were kept on ice and used on the day of preparation.

2.16.2 Linearisation of pPICZ B

The plasmid pPICZ B-QGAP1 and pPICZ B, which was used as a control were linearised before transformation into *Pichia*. The plasmid was digested with *Mss*I (Thermo Scientific). The reaction was incubated at 37 °C overnight and then linearised plasmid was purified using a PCR purification kit (Qiagen). Eluted DNA was concentrated with 1/10 volume of 3 M sodium acetate pH 5.2 and 2 volume of ice-cold absolute ethanol. The DNA sample was stored at -20 °C for at least 1 hour and pelleted by centrifugation at 16,060 x g for 20 minutes. The supernatant was removed, and the pellet was washed with 70% v/v ethanol, then air-dried. DNA was

re-suspended with 10 µl of nuclease-free water and the concentration measured using a Nanodrop spectrophotometer (Thermo Fisher Scientific).

2.16.3 Transformation of *Pichia* by electroporation

Pichia competent cells (80 µl) were mixed with 5 ng of linearised pPICZ B or pPICZ B-IQGAP1. The reaction was transferred into an ice-cold 0.2 cm electroporation cuvette and incubated on ice for 5 minutes. The cells were pulsed using 25 µF, 2 kV and 200 Ω and then 1 ml of ice-cold 1 M sorbitol was immediately added to the cuvette. Contents in the cuvette were transferred into a sterile 15 ml tube and incubated at 30 °C for 2 hours without shaking. Cells were plated on YPDS agar plates (1% w/v yeast extract, 2% w/v peptone, 2% w/v glucose, 1 M sorbitol and 2% w/v agar) supplemented with 100 µg/ml of Zeocin™ (Thermo Fisher Scientific) and incubated at 30 °C for 4 days. A few colonies were picked and streaked for single colonies on fresh YPDS plates containing 2,000 µg/ml Zeocin™. The colonies that were able to grow on that high concentration of Zeocin™ were subjected to colony PCR to detect the plasmid containing the IQGAP1 gene insert.

Additionally, transformant of *P. pastoris* GS115 strains were confirmed to be of the Mut^+ phenotype (Methanol utilisation plus) which is the ability of strains to metabolise methanol as the sole carbon source. A colony was picked and patched on an MMH plate (13.4 g/L yeast nitrogen base, 4 x 10^{-5}% v/v biotin, 0.04 g/L histidine, 0.5% v/v methanol and 15 g/L agar) first. After growth on the MMH plate, the strain was patched onto an MDH plate (13.4 g/L yeast nitrogen base, 4 x 10^{-5}% v/v biotin, 0.04 g/L histidine 2% g/L dextrose, and 15 g/L agar). The controls, GS115(Mut^S) albumin and GS115 pPICZ-lacZ (Mut^+) were also patched onto the MDH and MMH agar plates. Plates were incubated at 30 °C for 2 days. Colonies that grew on both plates were Mut^+ strains and were further screened for protein expression. Whereas Mut^S strains (that grew on the MDH plate but not on the MMH plate) were discarded.

2.17 Protein expression and purification

2.17.1 MBP-IQGAP1 fusion proteins

To express full-length IQGAP1 fused with maltose-binding protein (MBP); MBP-FL-IQGAP1 and C-terminal IQGAP1-MBP fusion protein (MBP-C-IQGAP1), a glycerol stock of *E. coli* Rosetta 2 (DE3) pLysS harbouring pMAL-p2X-FL-IQGAP1 or pMAL-p2X-C-IQGAP1 was inoculated into LB broth containing appropriate

antibiotics and incubated at 37 °C overnight with shaking. For induction of MBP-FL-IQGAP1, IPTG was added into the overnight culture to a final concentration of 0.3 mM and then incubated at room temperature for 6 hours with shaking. With the same concentration of IPTG, MBP-C-IQGAP1 was induced for 3 hours at 37 °C with shaking.

For *E. coli* Rosetta 2 (DE3) pLysS harbouring N-terminal half of IQGAP1 (MBP-N-IQGAP1) and pMAL-p2X, overnight cultures were sub-cultured in a ratio of 1:10 into fresh medium. After 3 hours of incubation at 37 °C with shaking, IPTG was added to 0.1 mM final concentration and then incubated at room temperature overnight. Induced *E. coli* cells were harvested by centrifugation and pellets were stored at -20 °C.

Pellets of induced *E. coli* were re-suspended with BugBuster Master Mix using 1/5 of the original culture volume and incubated on a rocker at room temperature for 10 minutes. Crude cell extract was then subjected to centrifugation at 16,060 x g for 3 minutes to separate the soluble (supernatant) and insoluble (pellet) fractions. Soluble protein was incubated with pre-washed amylose resin (New England Biolabs) at room temperature on a rocker for 15 minutes. The supernatant was then removed after centrifugation at 16,060 x g for 1 minute. The amylose resin was washed profusely with 20 mM Tris-HCl pH 7.5. MBP-fusion protein bound to amylose resin was kept at 4 °C. Alternatively, the protein was eluted at room temperature with 20 mM Tris-HCl pH 7.5 containing 50 mM maltose. Eluted MBP-fusion full-length, N-terminal and C-terminal IQGAP1 proteins were concentrated using centrifugal concentrators at a molecular weight cut-off (MWCO) 100 kDa (GE Healthcare).

2.17.2 N-IQGAP1 purification

E. coli Rosetta 2 (DE3) pLysS harbouring pMAL-p2X-N-IQGAP1 was inoculated into 50 ml of LB broth containing 100 μg/ml ampicillin and 34 μg/ml chloramphenicol and incubated at 37 °C overnight with shaking. The overnight culture was washed with PBS twice. The bacterial cells were re-suspended in 50 ml of LB broth and sub-cultured in a ratio of 1:100 into 4 litres of LB broth supplemented with the antibiotics and incubated at 37 °C for 3 hours. The culture was cooled down on ice and then IPTG was added at a final concentration of 0.1 mM. IPTG induction was conducted at 16 °C overnight with shaking. Bacterial cells were harvested by centrifugation and washed with PBS. Cell pellets were kept at -70 °C.

To purify MBP-N-IQGAP1, every 1 gram of bacterial cell paste was re-suspended with 5 ml of lysis buffer (1% w/v Octylthioglucoside (OTG) in 20 mM Tris pH 7.5, 200 mM NaCl, 1 mM EDTA, 1 mM DTT and 0.1% v/v Triton X-100). Lysonase™ Bioprocessing Reagent (Novagen) was also included in the cell suspension using 10 µl per 1 gram of cell paste and incubated on a rocker at room temperature for 30 minutes. The insoluble fraction was separated by centrifugation at 16,000 × g for 20 minutes at 4 °C. The supernatant was cleared with a 0.45-µm filter. Next, the soluble protein was purified by affinity chromatography on an MBPTrap™ HP column (GE Healthcare) coupled to an ÄKTApurifier system. Then the column was washed with washing buffer (20 mM Tris pH 7.5, 200 mM NaCl, 2 mM $CaCl_2$). MBP-tag was cleaved while bound to the amylose resin by injection of 50 µg of FactorXa (New England Biolabs) into the column and incubation at 4 °C for 48 hours. The digested protein was removed from the column by washing with washing buffer. Each fraction was examined for the presence of protein using Bradford reagent (Sigma-Aldrich) and confirmed by SDS-PAGE with Coomassie blue staining. Fractions showing the presence of protein were pooled and subjected to gel filtration using HiPrep 16/60 Sephacryl S-100 HR (GE Healthcare) to separate N-IQGAP1 from MBP. The proteins were collected in washing buffer. Two microliters from each fraction were subjected to dot blot on a nitrocellulose membrane to detect IQGAP1. Positive fractions were pooled and concentrated using an Amicon® Ultra-4 centrifugal filter device at 3 kDa MWCO (Merck Millipore). The concentration of purified N-IQGAP1 protein was measured by Nanodrop spectrophotometry before snap-freezing and storage of aliquots at −70°C.

2.17.3 IQGAP1-6xHis expression in *Pichia* and purification

A recombinant strain with the highest expression of IQGAP1, GS115/IQGAP1#15, was cultured from a single colony in 25 ml of Buffered Glycerol-complex Medium (BMGY; 1% w/v yeast extract, 2% w/v peptone, 100 mM potassium phosphate, pH 6.0, 1.34% w/v YNB, 4×10^{-5}% w/v biotin, and 1% v/v glycerol). Cells were pelleted and re-suspended in Buffered Methanol-complex Medium (BMMY; 1% w/v yeast extract, 2% w/v peptone, 100 mM potassium phosphate, pH 6.0, 1.34% w/v YNB, 4×10^{-5}% w/v biotin, and 0.5% v/v methanol) to an OD600 of 1.0. The induction was conducted at 30 °C with shaking. Methanol was added to the culture to a final concentration of 0.5% v/v every 24 hours. To determine the optimal time

post-induction, cells were harvested every 24 hours for 4 days. Total protein was analysed for IQGAP1 expression by Western blotting.

To purify 6xHis-IQGAP1, the strain was cultured in 400 ml media at 30 °C for 3 days by adding methanol to a final concentration of 0.5% v/v every 24 hours. Cells were re-suspended with *Pichia* lysis buffer (1 mM PMSF, 5% v/v glycerol, 50 mM sodium phosphate, pH 7.4) in a ratio of 1 gram of cell paste weight to 4 ml of *Pichia* lysis buffer. Cells were lysed using a One-Shot Model cell disruptor (Constant Systems) at 16,000 psi for 2 passes. Total cell lysate was centrifuged at 16,000 × g for 30 minutes at 4 °C. The supernatant was cleared with a 0.45-µm filter and diluted in binding buffer (500 mM NaCl, 1% v/v TritonX-100, and 5% v/v glycerol, 50 mM sodium phosphate, pH 7.4) in a ratio of 1:2. Then the protein was purified by affinity chromatography on a HiTrapTalon Crude column (GE Healthcare) coupled to an ÄKTApurifier system. After washing the column with washing buffer (500 mM NaCl, 1% v/v TritonX-100, 5% v/v glycerol and 5 mM imidazole, 50 mM sodium phosphate, pH 7.4), the 6xHis-tagged protein was eluted in the elution buffer (50 mM sodium phosphate, pH 7.4, 500 mM NaCl and 500 mM imidazole). Each fraction was examined for the presence of protein using Bradford reagent (Sigma-aldrich) and subjected to SDS-PAGE with Coomassie blue staining and Western blot analysis.

2.17.4 GST and GST-BimA$_{54-455}$ expression and purification

A construct for the expression of amino acid residues 54 to 455 of *B. pseudomallei* strain 10276 BimA with a GST fusion protein was described in the previous study (Sitthidet et al., 2010). A single colony of *E. coli* harbouring pGEX-BimA and pGEX-4T-1, which expressed GST-BimA$_{54-455}$ and GST protein respectively, was inoculated in LB broth containing 100 µg/ml ampicillin and 10 µg/ml chloramphenicol and incubated overnight. One millilitre of overnight culture was sub-cultured in 100 ml LB containing appropriate antibiotics. After 3 hours of incubation with shaking, IPTG was added to a final concentration of 0.25 mM and then incubated for a further 3 hours at 37 °C. The induced *E. coli* cells were pelleted and re-suspended in BugBuster Master Mix (Novagen) and incubated on a rocker for 10 minutes at room temperature. Insoluble debris was separated by centrifugation at 16,060 x g for 3 minutes. The supernatant was transferred to a new tube containing 200 µl of prewashed glutathione sepharose 4B beads (GE Healthcare) and incubated on a rocker at room temperature for 30 minutes. The beads were washed

4 times with 1 ml of PBS and kept at 4 °C. Otherwise, the protein was eluted with elution buffer. The eluted solution was cleared by a 2-ml spin filter column (Novagen) and equilibrated into 50 mM Tris-HCl, pH 7.5 by using centrifugal concentrators at MWCO 3 kDa (Sartorius).

For a large-scale production, 1 litre culture of induced *E. coli* cells was lysed using 1% w/v OTG in PBS in a ratio of 1 gram of cell paste per 5 ml of lysis buffer supplemented with 10 µl Lysonase™ Bioprocessing Reagent (Novagen). The cell suspension was incubated on a rocker at room temperature for 20 minutes. Insoluble debris was separated by centrifugation at 16,000 × g for 20 minutes at 4 °C. The supernatant was cleared using a 0.45-µm filter and then purified by affinity chromatography on a GSTrap™ 4B column (GE Healthcare) coupled to an ÄKTApurifier system. The column was washed with PBS and then the protein was eluted with elution buffer (10 mM reduced glutathione in 50 mM Tris-HCl pH 8.0). The eluted solution in each fraction was determined the presence of protein using Bradford reagent. The fractions that turned the reagent to blue were pooled and equilibrated into 50 mM Tris-HCl, pH 7.5 by dialysis using D-Tube Dialyzers Maxi, MWCO 3.5 kDa (Novagen) at 4 °C. The protein concentration was measured using Nanodrop spectrophotometer and subjected to SDS-PAGE with Coomassie blue staining.

2.17.5 $BimA_{54-470}$ -6xHis expression and purification

A few colonies of *E. coli* Rosetta 2 (DE3) pLysS harbouring pET-21b (+)/$BimA_{54-470}$ were screened for protein expression. A single colony was inoculated into 5 ml of LB broth supplemented with 100 µg/ml ampicillin and 34 µg/ml chloramphenicol and incubated at 37 °C overnight with shaking. Then the overnight culture was subcultured in a ratio of 1 in 100 to a fresh media and incubated at 37 °C for 3 hours with shaking. IPTG was added to a final concentration at 0.5 mM and induced at 37 °C for 2 hours. Total cell lysate was subjected to SDS-PAGE with Coomassie blue staining and Western blot analysis.

A selected colony was cultured in a large-scale production (2 litres) and induced protein expression at 16 °C overnight with shaking. After harvesting, bacterial cells were re-suspended with lysis buffer (1% w/v OTG in 50 mM sodium phosphate pH 7.4, 500 mM NaCl, 5% v/v glycerol) and incubated at room

temperature for 20 minutes on a rocker. The soluble protein was collected by centrifugation at 16,000 ×g for 20 minutes at 4 °C. The supernatant was cleared using a 0.45 µm-filter and diluted with 2 volumes of the binding buffer (50 mM sodium phosphate pH 7.4, 500 mM NaCl, 1% v/v Triton X-100, and 5% v/v glycerol) then subjected to affinity chromatography on a HiTrap TALON crude column (GE Healthcare) coupled to an ÄKTApurifier system. After washing the column with washing buffer (50 mM sodium phosphate pH 7.4, 500 mM NaCl, 1% v/v Triton X-100 and, 10% v/v glycerol, 1 mM DTT and 5 mM imidazole), the protein was eluted in elution buffer (500 mM NaCl, 500 mM imidazole, 50 mM sodium phosphate pH 7.4) and determined the presence of protein using Bradford reagent. The protein was then dialysed using D-Tube™ Dialyzers with molecular weight cutoffs (MWCO) 3.5 kDa (Novagen).

2.17.6 MBP-BimA$_{54-470}$ expression and purification

To determine protein expression in *E. coli* Rosetta 2 (DE3) pLysS harbouring pMAL-p2X-BimA$_{54-470}$, a few colonies were cultured in 10 ml of LB supplemented with appropriate antibiotics at 37 °C for 3 hours and induced with IPTG at a final concentration of 0.3 mM at 37 °C for 2 hours. The cell lysate was subjected to SDS-PAGE with Coomassie blue staining and BimA expression was confirmed by Western blot analysis. A colony showing BimA expression was selected for a pilot experiment of protein purification as described below. One millilitre of overnight culture was inoculated into 100 ml of LB supplemented with 0.2% w/v glucose and incubated at 37 °C with shaking to an OD600 of 0.5. IPTG was added to a final concentration of 0.3 mM and incubation continued at 37 °C for 2 hours. Cells were harvested by centrifugation at 3,200 x g for 15 minutes. Cells were re-suspended in 5 ml of 1% w/v OTG in column buffer (200 mM NaCl and 1 mM EDTA, 20 mM Tris-HCl pH 7.4). The cell lysate was centrifuged at 16,000 × g for 20 minutes at 4 °C. The supernatant was cleared using a 0.45 µm-filter. Pre-washed amylose resin (~200 µl) was added to the supernatant and incubated on a rocker at room temperature for 2 hours. The resin was washed with column buffer extensively and the fused protein was eluted in 200 µl of 50 mM maltose in column buffer. After incubation at room temperature for 10 minutes, the resin and eluted protein were separated by centrifugation. The supernatant was incubated with FactorXa (New Biolabs) following the manufacturer's instruction. The digestion was performed at room temperature for

12 hours. The protein samples were subjected to SDS-PAGE with Coomassie blue staining and Western Blot analysis.

2.18 Pull-down assay

2.18.1 GST pull-down

Immobilised fusion-tagged protein, GST and GST-BimA$_{54-455}$ (Sitthidet et al., 2011) bound to glutathione sepharose 4B beads were blocked with 5% w/v BSA in PBS at room temperature for 30 minutes and washed twice with PBS. The immobilised protein was incubated with 1 µg of purified MBP-fusion protein for 2 hours at room temperature in 1X polymerisation buffer (500 mM KCl, 20 mM $MgCl_2$, 10 mM ATP, 100 mM Tris-HCl pH 7.5) containing 500 µM ATP and 100 µM $CaCl_2$. The beads were washed with PBS extensively and the supernatant was removed as much as possible. Then the beads were suspended in 2X SDS-PAGE loading buffer containing 2% v/v β-mercaptoethanol. The samples were heated at 99 °C for 5 minutes and separated by SDS-PAGE. The interaction of GST-BimA and IQGAP1 was determined by anti-MBP Western blot analysis.

2.18.2 MBP pull-down

Non-specific binding sites of immobilised MBP-tagged proteins, MBP, MBP-FL-IQGAP1, MBP-N-IQGAP1 and MBP-C-IQGAP1 bound to amylose resin were blocked with 5% w/v BSA in PBS at room temperature for 30 minutes. The resin was washed with PBS twice and then incubated with 5 µg of purified GST-fusion protein for 2 hours at room temperature in 1X polymerisation buffer containing 500 µM ATP and 100 µM $CaCl_2$. After stringent washing steps with PBS, the supernatant was removed. Beads were re-suspended in 2X SDS-PAGE loading buffer containing 2% v/v β-mercaptoethanol. The samples were heated at 99 °C for 5 minutes and proteins in the supernatant were separated by SDS-PAGE. The interaction of GST-BimA and IQGAP1 was examined by anti-GST Western blot analysis.

2.19 Yeast two-hybrid

2.19.1 Yeast transformation

Saccharomyces cerevisiae AH109 containing pGBKT7-BimA$_{54–455}$ (AH109 pGBKT7-BimA) was generated previously in our laboratory. To test the interaction between BimA and IQGAP1 or actin, pGADT7-IQGAP1 or pGADT7-actin was

transformed into *S. cerevisiae* AH109 expressing BimA on the bait plasmid (pGBKT7-BimA$_{54–455}$) by the LiAc/SS Carrier DNA/PEG method (Gietz and Woods, 2002). A single colony (~2 mm in size) of the *S. cerevisiae* AH109 harbouring pGBKT7-BimA$_{54–455}$ was inoculated into 5 ml of SD medium lacking tryptophan (SD/−Trp) and incubated on a shaker at 30 °C with shaking. The overnight culture was harvested at 1,000 × g for 10 minutes and some of the supernatant was removed. Cells were re-suspended before transferring to a new micro-centrifuge tube and pelleted at 16,060 x g for 30 seconds. The supernatant was discarded. The reagents were added to the cells in the following order: 240 µl of 50% w/v filter sterilised PEG BioUltra 3,500 (Sigma), 36 µl of 1.0 M LiAc, 10 µl of 10 mg/ml chilled Herring Testes Carrier DNA, denatured (Clontech), 2 µl of plasmid DNA (~1 µg) and 72 µl of sterilise water. The tube was incubated in a water bath at 42 °C for 3 hours. After that, the transformation mixture was pelleted by centrifugation at 16,060 x g for 30 seconds. One millilitre of sterile water was added to the pellet to re-suspend the cells, by pipetting and vortex mixing vigorously. 100 µl samples were inoculated onto SD agar plates lacking leucine and tryptophan (double dropout media; DDO) plates and incubated at 30 °C for 3-4 days to generate the strains AH109 pGBKT7-BimA pGADT7-IQGAP1 and AH109 pGBKT7-BimA pGADT7-actin.

2.19.2 Yeast two-hybrid assay

Colonies of yeast strains AH109 pGBKT7-BimA pGADT7-IQGAP1 and AH109 pGBKT7-BimA pGADT7-actin from DDO agar plates were suspended in 20 µl of water. Then 5 µl of cell suspension was dotted onto SD agar plates lacking leucine, tryptophan, adenine, and histidine or quadruple drop out (QDO) supplemented with 20 µg/ml of X-α-galactosidase. Plates were incubated at 30 °C for 24 hours before observing the appearance of the colonies until 72 hours. Interaction controls supplied with the Matchmaker GAL4 Two-Hybrid System 3 (Clontech) were included using pGADT7-T antigen pGBKT7-p53 as a positive control and pGADT7-T antigen pGADT7-Lamin C as a negative control.

2.20 Pyrene-actin assembly assay

Pyrene-actin polymerisation assay conditions were described previously (Stevens et al., 2005a) using the commercial actin polymerisation Biochem kit™ (Cytoskeleton). The reagents were prepared, and reactions performed as per the

manufacturer's instructions with some modification. In brief, an aliquot of pyrene-actin (1 mg) was suspended in 50 µl water and diluted with 2.450 ml of ice-cold G-buffer (10mM Tris pH 7.5, 0.2 mM $CaCl_2$, 0.2 mM ATP and 1 mM DTT). After vortexing, the pyrene-actin was incubated on ice in the dark for 1 hour and then centrifuged at 100,000 × g for 2 hours at 4°C. The supernatant (2 ml) was transferred to a chilled tube and kept on ice and in the dark. The concentration of this G-actin stock was measured using a NanoDrop spectrophotometer.

Assays were performed in the FLUOstar OPTIMA (BMG LABTECH) and set up in black opaque 96-well plates. To study the effect of IQGAP1 on actin polymerisation mediated by BimA, 200 nM GST or GST-BimA protein (with or without 50 nM N-IQGAP1) were added into test wells and incubated with 1X polymerisation buffer. Next, test reactions were initiated by the addition of 1 µM G-actin and run with a kinetic cycle with the emission of fluorescence at 407 nm data (after excitation at 365 nm) collected every 1 minute up to 1 hour. Rates of polymerisation were calculated as the rise in fluorescence units per second during the linear phase of polymerisation.

Table 2.3: Molecular weight of proteins in this study

Protein	Relative Molecular weight; Rmw (Da)
Actin	~43,000
GST	27,897
GST-$BimA_{54-455}$	66,779
N-IQGAP1	99,805

2.21 Statistical Analysis

Data from at least three individual experiments from each condition were analysed using an unpaired two-sample Student's *t*-test in GraphPad Prism software. *p* values of ≤0.05 were taken as significant.

Chapter 3
Dissecting the role of IQGAP1 in *B. pseudomallei* actin tail formation using siRNA-mediated knockdown

3.1 Introduction

B. pseudomallei requires BimA, a bacterial protein which is located at the pole of the bacterial cell, to move within and between host cells by actin-based motility (Stevens et al., 2005a). The mechanism by which BimA subverts the cellular actin machinery is ill-defined. Following previous studies to identify host cell proteins required for actin-based motility of *L. monocytogenes* (David et al., 1998, Van Troys et al., 2008), our laboratory has previously performed a proteomic analysis in a similar manner.

Prior to this present thesis, the Stevens laboratory generated bacteria expressing BimA by electroporation of pBHR2-virAG plasmid (Schell et al., 2007) into *B. pseudomallei* strain 10276 wild-type and bimA mutant (Stevens et al., 2005a). This resulted in constitutive expression of BimA protein in the wild-type strain in vitro (10276 pBHR2-virAG; BimA+) and a lack of expression in a bimA insertion mutant (10276 bimA::pDM4 pBHR2-virAG; BimA-). The bacterial strains were subjected to an affinity purification in murine splenic lysate supplemented with a buffer that promotes BimA-mediated actin polymerisation (Stevens et al., 2005a). By affinity purification, interacting proteins were isolated and eluted. Protein samples were separated by SDS-PAGE and stained. Bands were excised and subjected to LC-MS/MS. Of the thirty proteins identified in the eluted proteins from BimA+ compared to BimA-, collected for three independent experiments. Several cytoskeleton proteins that have previously been found in the tails of other bacterial pathogens, for example, α-actinin and cofilin, were identified. Some host cell proteins that were identified in 2 and 3 experiments were validated by immunoblotting. The data set of host cellular protein identified has now been published following peer-review (Jitprasutwit et al., 2016) and the experimental workflow that had been done before this thesis is shown in Figure 3.1.

Comparison of the affinity purification results to proteins involved in *Listeria* or *Shigella* actin-based motility identified HSP90 and IQGAP1 as novel proteins involved in actin-based motility. IQGAP1 was of particular interest as it has not

previously been shown to be involved in the actin-based motility of any intracellular bacterial pathogen studied to date, but also, since IQGAP1 is a key regulator of cellular actin dynamics. Moreover, the presence of IQGAP1 in *B. pseudomallei* actin tail had been seen from a preliminary observation by Stevens laboratory. It was hypothesised that IQGAP1 was required for *B. pseudomallei* actin-based motility. Thus, this thesis aimed to confirm the IQGAP1 localisation and explore the function of IQGAP in *B. pseudomallei* actin-based motility using siRNA technique. Results from the study of the interaction between IQGAP1 and BimA presented here (Chapter 5) have been included in a peer-reviewed publication, a copy of which is included as an appendix in Chapter 7.

From the previous study using an RNAi screen targeting cytoskeleton proteins uncovered a core set of proteins that play roles in *Rickettsia* actin-based motility, demonstrated that the host cell proteins which were localised in the bacterial actin tails could be functionally important for actin-based motility as well as the efficiency of infection (Serio et al., 2010). The roles of IQGAP1 in the actin-based motility were explored in this study using an siRNA-mediated knockdown approach.

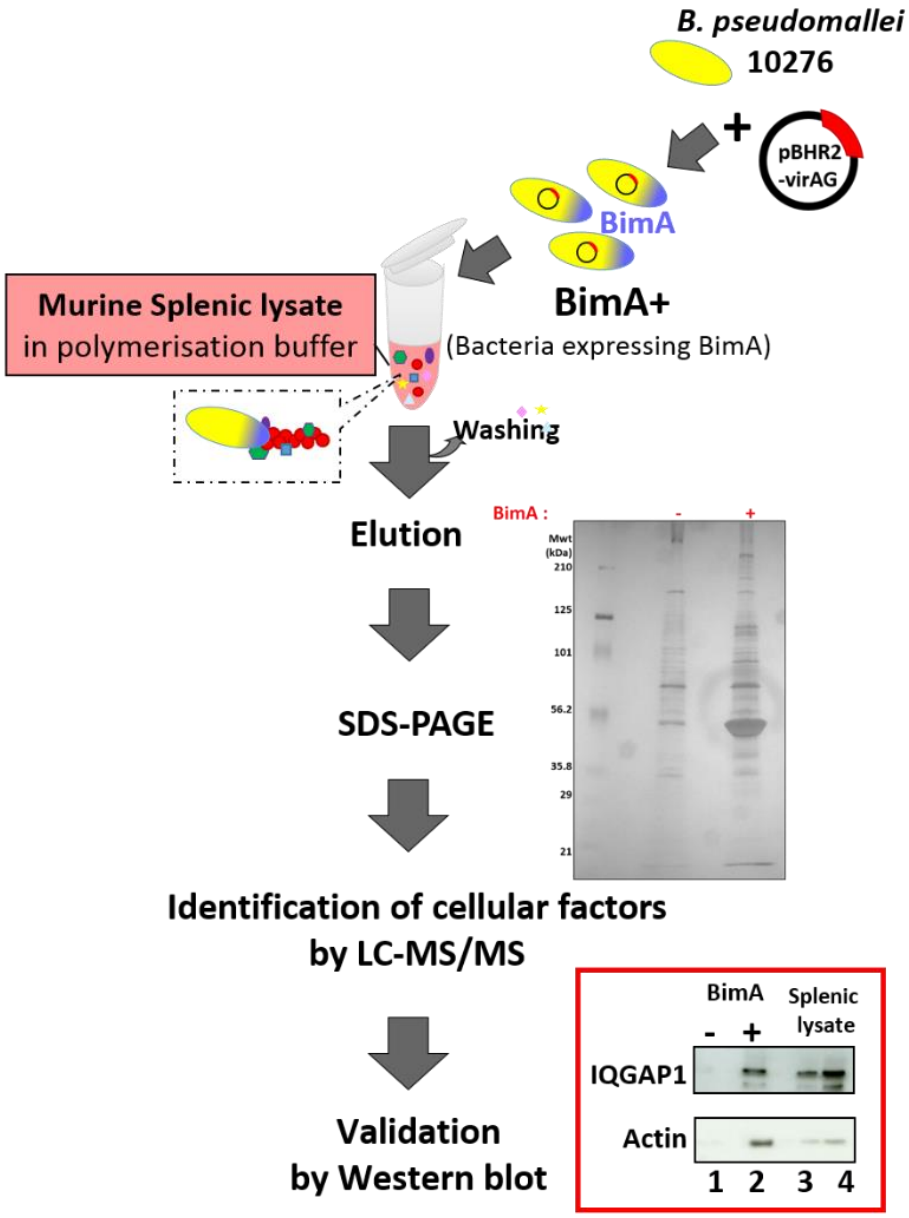

Figure 3.1: Schematic diagram illustrating the method to identify host cell proteins recruited to bacteria expressing BimA

pBHR2-virAG was introduced into *B. pseudomallei* 10276 to obtain bacteria over-expressing BimA (BimA+). Interacting host cell proteins from murine splenic lysate were isolated by affinity purification under conditions supporting actin polymerisation. After washing, interacting proteins were eluted and then separated by SDS-PAGE. Each protein band was excised from the gel for identification by mass spectrophotometry. Identified proteins were validated with a specific antibody by immunoblotting. (Data from Jitprasutwit et al., 2016).

Small or short interfering RNA (siRNA) is a non-coding RNA involved in a mechanism called RNA interference (RNAi) for silencing gene expression. RNAi is an innate defence mechanism against foreign nucleic acids such as invading viruses. This biological process occurs naturally in eukaryotic organisms by introduction of a double-stranded RNA (dsRNA), such as viruses, resulting in degradation of mRNAs with complementary RNA targets. RNAi is triggered by the presence of double-stranded RNA (dsRNA) in the cytoplasm. Then this dsRNA is cleaved by Dicer, a ribonuclease (RNase)-like enzyme, into a 21–23 nucleotides RNA which is known as siRNA. The siRNA duplex is taken up by the RNA-induced silencing complex (RISC) that requires endonuclease Argonaute 2 (AGO2) to catalyse the unwinding of the siRNA duplex. The central AGO2 cleaves the sense strand of the siRNA while the antisense strand (guide strand) remains associated with the RISC. The guide strand only binds to mRNA by Watson-Crick base pairing and the active RISC targets specific mRNA targets for cleavage by AGO2, resulting in specific gene silencing. The activated RISC-siRNA complex can then be recycled to destroy additional mRNA targets. As a result, the gene silencing process continues.

RNAi-mediated mechanisms are a powerful tool to explore the function of target genes. In experimental approaches, siRNA can be synthetically produced and introduced into cells directly to suppress gene expression (Reviewed in Shan, 2010). An RNAi screen identified a core set of host factors that were important for *R. parkeri* actin tail formation (Serio et al., 2010). Besides, many groups have succeeded in repressing IQGAP1 expression and explored its function in bacterial infection. For example, a previous study using siRNA knockdown investigated the role of IQGAP1 in *Salmonella* cell invasion. IQGAP1 expression was decreased by 75% leading to reduced host cell invasion. It revealed that IQGAP1 was required for invasion by regulating actin polymerisation in the phagocytic cup (Brown et al., 2007).

It was hypothesised that IQGAP1 may be a key mediator of BimA-dependent actin polymerisation. The aim of this chapter was to investigate the role of IQGAP1 in *B. pseudomallei* actin-based motility using RNAi technology.

3.2 Results

3.2.1 Co-localisation of IQGAP1 with *B. pseudomallei* actin tails in host cells

From the proteomic experiment using bacteria expressing BimA, IQGAP1 was detected and validated by Western blot analysis with specific antibodies, confirming the association with BimA-expressing bacteria *in vitro* (Figure 3.1, Jitprasutwit et al., 2016). Hence, IQGAP1 was identified as a putative component of *B. pseudomallei* actin tails. In this study, localisation of IQGAP1 in *B. pseudomallei*-infected cells was investigated using immunofluorescence confocal microscopy. Firstly, a series of antibody dilutions in a titration experiment was performed to determine the optimum concentration with the best staining and minimum background (Supplemental figure 7.1). Sub-cellular localisation of IQGAP1 in control HeLa cells was observed in the cytoplasm and the cell membrane. Microscopy showed an overlap in the fluorescence signals of IQGAP1 (red) and F-actin, which is selectively labelled by phalloidin (green) in yellow, representing co-localisation of IQGAP1 with actin filaments (Figure 3.2a).

Next, the localisation of IQGAP1 in *B. pseudomallei* infected cells was observed at different time points (8, 16, 24, and 32 hours post-infection). At each time point, the presence of IQGAP1 in *B. pseudomallei* actin tails were detected. At 16 hours post-infection showed the greatest number of bacteria displayed actin tails. Figure 3.2b showed the localisation of IQGAP1 throughout the *B. pseudomallei* actin tail implied that this protein may be required for actin tail formation. From this promising result, the role of IQGAP1 was further examined in this study.

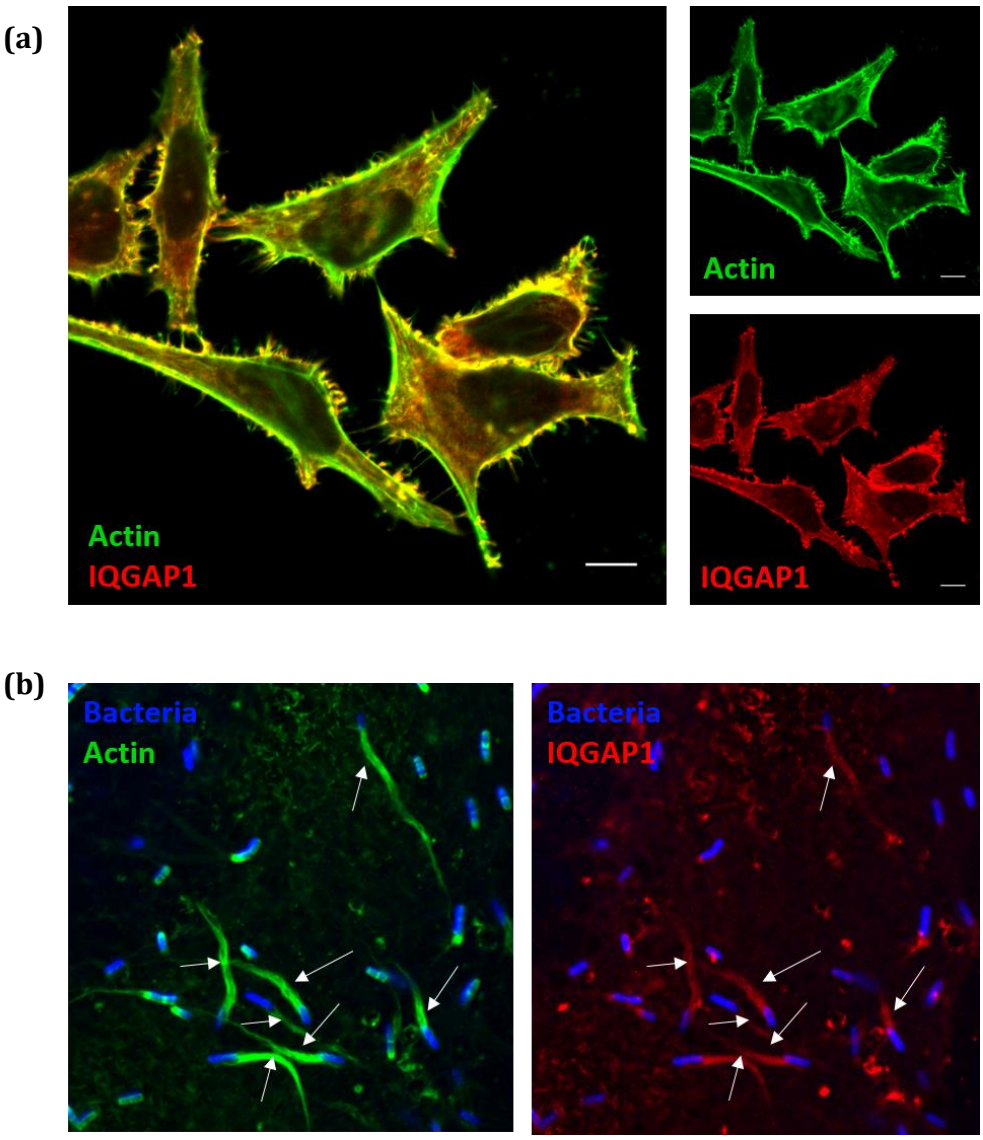

Figure 3.2: IQGAP1 localises with actin tails of *B. pseudomallei*
Representative confocal laser scanning micrographs of uninfected HeLa cells **(a)** and HeLa cells infected with the *B. pseudomallei* 10276 at 16 hours post-infection **(b)**. Bacteria (blue) were stained using mouse monoclonal anti-*B. pseudomallei* lipopolysaccharide antibody that was detected with anti-mouse Ig-Alexa Fluor 405. F-actin (green) was stained with Alexa Fluor 488-conjugated phalloidin. IQGAP1 (red) was stained with a rabbit polyclonal antibody and detected with anti-rabbit Ig-Alexa Fluor 568. Arrows denote actin tails where IQGAP1 was recruited.
Scale bar = 10 μm.

3.2.2 Optimisation of IQGAP1 knockdown in HeLa cells

To study the function of IQGAP1 in *B. pseudomallei* actin tail formation, siRNA technique was used to repress IQGAP1 expression in HeLa cells. The efficiency of siRNA transfection was maximised by optimisation of the amount of siRNA and transfection reagent. A commercial siRNA targeting exon 31 (from a total of 39 exons) of the *Homo sapiens* IQGAP1 gene was available from Ambion (siRNA IQGAP1, ID S16837; Silencer Select). The siRNA duplex was delivered into HeLa cells using the cationic-lipid transfection reagent Lipofectamine RNAiMAX, following the manufacturer's protocol. Optimisation of RNAi induction was validated by immunoblotting to detect IQGAP1 protein in total cell lysates. Figure 3.3 shows a workflow of siRNA transfection performed in this study. Briefly, one day before transfection, HeLa cells (diluted in DMEM without antibiotics) were plated into a 24-well plate at a low confluency. The cells were transfected with siRNA IQGAP1 duplex and Lipofectamine RNAiMAX in Opti-MEM. At a specific time post-transfection, the cells were washed with PBS and lysed with BugBuster. Total cell lysate was subjected to Western blotting. For each sample, the level of protein expression was acquired by measuring the band intensity of IQGAP1 and actin on the blot using an Odyssey infrared imager. The signal value was obtained using Image studio software and the level of IQGAP1 expression normalised with actin in each sample. The percentage of IQGAP1 expression was calculated by comparing with non-transfected control samples, which were taken as 100%.

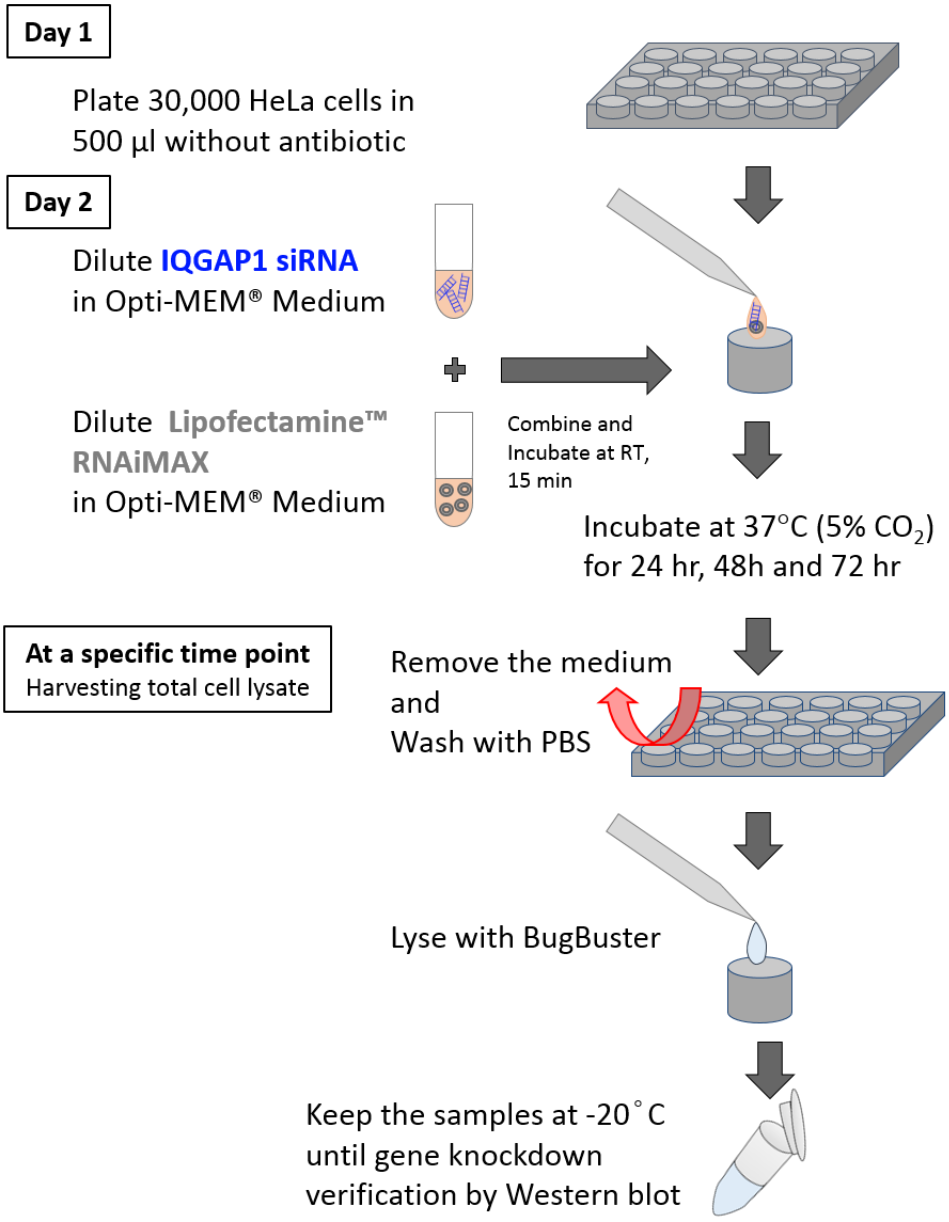

Figure 3.3: Workflow for siRNA transfection into HeLa cells using Lipofectamine RNAiMAX
A low density of HeLa cells was seeded into a 24-well plate one day before transfection. For transfection, RNAi duplex and Lipofectamine RNAiMAX were diluted in Opti-MEM and combined. The RNAi duplex-Lipofectamine RNAiMAX complex was added into each well and cells incubated at 37°C in a 5% CO_2 incubator. At a specific time point, HeLa cells were washed and lysed with BugBuster to obtain a total cell lysate. IQGAP1 protein expression was determined by Western blot analysis.

Initially, several siRNA concentrations and amount of transfection reagent were employed to optimise conditions for knockdown of IQGAP1 in a pilot experiment analysing single samples from each treatment. At 48 hours post-transfection, immunoblotting analysis (after normalisation of the IQGAP1 signal with that of actin) showed that increasing the siRNA concentration (3, 15, and 24 pmol) did not result in an improvement in IQGAP1 knockdown (Figure 3.4a). Although the level of IQGAP1 knockdown was more efficient with the lower concentration of transfection reagent (Figure 3.4b). This was followed by comparing the level of knockdown achieved between a single or double transfection method. For single transfection, HeLa cells were transfected with siRNA by Lipofectamine RNAiMAX only once. On the other hand, for the double transfection method, HeLa cells were transfected twice with the same amount of siRNA duplex and Lipofectamine RNAiMAX, at a 24 hours interval. A pilot experiment was set up where the efficiency of each condition was determined from one sample. In contrast, when the siRNA IQGAP1 concentration was increased by the use of a double transfection technique, IQGAP1 expression was lower than cells that had only been transfected once (Figure 3.4c and 3.4d). From the quantitative immunoblotting results shown in figure 3.4, we decided to further optimise the double transfection method with a total amount of 6 pmol siRNA IQGAP1 and 2 μl transfection reagent to determine the time point post transfection that demonstrated the greatest level of knockdown.

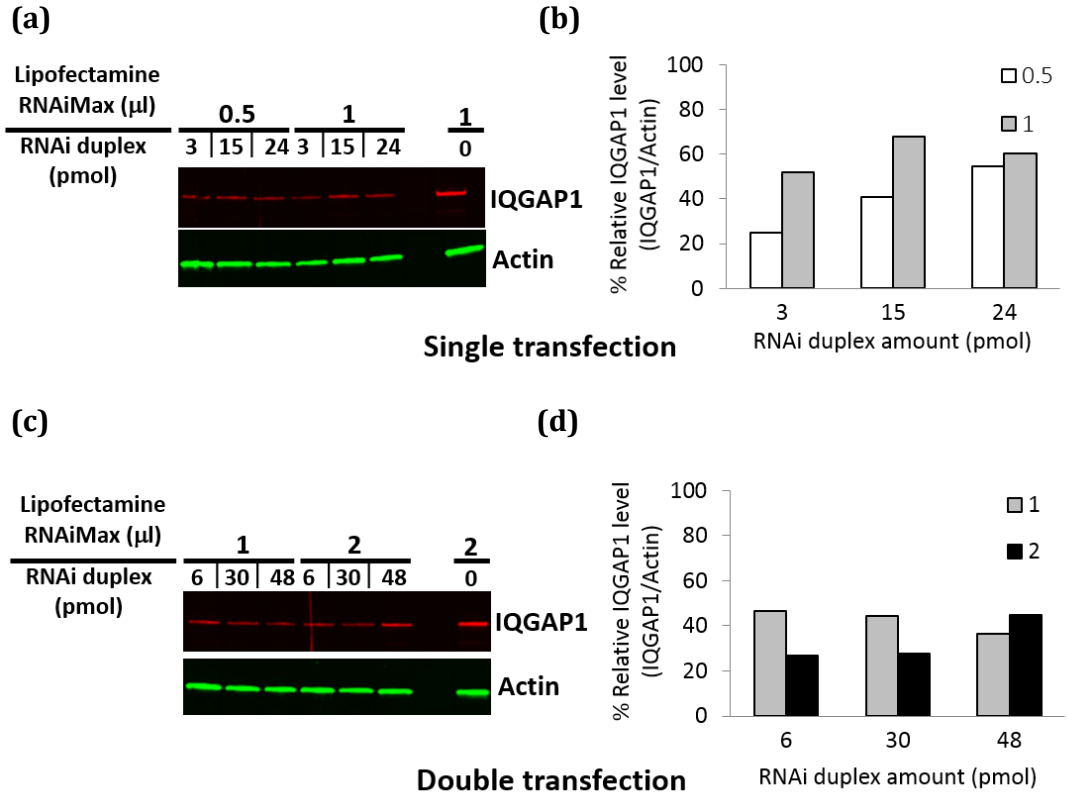

Figure 3.4: IQGAP1 expression was suppressed in a siRNA dose-dependent manner

HeLa cells were transfected with a range of siRNA IQGAP1 and Lipofectamine RNAiMAX concentrations. Cells were incubated for 48 hours and cell lysates immunoblotted for IQGAP1 and actin. Quantitation of IQGAP1 expression was calculated by measuring the intensity of the IQGAP band normalised with the actin band in each lane. Control sample that was treated with the same volume of Lipofectamine RNAiMAX was taken as 100%. Total volume of Lipofectamine RNAiMAX was either 0.5 µl (white bar), 1 µl (grey bar) or 2.0 µl (black bar) in each sample. The data were obtained and calculated from one individual sample (n=1).

(a) Western blot analysis of IQGAP1 and actin in transfected HeLa cells from single transfection.

(b) The expression level of IQGAP1 in HeLa cells from single transfection was analysed from the immunoblot in (a) using an Odyssey infrared imager and Image Studio software.

(c) Western blot analysis of IQGAP1 and actin in transfected HeLa cells from double transfection.

(d) The expression level of IQGAP1 in HeLa cells from single transfection was analysed from the immunoblot in (c) using an Odyssey infrared imager and Image Studio software.

3.2.3 Further optimisation of IQGAP1 silencing

To further optimise the transfection conditions for efficient silencing of IQGAP1 expression, a range of incubation times were tested. From the previous result in section 3.2.2, HeLa cells double-transfected with 6 pmol siRNA IQGAP1 duplex and 2 µl of Lipofectamine RNAiMAX, and incubated for 48 hours, showed the lowest level of IQGAP1 expression. The protocol for double transfection was modified in this experiment by adding the second transfection reagent at 6 hours after the first transfection. For this pilot experiment, only one sample was collected per condition at 24, 48 and 72 hours post-transfection. In this experiment, single and double transfections with the same amount of total siRNA IQGAP1 duplex (6 pmol) and Lipofectamine (2 µl) were compared once again. Controls for this experiment included cells treated with only Opti-MEM (no Lipofectamine or siRNA IQGAP1) to examine the basal levels of IQGAP1 expression. Total cell lysate from each condition was subjected to Western blotting, probing with anti-IQGAP1 and anti-actin antibodies. Cells treated with Opti-MEM and Lipofectamine showed similar signal intensities of actin and IQGAP1 (Figure 3.5a and 3.5b). This implies that Lipofectamine did not affect the baseline actin and IQGAP1 protein levels at the concentration used. From this result, the percentage of IQGAP1 expression was calculated by comparing with Lipofectamine-treated control samples which were taken as 100%.

Comparing the different methods for transfection of siRNA IQGAP1 into HeLa cells, showed that the level of IQGAP1 expression gradually decreased over time from approximately 50% at 24 hours post-transfection to below 20% at 72 hours post-transfection by both protocols, whether by single or double transfection. (Figure 3.5c). In particular, the single transfection method was more efficient than using double transfection to suppress IQGAP1 expression. Therefore, in the following experiments, HeLa cells were transfected with 6 pmol of siRNA IQGAP1 duplex and 2 µl of Lipofectamine RNAiMAX by the single transfection method and incubated for 72 hours for a maximal knockdown.

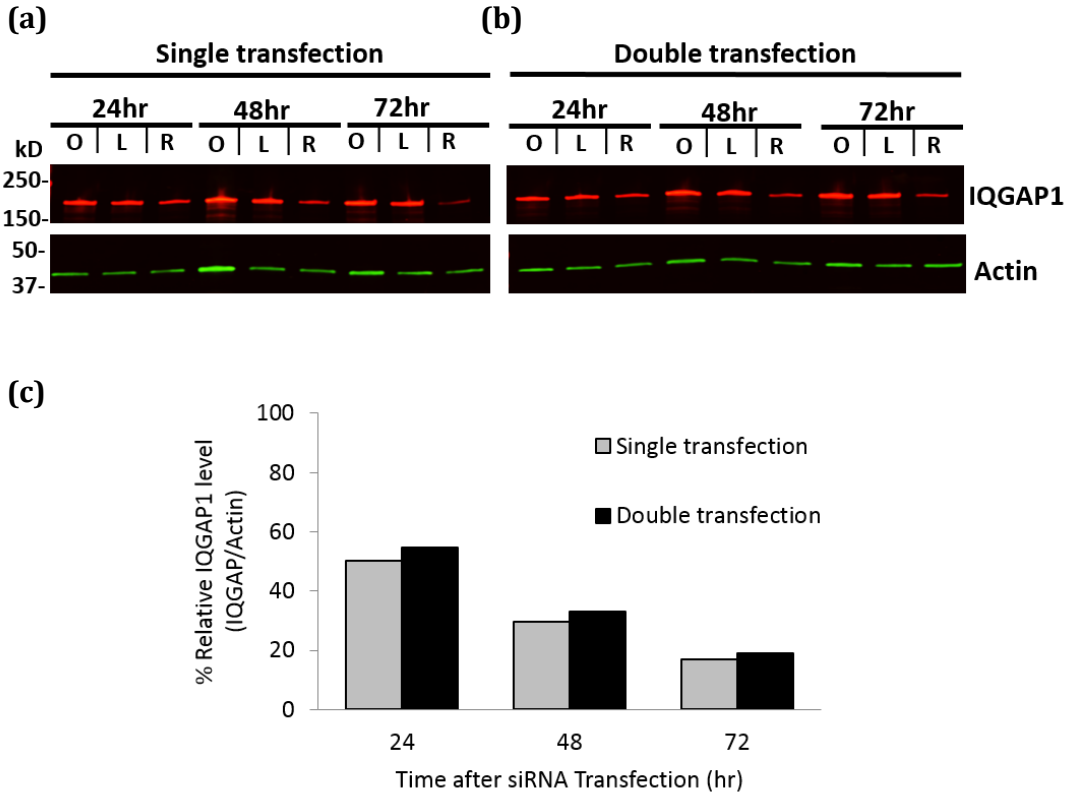

Figure 3.5: The level of IQGAP1 expression in siRNA transfected cells reduced over time

HeLa cells were transfected with siRNAs targeted to IQGAP1 with 6 pmol of siRNA IQGAP1 and 2 µl of Lipofectamine RNAiMAX (R). Cells were incubated for a range of time points before lysis and immunoblotting for IQGAP1 and actin (which was used as a protein loading control). Quantitation of IQGAP1 level was calculated by measuring the intensity of the IQGAP band normalised with the actin band in each sample. For negative controls, HeLa cells were treated with Opti-MEM (O) or Lipofectamine (L). IQGAP1 expression of mock transfection control was considered as 100%. The data was calculated from one individual sample (n=1).

(a) Western blot analysis of IQGAP1 and actin in transfected HeLa cells from single transfection.

(b) Western blot analysis of IQGAP1 and actin in transfected HeLa cells from double transfection.

(c) The expression level of IQGAP1 in HeLa cells was analysed using an Odyssey infrared imager and Image Studio software. From the immunoblot in (a), the level of IQGAP1 expression using single transfection method is shown in grey bar. From double transfection (b) the level of IQGAP1 expression using double transfection method is shown in the black bar.

3.2.4 Confirmation of efficient IQGAP1 knockdown in HeLa cells

To validate IQGAP1 expression in siRNA-mediated IQGAP1 (siIQGAP1) knockdown cells and determine if the siRNA IQGAP1 was having any non-specific effect, such as cell death, a siRNA with a sequence that does not target a known gene was included as a non-silencing siRNA control. A commercial negative control siRNA was utilised for assessing any 'off-target' effect associated with siRNA transfection. HeLa cells were transfected with 6 pmol of siRNA IQGAP1 duplex or siRNA negative control with the same amount of Lipofectamine RNAiMAX and incubated for 72 hours.

From three individual experiments, it was clear that the level of IQGAP1 expression in siIQGAP1 knockdown cells was decreased (Figure 3.6a), and the signal intensity of IQGAP1 from siIQGAP1 knockdown cells was lower than those from siRNA negative control cells (Figure 3.6b). IQGAP1 expression was reduced by 70%, a highly statistically significant difference from the negative siRNA control (Student's *t*-test, $p = 0.0007$) (Figure 3.6b). In addition to immunoblotting, suppression of IQGAP1 expression in siIQGAP1 cells was validated compared with control HeLa cells (Lipofectamine-treated cells) by confocal laser scanning microscopy. The cells were stained to detect IQGAP1 and actin. The result showed cytoplasmic and membrane localisation of IQGAP1 in the control cells, whereas siIQGAP1 knockdown cells showed only weak IQGAP1 expression (Figure 3.6c). The morphology of siRNA IQGAP1-transfected HeLa cells and control cells were not obviously different, indicating that IQGAP1 knockdown by siRNA IQGAP1 did not affect gross cellular morphology.

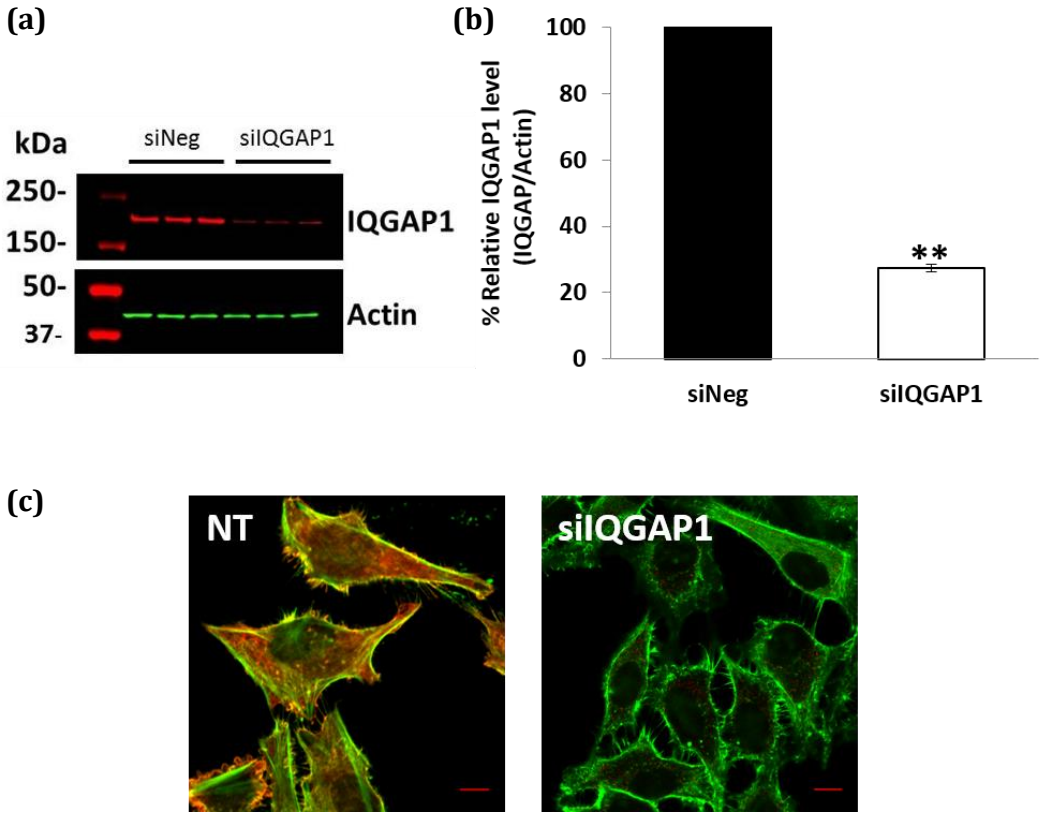

Figure 3.6: Characterisation of IQGAP1 knockdown cells

IQGAP1 knockdown at 72 hours post-transfection with 6 pmol of siRNA IQGAP1 and 2 µl of Lipofectamine RNAiMAX.

(a) Equal total whole cell lysate from negative siRNA control (siNeg) and siRNA-IQGAP1 (siIQGAP1) transfected HeLa cells from 3 independent experiments were resolved by SDS-PAGE. Western blot was probed with anti-IQGAP1 (red) and anti-actin (green) antibodies.

(b) IQGAP1 expression was quantified by signal intensity using Image Studio and normalised with actin expression. Data show the mean ± SEM from three independent experiments (n=3), with negative siRNA control-transfected cells considered as 100%. $p = 0.0007$ (Student's *t*-test).

(c) Representative confocal laser scanning micrographs of HeLa non-transfected cells (NT) and siIQGAP1 knockdown cells. F-actin (green) was stained with Alexa Fluor 488-conjugated phalloidin. IQGAP1 (red) was stained with a rabbit polyclonal antibody and detected with anti-rabbit Ig-Alexa Fluor 568. Scale bar= 10 µm.

3.2.5 Cytotoxicity of siRNA transfected HeLa cells

With an efficiency of IQGAP1 knockdown of more than 70% achieved by using 6 pmol of siRNA IQGAP1 and 2 µl of Lipofectamine RNAiMAX at 72 hours post-transfection, the potential effect of cytotoxicity was assessed by a colorimetric assay. When cells die they release lactate dehydrogenase (LDH) into the culture medium that can be quantified by a coupled enzymatic reaction and measured using a spectrophotometer. LDH catalyses lactate to pyruvate by reduction of NAD^+ to NADH. Then the catalyst (diaphorase) uses NADH to reduce a tetrazolium salt to a red formazan product that can be absorbed by a visible wavelength (490 nm). To examine the effect of IQGAP1 knockdown on cell viability, cytotoxicity was evaluated after 72 hours of transfection compared to the maximum LDH released from lysed control cells taken as 100%. The value of maximum LDH was determined from HeLa cells cultured in DMEM without antibiotics and lysed with BugBuster to break the cells. Cell debris was separated by centrifugation. The supernatant was diluted in the same growth media which was used as a blank control for spectrophotometry. As shown in figure 3.7a, there was little difference in cytotoxicity between non-transfected controls, siRNA negative control and siIQGAP1 knockdown cells. However, negative siRNA control transfected cells showed slightly higher cytotoxicity than siRNA IQGAP1-treated cells but with no statistical significance (Student's *t*-test, $p = 0.1774$). Notably, the three independent experiments involved the use of HeLa cells of increasing passage number. Cytotoxicity continually increased with passage number from set 1 to set 3, though at a low rate (Figure 3.7b). From this finding, HeLa cells at early passage (not more than 25 passages) were used in this study.

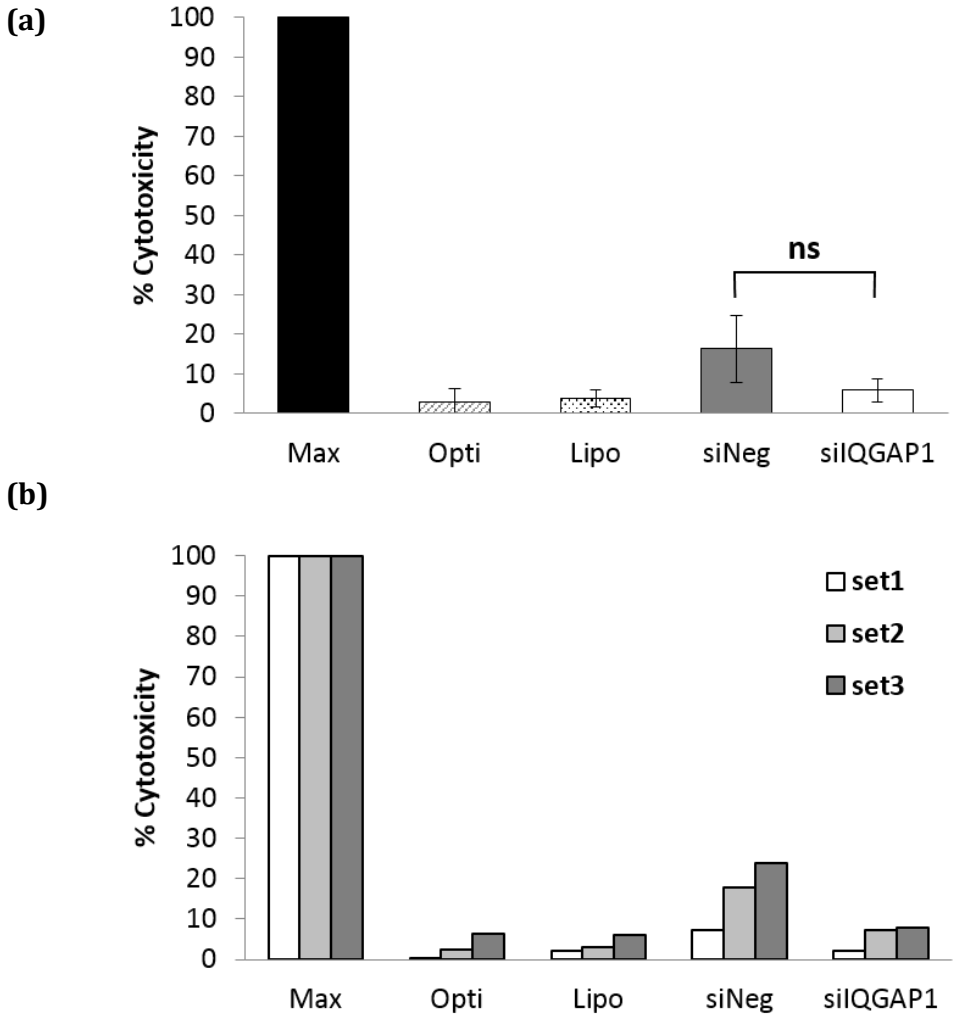

Figure 3.7: Cytotoxic effect of siRNA transfection

Cytotoxic effect of siRNA on the HeLa cells after 72 hours incubation with 6 pmol of siRNA and 2 µl of Lipofectamine RNAiMAX. The percentage of cytotoxicity was calculated from OD 490 nm measuring LDH release from cells into the supernatant. The value of maximum LDH released from control cells (Max) taken as 100%, compared with those from Opti-MEM-treated cells (Opti), Lipofectamine-treated cells (Lipo), siRNA negative control-treated cells (siNeg) and siRNA IQGAP1-treated cells (siIQGAP1).

(a) Data shown are mean ± SD representative of triplicate independent experiments (n=3) with no statistical significance (Student's t-test, $p = 0.1774$).

(b) The same samples in (a) showing individual data from three independent experiments in cells of increasing passage number.

3.2.6 Actin-based motility of *B. pseudomallei* in IQGAP1 knockdown cells

To assess if IQGAP1 is necessary for actin-based motility of *B. pseudomallei*, IQGAP1 knockdown cells and control cells were infected and assessed for actin tail formation by confocal microscopy. In this preliminary observation, after transfection of siRNA IQGAP1 into HeLa cells for 48 hours, the treated cells were infected with *B. pseudomallei* 10276. Actin tail formation of *B. pseudomallei* 10276 at 8, 16, 24 and 32 hours post-infection in cells transfected with negative siRNA control and siRNA IQGAP1 were observed and compared with non-transfected cells. At the specific time point, cells were washed twice in PBS before fixation with 4% PFA/PBS overnight. After permeabilisation with 0.5% Triton X-100 in PBS for 15 minutes, cells were stained with phalloidin and anti-IQGAP1, while the bacteria were stained with anti-LPS antibody. The z-stack images were acquired with identical laser settings using an LSM710 confocal laser scanning microscope. At each of the time points IQGAP1 co-localised with the actin tail of *B. pseudomallei* in non-transfected cells and negative siRNA control-transfected cells. In contrast, some actin tails of *B. pseudomallei* in the IQGAP1 knockdown cells showed a lack of IQGAP1 co-localisation (Figure 3.8 – 3.11). This suggested that *B. pseudomallei* was able to form an actin tail without IQGAP1.

Furthermore, it was noticeable that there was a decrease in cell viability of the *B. pseudomallei* infected negative siRNA control-treated HeLa cells. This is consistent with the previous result of cytotoxicity in the previous section (3.2.5). Negative siRNA control-treated cells showed a higher level of cytotoxicity than other controls and siRNA IQGAP1-transfected cells (Figure 3.7). In spite of the fact that there was no statistical difference of cytotoxicity between the controls, HeLa cells treated with the transfection reagent alone (mock control) was used for further infection experiments.

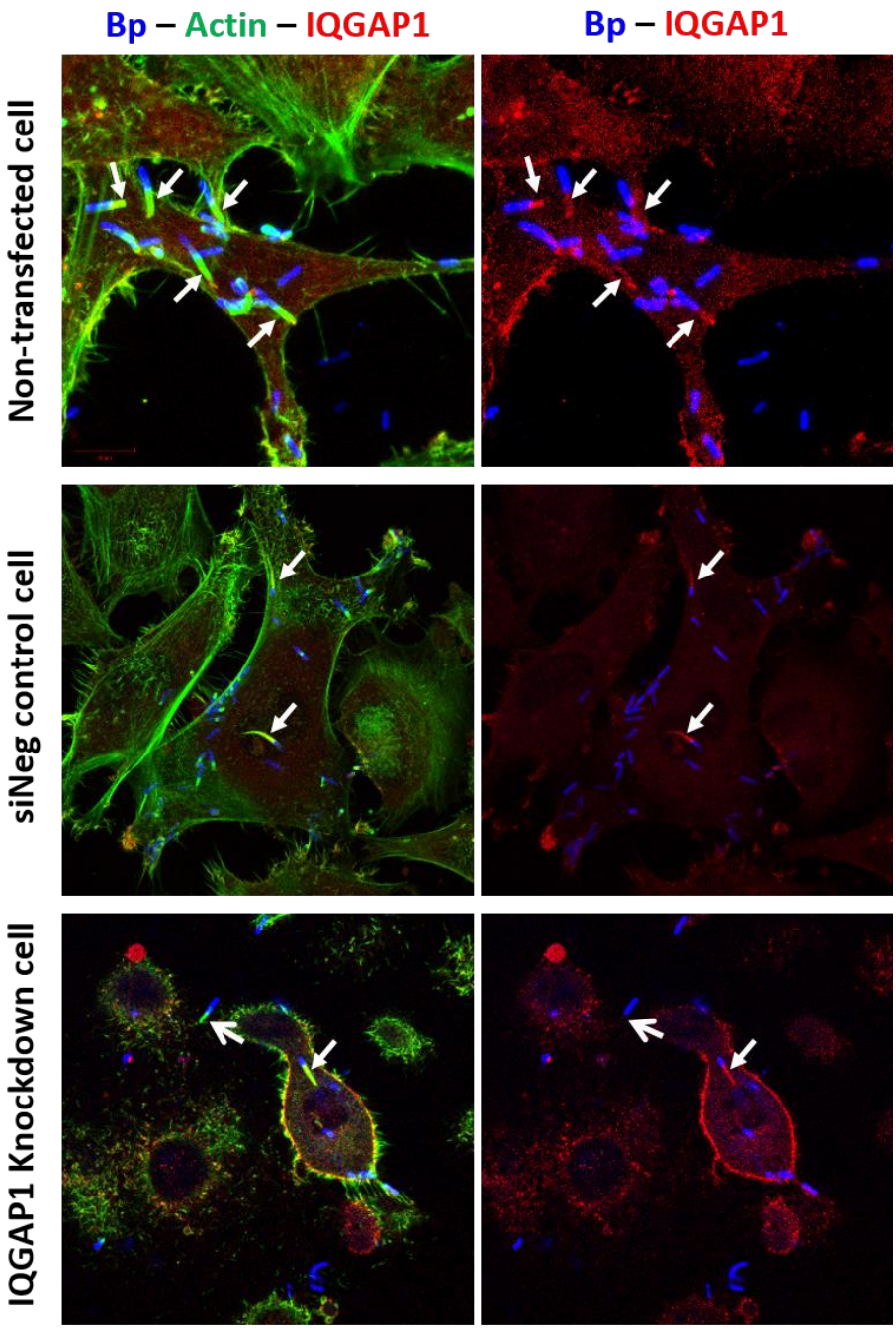

Figure 3.8: Actin tail formation by *B. pseudomallei* in control cells and IQGAP1 knockdown cells at 8 hours post-infection
Confocal micrographs of HeLa cells infected with wild-type *B. pseudomallei* 10276. The left-hand panel shows a merged image of three channels. Bacteria were stained with anti-LPS antibody in blue and cellular proteins, actin and IQGAP1 were stained in green and red respectively. The right-hand panel shows the bacteria and IQGAP1 localisation. → indicates IQGAP1 co-localised with actin in an actin tail. → shows actin tail formation without IQGAP1 co-localisation.

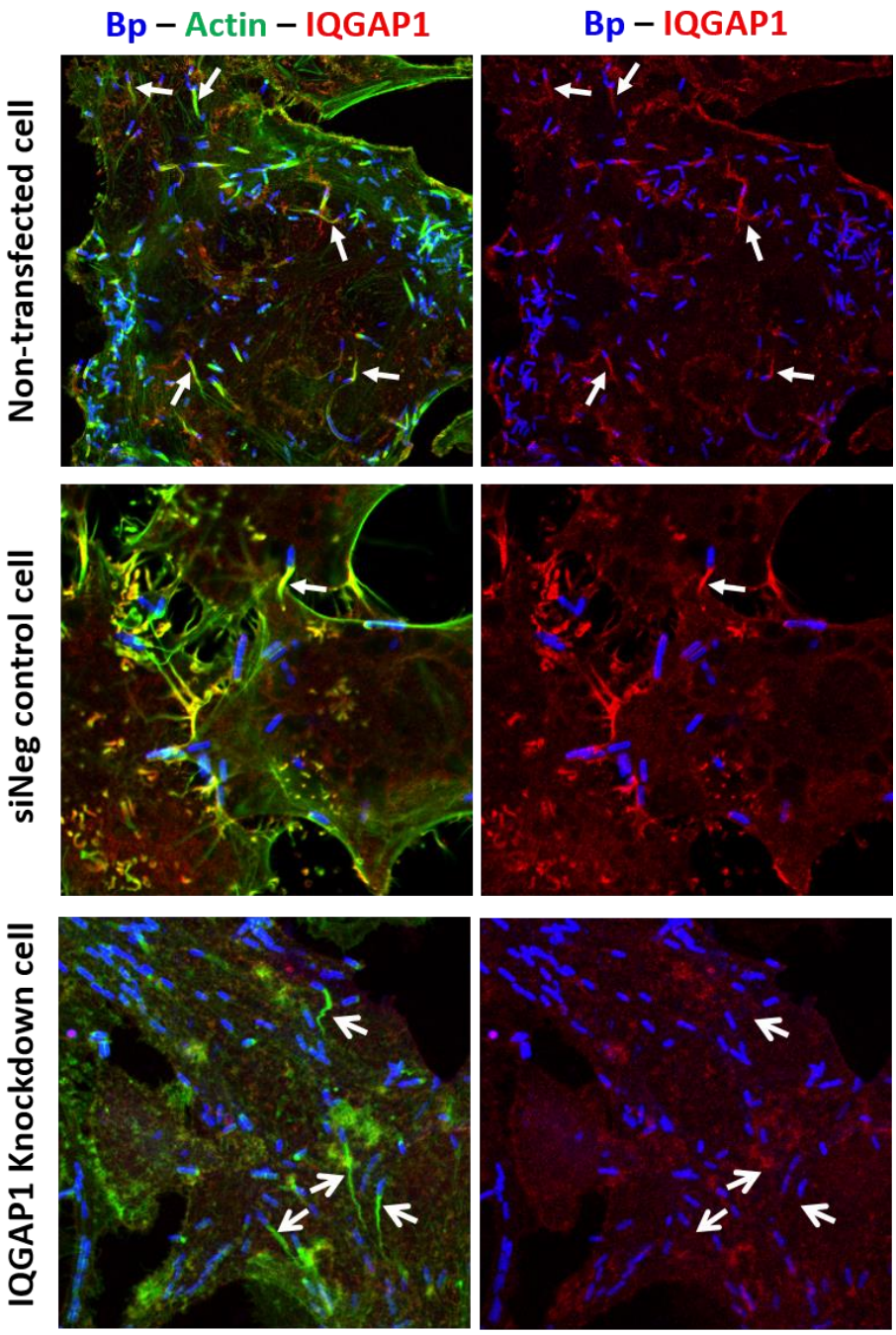

Figure 3.9: Actin tail formation by *B. pseudomallei* in control cells and IQGAP1 knockdown cells at 16 hours post-infection

Confocal micrographs of HeLa cells infected with wild-type *B. pseudomallei* 10276. The left-hand panel shows a merged image of three channels. Bacteria were stained with anti-LPS antibody in blue and cellular proteins, actin and IQGAP1 were stained in green and red respectively. The right-hand panel shows the bacteria and IQGAP1 localisation. → indicates IQGAP1 co-localised with actin in an actin tail. → shows actin tail formation without IQGAP1 co-localisation.

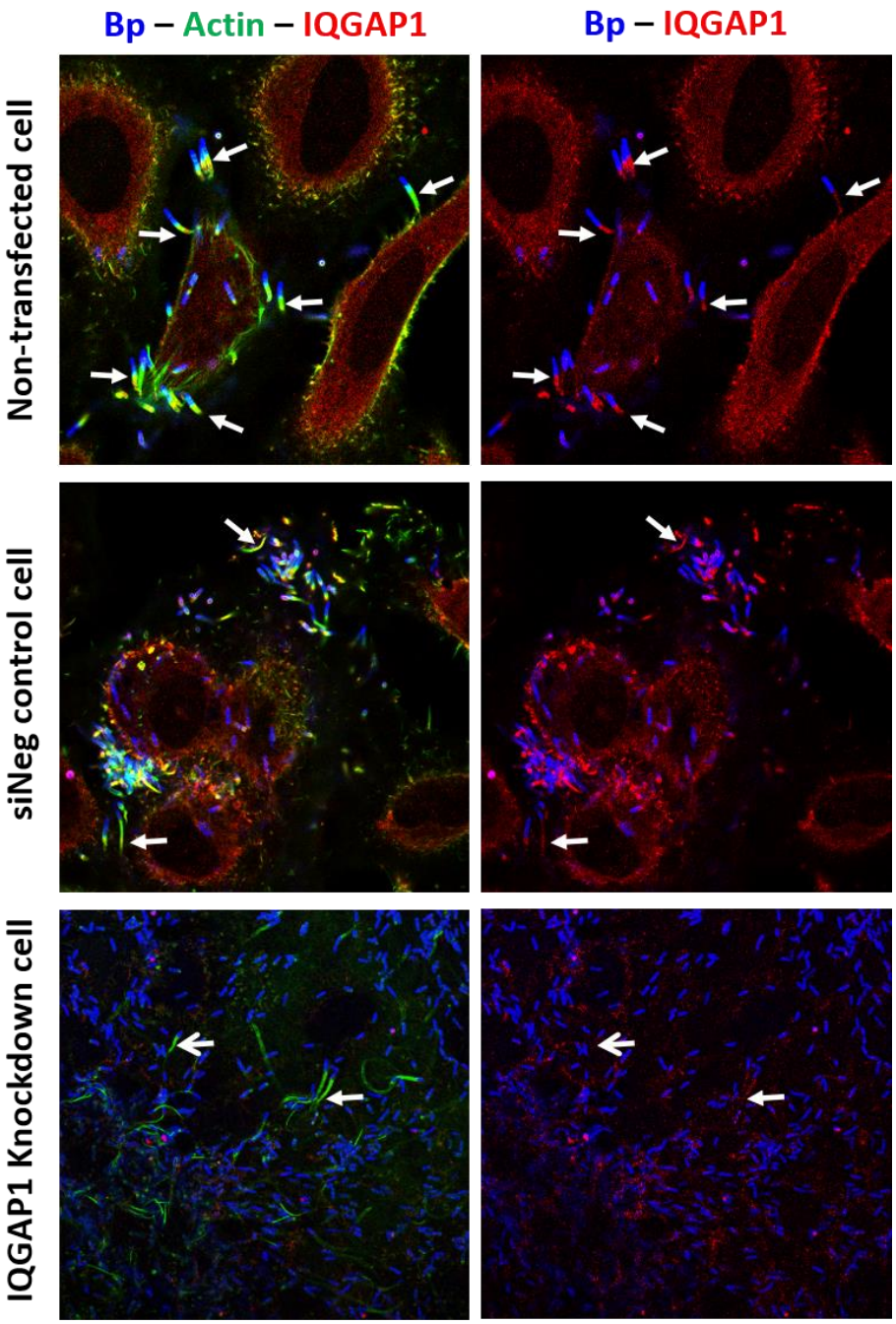

Figure 3.10: Actin tail formation by *B. pseudomallei* in control cells and IQGAP1 knockdown cells at 24 hours post-infection
Confocal micrographs of HeLa cells infected with wild-type *B. pseudomallei* 10276. The left-hand panel shows a merged image of three channels. Bacteria were stained with anti-LPS antibody in blue and cellular proteins, actin and IQGAP1 were stained in green and red respectively. The right-hand panel shows the bacteria and IQGAP1 localisation. → indicates IQGAP1 co-localised with actin in an actin tail. → shows actin tail formation without IQGAP1 co-localisation.

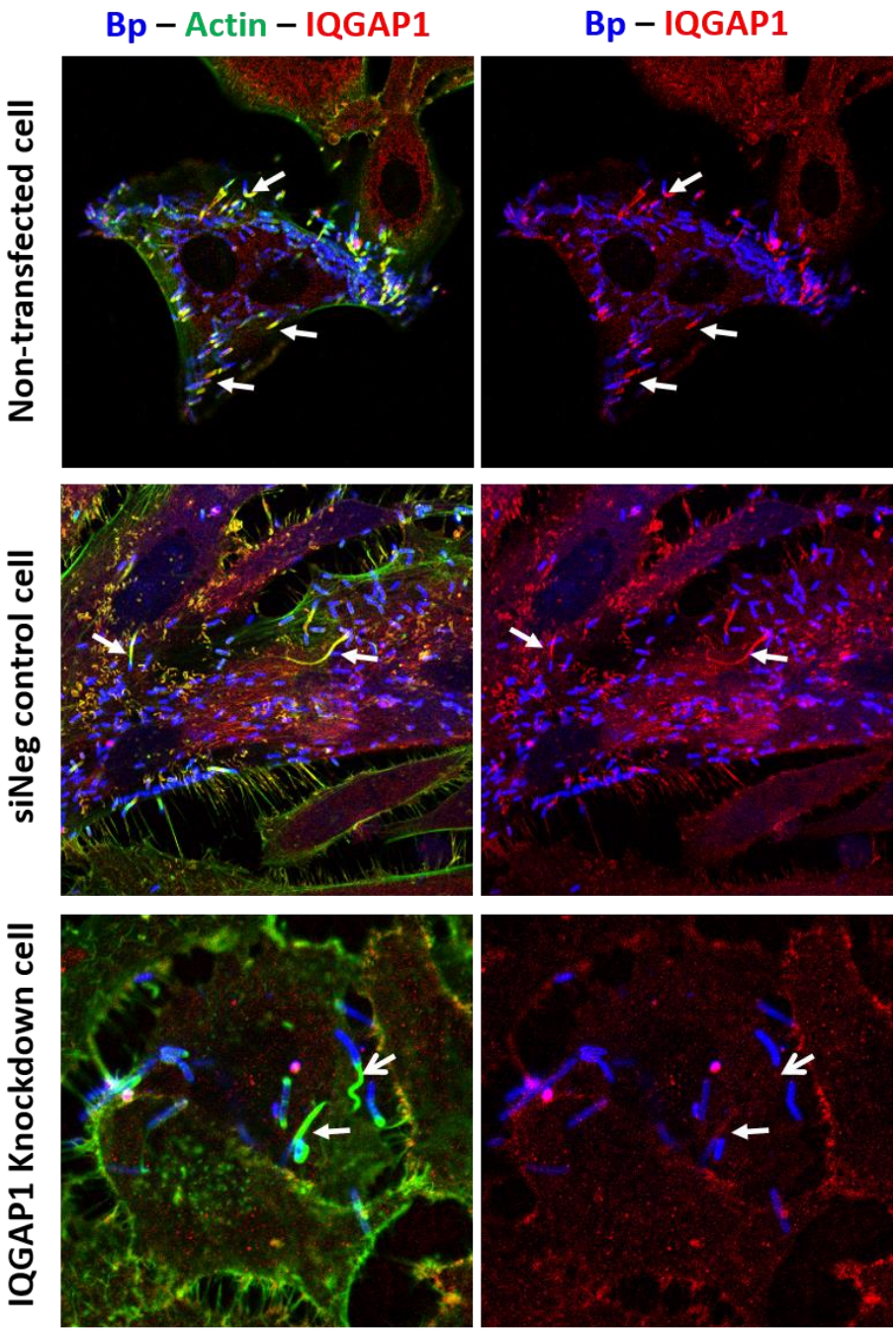

Figure 3.11: Actin tail formation by *B. pseudomallei* in control cells and IQGAP1 knockdown cells at 32 hours post-infection
Confocal micrographs of HeLa cells infected with wild-type *B. pseudomallei* 10276. The left-hand panel shows a merged image of three channels. Bacteria were stained with anti-LPS antibody in blue and cellular proteins, actin and IQGAP1 were stained in green and red respectively. The right-hand panel shows the bacteria and IQGAP1 localisation. → indicates IQGAP1 co-localised with actin in an actin tail. → shows actin tail formation without IQGAP1 co-localisation.

3.2.7 IQGAP1 expression after *B. pseudomallei* infection

To give an assurance that IQGAP1 expression was suppressed when HeLa cells were infected with *B. pseudomallei* 10276, the infected HeLa cells were analysed by immunoblotting to examine IQGAP1 expression in control cells and siIQGAP1 knockdown cells. Remarkably, quantification of IQGAP1 expression by signal intensity, using actin expression as a loading control, showed that the level of IQGAP1 expression in infected cells was statistically greater than in uninfected cells at 24 hours post-infection (Student's *t*-test, $p = 0.0299$) and at 32 hours post-infection (Student's *t*-test, $p = 0.0288$), as shown in figure 3.12a. The same samples were subjected to Western blotting with anti-IQGAP1 and anti-GAPDH antibodies. Figure 3.12b shows that IQGAP1 expression normalised with GAPDH in uninfected siRNA knockdown cells was not significantly different compared to infected cells (Student's *t*-test $p = 0.2086$ and 0.7935 at 24 and 32 hours post-infection respectively). This is an intriguing finding implying that infection of HeLa cells with *B. pseudomallei* alters the total cellular levels of actin.

Next, an experiment was performed to determine the optimal time point post-infection to study *B. pseudomallei* actin tail formation. HeLa cells were transfected with siRNA IQGAP1 and then infected with *B. pseudomallei* for 8, 16, 24 and 32 hours. At each of these time points, the cells were lysed and the level of IQGAP1 knockdown assessed by Western blotting, normalising IQGAP1 levels with the housekeeping protein GAPDH. The initial data showed the lowest expression of IQGAP1 was at 16 hours post-infection and then the levels increased afterwards (Figure 3.13). Additionally, the largest number of bacteria that displayed actin tails in the control cells was observed using confocal microscopy at 16 hours post-infection (Supplemental figure 7.2). Thus, *B. pseudomallei* actin tail formation was examined in the next experiments by infecting cells at 48 hours post-transfection and incubating them for a further 16 hours.

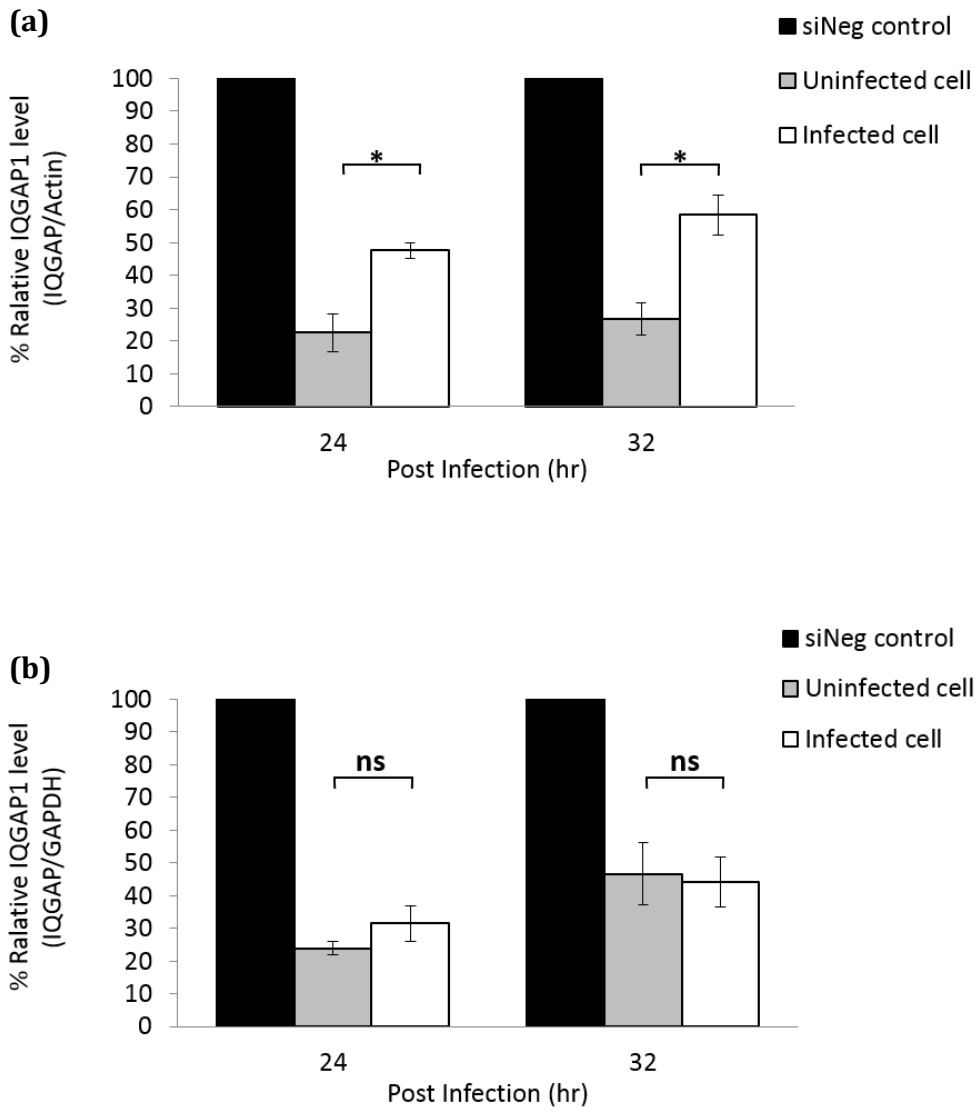

Figure 3.12: Assessment of IQGAP1 levels using actin and GAPDH for normalisation

Level of IQGAP1 expression in uninfected siIQGAP1 knockdown cells (grey bar) compared with *B. pseudomallei* infected-siIQGAP1 knockdown cells (white bar) at 24 and 32 hours post-infection, compared with negative siRNA control-transfected cells (black bar), which were taken as 100%. Data represent mean ± SD of two samples from one experiment (n=2).

(a) Band intensity of IQGAP1 expression was quantified and normalised with actin expression (Student's *t*-test, $p = 0.0299$ at 24 hours post-infection and $p = 0.0288$ at 32 hours post-infection).

(b) Band intensity of IQGAP1 expression was quantified and normalised with GAPDH expression (Student's *t*-test $p = 0.2086$ at 24 hours post-infection and $p = 0.7935$ at 32 hours post-infection).

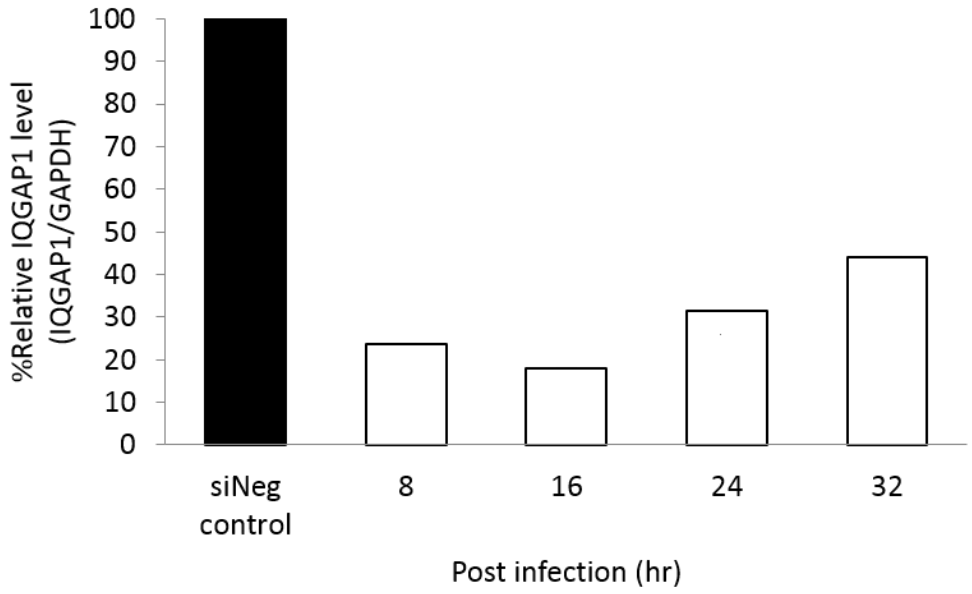

Figure 3.13: IQGAP1 expression in siIQGAP1 knockdown cells after *B. pseudomallei* infection at different time points
Percentage of IQGAP1 expression when normalised with GAPDH, and compared with negative siRNA control that was set as 100%. The data represent an analysis of single samples (n=1).

3.2.8 Analysis of actin tail formation in IQGAP1 knockdown and control cells

To further investigate the role of IQGAP1 in actin-based motility of *B. pseudomallei*, the formation of actin tails in Lipofectamine-treated cells (mock control) and siIQGAP1 knockdown cells were analysed qualitatively. Initially, a total number of 6,847 bacteria were scored manually for the presence of an actin tail, 2,322 bacteria were analysed in control cells and 4,525 bacteria in siIQGAP1 knockdown cells. The proportion of bacteria that were associated with actin in control cells and siIQGAP1 knockdown cells were similar (Figure 3.14a). Next, the bacteria associated with actin were categorised into 4 phenotypes: 'no tail' (no actin was recruited to the bacterial surface), 'barcode' (displayed a pattern of parallel lines of varying widths of actin across the bacterium), 'short tail' (where the length of the actin tail was shorter than the 2 μm length of the bacterium), and 'long tail' (where the length of the actin tail was longer than 2 μm) (Figure 3.14b). From this categorisation, no significant differences were observed between actin tails formed by *B. pseudomallei* in control cells with those in siIQGAP1 knockdown cells (Figure 3.14c).

Then, the bacteria with long actin tails (≥2 μm) were classified into a further 3 types. The first one was called 'comet tail' in which the actin was condensed to form classic 'rocket-like' tails. The second one was 'thin tail' in which the width of the actin tail was smaller than the width of the bacterium. The last type was 'loose tail' which showed faint actin staining. The representative images for each actin tail type are shown in figure 3.15a. A total of 512 bacteria were analysed in control cells and 781 bacteria in siIQGAP1 knockdown cells. Figure 3.15b shows the majority of bacteria displayed a comet tail (black box), whilst the number of bacteria with thin tails showed the smallest proportion (grey box). Although, the number of bacteria with a comet tail in normal control cells was greater than in IQGAP1 knockdown cells. Conversely, bacteria with a loose tail were present in higher number in siIQGAP1 knockdown cells than in normal control cells. Next, the images were analysed with ImageJ software to obtain quantitative data.

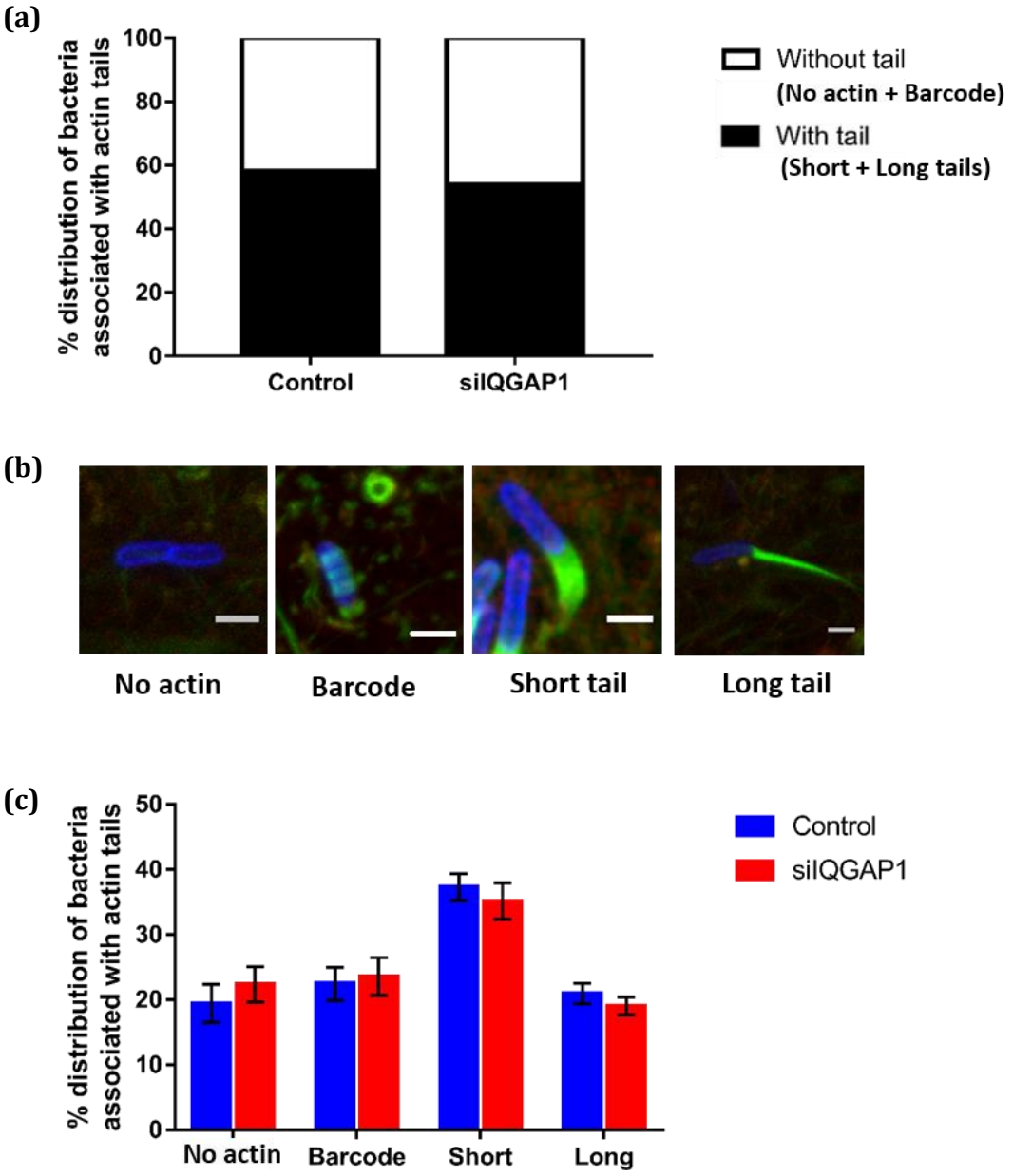

Figure 3.14: Analysis of *B. pseudomallei* actin tail formation in control and siIQGAP1 knockdown cells from performing of three independent experiments.

(a) Distribution of bacteria associated with or without an actin tail (Student's *t*-test, p = 0.3452 for bacteria with and without tail, n = 16 for control cells and n = 17 for siIQGAP1 cells).

(b) Confocal micrographs showing a representative image of the different actin tail morphology formed by *B. pseudomallei* (Student's *t*-test, p = 0.4620 for no tail, p = 0.7745 for barcode, p = 0.5402 for short tails and p = 0.3667 for long tails, n = 16 for control cells and n = 17 for siIQGAP1 cells).

(c) Percentage distribution of bacteria associated with actin tails of each morphology in control cells (blue bar) compared to siIQGAP1 knockdown cells (red bar) from 3 independent experiments. Add stat

(a)

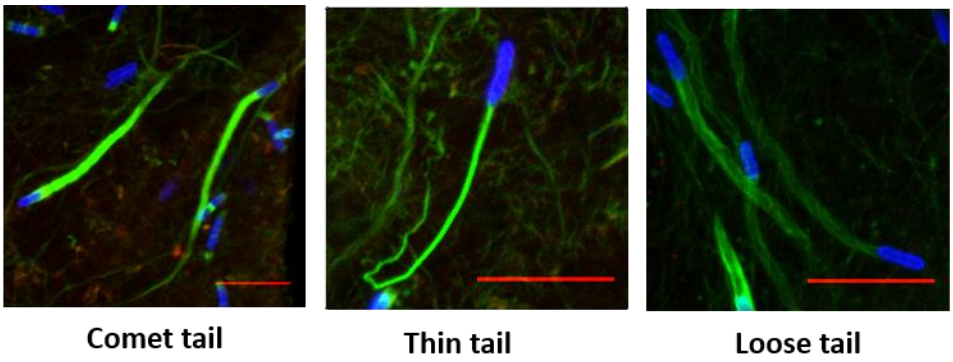

(b)

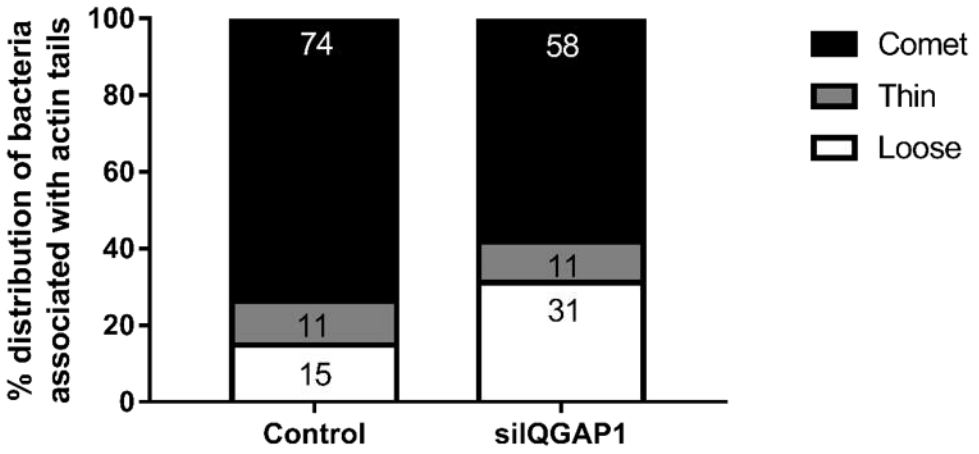

Figure 3.15: Qualitative analysis of the morphology of actin tail formed by *B. pseudomallei* in control and siIQGAP1 knockdown cells

(a) Confocal micrograph of HeLa cells infected with *B. pseudomallei* 10276 showing actin tail phenotypes. Scale bar = 10 μm.

(b) Percentage of bacteria tail morphologies (≥2 μm long) in control HeLa and siIQGAP1 knockdown cells.

3.2.9 IQGAP1 plays a role in determining the actin density and length of actin tails formed by *B. pseudomallei*

In the previous section, over 2000 bacteria were imaged from each infected cell type across 3 biological replicates and scored manually for actin tail morphology. The proportion of bacteria with and without actin tails were similar in control cells and IQGAP1 knockdown cells. However, the actin tails appeared to have a lower actin density in siIQGAP1 knockdown cells. To substantiate this finding, ImageJ software was used to measure the length of the actin tail and quantify the actin density by measuring the fluorescence intensity along the tail structure. One hundred actin tails with the length longer than 2 μm from control and siRNA IQGAP1 transfected HeLa cells, across 3 biological replicates, were analysed from maximum intensity projection z-stack images that were captured with identical laser settings using an LSM710 laser scanning confocal microscope. The data showed a statistically significant increase in overall tail length (p = 0.0033, Figure 3.16a), with a concomitant decrease in actin density (p = 0.0001, Figure 3.16b), in siIQGAP1 knockdown cells compared with control cells. RNAi-mediated knockdown of IQGAP1 expression in Hela cells resulted in a significant increase in the length of actin tails, a mean length of 20.5 μm compared to a mean length of 14.8 μm in control cells (Figure 3.16a). Although longer in length, the actin density of tails generated in siIQGAP1 knockdown cells was lower with a mean signal of 1,036 A.U. compared to a mean signal of 2,522 A.U. measured for tails in control cells (Figure 3.16b). Taken together, this result supports a role for IQGAP1 in controlling *B. pseudomallei* actin tail length and density.

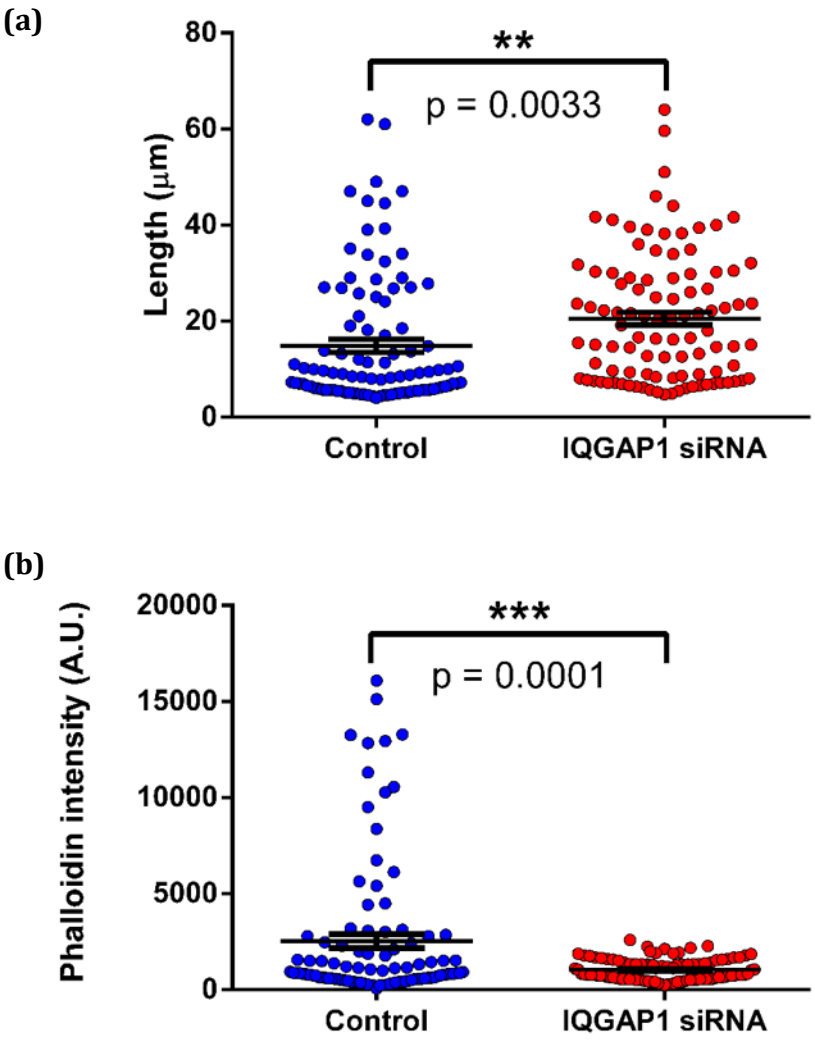

Figure 3.16: IQGAP1 affects *B. pseudomallei* actin tail length and density
HeLa cells were infected with *B. pseudomallei* 10276 for 16 hours post-infection before fixing. Bacteria, IQGAP1 and actin were stained and images captured by confocal microscopy. Length of actin tail and signal intensity were quantified using ImageJ software. 100 bacteria from three independent experiments of each sample, control cells and IQGAP1 knockdown cells were observed (n=3).

(a) Scatter plot indicating the length of actin tail formed by individual bacteria displaying tail longer than 2 μm. The data represent mean ± SEM and asterisks denote lengths are significantly different from each other (Unpaired *t*-test; p = 0 .0033).

(b) Scatter plot indicating the intensity of actin recruited by individual bacteria displaying tail longer than 2 μm. The data represent mean ± SEM and asterisks denote actin intensity is significantly different from each other (Unpaired *t*-test; p = 0 .0001).

3.2.10 Expression of IQGAP2 and IQGAP3 in HeLa cells

The preliminary result showed that IQGAP1 co-localises with the actin tails of *B. pseudomallei* in non-transfected cells and negative siRNA control-transfected cells. In contrast, IQGAP1 knockdown cells showed some actin tails of *B. pseudomallei* without any IQGAP1 co-localisation. This suggested that *B. pseudomallei* was able to form an actin tail without IQGAP1. However, an explanation for this observation could be that the lack of IQGAP1 expression may be compensated by the expression of IQGAP2 and IQGAP3 isoforms in the cells.

IQGAPs are differentially expressed in tissues. The Human Protein Atlas (http://www.proteinatlas.org/) indicates that the mRNAs for the IQGAP2 and IQGAP3 genes are expressed in HeLa cells (Supplemental figure 7.3). To test the presence of IQGAP2 and IQGAP3 in HeLa cells, Western blot analysis was performed. Figure 3.17 shows that IQGAP2 and IQGAP3 are both expressed in HeLa cells. Unfortunately, despite testing a wide range of commercially-available antibodies against the IQGAP2 and IQGAP3 proteins, none were suitable for confocal microscopy analysis. This leaves open the possibility that the IQGAP1-negative tails detected in this study may have arisen from the functional compensation of IQGAP1 by the other IQGAP family members.

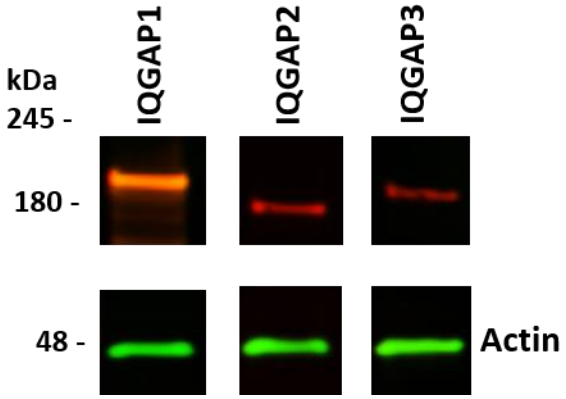

Figure 3.17: IQGAP2 and IQGAP3 expression in HeLa cells
The same amount of total HeLa cell lysate was resolved by SDS-PAGE and probed with anti-IQGAP1, anti-IQGAP2 (sc-17835), and anti-IQGAP3 (Ab136976) in red and anti-actin antibodies in green. Using the same sample blotted on the same membrane, to detect each protein, the membrane was cut and probed with the specific antibody. To detect IQGAP2 and IQGAP3, the membranes were scanned with a higher intensity than IQGAP1 using an Odyssey infrared imager.

3.3 Discussion

The work described in this chapter arose from the valuable data set of 30 host cellular proteins identified by an affinity approach using bacteria expressing BimA under actin polymerising conditions *in vitro* (Jitprasutwit et al., 2016). From the protein list generated previously in our laboratory, IQGAP1 was identified as an interesting candidate host protein to study its functional role in *B. pseudomallei* actin-tail formation. Despite many studies on the actin-based motility of other intracellular bacterial pathogens, none showed localisation of IQGAP1 in the actin tail. Many studies demonstrated that pathogens target IQGAP1 to regulate the host cell cytoskeleton to facilitate their infection. In fact, a recent study showed the interaction between the OspB *Shigella* effector and IQGAP1 limits *Shigella* spreading within a cell monolayer (Lu et al., 2015b). In spite of this, subcellular localisation of IQGAP1 with the *Shigella*-actin tail in infected cells was not reported (Lu et al., 2015b). Taken together, IQGAP1 was selected for investigation in this study because IQGAP1 is a novel cellular protein identified in actin-based motility of *B. pseudomallei* and potentially other bacteria that display actin-based motility.

In this study, confocal microscopy revealed that IQGAP1 is recruited to the *B. pseudomallei* actin tail. Then the localisation of IQGAP1 in *B. pseudomallei* infected cells over a time course was examined. The results showed that at even the earliest time point of the study (8 hours post-infection), IQGAP1 co-localised with *B. pseudomallei* actin tails. Similarly, at later time points (16, 24 and 32 hours post-infection), IQGAP1 was recruited throughout the tail of *B. pseudomallei*, indicating that IQGAP1 is possibly involved in actin-based motility. At 16 hours post-infection, the greatest number of bacteria associated with actin tails were observed. It could be seen that most of the bacteria displayed a compact (comet-like) actin tail. However, the bacteria did not form actin tails with a specific uniform structure. In fact, a proportion of bacteria were associated with actin tails composed of loosely bundled actin filaments. This observation is in agreement with a recent report by Benanti and co-authors (Benanti et al., 2015). The loosely bundled tail is reminiscent of those described for certain *Rickettsia* species reliant on the formin-like Sca2 autotransporter for actin polymerisation (Haglund et al., 2010). Furthermore, it was noticeable that IQGAP1 was recruited in each of the actin tail structures formed by *B. pseudomallei*. This may imply that other host cellular proteins play a role in actin tail

formation which might lead to a variety of actin tail morphology, possibly using IQGAP1 as a scaffold to act in concert to regulate actin-based motility.

To dissect the role of IQGAP1 in *B. pseudomallei* actin-based motility, RNAi-mediated gene knockdown was performed. In this study, conditions of transfection were optimised to obtain the greatest level of IQGAP1 knockdown. After adjustment of the transfection conditions, IQGAP1 expression was decreased by more than 70% as assessed by IQGAP1 immunoblotting. Upon depletion of IQGAP1 by siRNA, it was found that the number of bacteria associated with actin tail was similar to those in control cells. There is a possibility that IQGAP1 is involved in the number of bacteria able to form tails, but the residual levels of IQGAP1 in knockdown cells is enough to support tail formation. Nevertheless, when the different actin tail morphologies were categorised (no tail, barcode, short and long tails) the number of bacteria with long loose tails was greater in IQGAP1 knockdown cells. To verify this observation, confocal images were analysed using ImageJ software. This present study revealed the length of actin tails formed by *B. pseudomallei* in HeLa cells showed a mean of 14.8 μm with the longest of 62 μm. A previous study on actin tail formation of *Burkholderia* species by Benanti and colleagues (2015) observed the length of actin tail formed by *B. pseudomallei* in A549 and Cos7 cells. They showed that the mean length of a *B. pseudomallei* actin tail was approximately 20 μm with the longest tails of 82 μm in A549 cells, and a mean of 15 μm with the longest tails of 65 μm in Cos7 cells (Benanti et al., 2015). This different value could be a result of experimental methods. Length of *B. pseudomallei* actin tail formation was observed at 16 hours post-infection in this study, whereas the study of Benanti and colleagues (2015) examined at 10 hours post-infection. Additionally, there may be significant differences in the proteins expressed by these different cell types that are able to support actin-based motility. Bacterial factors also should be taken into account because *B. thailandensis* strains engineered to have different BimA orthologues were subjects of their study (Benanti et al., 2015).

Comparison between control HeLa cells and IQGAP1-depleted cells showed a significant difference in density and length of *B. pseudomallei* actin tail. The bacterium formed tails with a lower actin density but a longer tail in cells with reduced IQGAP1 expression. These results suggested that IQGAP1 plays role in controlling the length and actin density of *B. pseudomallei* actin tails. Previous studies

showed a defect in actin tail formation in length and morphology could influence motility rate and affected bacterial infectivity. For example, SFG *R. perkeri* showed abnormal actin tails with a shorter actin tail in profilin-depleted cells (Serio et al., 2010). Although this work demonstrated the localisation of profilin to *Rickettsia* actin tails in mammalian cells, the absence of this host factor in the *Rickettsia* tail in profilin siRNA-treated cells control was not reported (Serio et al., 2010). The reduction of profilin in the RNAi cells caused a reduction of motility rate of *Rickettsia* but not *L. monocytogenes* (Serio et al., 2010). This suggested that host factors are exploited by the bacterial pathogens with a specific and distinct role.

In spite of this, it was evident that *B. pseudomallei* could still form actin tails in the knockdown cells. This may be a result of compensation by the related IQGAP proteins IQGAP2 or IQGAP3, which are also expressed in HeLa cells as verified by Western blot analysis. This finding disagrees with a previous study that used RT-PCR and immunoblotting with specific antibodies and showed the expression of IQGAP1 and IQGAP3, but not IQGAP2, in HeLa cells (Adachi et al., 2014). A reason for the discrepancy may, in fact, be the specificity of antibodies. To verify whether the loss of IQGAP1 is compensated by IQGAP2 or IQGAP3 for actin-based motility of *B. pseudomallei*, confocal microscopy of infected cells would be required. However, this speculation could not be confirmed because of a lack of specific antibodies available for immunostaining to detect IQGAP2 and IQGAP3 in *B. pseudomallei* infected cells. Compensation mechanisms in the IQGAP family would be possible because of the conservation of multiple functional domains. Indeed, one report indicated that IQGAP3 partially compensates for the functions of IQGAP2 to promote axon outgrowth in hippocampal neurons (Wang et al., 2007). However, there is no evidence in the literature that the loss of IQGAP1 can be compensated with other IQGAPs. From the similarity of domain structure of these proteins and the fact that they have common interacting partners, such as actin, it is a possibility that these IQGAP2 and IQGAP3 isoforms could compensate for the loss of IQGAP1 in our assay. However, this would require further experimentation to investigate. For example, double knockdown, suppression of both IQGAP1 and IQGAP2, or both IQGAP1 and IQGAP3, and reconstituting IQGAP1-knockdown cells with wild-type IQGAP1 could be performed.

Additionally, the residual IQGAP1 expression in the siIQGAP1 knockdown cells may be a reason why the bacteria can still form actin tails, although confocal microscopy revealed that there was no IQGAP1 recruitment in some actin tails. An approach to understanding whether IQGAP1 plays a role in actin-based motility of *B. pseudomallei* or not could utilise cells derived from IQGAP1 knockout mice (Li et al., 2000). A study of the role of IQGAP1 in *Salmonella* cell invasion revealed that IQGAP1 was required for invasion by regulating actin polymerisation in the phagocytic cup (Brown et al., 2007). By using siRNA knockdown, which decreased IQGAP1 expression by 75%, the percentage of *Salmonella* Typhimurium SL1344 invasion was reduced by 33%. When invasion was tested on mouse embryonic fibroblasts (MEFs) from IQGAP1 knock-out mice, the number of intracellular bacteria was significantly lower than those in control MEFs, 77% (Brown et al., 2007). A similar finding was published showing that IQGAP1-null MEFs were less able to support actin pedestal formation by EPEC (Brown et al., 2008). A study of *S. flexneri* intercellular spreading using the MEFs lacking IQGAP1 showed that the area of bacterial spread increased in the absence of IQGAP1, suggesting a role for IQGAP1 in restriction of *S. flexneri* spread in cell monolayers (Lu et al., 2015b). However, in our hands, siIQGAP1 knockdown cells were not useful for studying the intracellular life of *B. pseudomallei* because IQGAP1 knockdown is transient. It should be noted that invasion and intracellular survival of *B. pseudomallei* in IQGAP1-depleted cells in this study were not statistically significant difference when compared to control cells (Supplemental figure 7.4). Moreover, a monolayer of siIQGAP1 knockdown cells could not be obtained to study cell-to-cell spreading.

Unfortunately, we did not have access to IQGAP1 knockout mice or MEFs. When this study was ongoing, the CRISPR-Cas9 technique was a new powerful technique to specifically knockout target genes in cell lines. This technique was applied to study the role of IQGAP1 in *B. pseudomallei* intracellular life in the next chapter.

Chapter 4
Investigating the role of IQGAP1 in intracellular life of *B. pseudomallei*

4.1 Introduction

Several studies have demonstrated the impact of actin-based motility on intracellular life of bacterial pathogens. Particularly, it is important for the cell-to-cell spread of bacteria. Bacterial mutants incapable of actin-based motility show defects in cell-to-cell spread in cultured cells, and are also compromised for virulence (Reviewed in Choe and Welch, 2016). The *Listeria monocytogenes actA* mutant strain, that was unable to accumulate actin around individual bacteria, was incapable of infecting adjacent cells and demonstrated significant attenuation of virulence (Domann et al., 1992, Kocks et al., 1992). Whilst the *actA* mutant did not show a defect in replication within L929 fibroblast cells, its ability to form plaques was compromised (Domann et al., 1992). Similarly, a *Shigella flexneri icsA* mutant that did not accumulate F-actin either on the surface or around the bacteria, lost its capacity to spread intracellularly and was impaired in plaque formation in confluent monolayers of HeLa cells (Bernardini et al., 1989). For *R. parkeri* both the *rickA* and *sca2* mutants exhibited significantly smaller plaque size than wild-type (Reed et al., 2014). Whilst the *rickA* mutant was impaired in actin tail formation in the early stage of infection (30 minutes post-infection) with no defect in late tail formation at 48 hours post-infection, the *sca2* mutant was partially defective in tail formation in the early stage but not able to form an actin tail in the later stage of infection (Reed et al., 2014). Moreover, the *sca2* mutant formed significantly smaller plaques than the *rickA* mutant (Reed et al., 2014), which agreed with the small plaques generated from *R. rickettsii sca2* mutant (Kleba et al., 2010). These results suggested that Sca2 is important in the later stage of *Rickettsia* infection to facilitate efficient cell spreading (Reed et al., 2014).

In addition to cell-to-cell spread, bacteria can manipulate the host cellular protective autophagy pathway using actin-based motility, allowing the bacteria to survive and replicate in infected cells. ActA, the bacterial surface protein of *L. monocytogenes* recruits host actin to avoid autophagic recognition (Yoshikawa et al. 2009). On the other hand, IcsA-mediated actin polymerisation of *S. flexneri*

stimulates autophagy by IcsA binding to the autophagy protein Atg5, resulting in *Shigella* uptake by autophagosomes followed by degradation (Ogawa et al., 2005). However, *Shigella* secretes a T3SS effector IcsB which inhibits the IcsA/Atg5 interaction and prevents the autophagic recognition of the bacterium (Ogawa et al., 2005). IcsB interacts with Toca-1 which is a host protein required for efficient actin tail formation of *S. flexneri* and for inhibition of recruitment of a marker of autophagy (LC3) around intracellular *S. flexneri* (Baxt and Goldberg, 2014, Leung et al., 2008). Moreover, another host cytoskeleton factor known as septin targets and traps *Shigella* by forming septin cages surrounding the bacteria to promote autophagy (Mostowy et al., 2010).

The mechanism of cell-to-cell spread by *Burkholderia* spp. is different from other bacteria that display actin-based motility. Whilst *Listeria* and *Shigella* spp. form double-membrane protrusions from an infected cell which are then engulfed by the adjacent uninfected cells, *Burkholderia* spp. induce multinucleated giant cell (MNGC) formation by fusion of infected cells with the neighbouring cells to mediate spreading (Kespichayawattana et al., 2000, French et al., 2011). *bimA* mutants show a significant defect in cell-to-cell spread without visible plaque formation (Sitthidet et al., 2011, French et al., 2011, Benanti et al., 2015). Understanding of how *B. pseudomallei* actin-based motility mediates escape from cellular detection and killing mechanisms is lacking. A recent study showed a reduction of net intracellular replication of a *bimA* mutant in J774.2 macrophage-like cells (Lazar Adler et al., 2015). In the same study, the authors also demonstrated that BimA plays a role in the virulence of *B. pseudomallei* since the *bimA* mutant had a 10-fold increased median lethal dose in a BALB/c mouse model of melioidosis compared to the wild-type *B. pseudomallei* 10276 (Lazar Adler et al., 2015). This finding agrees with our own unpublished observations that a *bimA* mutant shows impaired intracellular survival, a lack of plaque formation in A549 cell monolayers, reduced virulence in a mouse model of infection (Figure 1.3 in Chapter 1) and reduced virulence in *Galleria mellonella*.

The results described in chapter 3 demonstrated that IQGAP1 play a role in actin tail formation of *B. pseudomallei*. To elucidate the role of IQGAP1 in *B. pseudomallei* intracellular life, IQGAP1 knockout cells were generated by CRISPR-Cas9 technique in this chapter. CRISPR-Cas9 is a new gene-editing technology that

can be programmed to cleave specific DNA target sites in living cells and organisms. This technique is adapted from the CRISPR-Cas systems that are found in bacterial and archaeal genomes as immune mechanisms to degrade foreign nucleic acid by inducing sequence-specific DNA double-stranded breaks (DSBs). The type II CRISPR-Cas from *Streptococcus pyogenes* has been widely used for targeted genome editing. **C**lustered **R**egularly **I**nterspaced **S**hort **P**alindromic **R**epeats (CRISPR) is a region in bacterial genomes required for pathogen defence by incorporating a variable sequence from the foreign genetic element. CRISPR locus contains a cluster of genes including nucleases called Cas9 (**C**RISPR-**as**sociated protein **9**) which recognises the target DNA via Watson-Crick base pairing and cleaves the target creating a DSB to prevent proliferation and propagation of invading genetic elements (Cong et al., 2013).

To modify the genome with high precision, a guide RNA (gRNA), also known as a single guide RNA (sgRNA), can be designed to define the genomic target to be modified, where the protospacer-adjacent motif (PAM) flanks the 3′ end of the DNA target site. Once a DSB has been created, it can be repaired via either the Non-Homologous End Joining (NHEJ) pathway or the Homology-Directed Repair (HDR) pathway. NHEJ pathway is rapidly activated to repair DSBs, but it generates random mutations with either nucleotide insertions or deletions (InDels) at the DSB site. These mutations on the target DNA result in changes in the amino acid sequence, in-frame or frameshift mutations. Premature stop codons can be introduced within the open reading frame (ORF) causing a loss-of-function mutation within the targeted gene. In contrast, the HDR pathway is less efficient but more accurate. The DSB can be repaired by introducing a specific mutation as a donor template that contains the desired mutation, insertion or modification, flanked by segments of DNA identical to the original DNA sequence at the DSB. The desired mutation is generated through recombination. The DSB is processed to create a 3’ overhang and then the invasion of the 3’ single-stranded DNA displaces one strand of the homologous donor DNA duplex. The invasive strand pairs with another strand before synthesis of new DNA using the homologous DNA sequence as a template to repair the DSB (Reviewed in Sander and Joung, 2014).

In this chapter, the first aim was to permanently disrupt IQGAP1 gene function by creating a HeLa IQGAP1 knockout cell line without regard for specific mutation. Thus, the NHEJ repair pathway was utilised to generate random loss-of-function mutations. Having generated an IQGAP1 knockout cell line, the impact of IQGAP1 on intracellular life of *B. pseudomallei* was then investigated.

4.2 Results

4.2.1 Optimisation of double nickase plasmid transfection

In this study, a commercial double nickase plasmid was employed to generate IQGAP1 knockout cells. The plasmid provided by the manufacturer (Santa Cruz Biotechnology) incorporates 20-bp sgRNAs designed to target exon 13 of the *Homo sapiens* IQGAP1 gene, which consists of a total of 39 exons (Gene ID: 8826, Genomic Sequence: NC_000015.10). The guide sequences were analysed by nucleotide BLAST using 'Human genomic plus transcript' search set to test the specificity of the sgRNAs to IQGAP1. Each sgRNA is followed by PAM 5′-NGG-3′ site which is a prerequisite for Cas9 cleavage.

From the NCBI Reference Sequence of the *Homo sapiens* IQGAP1 gene (NM_003870.3), the sgRNAs target the opposite strand, at base 1474-1493 and 1465-1446. Thus, the distance between the PAM-distal 5′ ends of the sgRNA pair was 8 bp, which created 42 bp 5′- overhangs (Figure 4.1). The offset of +8 bp was in the range of an optimum gap (0-20 bp) between sgRNA pairs to allow for specific Cas9-mediated double nicking of the genomic DNA mimicking a DSB (Ran et al., 2013). The expected consequence of double-strand break-mediated InDels is the production of a stop codon or nonsense mutation leading to a premature mRNA which is marked for degradation and the protein cannot be expressed.

The double nickase plasmids used in this study consists of a pair of plasmids each encoding a Cas9n (D10A) nuclease and sgRNA which is chimeric between crRNA and tracrRNA targeting opposite strands of the human IQGAP1 locus. In the pair, one plasmid contains a GFP marker for monitoring transfection efficiency and another one contains a puromycin-resistance gene for selection. In addition, each plasmid contains the U6 RNA polymerase III promoters for sgRNA expression. Two nuclear localisation signals (NLSs) that efficiently target Cas9 to the nucleus were included (Cong et al., 2013). A chicken β-actin hybrid (CBh) promoter controls Cas9n and puromycin resistance gene expression. A small sequence encoding a 2A-peptide, which is a self-cleaving peptide, was also included to produce two individual proteins from one transcript allowing the production of Cas9 and either puromycin resistance or GFP from the same CBh promoter.

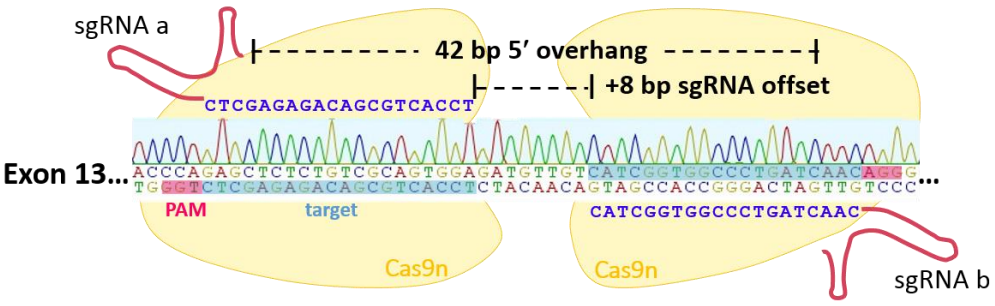

Figure 4.1: Double nickase mediates a DNA double-strand break within the target DNA

Schematic illustrating DNA double-stranded breaks generated from a pair of sgRNA that was designed for the human IQGAP1 locus targeting within exon 13. The distance between the 5′-ends of the guide sequence is 8 bp. The pair of sgRNA-Cas9n complexes nicks both strands creating 5′ overhangs.

HeLa cells were used to generate IQGAP1 knockout cells using the commercial double nickase plasmids described earlier. Lipofectamine® 2000 reagent was used for delivery of the plasmid into HeLa cells. For a successful transfection, the amount of Lipofectamine was optimised. Firstly, a control plasmid (pECFP-C1) expressing cyan fluorescent protein (CFP) was utilised to determine the optimum amount of transfection reagent to use in this cell line. One day before transfection, HeLa cells were cultured on a coverslip in a 6-well plate to obtain 70-90% confluency on the day of transfection. The same amount of plasmid (2.5 μg) was tested with four concentrations of Lipofectamine 2000 reagent by adding 0, 6, 9, and 12 μl into the reaction. The plasmid and transfection reagent were mixed and diluted in the Opti-MEM medium before transfection. A negative control of HeLa cells cultured in Opti-MEM (without plasmid or Lipofectamine) was also included in the experiment, providing a baseline of cell viability of non-treated cells. CFP expression was observed after 24 hours post-transfection. Actin was stained in red with Alexa Fluor® 568 phalloidin. Cells with CFP expression were visualised under a confocal microscopy. The result in figure 4.2 shows there were no CFP-expressing cells in either cell treated with only Opti-MEM or plasmid without transfection reagent. The number of CFP-expressing cells increased with higher amounts of Lipofectamine, although the presence of cell debris was found because of the cytotoxic effect of the transfection reagent. From this experiment 12 μl of Lipofectamine® 2000 reagent showed the highest transfection efficiency and was used for further experiments.

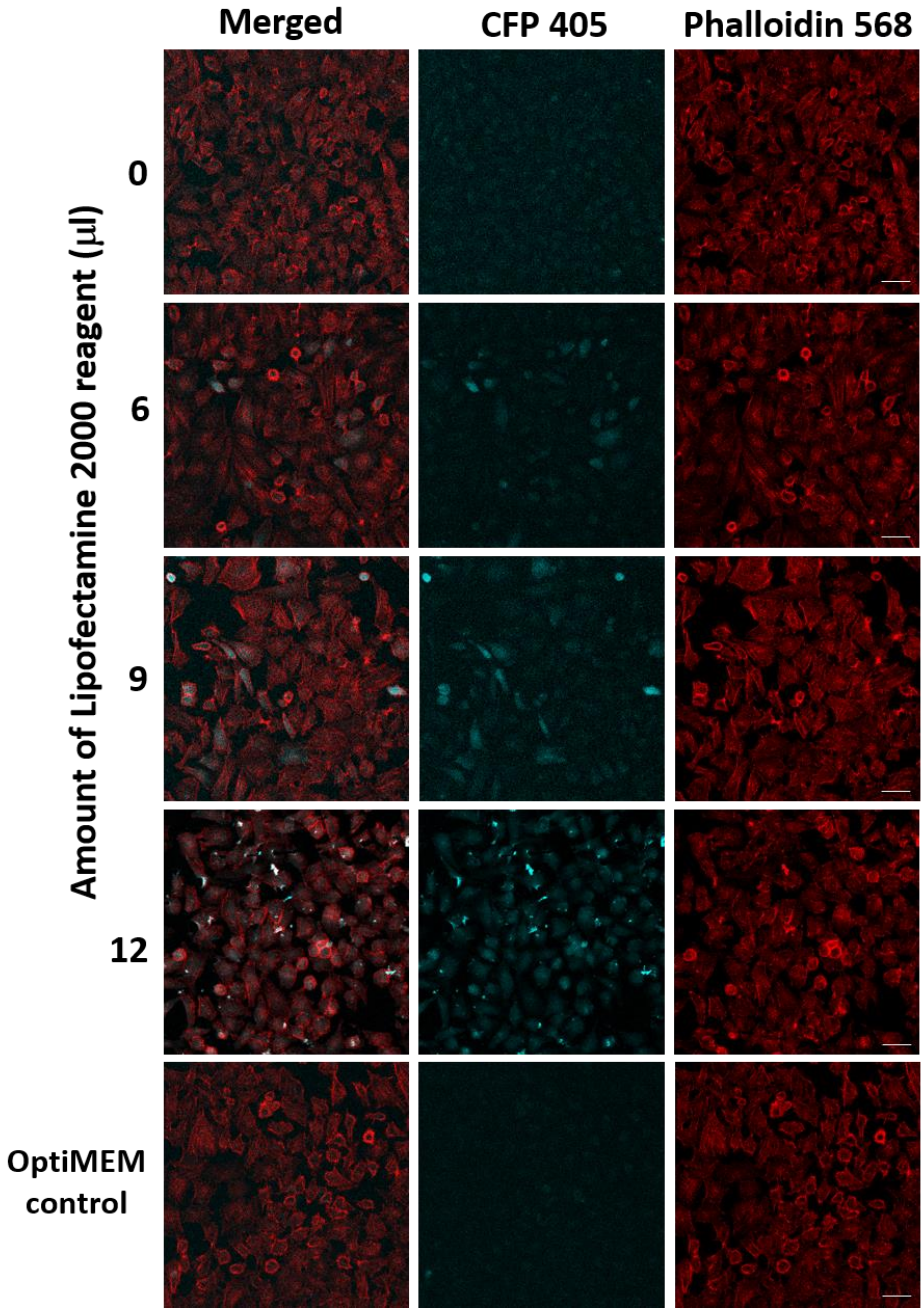

Figure 4.2: Optimisation of HeLa cell transfection
HeLa cells were transfected with pECFP-C1 with varying amounts of Lipofectamine 2000: 6, 9 and 12 µL. The cyan fluorescent protein expression was observed under a confocal microscope, compared with the negative controls which were Lipofectamine-treated cells (treated with plasmid only) and Opti-MEM-treated cells. Scale bar = 50 µm.

4.2.2 Generation of IQGAP1 knockout cell lines

Knockout of IQGAP1 in this study was conducted in HeLa cells using the commercial double nickase plasmid. The overview of this experiment is shown in figure 4.3. In brief, HeLa cells were seeded in a 6-well plate one day before transfection. To monitor transfection efficiency, a cover slip was included in an extra well. The cells were approximately 70-90% confluent on the day of transfection. Then, 2.5 μg of the double nickase plasmids were delivered into the cells using 12 μl of Lipofectamine 2000. At 24 hours post-transfection, the transfected cells on the coverslip were observed for GFP expression under a fluorescence microscope. GFP-expressing cells indicate the cells were transfected with the plasmid successfully. However, the transfected cells could contain only one plasmid encoding GFP or both two plasmids encoding GFP and the puromycin resistance gene. After that, the cells containing the plasmid encoding puromycin resistance were selected by adding puromycin on day 3 of transfection and incubating for 2 days. In this step, the cells that contain only one plasmid encoding GFP are not resistant to puromycin, causing rapid cell death of this population of cells. Following this step, any viable cells could contain only one plasmid encoding puromycin resistance or both plasmids. To generate IQGAP1 knockout cell lines by CRISPR Cas9-mediated genome editing, the cells must contain both plasmids to induce a DSB. Single clonal cell lines of the desired mutation were then isolated by serial dilution method.

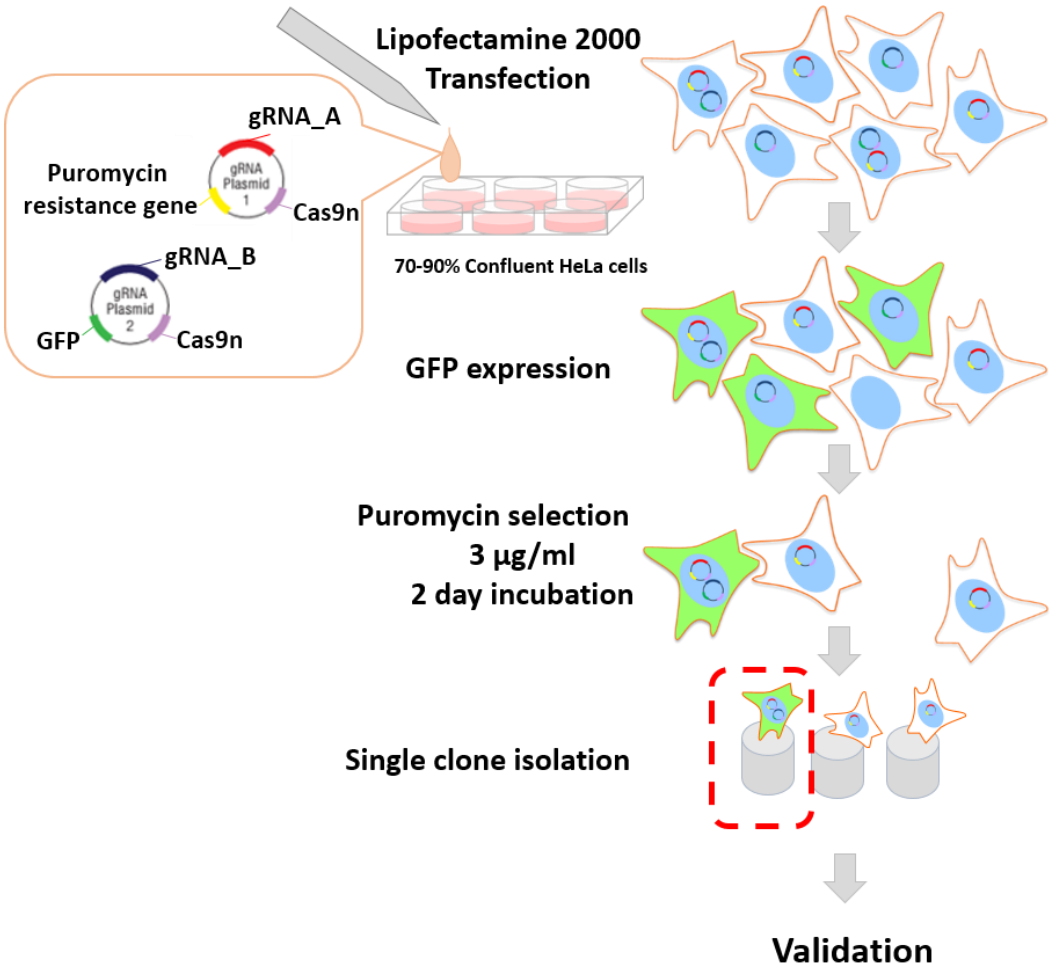

Figure 4.3: Overview of experiments for genome editing using a pair of double nickase plasmids

HeLa cells were transfected with a pair of sgRNA and Cas9n expressing plasmids using Lipofectamine. At 24 hours, the cells were observed for GFP expression to indicate the transfection efficiency. Cells harbouring both plasmids, or one plasmid that contains the puromycin resistance gene, were selected by adding puromycin at 3 µg/ml for 2 days. Single cells were isolated by serial dilution before expanding and validation.

In this study, after transfection of IQGAP1 double nickase plasmid for 24 hours, the cells plated onto a coverslip were washed and fixed with 4% PFA/PBS for further staining and observation of GFP expression. DNA staining with DAPI allowed all cells to be visualised. The efficiency of transfection was observed from GFP-expressing cells under a fluorescence microscope. Figure 4.4b shows a number of cells expressed GFP indicating transfection of double nickase plasmid into HeLa cells was successful despite low efficiency, compared with the control in figure 4.4a. Bright field images showed a small number of cells with brighter round shape indicating some cytotoxicity in both transfected and control cells (Figures 4.4c and 4.4d).

From this observation, the transfected cells were further subjected to puromycin selection. The cells were incubated with 3 μg/ml puromycin for 2 days. This step was conducted twice to ensure that all non-transfected cells died. The viable cells were expanded and then dissociated from the transfected wells. To obtain a single clonal cell line after puromycin selection, the media was replaced with fresh media without puromycin and the viable cells were allowed to expand for 4 days. Then, the cells were trypsinised and counted before performing a serial dilution into 96-well plates. The isolated cells were incubated at 37 °C in a CO_2 incubator until colonies developed. The round colonies radiating from a central point, representing a single clonal cell line, were kept and expanded for validation by Western blot analysis.

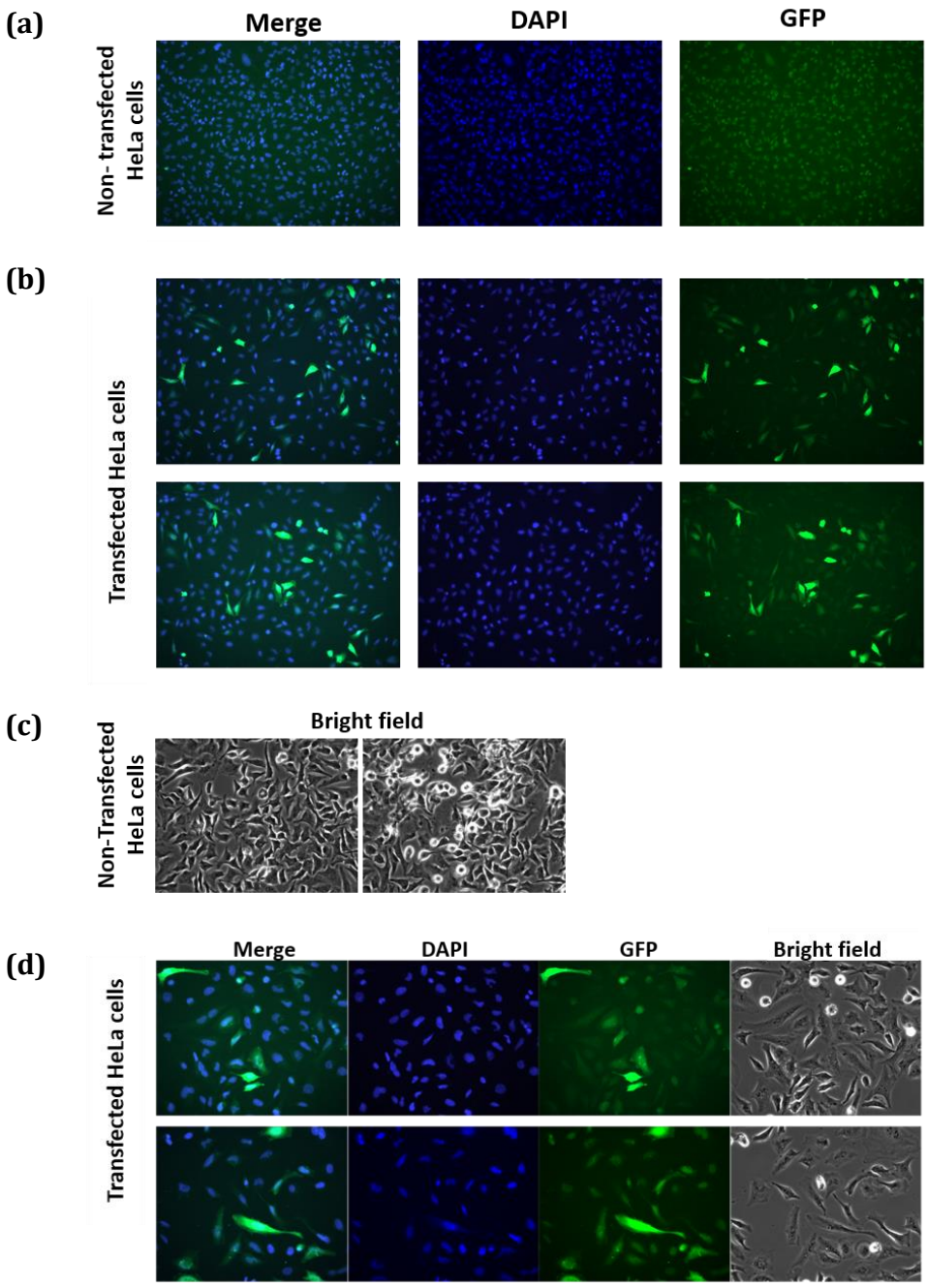

Figure 4.4: GFP-expression in HeLa cells after transfection with double-nickase plasmid using Lipofectamine® 2000

HeLa cells were transfected with 2.5 µg of the double nickase plasmid and 12 µl of Lipofectamine. After 24 hours, the cells were washed and fixed with 4% PFA/PBS before staining with DAPI.

(a) 20X fluorescence images of non-transfected cells (Lipofectamine-treated cells) control.

(b) Expression of GFP was detectable under a fluorescence microscope (40X) in HeLa cells transfected with double nickase plasmid.

(c) 100X bright field images of non-transfected HeLa cells.

(d) 100X fluorescence and bright field images of transfected-HeLa cells.

4.2.3 Screening of IQGAP1 knockout cells

After isolation of clonal cell lines by serial dilution, individual clones were validated by immunoblotting for IQGAP1. Cell pellets from each clone were washed with PBS twice before lysis to obtain a total protein that was subjected to Western blot analysis. The commercial antibody used for detection of IQGAP1 was raised against amino acids 314-422 of human IQGAP1 encoded by exons 10 to 12. Since the gRNA for editing targets exon 13 (encoding amino acids 443-495 of human IQGAP1), this antibody should detect both native and any truncated IQGAP1 isoforms as well as the absence of full-length IQGAP1.

From a total of 17 clones, the cell lysates were subjected to SDS-PAGE and immunoblotting probed with anti-IQGAP1 and anti-actin which was used as a loading control. Three clones (clone C3, G12 and H5) showed an absence of IQGAP1 at the expected size of 190 kDa (Figure 4.5a). From this preliminary result, only these clones were passaged and expanded to obtain a higher number of cells and screened a second time. From figure 4.5b, it was clear that all selected clones could not express IQGAP1. In addition to the immunoblotting result, the selected clones were plated on a coverslip in a 24-well plate to observe cell morphology and IQGAP1 expression by confocal microscopy. The images in figure 4.6 show that IQGAP1 was expressed ubiquitously in the cytosol and cell membrane in the control cells, whilst all the edited clones showed the absence of IQGAP1 expression. Moreover, the cellular morphology of these selected clones was similar to the wild-type control cell. Taken together, this suggested that IQGAP1 gene editing was successful using CRISPR Cas9 technique. The selected IQGAP1 knockout clones were further characterised by sequencing their genetic mutations.

(a)

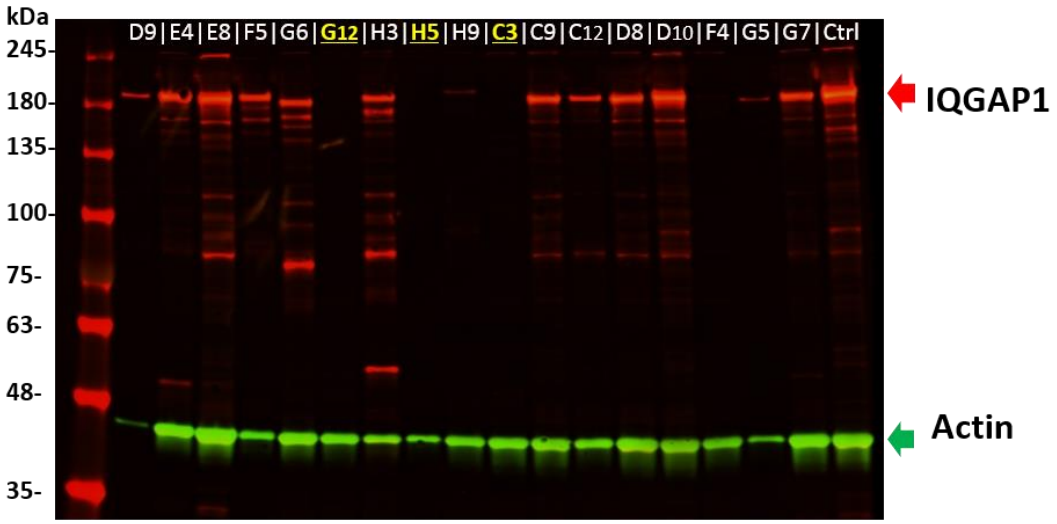

(b)

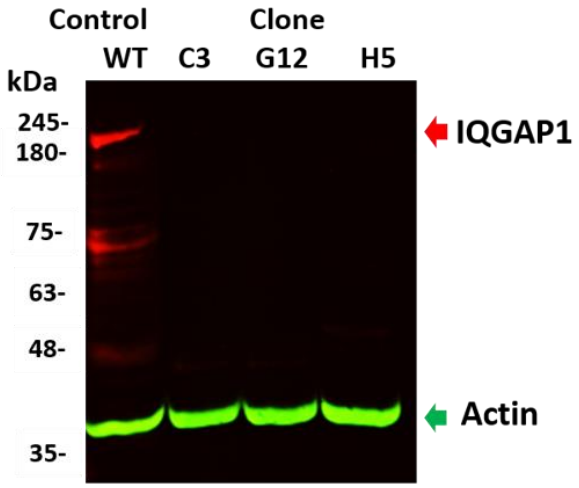

Figure 4.5: Screening and validation of IQGAP1 knockout cells using immunoblotting

HeLa cell lysates were subjected to SDS-PAGE and immunoblotting using rabbit anti-IQGAP1, and goat anti-actin antibodies which were used as a loading control.

(a) Screening of IQGAP1 knockout cells was examined by Western blotting. HeLa cell lysates were resolved by 4-15% SDS-PAGE. Western blot was probed with anti-IQGAP1 (red) and anti-actin (green) antibodies.

(b) The lack of IQGAP1 expression in selected clones was confirmed by 8% SDS-PAGE and immunoblotting with anti-IQGAP1 (red) and anti-actin (green) antibodies.

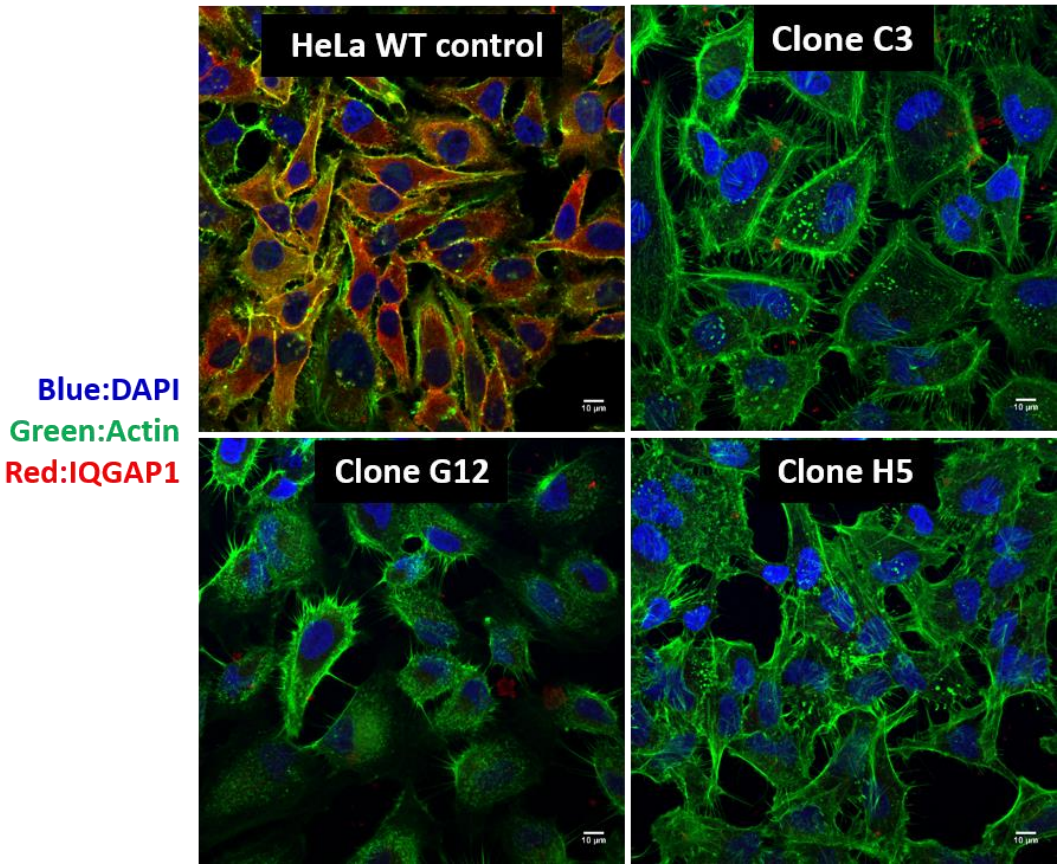

Figure 4.6: Validation of IQGAP1 knockout cells by immunofluorescence microscopy

Representative confocal laser scanning micrographs of HeLa cells, wide-type (WT) control cell and selected clones, C3, G12 and H5. F-actin (green) was stained with Alexa Fluor 488-conjugated phalloidin and nuclei was stained with DAPI (blue). IQGAP1 (red) was stained with a rabbit polyclonal antibody and detected with anti-rabbit Ig-Alexa Fluor 568. Scale bar= 10 μm.

4.2.4 Validation of IQGAP1 knockout cells

To characterise the genotype of these edited cells, primers for amplification of the region flanking exon 13 of the human IQGAP1 gene were designed from the Reference genome sequence (NC_000015.10). Figure 4.7a shows the position of exon 13 on the human IQGAP1 gene, target sites of sgRNAs and the sequencing primers.

Genomic DNA (gDNA) was extracted from WT HeLa cells using phenol/chloroform/isoamyl alcohol before precipitation with ethanol. The gDNA pellet was re-suspended in TE buffer and subjected to PCR amplification using a high-fidelity DNA polymerase. Firstly, the annealing temperature to amplify the region from control cell gDNA was titrated from 56 – 67 °C to avoid nonspecific priming. The result in figure 4.7b shows one specific band of PCR product at the expected size of 410 bp, at all annealing temperatures tested. The amplicons were extracted from the gel and purified before sequencing using the primers used for amplification. The sequencing result was blasted against the human genome to confirm that the product was derived from the IQGAP1 gene (Supplemental figure 7.5). Figure 4.7c shows a Sanger sequencing chromatogram indicating the site of gRNAs targeted on exon 13. From this result, these primers were used to verify gene editing in the selected clones.

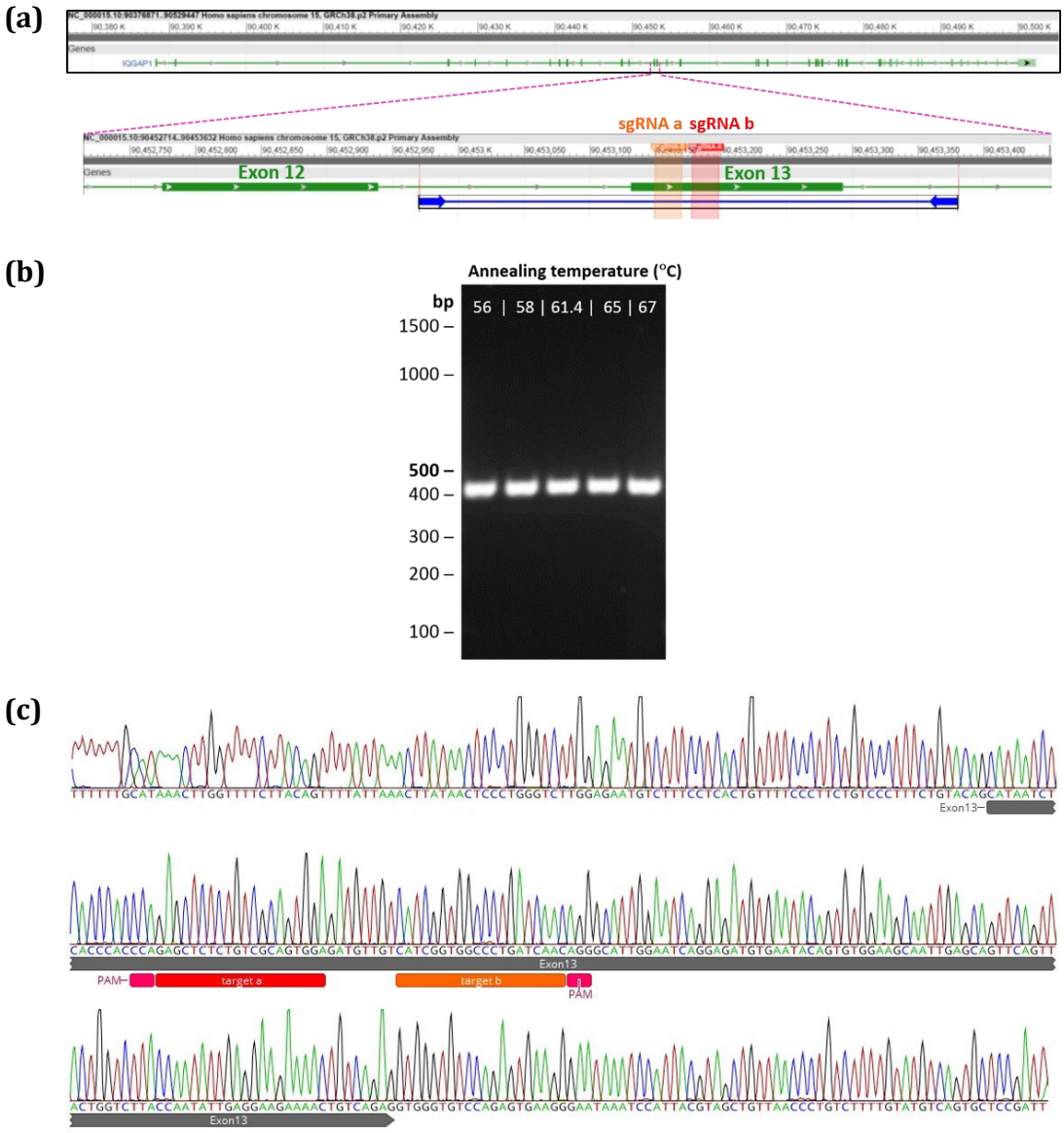

Figure 4.7: PCR-based protocol for identifying mutations induced by CRISPR-Cas9 in HeLa cells

(a) Schematic diagrams showing sequence viewer of *Homo sapiens* chromosome 15, GRCh38.p7 Primary Assembly (NCBI Reference Sequence: NC_000015 in the range: 90388241..90502243) (top panel). Pink dashed lines indicate sequenced regions containing exon 12 and exon 13. sgRNAs target exon 13. A pair of primers (blue arrows) were designed to prime outside exon 13 of the RefSegGene human IQGAP1, to detect mutations in the target site.

(b) PCR products amplified from genomic DNA extracted from HeLa cell WT control cell using the primers flanking the target region with varying annealing temperatures. The expected size of amplicons was 410 bp.

(c) Sanger sequencing chromatogram of purified PCR products around the sgRNA binding site. The target of sgRNAs are indicated in red and orange boxes, and PAMs are indicated pink boxes.

To validate mutations in the knockout cell lines, the region flanking the target for Cas9n editing at exon 13 of the RefSeq IQGAP1 sequence was amplified by PCR. Genomic DNA from three individual clonal populations was extracted and used as a template. The amplicons were analysed on an agarose gel. After gel electrophoresis, PCR products from the clones revealed different sizes and patterns indicative of the expected error-prone mutations at the target site following NHEJ-mediated repair (Figure 4.8). In clone C3, there was only one band present on the agarose gel that migrated faster than the product from the control cells. This suggested that a deletion had been engineered by the CRISPR/Cas9 technique. To confirm this deletion, the PCR band from the gel was extracted and the DNA sequenced. The result of the sequencing trace showed multiple sequence peaks at the same location with an ambiguous sequence read (Figure 4.9a). This indicated a mixed population of mutated alleles in clone C3. Analysis of PCR products of this clone was repeated. The PCR product was subjected to an extended period of gel electrophoresis to separate out any similarly sized DNA products. The result revealed two smaller bands that were excised from the gel and subjected to sequencing (Supplemental figure 7.6), which confirmed the mixed population of this clone. For clone G12, there were three distinct PCR product amplicons present on the gel, this also indicated a mixed population in this clone. Each band was excised from the gel and purified for sequencing and showed mutation had occurred either by insertion or deletion (Supplemental figure 7.7). From clone H5, the size of the PCR product was larger than the control, representing an insertion mutant. The result of Sanger sequencing of clone H5 showed the addition of nucleotide bases with single peaks, indicating this insertion mutant cell line was a homozygous single clone (Figure 4.9b).

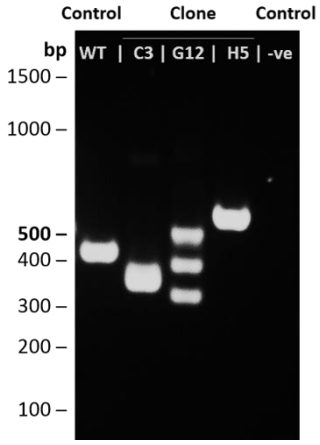

Figure 4.8: Validation of IQGAP1 knockout cell lines by PCR
Genomic DNA extracted from non-transfected control cells (WT) and clonal IQGAP1 KO isolates (clone C3, G12 and H5). For the negative control, the PCR reaction was set up identically to the experimental PCR, but without template DNA. PCR products amplified using primers upstream and downstream of exon 13 of IQGAP1. The amplicons were analysed on a 2% agarose gel.

(a)

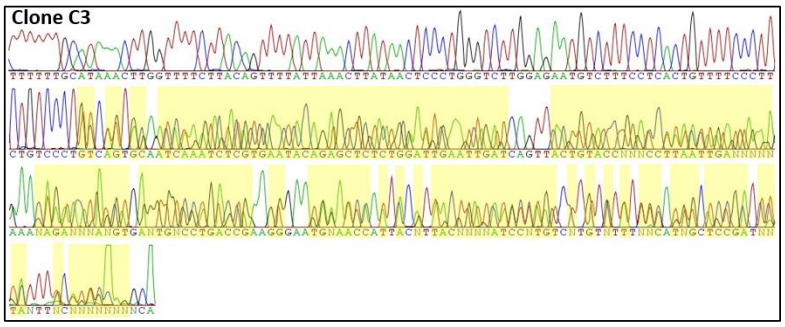

(b)

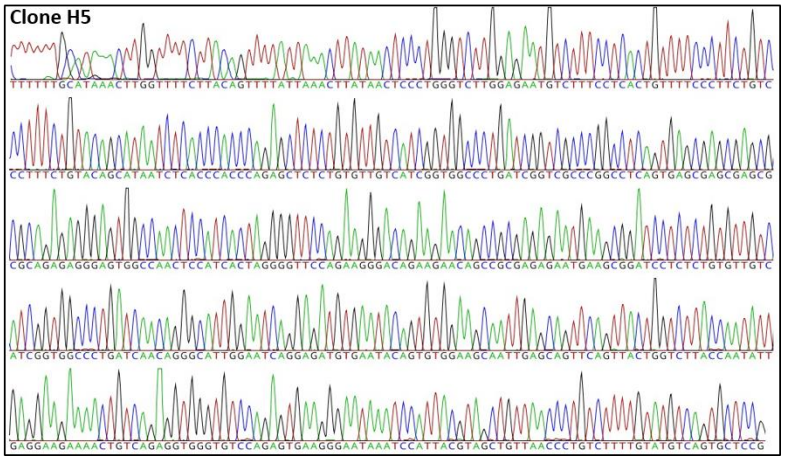

Figure 4.9: Sanger sequencing analysis of clone C3 and H5
Chromatograms from Sanger sequencing of purified PCR products using primers from the flanking regions of exon 13 of human IQGAP1.
(a) Chromatogram of clone C3 (Yellow highlights the areas of mixed sequence)
(b) Chromatogram of clone H5

Sanger sequencing of all PCR products from the 3 selected clones demonstrated gene editing at the target site in all cases. Two of them showed a mixed population, only cell line H5 was clonal and was further analysed for protein expression. The genomic DNA sequencing result of the exon 13 region of clone H5 showed 10 substituted nucleotides and 128 inserted nucleotides in the region. The resulting translated protein was predicted using an online tool (http://www.expasy.org/). The predicted consequence of this mutation generated a truncated protein with 40 new amino acids and a premature stop codon (Figure 4.10). This protein mutation can be described by the Human Genome Variation Society (HGVS) nomenclature (den Dunnen et al., 2016) as pAla453Leufs*41 and results in a protein with a predicted molecular weight at 55.4 kDa.

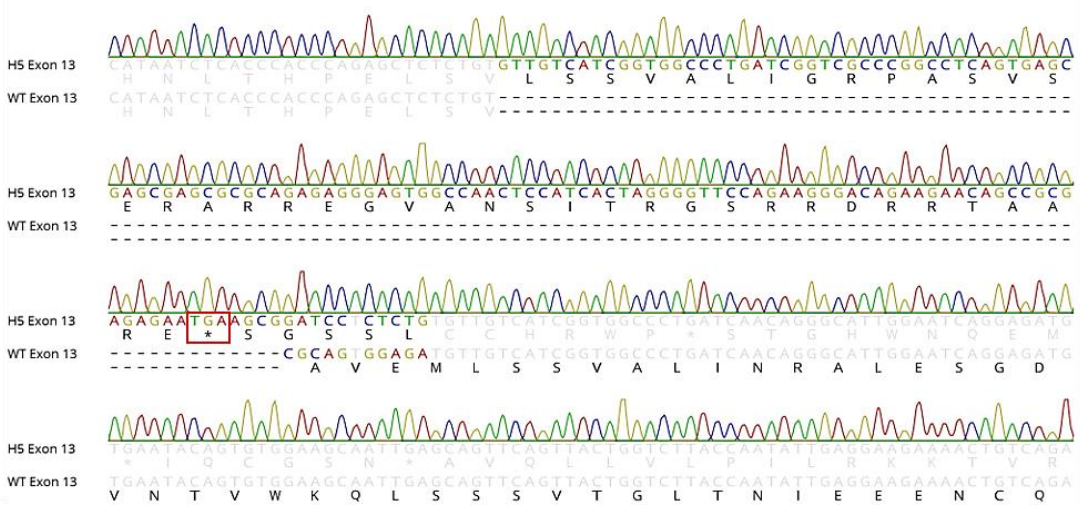

Figure 4.10: Validation of IQGAP1 KO cells by sequencing
Nucleotide and deduced amino acid sequences of exon 13 of human IQGAP1 from WT and from the mutant clone H5 are aligned. The nucleotide sequence is shown in the top lines and its deduced amino acid sequence in the single letter code is shown below. Nucleotide mutations are highlighted and the asterisk in the red box indicates the first premature stop codon produced in clone H5.

4.2.5 Lack of IQGAP1 was confirmed by immunoprecipitation

The predicted truncated protein of clone H5 is very likely to yield a non-functional protein sequence. To detect the truncated protein that may be produced in the knockout cell line, immunoprecipitation was performed. The antibody that was used to isolate IQGAP1 from the precleared lysates of control and knockout cells was raised against human IQGAP1 recognising amino acids 314-422. The predicted amino acid sequence of IQGAP1 from knockout cells showed the mutation occurs downstream of amino acid 453, which indicated that this antibody would be capable of recognising and immunoprecipitating both normal and truncated IQGAP1 from cell lysates. The antigen-antibody complexes were captured with Protein A agarose beads and then washed extensively to remove non-specific binding proteins. Immunoprecipitates were resolved by SDS-PAGE and stained with Coomassie blue. From figure 4.11a, the endogenous IQGAP1 was immunoprecipitated from the control lysates at the expected molecular weight of full-length IQGAP1 at 190 kDa. In addition, there was another band with a higher molecular weight that was isolated from the control cell lysate. In order to verify this band, 1/10 of the same immunoprecipitated sample was subjected to Western blot analysis probing with the anti-IQGAP1 antibody. The result revealed that both protein bands were specific to the antibody, representing the monomer and dimer of IQGAP1 respectively (Figure 4.11b). This finding supports a previous study that showed native IQGAP1 comprises two subunits of 190 kDa each subunit (Bashour et al., 1997). This also agreed with the study of Ren and colleagues that demonstrated oligomerisation of purified IQGAP1 using gel filtration chromatography (Ren et al., 2005).

In the knockout cell lysate, the full-length IQGAP1 was not isolated after precipitation (Figure 4.11a). The absence of IQGAP1 in the knockout cell was confirmed by Western blot analysis using the same anti-IQGAP1 antibody used for immunoprecipitation (Figure 4.11b). Moreover, it was unable to detect any distinct lower molecular weight protein in this knockout cell line, compared to the negative controls. This finding was proved by increasing the total protein of knockout cells (10-fold) and demonstrating a lack of truncated IQGAP1 protein from the knockout cells (Supplemental figure 7.8). This showed that clone H5 completely lacked expression of IQGAP1 and it was used for further experiments to determine the role of IQGAP1 in the intracellular life of *B. pseudomallei.*

(a)

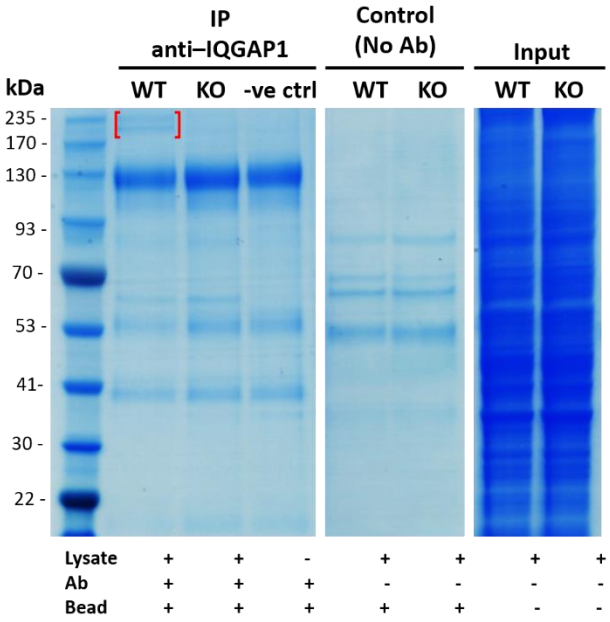

(b)

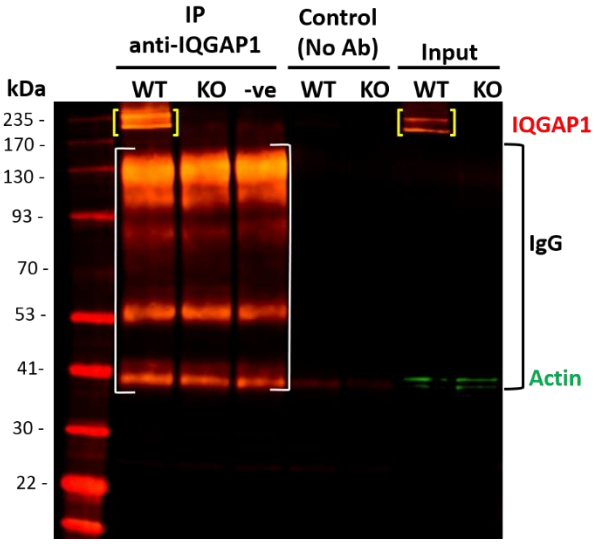

Figure 4.11: Immunoprecipitation of IQGAP1 from control and knockout cells
Precleared HeLa cells lysates were incubated with anti-IQGAP1 antibody and immunoprecipitated with protein A-Sepharose beads. After washing, the proteins were separated on a 4-12% Bris-Tris gel electrophoresed in MOPS buffer. Immunoprecipitates were analysed by Coomassie blue staining and immunoblotting. WT: Lysate of control HeLa cells; KO: Lysate of knockout cells (clone H5).
(a) Coomassie blue staining
(b) Western blot analysis with anti-IQGAP1 and anti-actin (as a loading control).

4.2.6 Role of IQGAP1 in invasion of HeLa cells by *B. pseudomallei*

In the previous chapter, the role of IQGAP1 in *B. pseudomallei* actin-based motility was studied in siIQGAP1 knockdown cells. It showed the impact of IQGAP1 on actin tail formation. However, there were no differences in invasion and intracellular replication of *B. pseudomallei* between control cells and siIQGAP1 knockdown cells. In this chapter, IQGAP1 knockout cells were used to validate these findings. Firstly, IQGAP1 knockout cells (clone H5) were subjected to a *B. pseudomallei* invasion assay. Control cells or IQGAP1 knockout cells were infected with *B. pseudomallei* 10276 at MOI of 130. After infection for 30 minutes, the media containing the bacteria was removed and replaced with fresh media supplemented with kanamycin to kill the extracellular bacteria. The infected cells were further incubated at 37 °C supplemented with 5% CO_2. At 2 hours post-infection, the infected cells were washed with PBS twice before lysis with Triton X-100. Released bacteria were serially diluted and colonies counted following plating on LB agar plates. The number of bacteria recovered from the infected cells was calculated as the number of colony forming units per millilitre (CFU/ml). To determine the percentage of invasion, the following equation was used:

(number of intracellular bacteria at 2 hours post-infection/ number of bacteria added) × 100

The result showed the bacterium was able to invade both control HeLa cells and IQGAP1 knockout cells at a similar efficiency, 0.00025% for control cells and 0.00034% for knockout cells. Although the number of recovered bacteria in the IQGAP1 knockout cells was slightly higher than those in the control cells, there was no significant statistical difference (Student's *t*-test, $p = 0.1699$) as shown in figure 4.12a. Similarly, when the cells were infected with a higher MOI of 260, there was no statistical difference of *B. pseudomallei* invasion between control and IQGAP1 knockout cells (Supplemental figure 7.9). In a previous study of *B. pseudomallei* 10276 invasion, HeLa cells were infected at MOI of 10 and showed a percentage of internalisation of about 0.5 (Stevens et al., 2003). The effect of multiplicity of infection was also found in *L. monocytogenes* which showed that a greater number of

bacteria were recovered when a low MOI rather than a high MOI was used (Francis and Thomas, 1996). However, in this study the recovery of bacteria could not be detected after 2- hours post-infection when using a low MOI (data not shown). From this observation, a high MOI (more than 100) was used in all experiments of *B. pseudomallei* infection HeLa cells in this study. A low invasion efficiency of *B. pseudomallei* in epithelial cells was found in a recent study that showed a low percentage of invasion of a clinical isolate of *B. pseudomallei* into A549 cells (0.000125-0.0002%) over a range of MOIs at 1 hour post-infection (Vellasamy et al., 2016).

It was hypothesised that this variability in bacterial invasion could be attributed to experimental conditions. To validate the invasion assay in this study, *Salmonella* invasion was performed using the IQGAP1 knockout cells. Whilst a previous study showed invasion efficiency of *Salmonella enterica* serovar Typhimurium SL1344 was reduced by 75% in IQGAP1-null MEFs (Kim et al., 2011a). When the H5 IQGAP1 knockout cells were infected with a spontaneous nalidixic acid resistant mutant of *S.* Typhimurium ST4/74 nal^R in this study, it showed no difference in the percentage of invasion between IQGAP1 knockout cells and control cells (Figure 4.12b). Using this invasive pathogen as the control for the invasion assay implied that this experiment requires further optimisation. However, it is also reasonable to assume that different cell types and bacterial strains can affect the invasion efficiency.

(a)

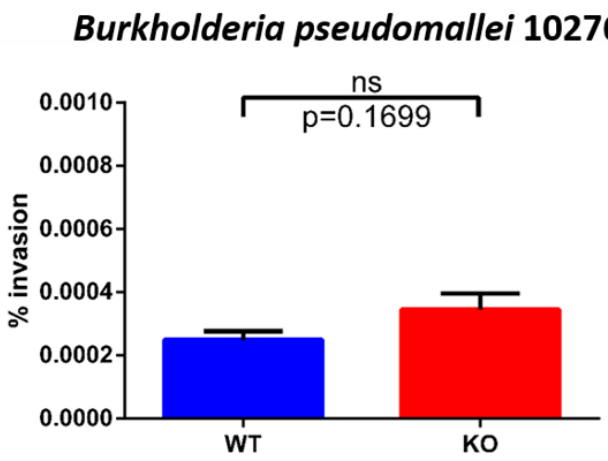

(b)

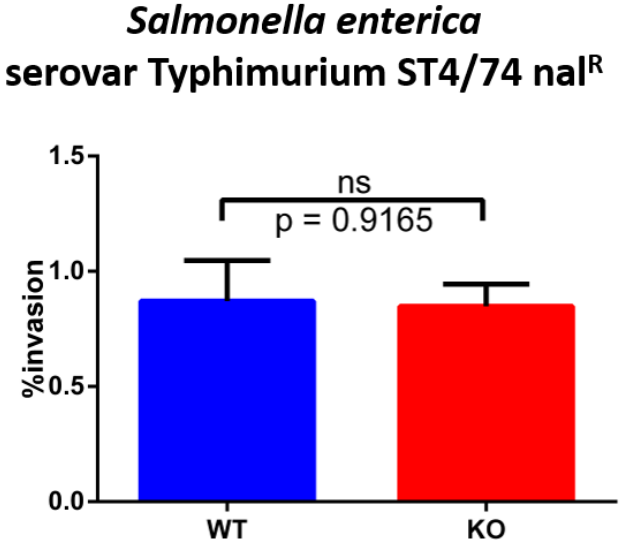

Figure 4.12: Percentage of invasion by *B. pseudomallei* and *Salmonella* Typhimurium strain ST4/74 in control HeLa cells (WT) and IQGAP1 knockout cells (KO)

(a) The cells were infected with *B. pseudomallei* at MOI of 130. Error bars represent standard errors of the mean for experiments performed in triplicate (n=3, Student's *t*-test, $p = 0.1699$).

(b) HeLa cells were infected with *S.* Typhimurium strain ST4/74 at MOI of approximately 15. After infection for 30 minutes, cells were incubated in 50 μg/ml gentamicin. At 2 hours post-infection, infected cells were lysed and the number of intracellular bacteria quantified. Data are expressed as the percentage of invasion calculated as follows: (the number of recovered bacteria/the number of bacterial inoculum) x 100 showing mean ± SEM from six separate experiments (n=6, Student's *t*-test, $p = 0.9165$).

4.2.7 IQGAP1 is essential for intracellular survival of *B. pseudomallei*

To assess the ability of bacteria to replicate in IQGAP1 knockout cells, the number of intracellular bacteria was determined at 6 and 24 hours after *B. pseudomallei* infection. Figure 4.13 shows the number of bacteria in control cells increased dramatically over time, but the numbers of intracellular bacteria only slightly increased over this period of time in IQGAP1 knockout cells. The number of viable bacteria at 6 hours post-infection in the control HeLa cells and IQGAP1 knockout cells was similar (Student's *t*-test, $p = 0.052$). On the other hand, a significantly higher number of bacteria were recovered from control cells after 24 hours post-infection, compared to IQGAP1 knockout cells (Student's *t*-test, $p = 0.0301$). This finding was confirmed by doubling the number of bacteria used to infect the cells and it showed a similar trend (Supplemental figure 7.9). Investigation of intracellular survival of this bacterium was also performed at a later point. At 48 hours post-infection, however, there was significant cell death in the control cells (as determined by LDH release assay) making it impossible to determine the actual number of viable bacteria at this time point (Supplemental figure 7.10). Thus, intracellular survival of *B. pseudomallei* in HeLa cells *in vitro* was only examined until 24 hours post-infection. Collectively, these results suggested that a lack of IQGAP1 causes a defect in the net replication and/or survival rate of intracellular *B. pseudomallei*.

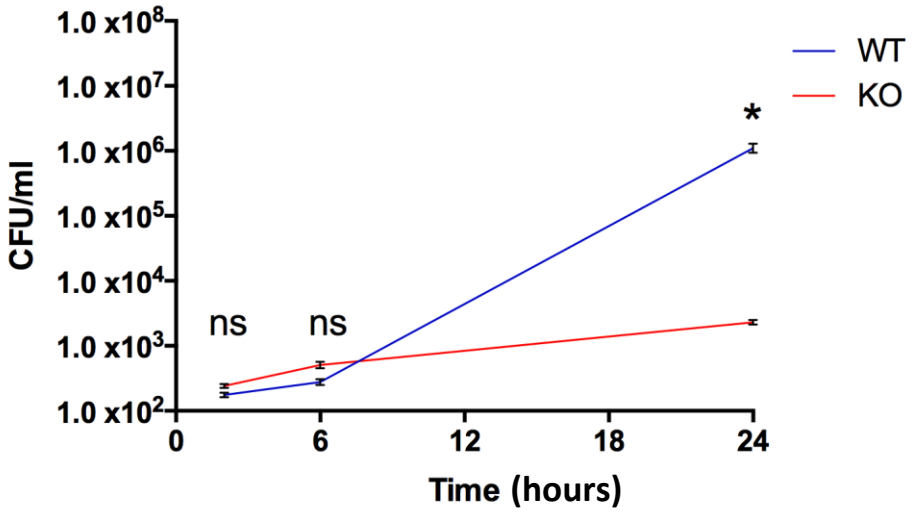

Figure 4.13: Intracellular survival of *B. pseudomallei* in control HeLa cells (WT) and IQGAP1 knockout cells (KO)
HeLa cells were infected by *B. pseudomallei* 10276 at MOI of 130. Intracellular bacteria were counted after lysing infected cells at 6 and 24 hours post-infection. The data of the number of recovered bacteria at 2 hours post-infection from figure 4.12 is also included. Asterisks indicate significant differences (Unpaired *t*-test; $p<0.05$) between control cells and knockout cells. Error bars represent standard errors of the mean for experiments performed in triplicate (n = 3, Student's *t*-test, $p = 0.052$ at 6 hours post-infection and $p = 0.0301$ at 24 hours post-infection).

4.2.8 Analysis of actin tail formation in IQGAP1 knockout and control cells

The use of siIQGAP1 knockdown cells in chapter 3 suggested that IQGAP1 plays a role in controlling the length and actin density of *B. pseudomallei* actin tails. In this chapter IQGAP1 knockout cells were utilised to transcend the limitation of residual IQGAP1 in the siIQGAP1 knockdown cells. From three independent experiments, a total number of bacteria in control cells and IQGAP1 knockout cells, 4,301 and 1,586 respectively, were examined at 16 hours post-infection for tail formation. The bacteria were categorised into two groups. The first group included the bacteria without a tail but which may still have recruited actin to the bacterial surface (termed 'barcode'), and those that were not associated with actin at all. The second group included bacteria with a tail, whether a short or long actin tail. This analysis showed a similar proportion of *B. pseudomallei* formed actin tails in control cells and IQGAP1 knockout cells (Figure 4.14a).

The same data was re-classified into four phenotypes: first, bacteria that were not associated with actin at all; second, bacteria that were associated with actin recruitment but not displaying an actin tail (barcode); third, bacteria displaying a short actin tail; fourth, bacteria displaying a long actin tail. Interestingly, as shown in figure 4.14b, the proportion of bacteria that were not associated with actin at all is greater in IQGAP1 knockout cells at 49.04% (Student's *t*-test, $p = 0.011$), whilst bacteria that demonstrated a barcode morphology is greater in control cells at 49.5% (Student's *t*-test, $p = 0.0018$). However, there was no statistically significant differences in the group of *B. pseudomallei* that displayed a short or long tail (Student's *t*-test, $p = 0.9790$ and 0.5835, respectively) in control cells and IQGAP1 knockout cells. Representative images of confocal micrographs in figure 4.14c shows the noticeably higher number of bacteria associated with actin in control cells. Additionally, it is noticeable that *B. pseudomallei* showed the barcode phenotype of parallel lines of varying widths of actin across the bacterium in control cells (Figure 4.14d), albeit at higher levels in knockout cells. This phenotype is reminiscent of septin-cages that entrap *Shigella* during host cell infection, where the septin rings were detectable next to actin around the bacterium in cage-like structures that restrict motility and cell-to-cell spread, and ultimately leads to elimination of the bacterium (Mostowy et al., 2010).

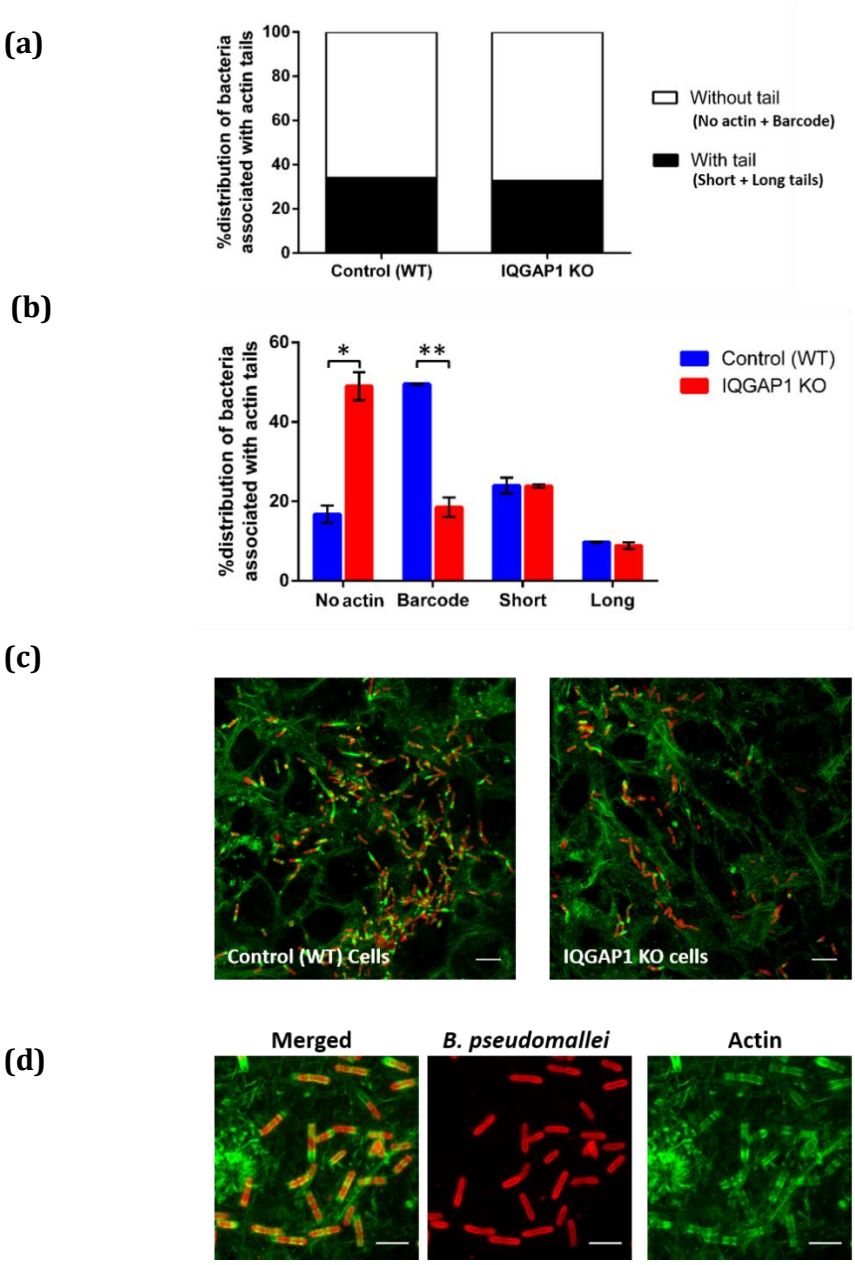

Figure 4.14: Qualitative analysis of the morphology of actin tails formed by *B. pseudomallei* in control and IQGAP1 knockout cells

(a) Distribution of bacteria associated with (short or long tail) or without an actin tail (no actin or barcode distribution of actin).

(b) Percentage distribution of bacteria in each category in control cells (blue bar) compared to IQGAP1 knockout cells (red bar). Data represents mean ± SEM (n = 3 Student's *t*-test, $p = 0.011$ for no actin, $p = 0.0018$ for barcode, $p = 0.9790$ for short tails and $p = 0.5835$ for long tails).

(c) Representative confocal micrographs of control HeLa and IQGAP1 knockout cells infected with *B. pseudomallei*. Bacteria were stained red, filamentous actin was stained in green. Scale bar = 10 µm.

(d) Representative confocal micrographs showing Hela cells infected with *B. pseudomallei* showing the barcode phenotype. Bacteria were stained red, filamentous actin was stained in green. Scale bar = 5 µm.

In the previous chapter, *B. pseudomallei* displayed an actin tail that was significantly longer but less actin dense in siIQGAP1 knockdown cells, compared with the control cells. To verify this finding, 100 bacteria displaying a tail with a length longer than 2 μm were selected randomly in each cell type for analysis. Actin tail length and density were measured and processed using ImageJ software. By using identical laser settings between *B. pseudomallei* infected control cells and IQGAP1 knockout cells, images were captured and analysed from maximum intensity z-projections of the stacked cell images. The results showed that the bacteria form an actin tail in control cells was longer than those in IQGAP1 knockout cells, with a mean length of 13.1 μm and 8.3 μm respectively (Figure 4.15a). However, actin density of *B. pseudomallei* actin tails measured by the fluorescence intensity in control cells was similar with those in IQGAP1 knockout cells (Student's *t*-test, $p = 0.1945$) (Figure 4.15b). Comparison with the finding in Chapter 3, actin tail formation of *B. pseudomallei* in IQGAP1 knockout cells did not follow the trend previously observed in siIQGAP1 knockdown cells. In fact, the proportion of bacteria displayed a short or long actin tail and bacteria did not display an actin tail (no actin recruitment and formed barcode morphology), compared with the control cells was consistent between in siIQGAP1 knockdown cells and in IQGAP1 knockout cells. Although, the greater number of bacteria with no actin association was observed only in IQGAP1 knockout cells, but not in siIQGAP1 knockdown cells. Conversely, the number of bacteria displayed barcode phenotype was shown in the control cells more than in IQGAP1 knockout cells, but this finding was not found in the siIQGAP1 knockout cells.

Taken together, it could be suggested that the IQGAP1 may be not essential to induce the formation of *B. pseudomallei* actin tail. Despite that, the results demonstrated that IQGAP1 is involved in the organisation of the architecture of the actin tails and recruitment of actin for forming barcode phenotype by *B. pseudomallei*.

(a)

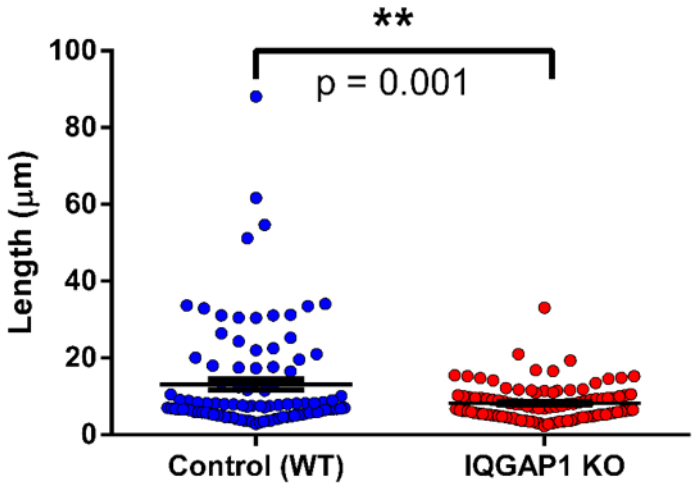

(b)

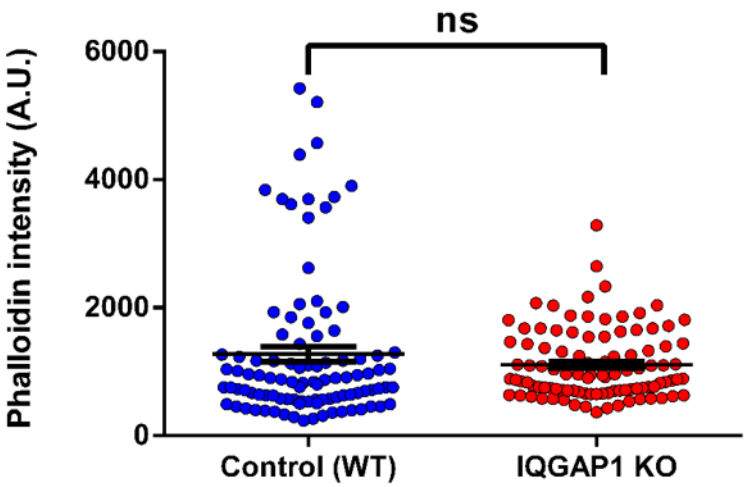

Figure 4.15: IQGAP1 affects *B. pseudomallei* actin tail length but not the density of the actin tail

HeLa cells were infected with *B. pseudomallei* 10276 WT for 16 hours post-infection before fixing. Bacteria, IQGAP1 and actin were stained and images captured by confocal microscopy. The length of the actin tails and signal intensity were quantified using ImageJ software. 100 bacteria from three independent experiments of each sample, control cells (WT) and IQGAP1 knockout cells (KO) were observed (n=3).

(a) Scatter plot indicating the length of actin tail formed by individual bacteria displaying a tail longer than 2 µm. The data represent mean ± SEM and asterisks denote lengths that are significantly different from each other (Unpaired *t*-test; p = 0 .001).

(b) Scatter plot indicating the intensity of actin in tails formed by individual bacteria displaying a tail longer than 2 µm. The data represent mean ± SEM (Unpaired *t*-test; p = 0 .1945).

4.2.9 IQGAP1 affects MNGC formation by *B. pseudomallei*

B. pseudomallei can spread directly to neighbouring cells by inducing the formation of a multinucleated giant cell (MNGC) which is promoted by actin-based motility. From the effect of IQGAP1 on actin tail formation, it was hypothesised that IQGAP1 could be a factor to support MNGC formation by *B. pseudomallei*. MNGC formation could not be assessed in siIQGAP1 knockdown cells because the cells could not form full monolayers, hence the IQGAP1 knockout cells were used to investigate MNGC formation in this chapter.

To assess MNGCs induced by *B. pseudomallei* in IQGAP1 knockout cells, cells were infected with the bacterium and incubated for 16 hours before fixing and staining, and quantification of the number of MNGCs. Infected cells were stained with phalloidin for F-actin and nuclei were stained with DAPI. To locate infected cells, the bacteria were stained red with mouse anti- *B. pseudomallei* LPS antibody followed by anti-mouse-Alexa568. MNGCs were defined as cells containing 3 or more nuclei. In a field of view, only nuclei of infected cells were quantified and used to calculate the percentage of MNGC formation as follows:

> (number of nuclei within multinucleated giant cells/ total number of nuclei in the field of view) × 100.

Figure 4.16a shows representative images of *B. pseudomallei* infected cells at 16 hours post-infection leading to MNGC formation in control HeLa cells (WT) and IQGAP1 knockout cells (KO). It is clear that the number of bacteria in control cells was greater than in IQGAP1 knockout cells, which agrees with the previous result of intracellular survival (Figure 4.13). Despite the lower number of bacteria in knockout cells, MNCG formation could be detected. On average, MNGC formation in control cells was 41% whilst in knockout cells, the bacteria induced MNGC at a much lower frequency of only 4.8% (Figure 4.16b). MNGC was monitored at later time points but MNCGs could not be detected in IQGAP1 knockout cells even at 72 hours post-infection. However, this is likely a result of a lack of intracellular bacteria at this time point.

(a)

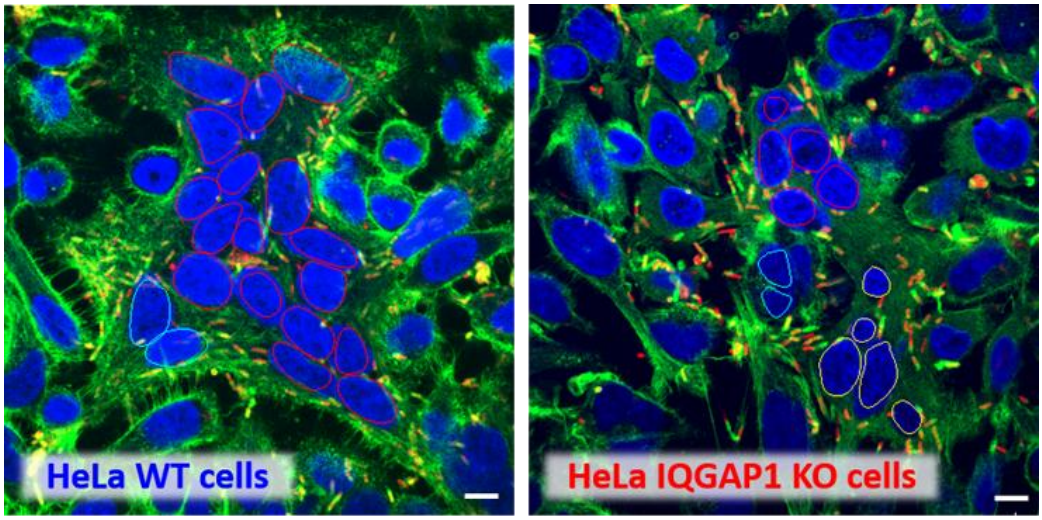

(b)

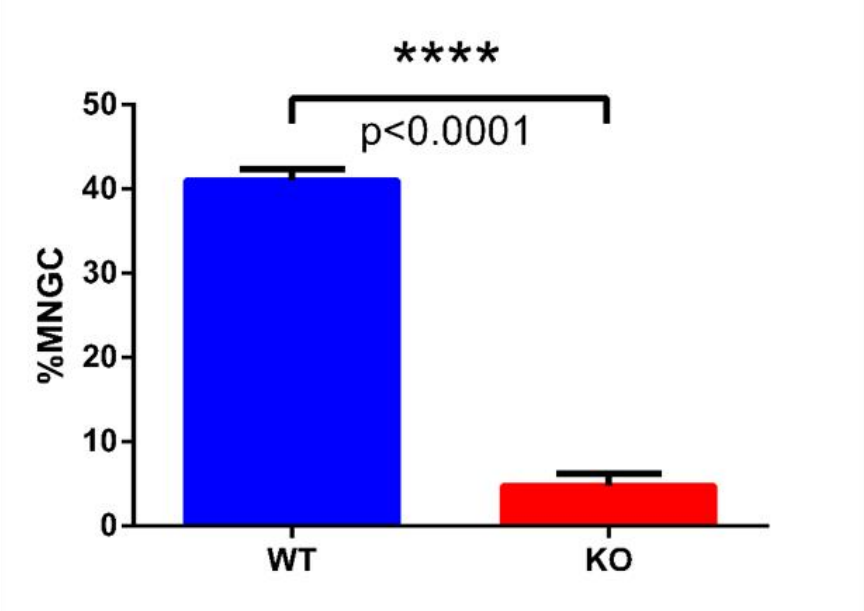

Figure 4.16: *B. pseudomallei* induced MNGC formation in control (WT) and knockout cells (KO)

HeLa cells were infected with *B. pseudomallei* 10276 WT at MOI of 130 for 16 hours post-infection before fixing. Bacteria, IQGAP1 and actin were stained and images captured by confocal microscopy.

(a) Confocal micrographs showing a representative image of an MNGC in control cells (WT) and IQGAP1 knockout cells (KO). Each colour of the circle represents a group of nuclei forming an MNGC.

(b) The percentages of MNGC formation in cells represent the mean ± SEM for experiments performed in triplicate (n=3) and asterisks indicate significant differences (Unpaired *t*-test; $p<0.0001$) between the control cells (WT) and IQGAP1 knockout cells (KO).

4.2.10 Defective plaque formation by *B. pseudomallei* in IQGAP1 knockout cells

The ability of *B. pseudomallei* to spread from cell-to-cell can be quantified by assessing the formation of plaques in a cell monolayer. This assay could not be performed in siIQGAP1 knockdown cells because these cells could not form a robust monolayer. To evaluate the role of IQGAP1 in plaque formation by *B. pseudomallei*, IQGAP1 knockout cells were used.

HeLa cells were infected with *B. pseudomallei* at MOI of approximately 100 and incubated for 24 hours before fixing and staining with crystal violet. At 24 hours post-infection, in control cells, the bacteria formed 24 plaques per well of a 24-well plate on average from 3 independent replicates. In contrast, there was no visible plaque formation in IQGAP1 knockout cells (Figure 4.17a). To confirm this phenotype, the infected cells were further incubated and observed for plaque formation at 48 and 72 hours post-infection. The results showed that the bacteria formed larger plaques over time in control cells (Figure 4.17b). However, the number of plaques could not be quantified at these time points because the plaques merged, thereby hindering accurate quantification. On the other hand, there was no visible plaque formation detected in *B. pseudomallei* infected IQGAP1 knockout cells even at 72 hours post-infection. At the later time points of infection, it is presumed that the number of intracellular bacteria decreased. The number of intracellular bacteria in *B. pseudomallei* infected IQGAP1 knockout cells were observed under a microscope and showed a very low number of bacteria at 48- and 72- hours post-infection, in agreement with this assumption (Supplemental figure 7.11). Collectively, IQGAP1 is assumed to play a role at a late stage of the *B. pseudomallei* intracellular life cycle, before reaching the plaque formation stage.

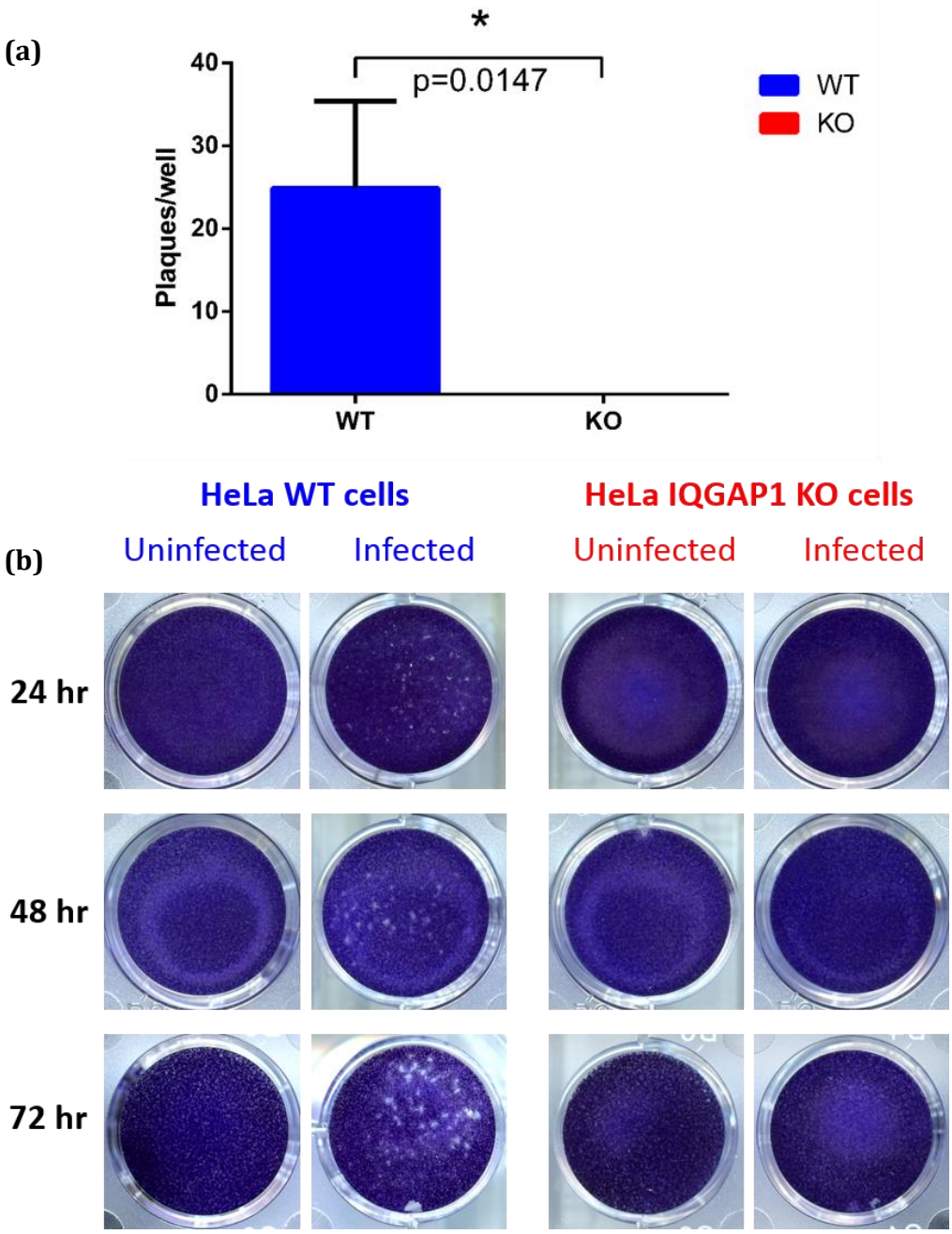

Figure 4.17: Plaque formation by *B. pseudomallei* in control (WT) and IQGAP1 knockout cells (KO)

HeLa cells were infected with *B. pseudomallei* 10276 at MOI of approximately 100. Plaque formation was observed by crystal violet staining.

(a) The total number of plaques formed at 24 hours post-infection in each well of a 24-well plate was counted. Data represent mean ± SEM for experiments performed in triplicate and asterisks indicate significant differences (n=3, Unpaired *t*-test, p = 0.0147) between groups.

(b) Representative images of the infected cell monolayers after infection with *B. pseudomallei* for 24, 48 and 72 hours and stained with crystal violet showing plaques in control cells but none in IQGAP1 knockout cells.

4.3 Discussion

The aim of the work presented in this chapter builds upon the previous chapter. It showed that IQGAP1 was present in the actin tail of *B. pseudomallei* with a proposed function to control the length and actin density of tails. To gain insight into the impact of IQGAP1 on the intracellular life of *B. pseudomallei*, IQGAP1 knockout cells were generated using the CRISPR-Cas9 technique. Transfections of siRNAs or CRISPR-Cas9 require optimisation to achieve the highest efficiency. RNAi is simple and can be validated by Western blot analysis to obtain a desired knockdown level of protein expression. On the other hand, CRISPR-Cas9 has additional steps of selection, clonal expansion and verification. One of the main differences between the mechanism to repress gene expression by siRNA and remove a gene by CRISPR-Cas9 is their action. Whilst RNAi results in decreases at the mRNA level and occurs in the cytoplasm, CRISPR-Cas9 targets at the DNA level in the nucleus. Consequently, the effect of RNAi is typically transient for 2–7 days and never fully eliminates expression of the targeted gene, whereas CRISPR-Cas9 edits the genome causing a permanent effect (Reviewed in Barrangou et al., 2015). With the benefits of the CRISPR-Cas9 approach, IQGAP1 knockout cells (clone H5) were produced to explore the roles of IQGAP1 in *B. pseudomallei* intracellular life. Studies show that actin-based motility affects bacterial intracellular life and is important for cell-to-cell spread (Reviewed in Kuehl et al., 2015). However, it is still under investigation how actin-based motility impacts the intracellular life cycle of *B. pseudomallei*. To explore the effect of IQGAP1 in the intracellular life of this bacterium, the IQGAP1 knockout cell was subjected to invasion, intracellular survival, MNGC and plaque formation assays.

IQGAP1 is a well-known regulator of *Salmonella* invasion (Brown et al., 2007, Kim et al., 2011a). However, this study showed that IQGAP1 is not required for *B. pseudomallei* invasion into HeLa cells. A very low percentage of *B. pseudomallei* invasion at 0.00025% and 0.00034% in control cells and IQGAP1 knockout cells respectively, was detected when the cells were infected at MOI of 130. This low percentage of invasion was also found upon infection of another epithelial cell line (A549) by a *B. pseudomallei* clinical isolate (Vellasamy et al., 2016). Due to a very low number of recovered bacteria obtained from infected cells, invasion by *B.*

pseudomallei into HeLa cells requires further optimisation to improve the level of detection. However, it was questionable whether the invasion assay performed in this study is reliable. To examine this, *S.* Typhimurium ST4/74 nal^R was used to infect the control or IQGAP1 knockout cells. The result showed a similar level of invasion efficiency of *Salmonella* into these cell types. This finding contradicts the previous study that showed a significant reduction (by 33%) of *Salmonella* invasion in HeLa cells with siRNA-mediated suppression of IQGAP1 (decreased ~75%) (Brown et al., 2007). Moreover, MEFs lacking IQGAP1 also showed a reduction of *S.* Typhimurium invasion by 75% (Kim et al., 2011a). However, when the MEFs lacking IQGAP1 were infected with *Shigella*, the number of internalised bacteria in the cells were greater than in control cells but with no statistical difference (Lu et al., 2015b). An explanation for this difference could be the specific mechanism used by these pathogens to gain entry into host cells or the origin of the cell types used in these experiments. It is also possible that the conditions used to culture *Salmonella* in the experiment described in this chapter were not optimal for T3SS expression. In future, temperature shift of the bacterial culture from 25°C to 37°C may be used to induce protein secretion by the *Salmonella* T3SS *in vitro.* For example, SopE that contributes to the entry process into HeLa cells and co-localises with IQGAP1 and phagocytic cups during *Salmonella* invasion could impact this process (Brown et al., 2007, Wood et al., 1996).

For intracellular survival, it is clear that the number of *B. pseudomallei* in control cells is greater than in IQGAP1 knockout cells at 24 hours post-infection. Although the number of bacteria that invaded and survived until 6 hours after infection in the knockout cells was slightly higher than in control cells, it was not significant. At 6 hours post-infection also mirrors the timing of BimA expression in *B. pseudomallei* infected cells (Jitprasutwit et al., 2016). The decreased number of bacteria in IQGAP1 knockout cells at the later time point indicates a defect in intracellular survival. The host defence mechanisms that affect the ability of the bacterium to survive and replicate include the harsh environment of the endosome and autophagy. After invasion of *B. pseudomallei* into non-phagocytic cells, the bacterium has evolved strategies to escape from the endocytic vesicle and survive in the cytosol. Comparison of intracellular growth of *B. pseudomallei* in control and IQGAP1 knockout cells at 2 hours to 6 hours after infection, demonstrated similar

numbers of bacteria. Several studies have demonstrated that *B. pseudomallei* T3SS mutants were able to escape into the cytosol by 6 hours post-infection (Reviewed in Allwood et al., 2011). Thus, it is probable that at 6 hours post-infection in this study the bacteria can escape from the endocytic vesicles and are free in the cytosol, suggesting that IQGAP1 does not impair the ability of the bacteria to escape from the vacuoles. Although this could be confirmed using a chloroquine and kanamycin protection assay or by LAMP1-staining.

In the cytosol, *B. pseudomallei* exploits host cellular actin to support its movement inside the cells and into the adjacent cells. *B. pseudomallei* was still able to form actin tails in IQGAP1 knockout cells, with the same proportion of bacteria displaying either a short or long tail, compared to the control cells. However, the length of the actin tail in control cells was significantly longer than in IQGAP1 knockout cells with no difference in actin density. Collectively, this data indicates a possible function of IQGAP1 to recruit actin to the bacteria and to promote actin polymerisation to form long tails. It should be noted that this finding differs significantly from that described in chapter 3 where siRNA mediated knockdown of IQGAP1 resulted in longer tails with less actin density. This can be explained by the fact that the residual IQGAP1 in siIQGAP1 knockdown cells are sufficient for forming a long actin tail. However, the depletion of IQGAP1 affected the structure of the actin tails causing a loose tail instead of a compact tail. On the other hand, in this chapter, a lack of IQGAP1 led to a shorter *B. pseudomallei* tail with no effect on actin density. This suggests that other unknown host factors may be involved in *B. pseudomallei* actin tail formation.

Actin-based motility is the ability of bacteria to propel themselves inside the cytoplasm and facilitate cell-to-cell spread by actin polymerisation. In addition, this motility promotes the avoidance of cellular innate immune responses. *B. pseudomallei* induces the fusion of cells for spreading from infected cells to neighbouring uninfected cells leading to MNGC formation. In this study, *B. pseudomallei* infected IQGAP1 knockout cells showed a significant defect in MNGC formation compared to control cells at 16 hours post-infection. This phenotype was confirmed by plaque assay which represents MNGC cell death and is a visual readout of the ability of the bacteria to spread directly from cell–to-cell. The defect of cell

fusion by *B. pseudomallei* in IQGAP1 knockout cells is supported because there was no visible plaque formation even up until 72 hours post-infection. Whereas in control cells a number of plaques could be detected at 24 hours post-infection which increased in size over time. This result could be expected given the rapid decrease in number of intracellular bacteria in IQGAP1 knockout cells. In the next chapter, the interaction between IQGAP1 and BimA was explored and the importance of IQGAP1 in an *in vitro* assay of actin polymerisation was assessed.

Chapter 5
Expression and purification of IQGAP1 to study its interaction with BimA

5.1 Introduction

Burkholderia actin-based motility requires BimA to mediate actin assembly at the bacterial pole. In order to understand what host cell proteins may be involved in this process, the bacterium was engineered to constitutively express BimA and IQGAP1 was identified as a potential interacting partner using an affinity approach (Jitprasutwit et al., 2016). In chapter 3, confocal microscopy revealed that IQGAP1 was recruited to *B. pseudomallei* actin tails in infected cells. In IQGAP1-depleted cells, the role for this protein in controlling the length and actin density of the actin tails was demonstrated. Moreover, a defect in intracellular survival of this bacterium was found in HeLa cells lacking IQGAP1 (chapter 4). A number of pathogen-derived IQGAP1 interaction partners were identified previously, with roles that seem to be specific for different pathogens (Reviewed in Kim et al., 2011b). For example, a T3SS-translocated effector protein, SseI, which plays a role in maintaining a long-term infection of *S. enterica* serovar Typhimurium in mice and is required to inhibit cell migration of primary macrophages and dendritic cells *in vitro*, has been identified as an IQGAP1 binding partner (McLaughlin et al., 2009). SseI binds directly to IQGAP1 *in vitro* and co-localises with IQGAP1 and actin at the cell periphery of bone marrow-derived macrophages during *Salmonella* infection (McLaughlin et al., 2009). Enteropathogenic *E. coli* (EPEC) also targets IQGAP1 through the translocated intimin receptor (Tir) of the T3SS which manipulates the actin cytoskeleton by associating with calmodulin to induce actin pedestal formation (Brown et al., 2008). Localisation of IQGAP1 with actin was revealed at the site of EPEC adhesion and an *in vitro* assay showed a direct interaction between IQGAP1 and Tir (Brown et al., 2008). Another novel T3SS effector protein in *E. coli*, Ibe (IQGAP1-binding effector), also interacts with IQGAP1 to induce pedestals and actin-rich membrane ruffles (Buss et al., 2009).

IQGAP1 is a scaffold protein with multiple roles including regulation of the cell cytoskeleton. Previous studies have shown that IQGAP1 directly binds and crosslinks filamentous actin (Bashour et al., 1997, Fukata et al., 1997). It also

enhances actin assembly *in vitro* via the Arp2/3 complex and N-WASP (Le Clainche et al., 2007, Bensenor et al., 2007). It has been proposed that IQGAP1 regulates actin polymerisation by capping the barbed end of actin filaments (Pelikan-Conchaudron et al., 2011). In this chapter, the role of IQGAP1 in BimA-mediated actin polymerisation has been studied. BimA is located at the pole of *B. pseudomallei*, binds monomeric actin and stimulates actin polymerisation *in vitro* in a manner independent of the cellular Arp2/3 complex (Stevens et al., 2005a, Sitthidet et al., 2010, Benanti et al., 2015). It is possible that IQGAP1 is recruited to the bacterial actin tail in infected cells either through a direct interaction with BimA or through its interaction with cellular actin. It is also possible that IQGAP1 augments BimA-mediated actin polymerisation. In this chapter, the interaction between IQGAP1 and BimA was examined. To determine if BimA can directly bind IQGAP1, an *in vitro* pull-down assay was performed with purified proteins. A yeast two-hybrid system approach was also utilised. In addition to protein-protein interaction assays, the ability of IQGAP1 to stimulate BimA-mediated actin polymerisation in an *in vitro* assay was also investigated.

5.2 Results

5.2.1 pMAL-IQGAP1 cloning for expression of MBP-IQGAP1

To test whether there is a direct interaction between IQGAP1 and BimA, recombinant plasmids encoding full-length and truncated IQGAP1 were constructed by PCR cloning. Primers were used to amplify either full-length, the N-terminus or the C-terminus of IQGAP1 at the expected size (approximately 5,000 bp, 2,400 bp and 2,500 bp respectively) using HeLa cell cDNA as template (Figure 5.1a). A positive control for amplification from the cDNA template was also included showing 838 bp fragments of the β–actin gene, whereas the absence of cDNA template was used as a negative control (Figure 5.1a). The PCR fragments were cloned into the pGEM-T Easy vector and transformed into *E. coli* XL-1 blue cells. And then, the fragments were sub-cloned into pMAL-p2X vector which is designed for protein expression in the periplasm to facilitate disulphide bond formation for correct folding of proteins. Using these vectors, IQGAP1 proteins were expressed as C-terminal MBP fusion proteins (Fig. 5.1b).

After identification of positive clones, the plasmid DNA was extracted and sequenced. Amino acid sequences of *Homo sapiens* IQGAP1 (NP_003861) and translation of the cloned genes were aligned using a web tool, Clustal Omega (https://www.ebi.ac.uk/Tools/msa/clustalo/). The full-length IQGAP1 (encoding aa1-1657) had 99% identity to the reference sequence, with substitutions of K201T (lysine was replaced by threonine at amino acid position 201) and D1244G (aspartic acid was replaced by glycine at amino acid position 1224). The N-terminus of IQGAP1 (encoding aa1-808) showed 99% identity with the reference IQGAP1 sequence with M185T and N299D substitutions (methionine was replaced by threonine at amino acid position 185 and asparagine was replaced by aspartic acid at amino acid position 299), while the C-terminal IQGAP1 (encoding aa809-1657) showed 100% identity to human IQGAP1 (Figure 5.2). The different positions of the mutations on each fragment suggested they had arisen from using the polymerase mix (Advantage 2 Kit; Clontech) that contained *Taq* DNA polymerase and a minor amount of a proof-reading polymerase to amplify the products, rather than the variation of IQGAP1 sequence. However, these mutations are located outside of the important conserved domains and were presumed to have negligible effect on IQGAP1 activity. These constructs were further used for protein expression and purification.

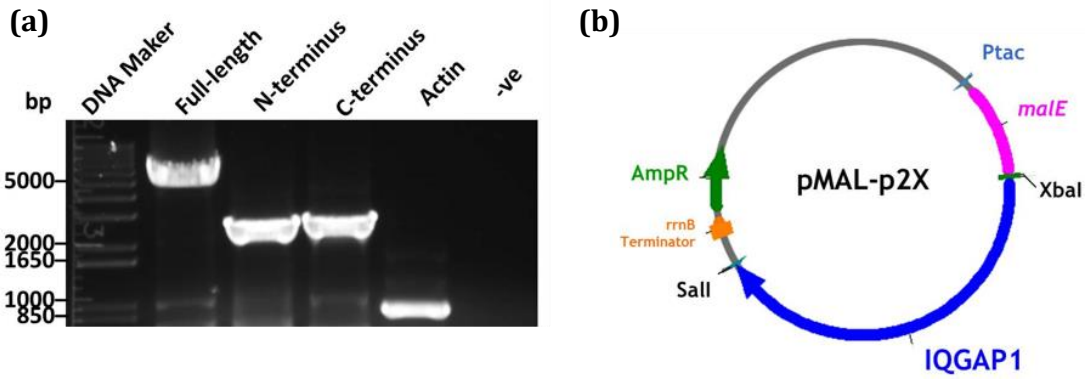

Figure 5.1: IQGAP1 cloning

(a) PCR product of full-length IQGAP1 (5,002 bp), IQGAP1 N-terminal half (2,444 bp) and IQGAP1 C-terminal half (2,578 bp) were separated by 1% agarose gel electrophoresis. Positive control for cDNA template showing 838 bp fragments of β –actin. No cDNA template used as a negative control (-ve).

(b) Schematic image of the pMAL-p2X-IQGAP1 constructs to express IQGAP1 under IPTG induction.

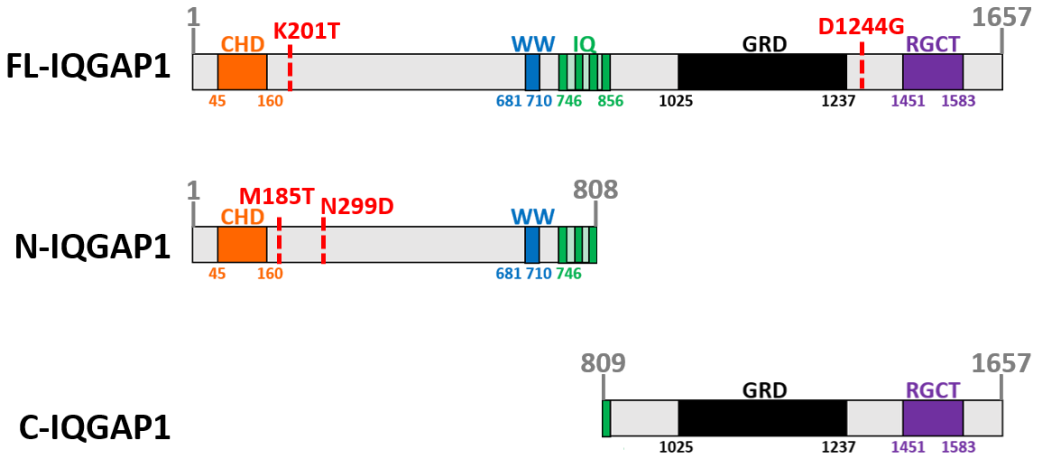

Figure 5.2: Schematic diagram of IQGAP1 constructs illustrating any differences in amino acid composition compared to the *Homo sapiens* IQGAP1 sequence (Accession number: NP_003861)

Known domains that interact with cellular proteins are highlighted. CHD; calponin homology domain, WW; polyproline binding region, IQ; calmodulin-binding IQ motifs, GRD; Ras GTPase-activating protein-related domain, RGCT; RasGAP C-terminus. Numbers indicate amino acid residues.

5.2.2 MBP-IQGAP1 expression and purification

To express IQGAP1 proteins, pMAL-p2X harbouring the full-length, N-terminal half and C-terminal half of the IQGAP1 gene were transformed into *E. coli* strain Rosetta 2 (DE3) pLysS that is suitable for expression of eukaryotic proteins with rarely used codons in *E. coli*. After IPTG induction, the recombinant protein from each of the constructs could be detected on an SDS-PAGE gel stained with Coomassie Blue dye (Figure 5.3). The culture and induction conditions were optimised to obtain the best conditions for expression and purification (Supplemental figure 7.12 and 7.13). Figure 5.3 shows the proteins were in both the soluble (S) and insoluble (P) fractions after lysis of induced cells in BugBuster buffer. SDS-PAGE showed several additional bands in the purified protein samples, including protein of the expected molecular weights of the MBP fusion proteins. Total cell lysate from IPTG-induced *E. coli* cells were analysed by Western blotting with antibodies specific to MBP to examine if the proteins were degradation products. Many bands of protein specific to anti-MBP could be detected from the expected molecular weight of the fusion protein to the size of MBP at 42.5 kDa (Supplemental figure 7.14). This suggested that the MBP-fusion proteins may be degraded by bacterial proteases. Another possibility for degradation could be protein folding improperly because of a high reducing potential in the *E. coli* cytoplasm. Direct the protein to the periplasm would be helpful for folding protein in *E. coli.* To improve this, the plasmids were transformed into *E. coli* Rosetta-gami B which is supplemented with a plasmid for expression eukaryotic proteins that are limited by codon usage of *E. coli*. Also, this engineered *E. coli* strain lacks neither the proteases reducing degradation of the expressed protein nor reductase for enhancing the formation of target protein disulphide bonds in the bacterial cytoplasm. However, this strain failed to express the IQGAP1-MBP fusion proteins (Supplemental figure 7.15). Therefore, the fusion proteins were expressed in *E. coli* Rosetta 2 (DE3) pLysS since they showed a high level of expression. The proteins were induced and purified, typical MBP-IQGAP1 fusion protein expression and purification profiles are shown in figure 5.3. Soluble MBP-fusion protein was bound on amylose resin and then eluted with maltose. The partially purified proteins were then used for pull-down assays.

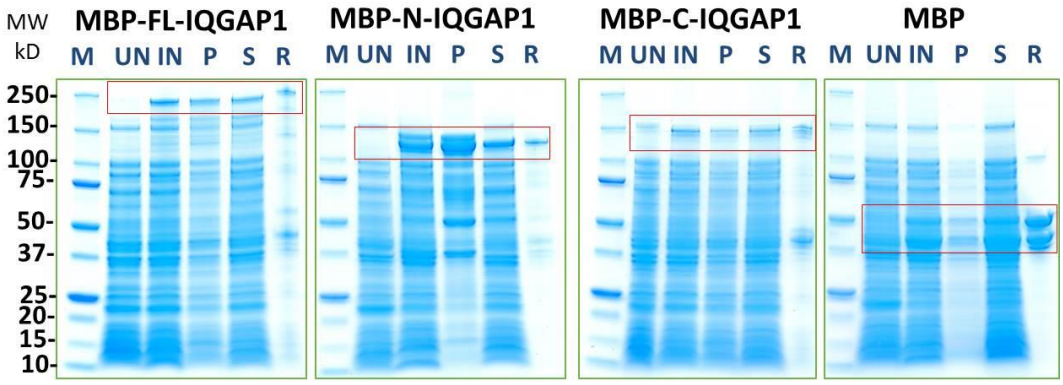

Figure 5.3: SDS–PAGE showing purification of MBP-IQGAP1 recombinant proteins expressed in *E. coli* Rosetta 2 (DE3) pLysS after IPTG induction
M: protein marker, UN: Uninduced cell, IN: Induced cell, P: Pellet of insoluble proteins, S: Soluble proteins and R: Protein bound to amylose resin.

5.2.3 Pull-down assay

To detect a direct interaction between BimA and IQGAP1, a pull-down assay was performed using GST-BimA$_{54-455}$ (Sitthidet et al., 2010) immobilised on GSH beads or MBP-IQGAP1 proteins; full-length, N-terminus and C-terminus immobilised on amylose resin. Comparison between the GST pull-down and MBP pull-down method is shown in figure 5.4. For the GST pull-down, purified MBP-IQGAP1 was added into the reaction containing GST or GST-BimA immobilised on GSH beads. After incubation, unbound proteins were removed from the beads by centrifugation and extensive washing. It was assumed that if IQGAP1 interacts with BimA, IQGAP1 would be eluted from the beads and could be detected by Western blotting using anti-MBP. In the same way, when IQGAP1 proteins were immobilised on amylose resin, BimA could be detected in the pull-down using anti-GST by immunoblotting if BimA is indeed an interacting partner of IQGAP1.

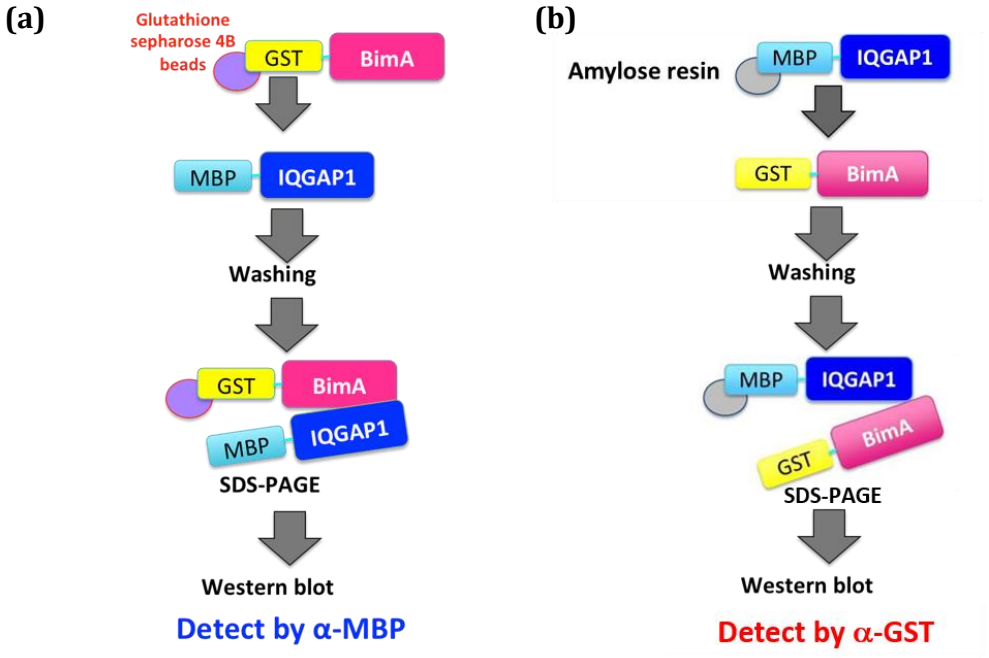

Figure 5.4: Schematic illustrating the pull-down assays

(a) GST pull-down assay. The BimA GST-tagged protein was captured by GSH agarose beads and incubated with the MBP-IQGAP1 proteins. After washing, if IQGAP1 interacts with BimA, it could be eluted and subjected to SDS-PAGE. The fusion MBP protein can be detected by Western blot using anti-MBP.

(b) MBP pull-down assay. The fusion MBP-IQGAP1 proteins were immobilised on amylose resin and incubated with BimA GST-tagged protein. After washing, if BimA interacts with IQGAP1, it could be eluted and subjected to SDS-PAGE. The GST fusion protein can be detected by Western blot using anti-GST.

1) Pull-down assay using immobilised GST-BimA

To perform a GST pull-down assay, the MBP-tag fusion proteins were produced after IPTG induction. The *E. coli* cells were harvested and lysed, and soluble protein was incubated with amylose resin. After washing, the MBP-tagged proteins were eluted with maltose (Figure 5.5a). The amount of eluted proteins was very low, and could only be detected by silver staining (Figure 5.5a). GST and GST-$BimA_{54-455}$ captured on beads were also produced for the pull-down assay as previously described (Sitthidet et al., 2010). The amount of protein on the beads is shown by Coomassie blue staining of the protein gel (Figure 5.5a).

Each MBP-tagged protein was incubated with GST or GST-$BimA_{54-455}$ immobilised on GSH beads. After extensive washing and electrophoresis of the GSH beads, Western blot analysis revealed that all MBP-tagged proteins, including the MBP protein alone were present in both the pull-down with either GST or GST-$BimA_{54-455}$ (Figure 5.5b). It indicated that there was non-specific binding between MBP and GST proteins or the GSH beads. Thus, the result from the GST pull-down was inconclusive.

2) Pull-down assay using immobilised MBP-IQGAP1

Next, IQGAP1 proteins fused with an MBP-tag were immobilised on amylose resin for MBP pull-down assays. SDS-PAGE gel followed by Coomassie blue staining in figure 5.6a showed a dominant band of MBP-tagged IQGAP1 proteins at the predicted molecular weight. The same amount of eluted GST or GST-$BimA_{54-455}$ was incubated with the MBP-proteins (Figure 5.6a). Similarly, to the situation described above, there was evidence of non-specific interaction of the tag proteins either with each other or the amylose resin used in the assays. At this point it could not be concluded that IQGAP1 and BimA are interacting partners and a separate independent approach was taken.

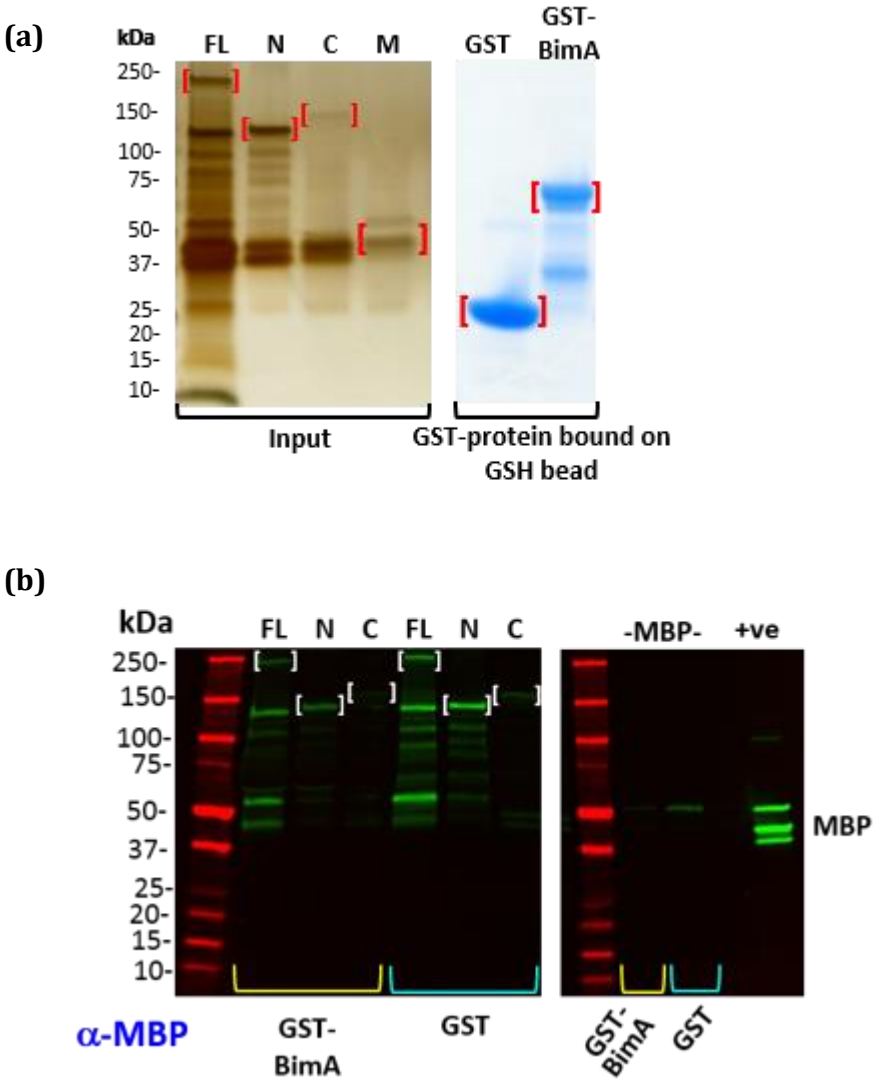

Figure 5.5: Pull-down assay using immobilised GST-BimA

After IPTG induction, protein was expressed and purified for pull-down assay. FL: MBP-full length IQGAP1, N: N-terminal IQGAP1, C: C-terminal IQGAP1, M: Maltose-Binding Protein.

(a) IQGAP1 proteins were eluted from amylose resin and subjected to SDS-PAGE with silver staining. GST and GST-BimA were immobilised on GSH beads and subjected to SDS-PAGE with Coomassie blue staining.

(b) GST pull-down assay; IQGAP1 proteins, full-length, N-terminus, and C-terminus were added to incubate with GST or GST-BimA that was immobilised on GSH beads. After washing extensively, the protein complex was subjected to SDS-PAGE and immunoblotting using anti-MBP.

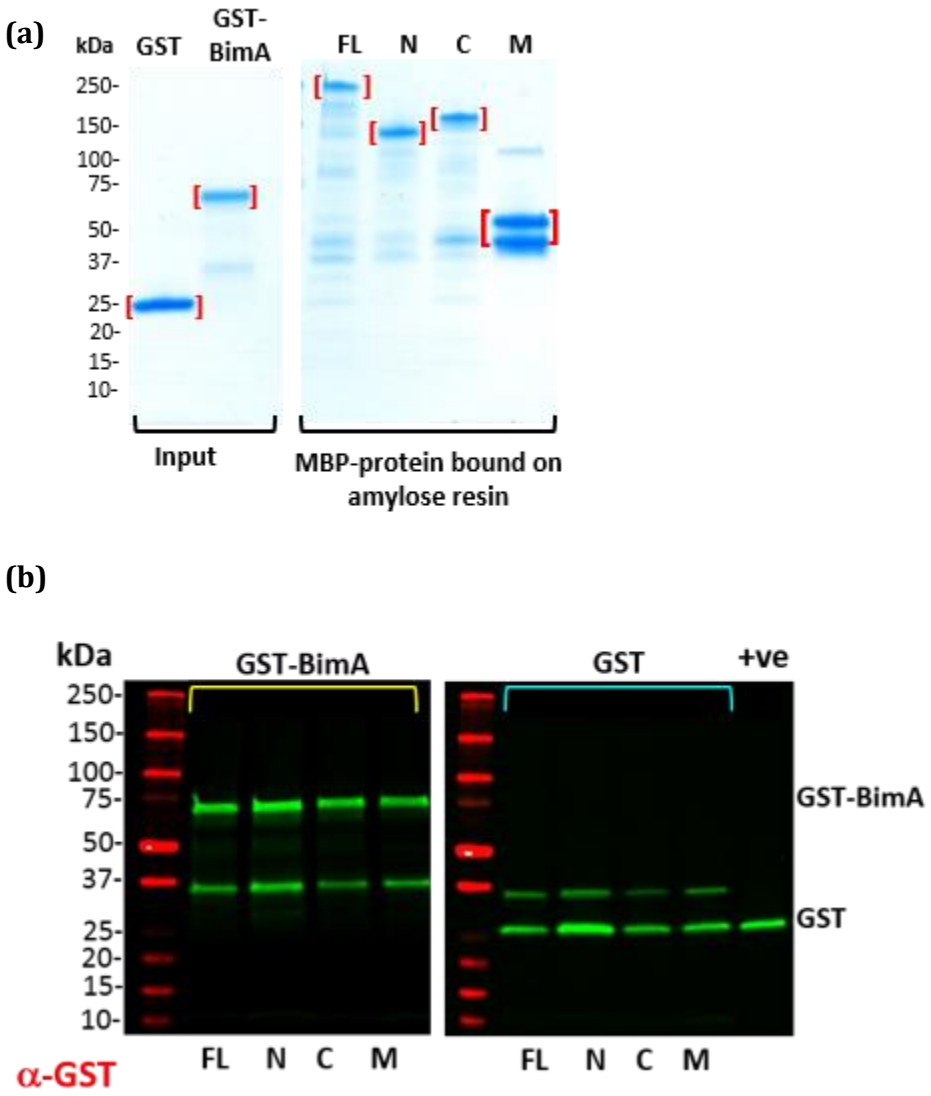

Figure 5.6: Pull-down assay using immobilised MBP-IQGAP1

(a) After IPTG induction, protein was expressed and purified for pull-down assay. FL: MBP- full length IQGAP1, N: N-terminal IQGAP1, C: C-terminal IQGAP1, M: Maltose-Binding Protein. GST and GST-BimA proteins were eluted from GSH beads whereas IQGAP1 proteins were immobilised on amylose resin. Proteins were subjected to SDS-PAGE with Coomassie blue staining.

(b) Eluted samples from the pull-down assays. MBP pull-down assay; GST and GST-BimA proteins were added to full-length, N-terminus, and C-terminus of IQGAP1 that was immobilised on amylose resin. After washing extensively, the protein complex was subjected to SDS-PAGE and immunoblotting using anti-GST. GST protein was loaded as a positive control (+ve).

5.2.4 Identification of a direct interaction between BimA and IQGAP1 using a yeast two-hybrid assay

The yeast two-hybrid (Y2H) assay is a powerful technique used to study protein-protein interactions in yeast cells allowing the detection of the interaction in the cellular environment. This system uses the modular nature of eukaryotic transcriptional activators that contain a DNA-binding domain (DNA-BD) and an activation domain (AD). These domains can be separated and are functionally and structurally independent. The DND-BD binds tightly to a DNA sequence called an upstream activating sequence (UAS), but does not activate transcription unless the AD is close enough to form a functional transcription unit. The reconstitution of the transcription factor activates the downstream reporter gene(s). In this study, the yeast GAL4 transcriptional activator was used to detect protein-protein interactions. A protein of interest (bait) is expressed as a fusion to the GAL4 DNA-BD, whereas another protein (prey) is expressed as a fusion to the GAL4-AD. The fusion proteins are expressed under the yeast alcohol dehydrogenase 1 promoter (P_{ADH1}) and targeted to the yeast nucleus where the interaction occurs. When the bait protein interacts with the prey protein, the AD is brought into close proximity with the DNA-BD forming an active transcription complex. The interaction is tested in the host strain *Saccharomyces cerevisiae* AH109 that utilises three reporters: *ADE2*, *HIS3*, and *MEL1*. The auxotrophic markers; *ADE2* and *HIS3* allow growth on minimal media or synthetically defined (SD) medium formulated to provide the carbon and nitrogen sources for the yeast to grow and is supplemented with essential amino acids lacking adenine and histidine, respectively. Additionally, α-galactosidase which is a secreted enzyme encoded by *MEL1* induces blue colonies on X-α-Gal indicator plates (Bruckner et al., 2009).

To perform a Y2H assay in this study, a bait plasmid; pGBKT7 containing the *TRP1* gene and the GAL4 DNA-BD was fused to amino acids residue 54–455 of BimA. This plasmid had been previously constructed in our laboratory. Yeast cells containing this plasmid were selected on minimal medium lacking tryptophan (SD/-Trp). The prey plasmid; pGADT7 encodes an *LEU2* nutritional marker that allows yeast to grow on SD media lacking leucine (SD/-Leu) as shown in figure 5.7a. The IQGAP1 gene was cloned into the prey plasmid and expressed in-frame with the GAL4-AD. IQGAP1 was amplified from a plasmid harbouring the full-length IQGAP1

(pGEMT-FL-IQGAP1) with 100% amino acid identity with the reference human IQGAP1 sequence. The nutritional selection markers encoded by the bait and prey plasmids allow yeast cells harbouring both bait ad prey plasmids to be selected on a double dropout media lacking both tryptophan and leucine (DDO or SD/–Leu/–Trp), as shown in figure 5.7b. When investigating the protein-protein interaction, the yeast cells were selected on a quadruple dropout (QDO/X) which is the SD media lacking adenine, histidine, leucine and tryptophan supplemented with X-α-Gal. This chromogenic substrate is used for detecting the positive interactions which results in formation of a blue yeast colony. To test whether proteins interact, positive and negative controls for the protein-protein interaction provided from the Matchmaker kit were transformed into *S. cerevisiae* AH109. A prey plasmid, pGADT7-T that encodes simian virus 40 large T-antigen fused with the GAL4-AD was co-expressed with pGBKT7-53 which is a bait plasmid that encodes a murine p53 fused with the GAL4 DNA-BD, generating the strain AH109 pGBKT7-53 pGADT7-T. These proteins are known interacting partners and used to demonstrate the positive interaction by the Y2H system. The interaction between the large T-antigen and p53 leads to reconstitution of the DNA-BD and the AD activating the transcription of *HIS3*, *ADE2* and *MEL1* genes leading to a blue colony on QDO/X plate (Figure 5.7c). Whereas the negative control yeast strain AH109 pGBKT7-Lam pGADT7-T harbours plasmids encoding a fusion of the DNA-BD with human Lamin C (pGBKT7-Lam) and pGADT7-T. Due to no interaction between these proteins, the DNA-BD is still bound on the UAS but it does not activate transcription because the AD is not close enough to activate transcription. Thus, the yeast cell cannot grow on a QDO/X plate (Figure 5.7c). In addition, β-actin was used as a positive control for the interaction with BimA (Stevens et al., 2005a). The β-actin gene was amplified from HeLa cell cDNA. PCR products were amplified and cloned into pGADT7. The resulting plasmids, pGADT7-IQGAP1 and pGADT7-actin, were extracted from *E. coli* for sequencing. Using the T7 promoter primer, the insertion of IQGAP1 and actin was confirmed to be in the correct direction and in-frame with the GAL4-AD (Supplemental figure 7.16). The plasmid, pGADT7-IQGAP1 or pGADT7-actin, was then transformed using the LiAc/SS Carrier DNA/PEG method into *S. cerevisiae* AH109 that harboured the bait plasmid, pGBKT7-BimA. The transformants were isolated on DDO media and then examined for interactions on QDO/X media

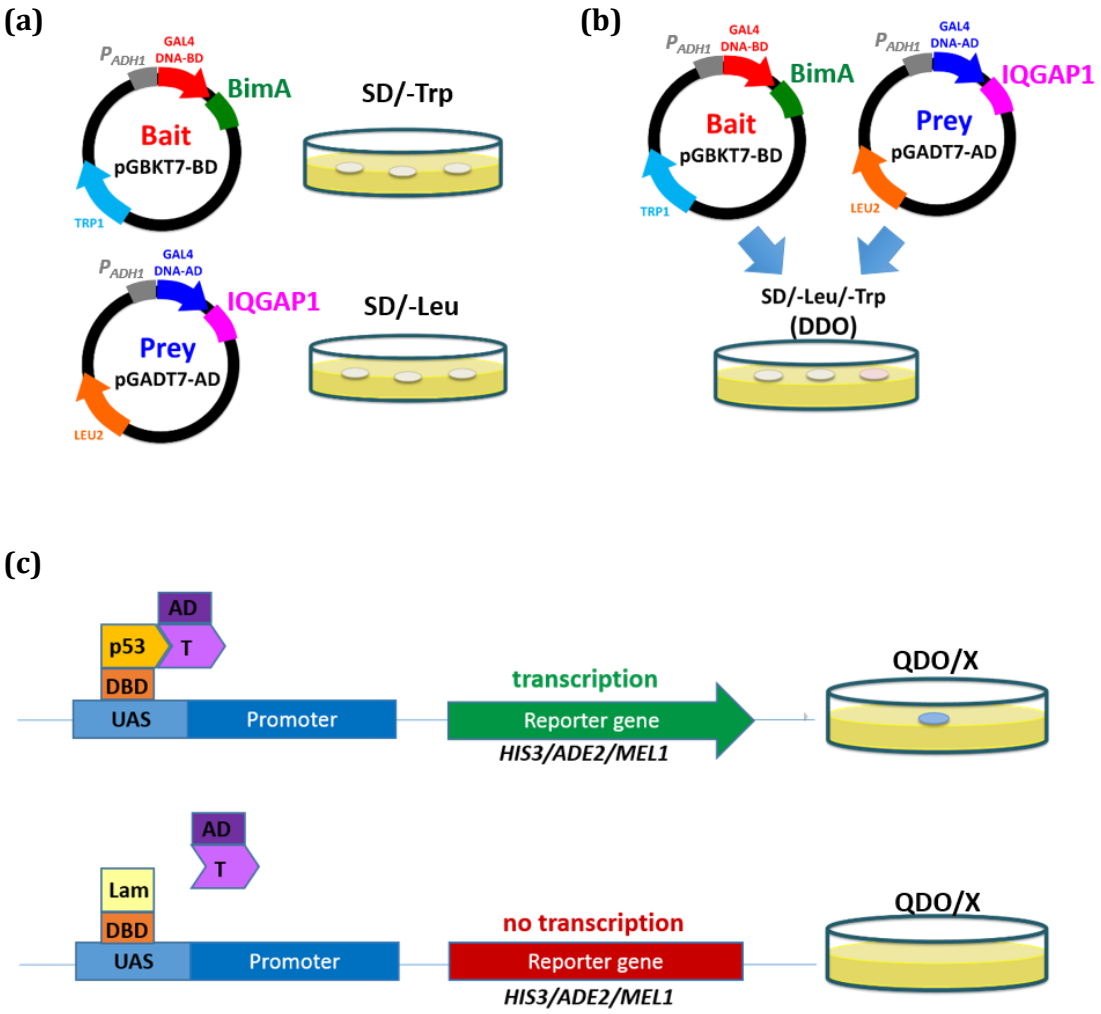

Figure 5.7: Yeast two-hybrid assay

(a) Yeast two-hybrid plasmid map shows important features. The ADH1 promoter is used to drive expression of the fusion proteins. A bait plasmid, pGBKT7 carrying *TRP1* allows growth on minimal media lacking tryptophan (SD/-Trp). The fusion protein, GAL4 DNA-BD-BimA was expressed by pGBKT7. The prey plasmid pGADT7 containing *LEU2* allows growth of the yeast on minimal media lacking leucine (SD/-Leu). The fusion protein GAL4-AD-IQGAP1 was expressed by pGADT7.

(b) When both bait and prey plasmid are introduced into yeast cells, it can be selected on minimal media lacking tryptophan and leucine (DDO).

(c) An example of protein-protein interactions showing the principle of yeast two-hybrid. The p53 and large T-antigen were expressed as DND-BD and AD fusion proteins, respectively in a yeast two-hybrid assay. The DNA-BD binds to upstream activating sequences (UAS). When the AD is close to the site transcriptional activation of the reporter genes occurs, consequently, yeast are able to grow and turn blue on a media lacking tryptophan, leucine, adenine and histidine supplemented with X-α-gal (QDO/X) plates. Whereas co-expressing T-antigen and human Lamin C which is on pGBKT7, yeasts are not able to grow on QDO because the proteins do not interact.

5.2.5 Yeast strain phenotype on SD media

To validate the phenotype of *S. cerevisiae* AH109 harbouring the plasmids, the cells were grown on various SD media. On the minimal medium lacking tryptophan, only cells containing pGBKT7 are able to grow e.g. cells harbouring pGBKT7-BimA, pGBKT7 pGADT7-actin and pGBKT7 pGADT7-IQGAP1, whereas cells that contains only pGADT7 (pGADT7-IQGAP1 or pGADT7-actin) cannot grow on this media (Figure 5.8a). On the other hand, cells harbouring pGADT7 are able to grow on media lacking leucine, whilst cells containing only pGBKT7 (pGBKT7-BimA$_{54\text{-}455}$) cannot survive on this medium (Figure 5.8a). On DDO medium (SD/-Trp/-Leu), cells must contain both bait and prey plasmids to survive. The result in figure 5.8a shows that there was no growth of cells containing only one plasmid on DDO medium. Collectively, all yeast strains displayed the expected phenotype, thus, these strains were then subjected to the Y2H assay.

Before testing protein-protein interactions, all strains carrying the vectors were tested for auto-activation to determine whether the protein fragments can activate the reporters in the absence of any binding partner thereby leading to a false positive result. To test this, the empty prey plasmid, pGADT7 was transformed into *S. cerevisiae* AH109 containing the bait protein (AH109 pGBKT7-BimA). The prey protein, IQGAP1 and actin, was also examined for false positives in the presence of the empty bait vector (pGBKT7). These negative control strains were tested on minimal media lacking histidine or adenine to investigate whether or not the *HIS3* and *ADE2* reporters are activated. Figure 5.8b shows that *S. cerevisiae* AH109 pGBKT7-BimA with the empty prey vector was capable of growing on the minimal media lacking histidine. This indicated that BimA is able to induce *HIS3* reporter gene activity. To eliminate yeast growth as a result of *HIS3* reporter leakage, a competitive inhibitor of the histidine synthase, 3-amino-1,2,4-triazole (3-AT) was included in the media. However, 3-AT could not reduce the background growth of AH109 pGBKT7-BimA pGADT7, despite use of a high concentration (Supplemental figure 7.17). Although BimA showed auto-activation of the *HIS3* reporter, the cells carrying pGBKT7-BimA could not grow on SD medium lacking tryptophan, leucine and adenine. Indeed, any strains tested in this experiment were unable to grow on this medium. Thus, the strong *ADE2* reporter was utilised for testing the protein-protein interaction in this study.

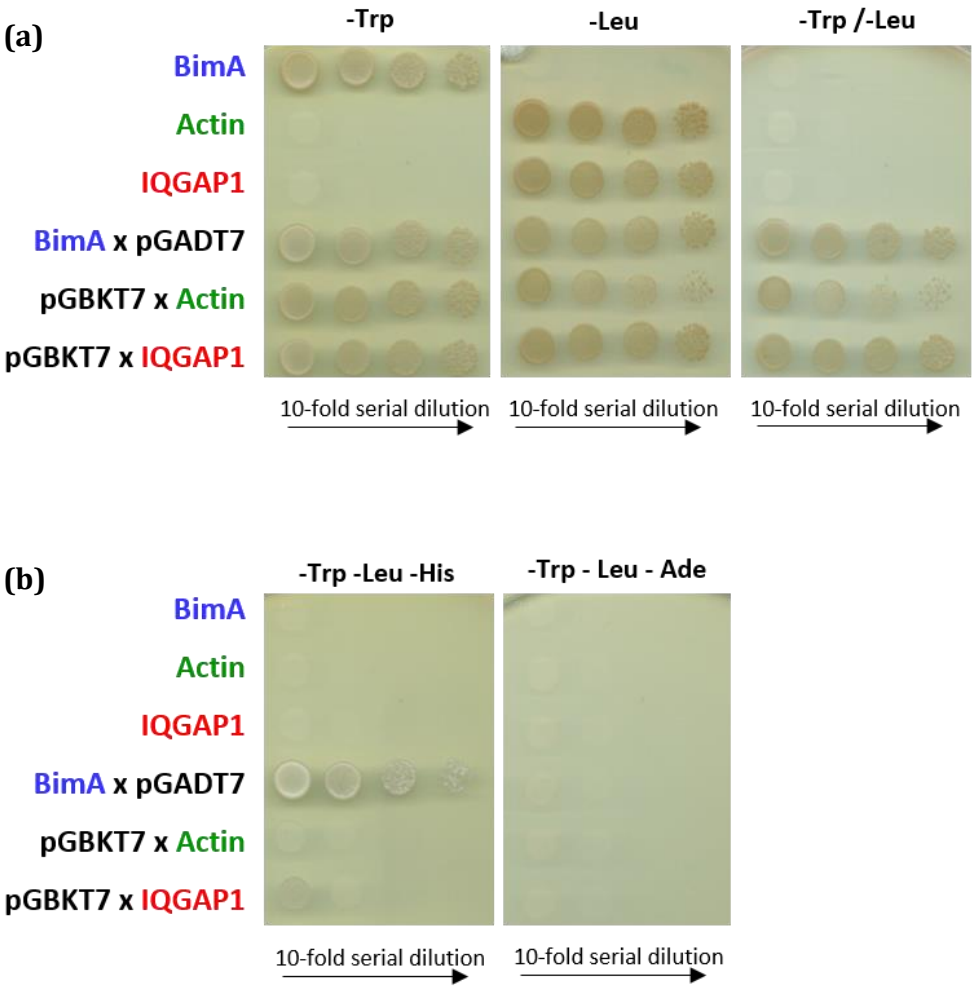

Figure 5.8: Yeast strain phenotype on minimal media (SD) lacking essential amino acid (s)

S. cerevisiae AH109 was transformed with pGBKT7 and/or pGADT7 with the fusion protein indicated in the figure. The yeast was cultured and a serial dilution was made. The cell suspension was dotted on the SD medium and incubated at 30°C for 24 hours.

(a) The minimal SD media lacking tryptophan (-Trp), or leucine (-Leu), or both (-Trp -Leu) showed the presence of plasmid in yeast cells.

(b) The minimal SD media lacking tryptophan, leucine and histidine or adenine (-Trp -Leu –His or -Trp -Leu -Ade) was tested auto-activation of the reporter genes.

5.2.6 Yeast two-hybrid assay

S. cerevisiae AH109 carrying both bait and prey plasmids were re-streaked on DDO media to isolate single colonies before testing for an interaction. From a single colony (after 5 days of incubation), a loop full from a single colony of *S. cerevisiae* AH109 containing both bait and prey plasmids was suspended in 20 µl of water. From the suspension, 5 µl was dropped onto the DDO or QDO/X plates. Figure 5.9 shows the growth of *S. cerevisiae* AH109 on DDO medium at 24 hours after inoculation which confirms that the cells harboured both bait and prey plasmids. To test the interaction, growth on QDO/X plates was observed. The result in figure 5.9 shows that AH109 pGBKT7-BimA pGADT7-actin generates blue colonies on QDO/X indicating an interaction between BimA and β-actin. This result is consistent with the previous finding that showed rhodamine-labelled actin was rapidly recruited to the surface of GST-BimA$_{48\text{-}384}$ coated sepharose beads without additional cellular factors (Stevens et al., 2005a). Although introduction of the vector expressing IQGAP1 as an activation domain fusion protein into the BimA yeast strain (AH109 pGBKT7-BimA pGADT7-IQGAP1) resulted in growth of the yeast strain on QDO media, the colonies remained white (Figure 5.9) even after extended incubation of up to 3 days (Supplemental figure 7.18). Growth on selective media in the absence of detectable α-galactosidase activity indicates that BimA$_{54\text{-}455}$ and IQGAP1 do not directly interact with each other.

The control yeast strains described in section 5.2.4 were also included in the assay and gave the expected phenotypes on DDO and QDO/X media (Figure 5.9).

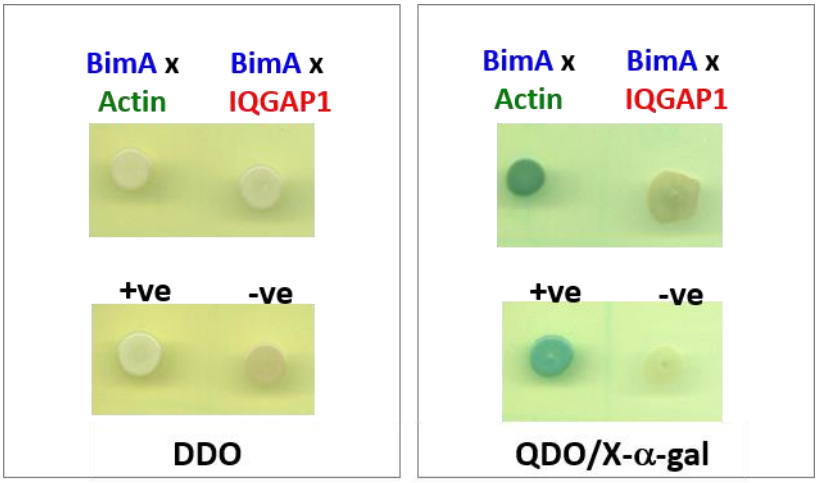

Figure 5.9: Yeast two-hybrid interactions
The pray plasmid expressing actin (pGADT7-actin) or IQGAP1 (pGADT7-IQGAP1) was transformed into *Saccharomyces cerevisiae* AH109 containing pGBKT7-BimA$_{54–455.}$ Cell suspensions were inoculated onto SD medium lacking leucine and tryptophan (DDO) to confirm the presence of plasmids. In addition, they were inoculated on SD medium lacking leucine, tryptophan, adenine and histidine (QDO) supplemented with X-α-Gal substrate to test for protein-protein interactions. Plates were observed at 24 hours after inoculation. The interaction controls were *S. cerevisiae* AH109 harbouring pGBKT7-53 and pGADT7-T (positive interaction control; +ve) and pGBKT7-Lam and pGADT7-T (negative interaction control; -ve).

5.2.7 Verification of protein expression

The fusion proteins from the Y2H cloning vectors were expressed under the yeast alcohol dehydrogenase 1 promoter (P_{ADH1}). The full-length ADH1 promoter leads to high-level expression of genes in pGADT7 during logarithmic phase of the yeast host cells growth. However, transcription is repressed in the late log phase by ethanol, which is a by-product of yeast metabolism that is accumulated in the medium. On the other hand, the bait vector pGBKT7 contains only a 700-bp fragment of the ADH1 promoter which leads to high-level constitutive expression of protein without ethanol repression (Reviewed in Van Criekinge and Beyaert, 1999).

In addition to the fact that the nucleotide sequencing results of pGADT7-IQGAP1 and pGADT7-actin showed the DNA insertions were in-frame with the AD sequence, the expression of fusion proteins was determined by Western Blot analysis. The construction of pGBKT7-$BimA_{54-455}$ was not generated in this study but immunoblotting using the specific antibody to test the actual BimA expression in the yeast was performed. Yeast strains were cultured in DDO medium lacking tryptophan and leucine to maintain the two plasmids. Cells were harvested and lysed with sample buffer to obtain total protein and subjected to SDS-PAGE and immunoblotting. To verify the expression of $BimA_{54-455}$ by pGBKT7, the protein was detected using the GAL4 DNA-BD antibody that binds specifically to the DNA-binding domain of the yeast GAL4 protein. Figure 5.10a shows a dominant protein band in each strain at a molecular weight consistent with the predicted size of the fusion protein. The approximate size of GAL4 DNA-BD is 22 kDa whilst the $BimA_{54-455}$ is about 40 kDa. As the result, the fusion GAL4 DNA-BD with BimA is about 62 kDa. This indicates that $BimA_{54-455}$ was expressed in-frame with the DNA-BD in *S. cerevisiae* AH109. Figure 5.10 also shows the protein band from the yeast lysate of AH109 pGBKT7-53 pGADT7-T which is a positive control for the yeast two hybrid interaction. The molecular weight of p53 fused in-frame to the GAL4 DNA-BD was predicted at 57 kDa, which was also detected using immunoblotting using antibody specific to GAL4 DNA-BD domain (Figure 5.10a).

To determine protein expression in pGADT7, IQGAP1 and actin were expressed as GAL4-AD fusion with a hemagglutinin epitope tag (HA-tag) which is located between the GAL4-AD and the prey protein. In addition to the GAL4-AD, the plasmid contains an N-terminal SV40 nuclear localisation signal (SV40 NLS) for

targeting the protein to the yeast nucleus where the interaction takes place to activate transcription. To detect the expression of IQGAP1 and actin in this study, anti-HA was used to probe the fusion proteins expressed in the yeast cells. Total protein from yeast strain AH109 pGBKT7-53 pGADT7-T was also included and used as a positive control for Western blotting to ensure that the antibody recognises the GAL4-AD-HA-tagged fusion proteins. Figure 5.10b shows the detection of specific proteins at the expected molecular weights in yeast cells strain AH109 pGBKT7-BimA pGADT7-actin and the control strain, but not in AH109 pGBKT7-BimA pGADT7-IQGAP1. GAL4-AD-HA-tagged T-antigen fusion protein is about 89 kDa and GAL4-AD-HA-tagged actin fusion protein is about 60 kDa. On the other hand, IQGAP1 fused with GAL4-AD-HA-tagged with a predicted molecular weight at about 210 kDa could not be detected by immunoblotting (Figure 5.10b). A reason for this could be the low level of expression as the full-length ADH1 promoter may be repressed by the ethanol that accumulated in the late-log phase of culture of the strain. To overcome this possibility, the cells were harvested after sub-culture or directly from plates, however, the expression of IQGAP1 still could not be detected by Western blotting in this study (Supplemental figure 7.19). Another reason for this could be that the sensitivity of Western blotting is limited. The protein-protein interactions in Y2H assay can be detected despite very low protein expression (Maple and Moller, 2007).

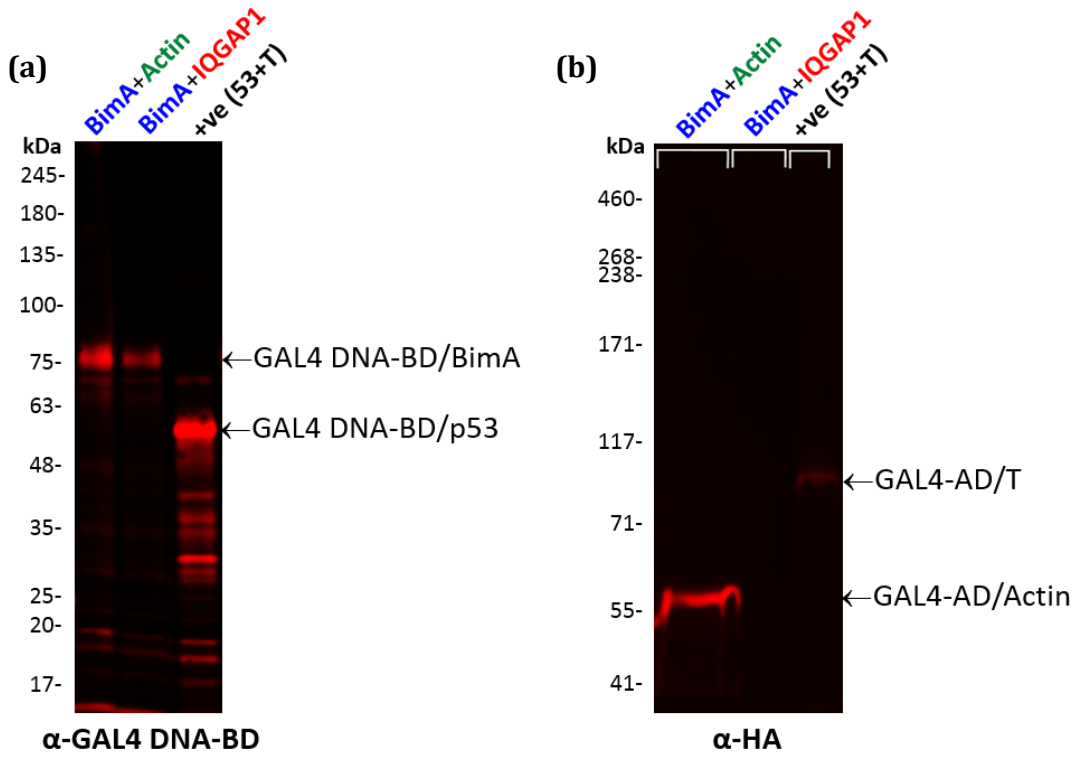

Figure 5.10: Western blot analysis showing expression of yeast fusion proteins in *S. cerevisiae* AH109

Overnight cultures of *S. cerevisiae* AH109 strains containing pGBKT7-BimA pGADT7-Actin (BimA+Actin), pGBKT7-BimA pGADT7-IQGAP1 (BimA+IQGAP1) and pGBKT7-p53 pGADT7-T (+ve) were harvested. The whole cell lysates were visualised by SDS-PAGE and probed by Western blotting.

(a) Protein expressed by pGBKT7 strains were detected using antibody specific to the GAL4 DNA-BD. Arrows indicate the binding domain fusion proteins.

(b) Protein expressed by pGADT7 strains were detected using antibody specific to the HA-tag. Arrows indicate the fusion proteins.

5.2.8 Cloning and expression of IQGAP1 in *Pichia*

Both *in vitro* and *in vivo* techniques failed to detect a direct interaction between IQGAP1 and BimA. Despite this, it was hypothesised that IQGAP1 was required for actin polymerisation mediated by BimA. To test this, purified IQGAP1 and BimA were required for an *in vitro* pyrene-actin assay. Previously, the full-length IQGAP1 was expressed in *E. coli* using pMAL-p2X. However, large-scale production of the full-length IQGAP1 could not be performed. It was assumed that stability of the plasmid and toxicity of the target protein in *E. coli* may be factors preventing large scale production and purification. To test this, the number of *E. coli* containing pMAL-p2X-FL-IQGAP1 after IPTG induction was quantified and it revealed a dramatic decrease in bacterial cell number on the LB plate containing the appropriate antibiotics compared with cells that had not been induced with IPTG (Supplemental figure 7.20). This plasmid instability and toxicity of the IQGAP1 to *E. coli* likely explains the low expression levels. From this result, the full-length IQGAP1 gene from the pMAL-p2X construct was sub-cloned into pPICZ B for expression of the protein intracellularly in *P. pastoris* to generate purified full-length IQGAP1. The plasmids were verified by sequencing to confirm that the IQGAP1 gene was in-frame with the polyhistidine (6x-His) tag (Supplemental figure 7.21). The plasmid was linearised and then transformed into *P. pastoris*. There are two different *P. pastoris* recombinant strains. Mut^{+} strain is capable of metabolising methanol as its sole carbon source (same as wild-type strain) and Mut^{S} phenotype has a slow growth phenotype on methanol medium. One phenotype may have better IQGAP1 expression than the other. Thus, both strains GS115 (Mut^{+}) and KM117H (Mut^{S}) were tested for IQGAP1 expression. *P. pastoris* GS115#15 showed the greatest expression of IQGAP1 estimated from GAPDH expression which was used as a loading control (Figure 5.11a). This strain was further optimised for a time point that yielded the greatest IQGAP1 production and showed IQGAP1 was produced increasingly over time until 4 days (Figure 5.11a). Then, the production was scaled up to 4 litres and the extracted protein was purified by affinity chromatography. Figure 5.11b shows that non-specific proteins were eluted from the Ni column and a protein of the expected molecular weight of IQGAP1 could not be detected, although it could be detected using Western blotting (Figure 5.11b). Thus, the amount of IQGAP1 was very low and would not be enough for further experiments.

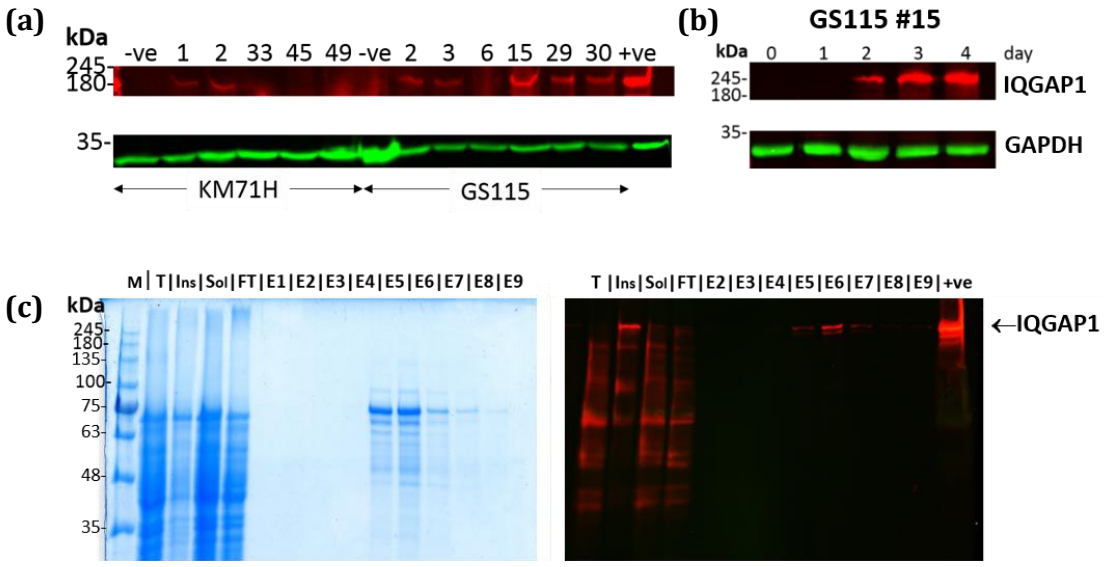

Figure 5.11: IQGAP1 expression and purification in *Pichia*

(a) Western blot probed with anti-IQGAP1 and anti-GAPDH as a loading control for screening of IQGAP1 expression in *Pichia* strains, GS115 (Mut^+) and KM117H (Mut^S).

(b) *P. pastoris* GS115#15 was selected for optimisation showing the greatest of IQGAP1 expression after 4 days of induction.

(c) IQGAP1 fused with 6xHis protein expressed in *Pichia* was affinity purified from 4 litres culture. Anti-IQGAP1 antibodies specifically recognised the full-length IQGAP1-6xHis protein by immunostaining of Western blots of samples from induced cell lysates, M: molecular weight marker, T: Total protein, Ins: Insoluble protein, FT: Flow through, E: Elutions.

5.2.9 Purification of N-IQGAP1

Since the full-length IQGAP1 could not be produced in a large-scale in either *E. coli* or *P. pastoris, E. coli* harbouring pMAL-p2X-N-IQGAP1 (described in section 5.2.2) was used for protein expression. From 4 litres of induced *E. coli* culture, MBP-N-IQGAP was purified by affinity chromatography. Figure 5.12a shows the protein was expressed and was bound on the amylose resin. The MBP-tag can be cleaved from the fusion protein using FactorXa, which is a site-specific endo-protease recognising a sequence that is introduced on the plasmid between sequence coding for MBP and the target protein. After digestion, the fused protein was cleaved efficiently resulting in N-IQGAP1 and MBP at the expected size (Figure 5.12a). FactorXa cleavage was performed with the fusion protein bound to the matrix. The digested protein was washed out and collected. Each fraction of proteins was tested for IQGAP1 protein by dot blot using anti-IQGAP1. Positive fractions were pooled and subjected to SDS-PAGE followed by Coomassie blue staining. Figure 5.12b shows the purified N-IQGAP1 protein that was used for a pyrene-actin polymerisation assay.

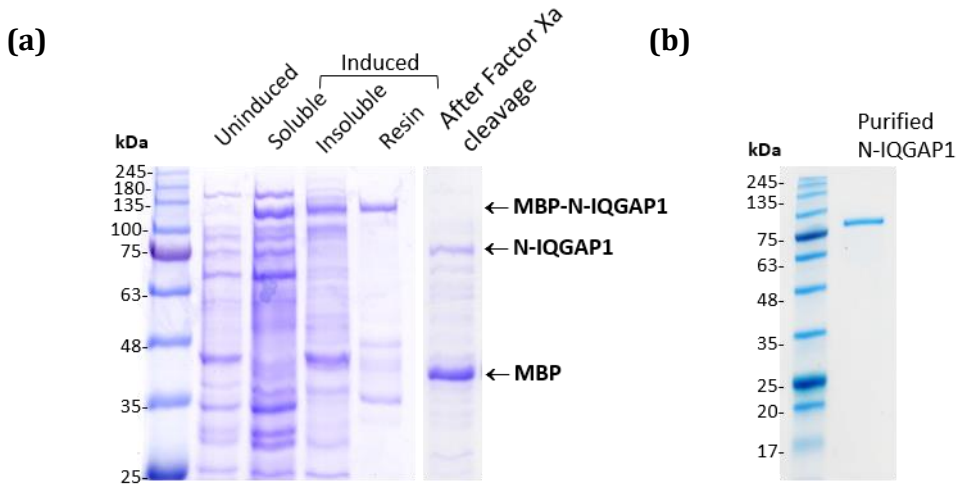

Figure 5.12: Purification of N-IQGAP1

(a) SDS–PAGE followed by Coomassie staining showing purification of MBP-N-IQGAP1 protein expressed in *E. coli* Rosetta 2 (DE3) pLysS after IPTG induction. Proteins were extracted from uninduced cells, soluble protein, insoluble proteins and the protein bound to amylose resin after elution. The eluted MBP-N-IQGAP1 protein was treated with FactorXa to cleave the MBP-tag off.

(b) SDS–PAGE followed by Coomassie staining showing the purified N-IQGAP1 used for pyrene-actin assay in this study. The protein was obtained from the on-column cleavage by FactorXa.

5.2.10 Cloning and expression of $BimA_{54-470}$

To study actin polymerisation *in vitro*, purified BimA was required. A recent study showed that the full passenger domain located at the C-terminus of BimA is important for oligomerisation and is required for full actin polymerisation activity (Benanti et al., 2015). In this study, BimA from amino residue 54 to 470 that includes the passenger domain and extends through the trimeric coiled coil region was produced. To amplify nucleotide sequence encoding $BimA_{54-470}$, pME-6032 harbouring full-length BimA from *B. pseudomallei* 10276 (Stevens et al., 2005b) was used as template for amplification. The PCR fragment was cloned into pET-21b(+) to generate $BimA_{54-470}$-6x-His. *E. coli* strains containing the plasmid were screened by PCR and then subjected to sequence analysis. The plasmid was transformed into *E. coli* Rosetta 2 (DE3) pLysS for protein expression and the transformants were screened for $BimA_{54-470}$ expression in a pilot experiment by Western blotting using antibody specific to $BimA_{48–384}$ (Stevens et al., 2005a) (Supplemental figure 7.22). Then a clone was selected for large-scale production (1 litre) and protein isolated by affinity purification. Figure 5.13a shows that proteins were eluted from the matrix, however the dominant band was not the expected size, it was bigger than the predicted molecular weight of the fusion protein (~44 kDa). To detect the His-tagged BimA protein, one of the elution fractions was further examined by immunoblotting using anti-BimA and anti-6xHis. Figure 5.13b revealed that the His-tagged BimA protein could be detected in the elution fraction after purification. Since the yield was so low, we next attempted to produce $BimA_{54-470}$ as an MBP-fusion protein.

(a)

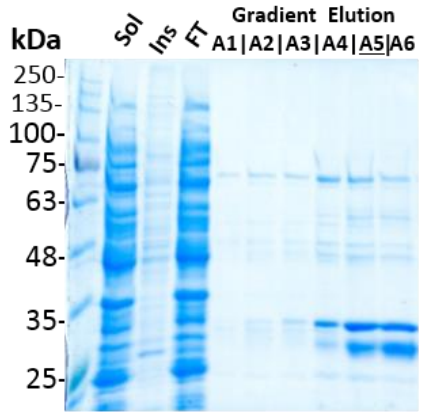

(b)

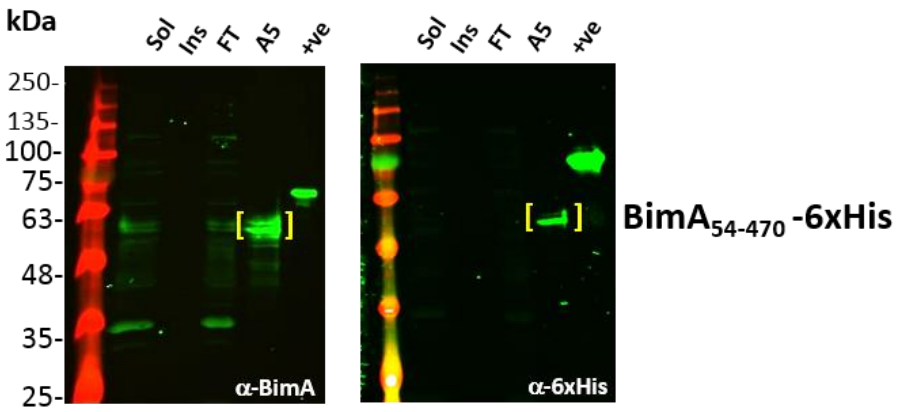

Figure 5.13: BimA$_{54-470}$-6xHis expression and purification

(a) SDS–PAGE followed by Coomassie staining showing purification of BimA$_{54-470}$-6xHis recombinant protein expressed in *E. coli* Rosetta 2 (DE3) pLysS after IPTG induction. Sol: Soluble protein, Ins: Insoluble proteins, FT: Flow-through, A1-A6: Gradient elution fractions.

(b) The same samples in (a) were subjected to immunoblotting using anti-BimA and anti-His. The positive controls for each antibody are GST-BimA$_{54-455}$ and a 6His tag protein kindly provided from Amy Richards.

To produce MBP-tagged $BimA_{54-470}$, the gene from pET-21b(+)-$BimA_{54-470}$ was sub-cloned into pMAL-p2X. The plasmids containing the $BimA_{54-470}$ insert were screened by PCR. A clone was selected for sequencing to confirm the MBP-tag was in-frame with $BimA_{54-470}$. Then a pilot scale protein expression and purification was performed. Figure 5.14a shows that expression of MBP-$BimA_{54-470}$ was induced and the soluble protein was bound to the amylose resin. The protein band after elution showed a dominant band of MBP-BimA, although the size of protein was not as expected. A reason for this may be the hydrophobicity of BimA causing the fusion protein to migrate faster than the predicted molecular weight (~88 kDa). To determine if the induced protein was BimA, the eluted fraction was subjected to Western blot analysis using anti-BimA. The result showed only one band specific to BimA having a molecular weight as same as the dominant band that shown in SDS-PAGE gel (Figure 5.14b in Panel 3). This suggested that MBP-$BimA_{54-470}$ was expressed in *E. coli* successfully showing a reasonable amount of protein that was enough for downstream purification.

An initial trial of the pyrene-actin polymerisation assay using purified MBP protein alone showed a high level of background nucleation activity, compared to control (actin alone) reactions that were used as a baseline for nucleation activity (Supplemental figure 7.23). Thus, we determined that the MBP-tag would need to be removed from the MBP-BimA fusion protein before using BimA in the actin polymerisation assay. Cleavage of MBP-$BimA_{54-470}$ by FactorXa was examined using a web tool (http://web.expasy.org/ peptide_cutter/) first. This tool confirmed that there is one FactorXa recognition site within the predicted MBP-$BimA_{54-470}$ protein sequence between the MBP and BimA proteins. This allows the cleavage of MBP after MBP-BimA purification. However, when MBP-BimA was digested with FactorXa, the molecular weight of the resulting protein products was not as expected. Figure 5.14b shows two bands of digested proteins with molecular weight at approximately 40 and 25 kDa. The molecular weight of MBP is about 42 kDa and the predicted molecular weight of $BimA_{54-470}$ is about 40 kDa. Immunoblotting with BimA antibodies revealed that the smaller band of the digested protein was BimA (Figure 5.14b). It was hypothesised that there was an additional unpredicted site for the FactorXa protease on BimA. To test this, GST-$BimA_{54-455}$ expressed and purified from a previous construct (Sitthidet et al., 2010) was used as the protein substrate for

FactorXa cleavage. Additionally, electrophoretic profiles of the BimA fragment was analysed in the absence of denaturing agents (Native-PAGE), a procedure commonly used for molecular mass determination of hydrophobic proteins. Surprisingly, both MBP-BimA and GST-BimA proteins showed evidence of proteolysis of the BimA portion of the fusion proteins (Figure 5.14c). Thus, MBP-$BimA_{54-470}$ could not be used for BimA purification because FactorXa cleavage also cut BimA at an additional unknown site, which may result in a loss of functional activity of the protein.

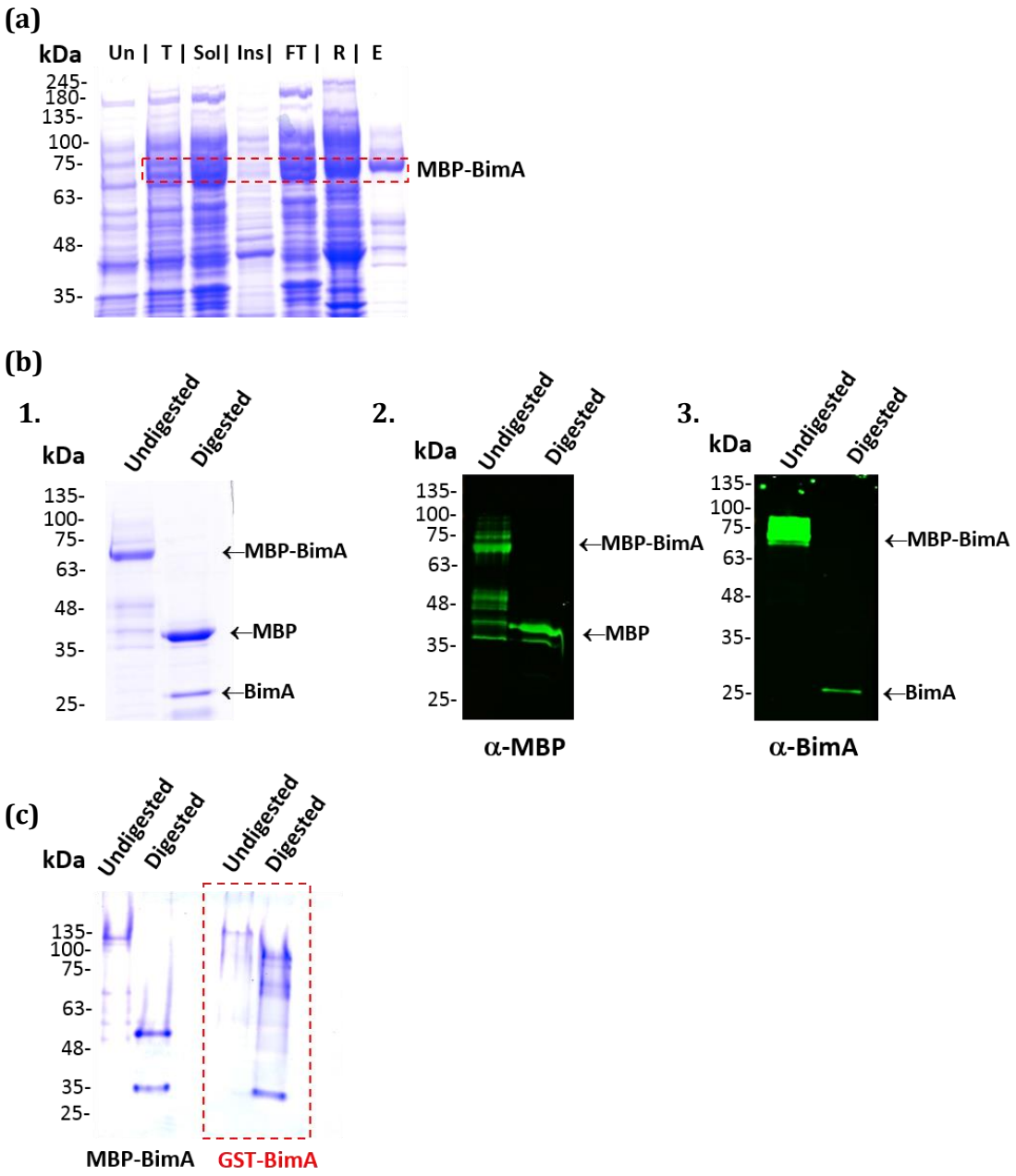

Figure 5.14: Generation of the recombinant fusion protein MBP-BimA$_{54-470}$

(a) SDS–PAGE followed by Coomassie staining showing purification of MBP-BimA$_{54-470}$ recombinant protein expressed in *E. coli* Rosetta 2 (DE3) pLysS after IPTG induction. UN: Uninduced cell, T: Total whole cell lysate from induced cell, Sol: Soluble protein, INS: Insoluble proteins, FT: Flow-through, R: Protein bound to amylose resin, E: Eluted protein.

(b) The MBP-BimA$_{54-470}$ was digested with and without FactorXa (1) and then were subjected to SDS–PAGE followed by Western blot using anti-MBP (2) and anti-BimA (3).

(c) Native–PAGE followed by Coomassie staining showing eluted MBP-BimA$_{54-470}$ and GST-BimA$_{45-544}$ proteins digested with FactorXa or treated with only buffer.

5.2.11 Purification of GST-BimA$_{54-455}$

A recombinant BimA$_{54-470}$ could not be generated in this study at sufficient quantities for the pyrene assay. The previous BimA protein from amino residues 54 to 455 fused with GST (Sitthidet et al., 2010) was used instead. Proteins (GST and GST-BimA) were expressed and purified by affinity chromatography from one litre cultures of induced *E. coli* Rosetta 2 (DE3) pLysS harbouring pGEX-BimA$_{54-455}$ or pGEX-4T-1. After elution and dialysis, proteins were subjected to SDS-PAGE with Coomassie blue staining. As shown in figure 5.15, the proteins were purified and then further used for pyrene assays.

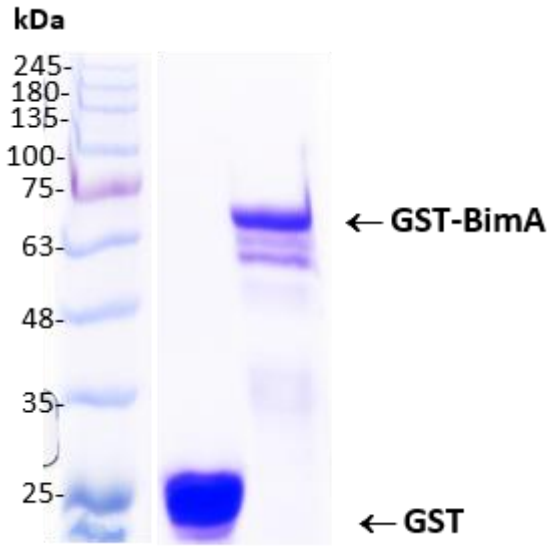

Figure 5.15: SDS-PAGE of recombinant GST and GST-BimA$_{54-455}$ proteins
GST and GST-BimA$_{54-455}$ were purified by affinity chromatography on a GSTrap™ 4B column. After elution from the column using reduced glutathione and then dialysis, the same amount of proteins was loaded for evaluation of purity by SDS-PAGE with Coomassie staining.

5.2.12 The effect of IQGAP1 on BimA-mediated actin polymerisation

IQGAP1 is a scaffold protein that binds actin filaments directly (Mateer et al., 2002) and crosslinks the actin filament through oligomerisation (Fukata et al., 1997). BimA also interacts with actin monomers directly (Stevens et al., 2005a) and enhances the rate of actin polymerisation *in vitro* (Stevens et al., 2005a, Benanti et al., 2015). It was hypothesised that IQGAP1 was required for maximal BimA-dependent actin polymerisation. In this study purified N-IQGAP1 (which contains the domain required for F-actin binding) was tested with GST-BimA$_{54\text{-}455}$ to study the effect of IQGAP1 on BimA-mediated actin polymerisation. The kinetics of actin polymerisation can be observed using pyrene-conjugated actin (Cytoskeleton). Enhanced fluorescence occurs over time when pyrene monomers are incorporated into filaments (Stevens et al., 2005a).

Pyrene-actin polymerisation assays were performed in three independent experiments with a total of 6 reactions using 1 µM actin containing 200 nM of GST protein or GST-BimA$_{54\text{-}455}$ in the presence or absence N-IQGAP (50 nM). Fluorescence data was collected every minute for up to 1 hour. During the linear phase of polymerisation, rates of fluorescence units per second were calculated. G-actin alone in the polymerisation buffer was used as a negative control for the spontaneous actin polymerisation, compared to those with the GST or N-IQGAP1 alone. The actin polymerisation rate of GST or N-IQGAP1 alone was similar (Figure 5.16) which is the same rate of G-actin alone (Supplemental figure 7.24). This suggested that GST and N-IQGAP1 do not have polymerising activity on its own. Moreover, the rate of polymerisation by GST was not enhanced by addition of N-IQGAP1 (Figure 5.16). On the other hand, the rate of BimA-mediated polymerisation markedly increased up to 18.5 units per second in average, compared to the controls which were about 5.8 units per second. The stimulation of actin polymerisation by BimA agreed with our previous studies (Sitthidet et al., 2010, Stevens et al., 2005a). Interestingly, addition of N-IQGAP1 in the reaction containing BimA$_{54\text{-}455}$ increased the polymerisation rate significantly to 21.50 units per second (p = 0.0026). This indicates that N-IQGAP1 enhances the rate of BimA-mediated actin polymerisation.

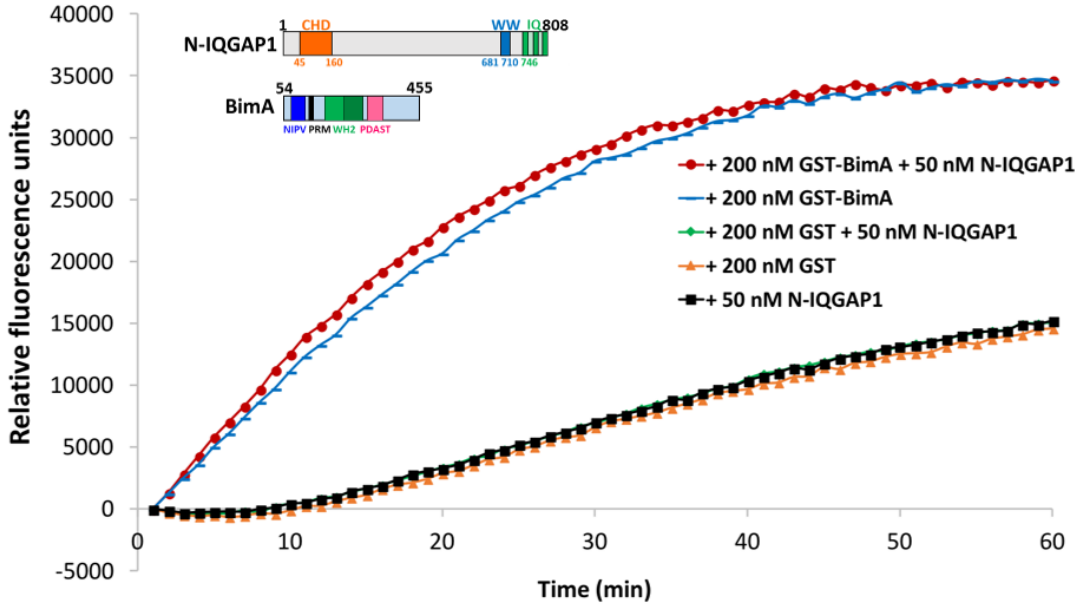

Protein	Polymerisation rate (Mean ± SEM; n = 3)	*p* value compared to the reaction of GST-BimA + N-IQGAP1
GST-BimA+N-IQGAP1	21.05 ± 0.16	n/a
GST-BimA	18.50 ± 0.35	0.0026464*
GST+N-IQGAP1	5.77 ± 0.12	0.0000002*
GST	5.87 ± 0.14	0.0000002*
N-IQGAP1	5.85 ± 0.21	0.0000006*

Figure 5.16: N-IQGAP1 enhances BimA-mediated actin polymerisation
Emission of fluorescence due to polymerisation of pyrene-labelled actin monomers by N-IQGAP1 and GST-BimA$_{54–455}$ proteins (red line) was increased compared with GST-BimA$_{54–455}$ alone (blue lines). While GST alone (orange lines), N-terminal IQGAP1 alone (black line) or GST and N-IQGAP1 (green line) showed spontaneous actin polymerisation. The graphs show the mean emission levels of fluorescence over time from three independent replicates in one assay. The rise in fluorescence units per second during the linear phase of polymerisation was calculated as rates of polymerisation showing the mean rates of fluorescence units per second ± SEM in the table below. Asterisks denote a significant difference in the rate of polymerisation compared to the reaction containing GST-BimA$_{54–455}$ and N-IQGAP1 ($p \leq 0.05$).

5.3 Discussion

BimA, which is located at one pole of the bacterium, was identified as a bacterial factor required for actin-based motility of *B. pseudomallei* (Stevens et al., 2005a). A host cellular protein, IQGAP1, was isolated from splenic lysates using an affinity approach using bacteria constitutively expressing BimA (Jitprasutwit et al., 2016). In this study, it was shown that IQGAP1 is present throughout the length of the actin tails of bacteria. It is possible that BimA interacts with IQGAP1 directly and is required for efficient actin tail formation by *B. pseudomallei*. To determine whether or not there is a direct interaction between these proteins, MBP pull-down and GST pull-down assays were performed. However, as demonstrated in this chapter, the results of the pull-down assays were inconclusive. It is possible that the interaction between IQGAP1 and BimA might require other host cellular proteins. Additionally, other bacteria factors that are regulated by the same VirAG two-component system might mediate the interaction (Schell et al., 2007). To test this, the fusion proteins could be investigated in experiments including lysates prepared from bacteria expressing BimA, with or without other host cellular proteins in splenic lysate. However, attempts to express and purify full length IQGAP1 proteins both in *E. coli* and *P. pastoris* were not successful in this study and would need further optimisation and troubleshooting.

Y2H was utilised to detect an interaction between IQGAP1 and BimA *in vivo* within the yeast cells. This system is very sensitive and the expressed proteins are more likely to be in their native conformations because they are produced in the eukaryotic cells intracellularly. However, this may lead to false positives because of high sensitivity. Thus, the multiple reporter systems in the yeast strain AH109 were selected to minimise false positives for testing the interaction between BimA and IQGAP1. The amino acid residues 54–455 of the BimA protein were expressed fused with the DNA-BD as the bait protein, whereas IQGAP1 was cloned in-frame with the AD as the prey protein. Additionally, β-actin was expressed and used as a positive control for a host cell protein that interacts with BimA.

To test for an interaction between the two proteins of interest, *S. cerevisiae* AH109 pGBKT7-BimA$_{54\text{-}455}$ pGADT7-IQGAP1 and AH109 pGBKT7-BimA$_{54\text{-}455}$ pGADT7-actin were inoculated on the minimal medium containing X-α-Gal substrate

but lacking leucine, tryptophan, adenine, and histidine (QDO/X), along with the control for interaction; AH109 pGBKT7-p53 pGADT7-T (positive control) and AH109 pGBKT7-Lam pGADT7-T (negative control). Plates were observed after 24 hours and up until 72 hours and showed that the yeast strain carrying pGBKT7-BimA$_{54-455}$ and pGADT7-actin produced blue colonies. This strong interaction was comparable with the positive interaction control between the p53 and large T-antigen, and is consistent with the previous result described by Stevens and colleagues (2005b). On the other hand, yeast strain AH109 pGBKT7-BimA$_{54-455}$ pGADT7-IQGAP1 resulted in growth on QDO/X media; however, the colonies remained white even after 3 days of incubation. This is similar to the AH109 pGBKT7-Lam and pGADT7-T strain, representing a negative control for the Y2H assay. The growth of yeast strain AH109 pGBKT7-BimA$_{54-455}$ pGADT7-IQGAP1 also implied that the fusion proteins were expressed although IQGAP1 expression could not be detected by Western blotting in this study. Only genuine positive interactions activate all reporters. Thus, this suggested that BimA$_{54–455}$ and IQGAP1 do not interact directly with each other.

In spite of the fact that IGAP1 does not interact with BimA directly, it was reasonable to hypothesise that IQGAP1 functions as a stabiliser for actin polymerisation by BimA. The previous studies demonstrated that BimA interacts with monomeric actin directly (Stevens et al., 2005a, Stevens et al., 2005b, Sitthidet et al., 2010). Also, BimA polymerises actin in a concentration-dependent manner, although this process is Arp2/3-independent (Benanti et al., 2015, Stevens et al., 2005a). In fact, a recent publication demonstrated that BimA mimics cellular Ena/VASP proteins with the ability to nucleate actin, elongate filaments at their barbed ends, and bundle the filament promoting actin polymerisation (Benanti et al., 2015). IQGAP1 has been recognised as a regulator of the cytoskeleton showing important roles in organising the actin cytoskeleton (Reviewed in Watanabe et al., 2015). IQGAP1 binds directly to filamentous actin and cross-links the filaments into bundles (Bashour et al., 1997, Fukata et al., 1997, Mateer et al., 2002). The binding site of the filamentous actin on IQGAP1 was demonstrated to be on the amino-terminal CHD domain (Fukata et al., 1997). However, the domains that are involved in the function of cross-linking by oligomerisation are unclear, it has been reported that this function is encoded between amino acids 216 - 683 (Fukata et al., 1997) or amino acids 763-863 (Ren et al., 2005). Nevertheless, these studies agree that

oligomerisation of IQGAP1 is important for its function of bundling or stabilising the actin filaments without any actin-related proteins. Further investigations also found that IQGAP1 stimulates branched actin filament assembly, thereby promoting Arp2/3-dependent actin polymerisation by binding to N-WASP (Bensenor et al., 2007, Le Clainche et al., 2007) with the barbed end capping activity which is located on the C-terminus of IQGAP1 (Pelikan-Conchaudron et al., 2011). Despite the fact that the exact mechanism of actin assembly regulation by IQGAP1 is still controversial, it is agreed that IQGAP1 is in an auto-inhibited conformation where the N-terminal domain of IQGAP1 interacts with the C-terminal region to stimulate Arp2/3-dependent actin assembly (Le Clainche et al., 2007, Pelikan-Conchaudron et al., 2011).

To determine the effect of IQGAP1 on BimA-mediated actin polymerisation, purified proteins were required for the pyrene assay. Although the full-length IQGAP1 could not be produced in this study, it is proposed that N-IQGAP1 containing the CHD domain and parts of the IQ motif with the capacity of F-actin binding and oligomerisation are enough to determine its function. Also, the purified $BimA_{54-470}$ which the passenger domain was extended through the trimeric coiled coil that mediates oligomerisation for full activity (Benanti et al., 2015), could not be produced in this study. The region of BimA encoding residues 54 to 455, that lacks the signal peptide and transmembrane domain, and fused with GST-tag from the previous study exhibited an ability to enhance the rate of pyrene-actin monomer polymerisation (Sitthidet et al., 2010). Thus, to investigate the effect of IQGAP1 on BimA-mediated actin polymerisation, the N-IQGAP1 and GST-$BimA_{54-455}$ proteins were used in the pyrene assays. In this assay, $BimA_{54-455}$ enhanced the rate of actin polymerisation, compared with the GST protein, consistent with the previous studies (Benanti et al., 2015, Sitthidet et al., 2010, Stevens et al., 2005b). It is noticeable that the reaction containing GST alone or N-IQGAP1 alone or the combination between GST and N-IQGAP1 showed an initial lag phase. After that, there is a phase of rapid filament elongation, during which subunits add quickly onto the ends of the nucleated filaments. On the other hand, the reaction containing only GST-$BimA_{54-455}$ lacked the lag phase, which indicated $BimA_{54-455}$ enhanced the nucleation rate which is a characteristic of actin nucleators. Whereas the nucleation rate in the reaction containing GST-$BimA_{54-455}$ and N-IQGAP1 was similar to the reaction containing only

GST-BimA$_{54-455}$, the rate of elongation was enhanced with increasing concentrations of F-actin in reaction. This suggested that N-IQGAP1 may function as a stabiliser of the actin filaments stimulated by BimA. To confirm this finding, further experiments are required, for example, by varying the concentration of N-IQGAP1 and including full-length IQGAP1. A previous study showed the concentration-dependent effects of IQGAP1, full-length and several N-terminal fragments of IQGAP1 on actin assembly (Bensenor et al., 2007). The full-length IQGAP1 showed the higher rate of actin polymerisation in the presence of the Arp2/3 complex and N-WASP (Bensenor et al., 2007). A reason for this could be the barbed end capping activity located on the C-terminal end of IQGAP1 (Pelikan-Conchaudron et al., 2011).

In conclusion, this chapter provides the first evidence that IQGAP1 enhances BimA-mediated actin polymerisation *in vitro*, despite no evidence of a direct interaction between these proteins in either a pull-down assay or a yeast two-hybrid assay.

Chapter 6
General Discussion

6.1 Impact of this study

The main objective of this study was to explore the mode of action and functional significance of IQGAP1 in the intracellular life of *Burkholderia pseudomallei*. This facultative intracellular bacterial pathogen has evolved mechanisms to harness the power of actin polymerisation for propelling itself inside the cytosol and providing the driving force for cell membrane protrusion into neighbouring cells. This process requires a putative Type V secreted protein, BimA that is located at one pole of the bacterial cell where actin nucleation occurs and the actin tail is formed (Stevens et al., 2005a). *B. pseudomallei* BimA influences intracellular survival, intercellular spread (Sitthidet et al., 2011) and virulence in mice (Lazar Adler et al., 2015 and our own unpublished data). However, the molecular mechanism by which it recruits and activates cellular factors to assemble actin is not fully understood. From valuable preliminary data obtained in our laboratory, IQGAP1 was one of 30 host proteins identified as a candidate host cell protein involved in BimA-mediated actin polymerisation. Many of the host cell candidate factors are common to both the actin-rich tails of *L. monocytogenes* and *B. pseudomallei*. However, IQGAP1 is a novel protein uniquely associated with the actin tails of *B. pseudomallei* (Jitprasutwit et al., 2016).

This present study revealed the localisation of IQGAP1 in *B. pseudomallei*-infected HeLa cells by confocal microscopy. This is the first demonstration of the presence of IQGAP1 in the actin tail of a bacterial pathogen. Additionally, siRNA-mediated IQGAP1 knockdown indicated a role for IQGAP1 in regulating *B. pseudomallei* actin tail morphology. This result is validated by the finding that the rate of BimA-mediated *in vitro* actin polymerisation could be enhanced by the N-terminal domain of this scaffold protein IQGAP1. This implies that the function of IQGAP1 is in the stabilisation of the actin filaments. Although, a direct interaction between IQGAP1 and BimA could not be detected in this present work.

The role of IQGAP1 in *B. pseudomallei* actin-based motility was investigated using IQGAP1 knockout cells generated using a CRISPR-Cas9 system. Interestingly, an impact of IQGAP1 was also shown on intracellular life of *B. pseudomallei*, in

intracellular survival, MNGC and plaque formation. Additionally, this thesis discloses the actin barcode morphology formed by this bacterium which is similar to septin cages-like structure in *Shigella*. Septin localises next to the actin around the surface of the bacteria, which is then targeted for autophagy and this protein restricts actin tail formation and cell-to-cell spread (Mostowy et al., 2010). In contrast, an incomplete septin ring was detected around the actin tail and body of *Listeria* suggesting that this bacterium avoids septin cage-like formation and escapes autophagy (Mostowy et al., 2010). Whilst septin prevents actin tail formation in *Shigella*, in this study the number of *B. pseudomallei* with this septin cage-like structure was decreased dramatically in IQGAP1 knockout cells, in which the number of viable bacteria was very low. This implies that IQGAP1 is involved in this structure and impacts the intracellular survival life *B. pseudomallei*.

6.2 Future work

6.2.1 Actin-based motility of *B. pseudomallei* in IQGAP1 knockdown cells and IQGAP1 knockout cells

B. pseudomallei is still able to form actin tails in both siIQGAP1 knockdown cells (Chapter 3) and IQGAP1 knockout cells (Chapter4). There is a contradiction between the data in chapter 3 and chapter 4. *B. pseudomallei* formed a longer and less actin dense tail in siIQGAP1 knockdown cells but formed a shorter tail with similar of actin density in IQGAP1 knockout cells, compared to the control cells. It should be noted that the control cells between these groups are different, Lipofectamine-treated cells were used as a control for the knockdown experiments, whereas non-treated cells were used as a control for the studies in the knockout cells. This can be explained by the different percentage of bacteria that displayed tails in these control cells. The proportion of *B. pseudomallei* displaying a tail in Lipofectamine-treated cells was 58% but in non-treated control cells only 34% of bacteria showed a tail, despite observing cells at the same time post-infection (16 hours post-infection). However, the results in the IQGAP1 knockdown and knockout system showed a similarity in the proportion of bacteria displaying actin tails and those without an actin tail. Both experiments showed that there was no difference between the ratio of bacteria without actin tail (no actin association and barcode

morphology) and with actin tail (short and long tails). This result may suggest that these cells could be comparable and agree that *B. pseudomallei* does not require IQGAP1 to induce or initiate actin polymerisation.

The ability of *B. pseudomallei* to form actin tail in either the siIQGAP1 knockdown cells or IQGAP1 knockout cells suggested that other host proteins participate in *B. pseudomallei* actin tail formation. Moreover, the function of IQGAP1 could be compensated by IQGAP2 or IQGAP3 isoforms. Although this study showed the expression of IQGAP2 and IQGAP3 detected by Western blotting was very low, compared with the level of IQGAP1. Further experiments to examine the presence of IQGAP2 or IQGAP3 in the actin tail of *B. pseudomallei* infected siIQGAP1 knockdown cells and IQGAP1 knockout cells using specific antibodies are needed to confirm this hypothesis.

Figure 6.1 shows a possible activity of IQGAP1 involved in *B. pseudomallei* actin tail formation. After *B. pseudomallei* BimA initiate actin polymerisation and the actin filaments are formed, IQGAP1 works with other unknown protein(s) to stabilise the actin filaments producing a compact comet tail, showing intense actin density when stained with fluorescently-labelled phalloidin. In siIQGAP1 knockdown cells, the remaining IQGAP1 is limited causing the actin filament to be looser and longer than those in control cells. In contrast, the ability to form a proper long actin tail is defective in IQGAP1 knockout cells, where the other host cell factor(s) may play a role in *B. pseudomallei* actin tail formation to result in a short actin tail.

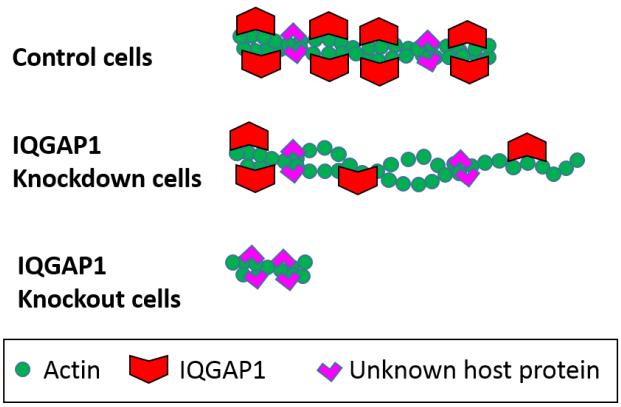

Figure 6.1: A possible function of IQGAP1 on actin filaments. Schematic representation of possible actin filament organisations in the HeLa control cells, siRNA-mediated IQGAP1 knockdown cells and IQGAP1 knockout cells.

The proportion of bacteria displaying tails (short and long tails) were similar between the control cells and the IQGAP1 knockout cells. Likewise, there was no difference in the number of bacteria with short and long tails between the control cells and the siIQGAP1 knockdown cells. Interestingly, within the group of bacteria that did not display tails, the number of bacteria with actin association in a barcode morphology was greater in the non-treated control cells, compared to the IQGAP1 knockout cells. Conversely, the number of bacteria without actin recruitment in the IQGAP1 knockout cells was greater than those in the non-treated control cells. However, this outcome was not found in the IQGAP1-depleted cells. The remarkable effect from the knockout cells could be more pronounced than in the knockdown cells. The remained IQGAP1 protein in the knockdown system may sufficient to partially induce the actin formation. In contrast, IQGAP1 is absent in the knockout cells. This could affect the downstream pathway if IQGAP1 may interact with others for proper actin-based motility of *B. pseudomallei*. Thus, comparison the results from these methods between knockdown and knockout system can be challenging. Particularly, studies on actin-based motility which is a rapid dynamic and highly complex process needs careful investigation. Live cell imaging by real-time video microscopy could be used for elucidating the stages of actin tail formation more precisely. However, this is a limitation to the study of *B. pseudomallei* which must be performed in the containment level 3 laboratory. Thus, a time course study is an alternative way to study this bacterium.

Collectively, both siRNA-mediated knockdown and CRISPR-Cas9 knockout of IQGAP1 demonstrate a role of IQGAP1 in *B. pseudomallei* actin-based motility and the intracellular life cycle of this bacterium.

6.2.2 Intracellular life of *B. pseudomallei* in IQGAP1 knockout cells

The main drawback of using siRNA-mediated knockdown cells in mammalian cells is that the suppression of gene expression is transient. This study showed that IQGAP1 expression recovered after transfection causing a difficulty in distinguishing the effects of IQGAP1 on intracellular survival at the later time points. Moreover, the study of plaque formation was also problematic because it requires a cell monolayer. To achieve the high siRNA transfection efficiency, the optimum cell density was 30-

50% confluence which could not be used to study cell-to-cell spreading in this knockdown system. Thus, studies on intracellular life of *B. pseudomallei* in the siIQGAP1 knockdown cells were only conducted until 16 hours post-infection because the expression of IQGAP1 decreased until this time point before recovery.

The role of IQGAP1 in *B. pseudomallei* invasion was not seen in this study whilst IQGAP1 participates in invasion of host cells by other bacteria. However, at 16 hours post-infection, when the level of IQGAP1 expression in siIQGAP1 knockdown cell was lowest, an impact of IQGAP1 in controlling actin tail length and actin density of *B. pseudomallei* was demonstrated. Bacterial actin tail architecture affects bacterial motility and impacts its pathogenesis. From the findings in siIQGAP1 knockdown cells, it was interesting to further understand the molecular basis of IQGAP1 function on *B. pseudomallei* infection. The CRISPR-Cas9 tool was utilised to knockout IQGAP1 in HeLa cells. To enhance specificity, double nickase plasmids were successfully used to generate the knockout cells. The single clone of IQGAP1 knockout cells, Clone H5, is an insertion mutant that causes a frameshift mutation introducing premature stop codons within the IQGAP1 gene. Eukaryotes evolved mechanisms to degrade this abnormal protein leading to loss of gene function. In this present study, Western blotting, immunofluorescence staining, and immunoprecipitation were used to validate the lack of IQGAP1 as well as the predicted truncated protein in this clone.

A bacterial invasion assay was performed to confirm the previous finding in siIQGAP1 knockdown cells. A low number of bacteria was recovered from the infected cells and showed similar number of bacteria in control and IQGAP1 knockout cells. Indeed, the bacteria could invade into IQGAP1 knockout cell readily but there was no statistical difference with the control cells. It was questionable whether the protocol to examine the invasiveness *in vitro* is repeatable. To test this, the invasive pathogen *Salmonella* was used to test the experimental conditions used in this study. Previous studies showed a defect of *Salmonella* Typhimurium SL1344 invasion into mouse embryonic fibroblasts (MEFs) derived from IQGAP1 knockout mice (Brown et al., 2007, Kim et al., 2011a). In this study, *Salmonella* Typhimurium 4/74 was used to infect the IQGAP1 knockout HeLa cells and the result was inconsistent with the previous studies. Variability could be attributable to experimental methods, the degree of invasiveness of a particular strain, the numbers

of the bacteria inoculated, the growth phase of bacteria, and the cell types as well as the maturity of cell line. This indicated that the protocol for this assay requires adjustment. Additionally, the percentage of invasion obtained for *B. pseudomallei* was relatively low. Alternative methods such as evaluation of the number of intracellular bacteria by confocal microscopy can be applied.

Despite the low number of bacteria recovered at 2 hours post-infection, the number of intracellular bacteria increased at 6 hours after infection in both control cells and IQGAP1 knockout cells but with no statistical difference. After that, the number of bacteria dropped dramatically in IQGAP1 knockout cells, whereas the growth of intracellular bacteria in control cells increased gradually at 24 hours post-infection. To further understand this phase of infection, additional time points before 24 hours post-infection may be required. However, the viability of bacteria was observed at 16 hours post-infection where actin tail formation was examined.

It was clear that the number of bacteria in IQGAP1 knockout cells was lower than in control cells at 24 hours post-infection. The increased number of bacteria in control cells can be explained by the ability of *B. pseudomallei* to spread to the adjacent cell obtaining more nutrients to replicate and subvert host immune responses. In contrast, the number of viable bacteria was reduced at the later time point in IQGAP1 knockout cell. A hypothesis for this is that the bacteria is killed by cell defence mechanisms, for example autophagy since the bacteria is trapped inside the cells. An assay using a protein marker of the autophagosomal membrane, LC3 conversion and turnover assays for monitoring autophagy could be performed to prove this. Additionally, it is evident that the number of *B. pseudomallei* with barcode morphology in control cells was greater than those in IQGAP1 knockout cells, whereas the greater number of bacteria without actin association (no actin recruitment at all) were observed in IQGAP1 knockout cells. The barcode feature that was revealed in this study is similar to *Shigella* that is trapped in septin cage-like structure and targeted to autophagy. However, there is no evidence of septin cages in *B. pseudomallei*. Staining of septins, which are a family of cytoskeletal proteins that play a role in cytokinesis in mammalian cells, can be performed in *B. pseudomallei* infected cells to confirm the localisation of this protein.

Moreover, the percentage of MNGC formation was approximately 10-fold less than those in control cells. Consequently, *B. pseudomallei* showed a defect in plaque formation in IQGAP1 knockout cells even after extended incubation times until 72 hours post-infection. This result agreed with the decrease in intracellular survival of bacteria in IQGAP1 knockout cells. A summary of the findings of the role of IQGAP1 in the intracellular life of *B. pseudomallei* in control and IQGAP1 knockout cells is depicted in figure 6.2.

The defect of *B. pseudomallei* intracellular survival in IQGAP1 knockout cells is one of the most striking results from this present study demonstrating the role of IQGAP1 in intracellular life of *B. pseudomallei*. This finding could be more convincing by restoring IQGAP1 in the knockout cells to rescue the *B. pseudomallei* ability to survive inside host cells. Full-length or some individual domains of IQGAP1 cDNA constructs could be transfected into the IQGAP1 knockdown cells to determine which domains of IQGAP1 are needed.

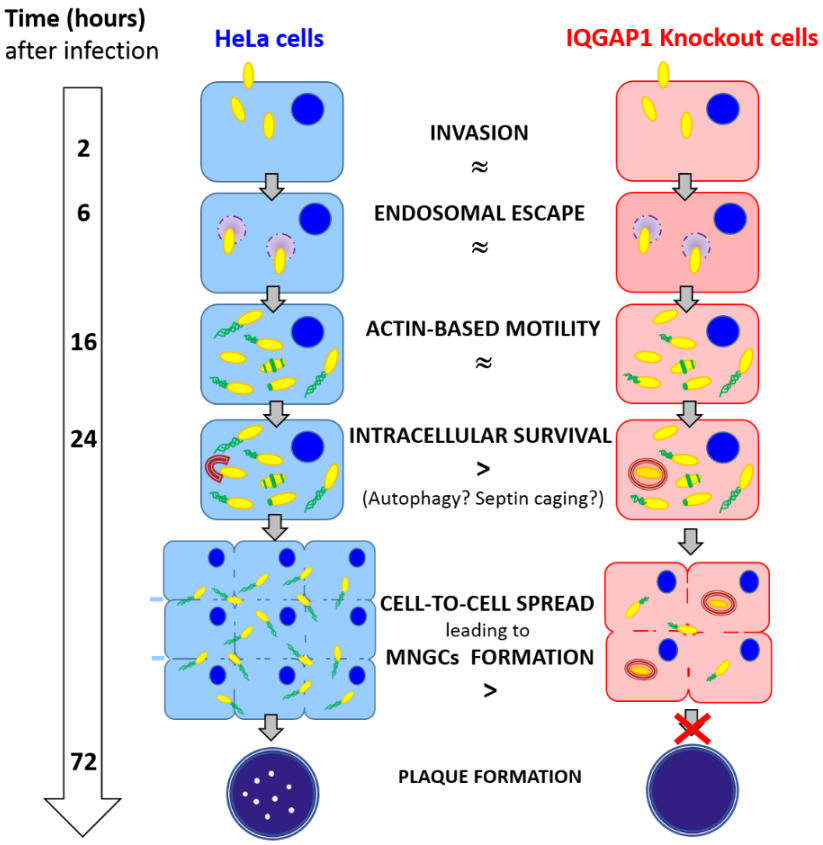

Figure 6.2: Possible fates of *B. pseudomallei* in HeLa control cells, compared to IQGAP1 knockout cells.
The mathematical symbols are based on the results of this study.

6.2.3 Investigation of the interaction between IQGAP1 and BimA

To study protein-protein interactions, the proteins of interest should be active and functionally in a native conformation. It can be difficult to express a protein in heterologous expression systems, especially target protein with inherent properties such as size and hydrophobicity. Choosing alternative expression systems or host strains can improve yield. However, purity of protein is also important to study the activity of proteins. A cell-free translation system may be an option for expressing troublesome proteins, although yield may be low.

The pull-down and yeast two-hybrid assays failed to demonstrate a direct interaction between IQGAP1 and BimA. The pulldown assays were compounded by the fact that the tagged-proteins bound non-specifically to the capture resin. Furthermore, the lack of a direct interaction in the Y2H assay may have been due to the undetectable levels of IQGAP1 fusion protein in the yeast. To overcome these caveats and definitively determine whether BimA and IQGAP1 directly interact with one another, Förster resonant energy transfer (FRET) could be used to study interactions within cells.

Despite the lack of evidence of a direct interaction of BimA with IQGAP1, this thesis shows the importance of N-IQGAP1 on BimA-mediated actin polymerisation. To complete this work, examination of the full-length IQGAP1 or individual domains, as well as including other host cellular factors, using the pyrene-actin polymerisation assay should be performed. Additionally, investigating the effects of IQGAP1 on actin depolymerisation would be interesting for a better understanding of this molecular mechanism.

6.3 Closing statement

B. pseudomallei causes a severe and fatal disease called Melioidosis, an emerging infectious disease with an expanding global distribution and with high mortality rates in the endemic areas. Particularly, this bacterial pathogen is classified as a bioterrorism agent because this agent is believed to be transmitted through the air and there is no available vaccine. Moreover, it is difficult to treat with antibiotics, thus, development of new therapeutic strategies is essential. Discovery of IQGAP1, which is a novel protein involved in *B. pseudomallei* actin-based motility in this study, could be a target for therapy in the disease. Using a therapeutic agent to transiently

suppress the target key protein that bacteria use to survive intracellularly could prevent the progress of disease which could improve management for treatment of severe sepsis.

Indeed, a preliminary observation in this study showed the presence of IQGAP1 in the actin tail of bacteria expressing BimA of another virulent *Burkholderia* species, *B. mallei* and also in the actin tail of an avirulent species, *B. thailandensis* (Figure 6.3). This implies that IQGAP1 is a common target protein that *Burkholderia* spp. exploit for actin tail formation. It is hypothesised that IQGAP1 may be used for actin-based motility in other pathogens with alternative mechanisms. Studying intracellular life of *B. pseudomallei* is essential not only to gain knowledge of the pathogenesis of actin-based motility but also to provide a better understanding of cell biology, both of which are critical to future treatment and prevention.

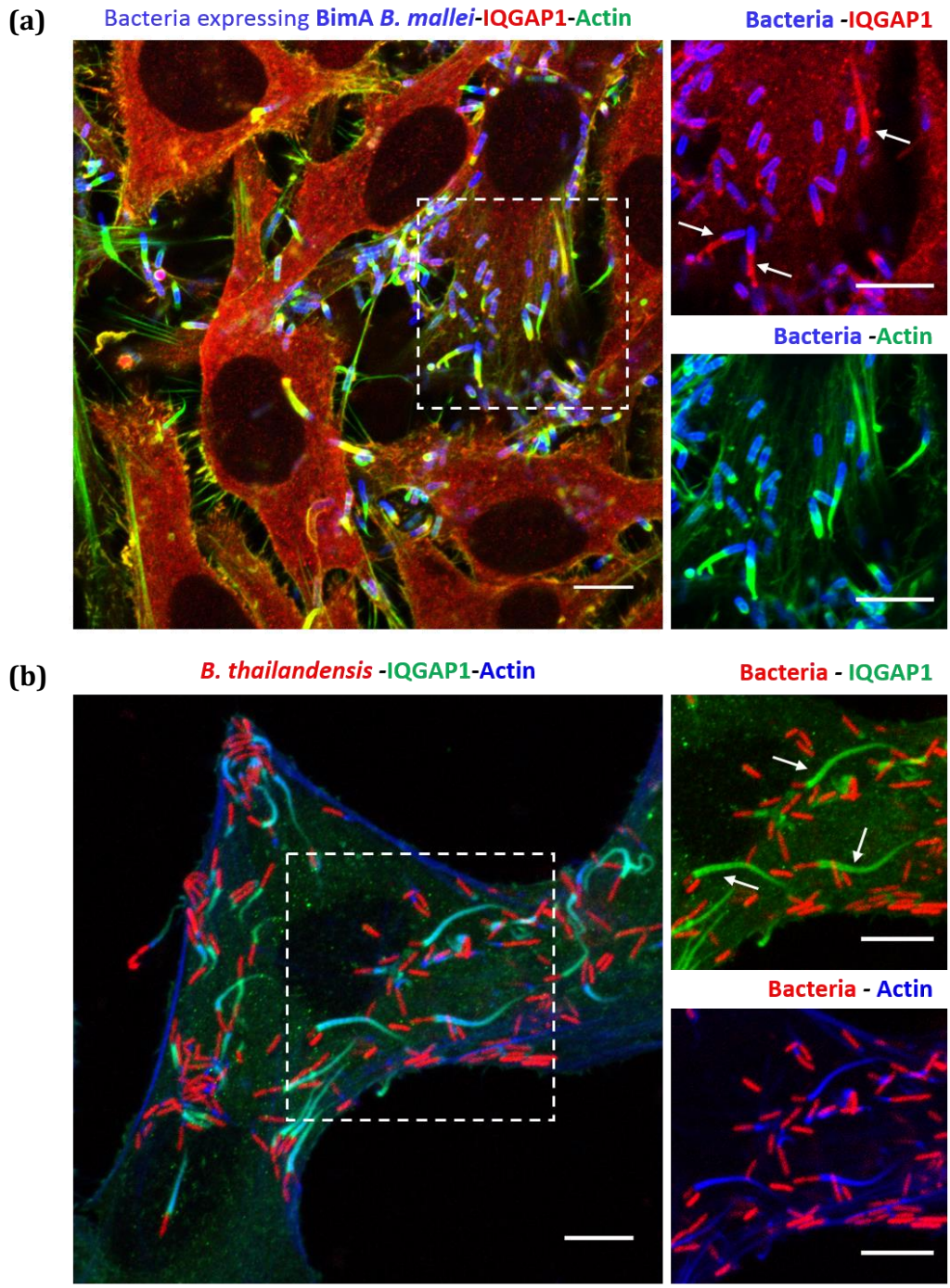

Figure 6.3: Localisation of IQGAP1 in HeLa cells infected with bacteria expressing BimA of *B. mallei* and *B. thailandensis*. Arrows indicate IQGAP1 is recruited into an actin tail.

(a) *B. pseudomallei* 10276 pDM4 :: BimA (pME- $BimA_{ma}$) infected HeLa cells at 16 hours post-infection *B. pseudomallei* expressing $BimA_{ma}$ was stained blue, actin was stained green and IQGAP1 was stained red. Scale bar = 10 µm.

(b) *B. thailandensis* E30 pBHR4-gros-RFP infected HeLa cell at 16 hours post-infection. *B. thailandensis* expressed red fluorescent protein, actin was stained blue and IQGAP1was stained green. (The plasmid is a kind gift from Richard Titball, University of Exeter, UK, (Wand et al., 2011)). Scale bar = 10 µm.

References

ADACHI, M., KAWASAKI, A., NOJIMA, H., NISHIDA, E. & TSUKITA, S. 2014. Involvement of IQGAP family proteins in the regulation of mammalian cell cytokinesis. *Genes Cells*, 19, 803-20.

AHMED, K., ENCISO, H. D., MASAKI, H., TAO, M., OMORI, A., THARAVICHIKUL, P. & NAGATAKE, T. 1999. Attachment of *Burkholderia pseudomallei* to pharyngeal epithelial cells: a highly pathogenic bacteria with low attachment ability. *Am J Trop Med Hyg*, 60, 90-3.

ALLWOOD, E. M., DEVENISH, R. J., PRESCOTT, M., ADLER, B. & BOYCE, J. D. 2011. Strategies for Intracellular Survival of *Burkholderia pseudomallei*. *Front Microbiol*, 2, 170.

ALLY, S., SAUER, N. J., LOUREIRO, J. J., SNAPPER, S. B., GERTLER, F. B. & GOLDBERG, M. B. 2004. *Shigella* interactions with the actin cytoskeleton in the absence of Ena/VASP family proteins. *Cell Microbiol*, 6, 355-66.

AUERBUCH, V., LOUREIRO, J. J., GERTLER, F. B., THERIOT, J. A. & PORTNOY, D. A. 2003. Ena/VASP proteins contribute to *Listeria monocytogenes* pathogenesis by controlling temporal and spatial persistence of bacterial actin-based motility. *Mol Microbiol*, 49, 1361-75.

BALDER, R., LIPSKI, S., LAZARUS, J. J., GROSE, W., WOOTEN, R. M., HOGAN, R. J., WOODS, D. E. & LAFONTAINE, E. R. 2010. Identification of *Burkholderia mallei* and *Burkholderia pseudomallei* adhesins for human respiratory epithelial cells. *BMC Microbiol*, 10, 250.

BARRANGOU, R., BIRMINGHAM, A., WIEMANN, S., BEIJERSBERGEN, R. L., HORNUNG, V. & SMITH, A. 2015. Advances in CRISPR-Cas9 genome engineering: lessons learned from RNA interference. *Nucleic Acids Res*, 43, 3407-19.

BASHOUR, A. M., FULLERTON, A. T., HART, M. J. & BLOOM, G. S. 1997. IQGAP1, a Rac- and Cdc42-binding protein, directly binds and cross-links microfilaments. *J Cell Biol*, 137, 1555-66.

BAXT, L. A. & GOLDBERG, M. B. 2014. Host and bacterial proteins that repress recruitment of LC3 to *Shigella* early during infection. *PLoS One*, 9, e94653.

BENANTI, E. L., NGUYEN, C. M. & WELCH, M. D. 2015. Virulent *Burkholderia* species mimic host actin polymerases to drive actin-based motility. *Cell*, 161, 348-60.

BENSENOR, L. B., KAN, H. M., WANG, N., WALLRABE, H., DAVIDSON, L. A., CAI, Y., SCHAFER, D. A. & BLOOM, G. S. 2007. IQGAP1 regulates cell motility by linking growth factor signaling to actin assembly. *J Cell Sci*, 120, 658-69.

BERNARDINI, M. L., MOUNIER, J., D'HAUTEVILLE, H., COQUIS-RONDON, M. & SANSONETTI, P. J. 1989. Identification of icsA, a plasmid locus of *Shigella flexneri* that governs bacterial intra- and intercellular spread through interaction with F-actin. *Proc Natl Acad Sci U S A*, 86, 3867-71.

BISHAI, E. A., SIDHU, G. S., LI, W., DHILLON, J., BOHIL, A. B., CHENEY, R. E., HARTWIG, J. H. & SOUTHWICK, F. S. 2013. Myosin-X facilitates *Shigella*-induced membrane protrusions and cell-to-cell spread. *Cell Microbiol*, 15, 353-367.

BOUJEMAA-PATERSKI, R., GOUIN, E., HANSEN, G., SAMARIN, S., LE CLAINCHE, C., DIDRY, D., DEHOUX, P., COSSART, P., KOCKS, C., CARLIER, M. F. & PANTALONI, D. 2001. *Listeria* protein ActA mimics WASp family proteins: it activates filament barbed end branching by Arp2/3 complex. *Biochemistry*, 40, 11390-404.

BRANDON, L. D., GOEHRING, N., JANAKIRAMAN, A., YAN, A. W., WU, T., BECKWITH, J. & GOLDBERG, M. B. 2003. IcsA, a polarly localized autotransporter with an atypical signal peptide, uses the Sec apparatus for secretion, although the Sec apparatus is circumferentially distributed. *Mol Microbiol*, 50, 45-60.

BRANDT, D. T., MARION, S., GRIFFITHS, G., WATANABE, T., KAIBUCHI, K. & GROSSE, R. 2007. Dia1 and IQGAP1 interact in cell migration and phagocytic cup formation. *J Cell Biol*, 178, 193-200.

BREITBACH, K., ROTTNER, K., KLOCKE, S., ROHDE, M., JENZORA, A., WEHLAND, J. & STEINMETZ, I. 2003. Actin-based motility of *Burkholderia pseudomallei* involves the Arp 2/3 complex, but not N-WASP and Ena/VASP proteins. *Cell Microbiol*, 5, 385-93.

BRETT, P. J., DESHAZER, D. & WOODS, D. E. 1997. Characterization of *Burkholderia pseudomallei* and *Burkholderia pseudomallei*-like strains. *Epidemiol Infect*, 118, 137-48.

BRETT, P. J., DESHAZER, D. & WOODS, D. E. 1998. *Burkholderia thailandensis* sp. nov., a *Burkholderia pseudomallei*-like species. Int J Syst Bacteriol, 48 Pt 1, 317-20.

BRIEHER, W. M., COUGHLIN, M. & MITCHISON, T. J. 2004. Fascin-mediated propulsion of *Listeria monocytogenes* independent of frequent nucleation by the Arp2/3 complex. *J Cell Biol*, 165, 233-42.

BROWN, M. D., BRY, L., LI, Z. & SACKS, D. B. 2007. IQGAP1 regulates *Salmonella* invasion through interactions with actin, Rac1, and Cdc42. *J Biol Chem*, 282, 30265-72.

BROWN, M. D., BRY, L., LI, Z. & SACKS, D. B. 2008. Actin pedestal formation by enteropathogenic *Escherichia coli* is regulated by IQGAP1, calcium, and calmodulin. *J Biol Chem*, 283, 35212-22.

BRUCKNER, A., POLGE, C., LENTZE, N., AUERBACH, D. & SCHLATTNER, U. 2009. Yeast two-hybrid, a powerful tool for systems biology. *Int J Mol Sci*, 10, 2763-88.

BRUNDAGE, R. A., SMITH, G. A., CAMILLI, A., THERIOT, J. A. & PORTNOY, D. A. 1993. Expression and phosphorylation of the *Listeria monocytogenes* ActA protein in mammalian cells. *Proc Natl Acad Sci U S A*, 90, 11890-4.

BUGALHAO, J. N., MOTA, L. J. & FRANCO, I. S. 2015. Bacterial nucleators: actin' on actin. *Pathog Dis*, 73, ftv078.

BURTON, E. A., OLIVER, T. N. & PENDERGAST, A. M. 2005. Abl kinases regulate actin comet tail elongation via an N-WASP-dependent pathway. *Mol Cell Biol*, 25, 8834-43.

BUSS, C., MULLER, D., RUTER, C., HEUSIPP, G. & SCHMIDT, M. A. 2009. Identification and characterization of Ibe, a novel type III effector protein of A/E pathogens targeting human IQGAP1. *Cell Microbiol*, 11, 661-77.

CAMPELLONE, K. G. & WELCH, M. D. 2010. A nucleator arms race: cellular control of actin assembly. *Nat Rev Mol Cell Biol*, 11, 237-51.

CARLIER, M. F., PERNIER, J., MONTAVILLE, P., SHEKHAR, S., KUHN, S., CYTOSKELETON, D. & MOTILITY, G. 2015. Control of polarized assembly of actin filaments in cell motility. *Cell Mol Life Sci*, 72, 3051-67.

CARLIER, M. F. & SHEKHAR, S. 2017. Global treadmilling coordinates actin turnover and controls the size of actin networks. *Nat Rev Mol Cell Biol*. 18(6):389-401

CHARLES, M., PEREZ, M., KOBIL, J. H. & GOLDBERG, M. B. 2001. Polar targeting of *Shigella* virulence factor IcsA in *Enterobacteriacae* and *Vibrio*. *Proc Natl Acad Sci U S A*, 98, 9871-6.

CHEWAPREECHA, C., HOLDEN, M. T., VEHKALA, M., VALIMAKI, N., YANG, Z., HARRIS, S. R., MATHER, A. E., TUANYOK, A., DE SMET, B., LE HELLO, S., BIZET, C., MAYO, M., WUTHIEKANUN, V., LIMMATHUROTSAKUL, D., PHETSOUVANH, R., SPRATT, B. G., CORANDER, J., KEIM, P., DOUGAN, G., DANCE, D. A., CURRIE, B. J., PARKHILL, J. & PEACOCK, S. J. 2017. Global and regional dissemination and evolution of *Burkholderia pseudomallei*. *Nat Microbiol*, 2, 16263.

CHOE, J. E. & WELCH, M. D. 2016. Actin-based motility of bacterial pathogens: mechanistic diversity and its impact on virulence. *Pathog Dis*.

CHOH, L. C., ONG, G. H., VELLASAMY, K. M., KALAISELVAM, K., KANG, W. T., AL-MALEKI, A. R., MARIAPPAN, V. & VADIVELU, J. 2013. *Burkholderia* vaccines: are we moving forward? *Front Cell Infect Microbiol*, 3, 5.

CHOI, K. H., KUMAR, A. & SCHWEIZER, H. P. 2006. A 10-min method for preparation of highly electrocompetent *Pseudomonas aeruginosa* cells: application for DNA fragment transfer between chromosomes and plasmid transformation. *J Microbiol Methods*, 64, 391-7.

CHONG, R., SWISS, R., BRIONES, G., STONE, K. L., GULCICEK, E. E. & AGAISSE, H. 2009. Regulatory mimicry in *Listeria monocytogenes* actin-based motility. *Cell Host Microbe*, 6, 268-78.

CHOY, J. L., MAYO, M., JANMAAT, A. & CURRIE, B. J. 2000. Animal melioidosis in Australia. *Acta Trop*, 74, 153-8.

CHUNG, L. K., PHILIP, N. H., SCHMIDT, V. A., KOLLER, A., STROWIG, T., FLAVELL, R. A., BRODSKY, I. E. & BLISKA, J. B. 2014. IQGAP1 is important for activation of caspase-1 in macrophages and is targeted by *Yersinia pestis* type III effector YopM. *MBio*, 5, e01402-14.

CHURUANGSUK, C., CHUSRI, S., HORTIWAKUL, T., CHARERNMAK, B. & SILPAPOJAKUL, K. 2016. Characteristics, clinical outcomes and factors influencing mortality of patients with melioidosis in southern Thailand: A 10-year retrospective study. *Asian Pac J Trop Med*, 9, 256-60.

CONG, L., RAN, F. A., COX, D., LIN, S., BARRETTO, R., HABIB, N., HSU, P. D., WU, X., JIANG, W., MARRAFFINI, L. A. & ZHANG, F. 2013. Multiplex genome engineering using CRISPR/Cas systems. *Science*, 339, 819-23.

COURSON, D. S. & ROCK, R. S. 2010. Actin cross-link assembly and disassembly mechanics for alpha-Actinin and fascin. *J Biol Chem*, 285, 26350-7.

CULLINANE, M., GONG, L., LI, X., LAZAR-ADLER, N., TRA, T., WOLVETANG, E., PRESCOTT, M., BOYCE, J. D., DEVENISH, R. J. & ADLER, B. 2008. Stimulation of autophagy suppresses the intracellular survival of *Burkholderia pseudomallei* in mammalian cell lines. *Autophagy*, 4, 744-53.

CURRIE, B. J. 2015. Melioidosis: evolving concepts in epidemiology, pathogenesis, and treatment. *Semin Respir Crit Care Med*, 36, 111-25.

DABIRI, G. A., SANGER, J. M., PORTNOY, D. A. & SOUTHWICK, F. S. 1990. *Listeria monocytogenes* moves rapidly through the host-cell cytoplasm by inducing directional actin assembly. *Proc Natl Acad Sci U S A,* 87, 6068-72.

DAVID, V., GOUIN, E., TROYS, M. V., GROGAN, A., SEGAL, A. W., AMPE, C. & COSSART, P. 1998. Identification of cofilin, coronin, Rac and capZ in actin tails using a *Listeria* affinity approach. *J Cell Sci*, 111 (Pt 19), 2877-84.

DAVIS BK, ROBERTS DM, TOCKER AM, TROIANI Z, JACOB K, TRIESCHMAN K, ET AL. IQGAP1 inhibits type I interferon production via interactions with NLRC3. The *Journal of Immunology*. 2017;198(1 Supplement):129.18-.18.

DEN DUNNEN, J. T., DALGLEISH, R., MAGLOTT, D. R., HART, R. K., GREENBLATT, M. S., MCGOWAN-JORDAN, J., ROUX, A. F., SMITH, T., ANTONARAKIS, S. E. & TASCHNER, P. E. 2016. HGVS Recommendations for the Description of Sequence Variants: 2016 Update. *Hum Mutat*, 37, 564-9.

DOMANN, E., WEHLAND, J., ROHDE, M., PISTOR, S., HARTL, M., GOEBEL, W., LEIMEISTER-WACHTER, M., WUENSCHER, M. & CHAKRABORTY, T. 1992. A novel bacterial virulence gene in *Listeria monocytogenes* required for host cell microfilament interaction with homology to the proline-rich region of vinculin. *EMBO J*, 11, 1981-90.

DOMINGUEZ, R. 2016. The WH2 Domain and Actin Nucleation: Necessary but Insufficient. *Trends Biochem Sci*, 41, 478-490.

DRAGOI, A. M., TALMAN, A. M. & AGAISSE, H. 2013. Bruton's tyrosine kinase regulates *Shigella flexneri* dissemination in HT-29 intestinal cells. Infect Immun, 81, 598-607.
EDWARDS, M., ZWOLAK, A., SCHAFER, D. A., SEPT, D., DOMINGUEZ, R. & COOPER, J. A. 2014. Capping protein regulators fine-tune actin assembly dynamics. *Nat Rev Mol Cell Biol*, 15, 677-89.
EGILE, C., LOISEL, T. P., LAURENT, V., LI, R., PANTALONI, D., SANSONETTI, P. J. & CARLIER, M. F. 1999. Activation of the CDC42 effector N-WASP by the *Shigella flexneri* IcsA protein promotes actin nucleation by Arp2/3 complex and bacterial actin-based motility. *J Cell Biol*, 146, 1319-32.
ESSEX-LOPRESTI, A. E., BODDEY, J. A., THOMAS, R., SMITH, M. P., HARTLEY, M. G., ATKINS, T., BROWN, N. F., TSANG, C. H., PEAK, I. R., HILL, J., BEACHAM, I. R. & TITBALL, R. W. 2005. A type IV pilin, PilA, Contributes to Adherence of *Burkholderia pseudomallei* and virulence in vivo. *Infect Immun*, 73, 1260-4.
FALZONE, T. T., LENZ, M., KOVAR, D. R. & GARDEL, M. L. 2012. Assembly kinetics determine the architecture of alpha-actinin crosslinked F-actin networks. *Nat Commun*, 3, 861.
FATTOUH, R., KWON, H., CZUCZMAN, M. A., COPELAND, J. W., PELLETIER, L., QUINLAN, M. E., MUISE, A. M., HIGGINS, D. E. & BRUMELL, J. H. 2015. The diaphanous-related formins promote protrusion formation and cell-to-cell spread of *Listeria monocytogenes*. *J Infect Dis*, 211, 1185-95.
FELGNER, P. L., KAYALA, M. A., VIGIL, A., BURK, C., NAKAJIMA-SASAKI, R., PABLO, J., MOLINA, D. M., HIRST, S., CHEW, J. S., WANG, D., TAN, G., DUFFIELD, M., YANG, R., NEEL, J., CHANTRATITA, N., BANCROFT, G., LERTMEMONGKOLCHAI, G., DAVIES, D. H., BALDI, P., PEACOCK, S. & TITBALL, R. W. 2009. A *Burkholderia pseudomallei* protein microarray reveals serodiagnostic and cross-reactive antigens. *Proc Natl Acad Sci U S A*, 106, 13499-504.
FIRAT-KARALAR, E. N. & WELCH, M. D. 2011. New mechanisms and functions of actin nucleation. *Curr Opin Cell Biol*, 23, 4-13.
FRADELIZI, J., NOIREAUX, V., PLASTINO, J., MENICHI, B., LOUVARD, D., SYKES, C., GOLSTEYN, R. M. & FRIEDERICH, E. 2001. ActA and human zyxin harbour Arp2/3-independent actin-polymerization activity. *Nat Cell Biol*, 3, 699-707.
FRANCIS, M. S. & THOMAS, C. J. 1996. Effect of multiplicity of infection on *Listeria monocytogenes* pathogenicity for HeLa and Caco-2 cell lines. *J Med Microbiol*, 45, 323-30.
FRENCH, C. T., TOESCA, I. J., WU, T. H., TESLAA, T., BEATY, S. M., WONG, W., LIU, M., SCHRODER, I., CHIOU, P. Y., TEITELL, M. A. & MILLER, J. F. 2011. Dissection of the *Burkholderia* intracellular life cycle using a photothermal nanoblade. *Proc Natl Acad Sci U S A*, 108, 12095-100.
FUKATA, M., KURODA, S., FUJII, K., NAKAMURA, T., SHOJI, I., MATSUURA, Y., OKAWA, K., IWAMATSU, A., KIKUCHI, A. & KAIBUCHI, K. 1997. Regulation of cross-linking of actin filament by IQGAP1, a target for Cdc42. *J Biol Chem*, 272, 29579-83.
GAO, L. Y., GUO, S., MCLAUGHLIN, B., MORISAKI, H., ENGEL, J. N. & BROWN, E. J. 2004. A mycobacterial virulence gene cluster extending RD1 is required for cytolysis, bacterial spreading and ESAT-6 secretion. *Mol Microbiol*, 53, 1677-93.
GEESE, M., LOUREIRO, J. J., BEAR, J. E., WEHLAND, J., GERTLER, F. B. & SECHI, A. S. 2002. Contribution of Ena/VASP proteins to intracellular motility of *Listeria* requires phosphorylation and proline-rich core but not F-actin binding or multimerization. *Mol Biol Cell*, 13, 2383-96.
GIETZ, R. D. & WOODS, R. A. 2002. Transformation of yeast by lithium acetate/single-stranded carrier DNA/polyethylene glycol method. *Methods Enzymol*, 350, 87-96.

GOLDBERG, M. B., BARZU, O., PARSOT, C. & SANSONETTI, P. J. 1993. Unipolar localization and ATPase activity of IcsA, a *Shigella flexneri* protein involved in intracellular movement. *J Bacteriol*, 175, 2189-96.
GOLDBERG, M. B. & THERIOT, J. A. 1995. *Shigella flexneri* surface protein IcsA is sufficient to direct actin-based motility. *Proc Natl Acad Sci U S A*, 92, 6572-6.
GOLEY, E. D. & WELCH, M. D. 2006. The ARP2/3 complex: an actin nucleator comes of age. *Nat Rev Mol Cell Biol*, 7, 713-26.
GONG, L., CULLINANE, M., TREERAT, P., RAMM, G., PRESCOTT, M., ADLER, B., BOYCE, J. D. & DEVENISH, R. J. 2011. The *Burkholderia pseudomallei* type III secretion system and BopA are required for evasion of LC3-associated phagocytosis. *PLoS One*, 6, e17852.
GOODE, B. L. & ECK, M. J. 2007. Mechanism and function of formins in the control of actin assembly. *Annu Rev Biochem*, 76, 593-627.
GOUIN, E., GANTELET, H., EGILE, C., LASA, I., OHAYON, H., VILLIERS, V., GOUNON, P., SANSONETTI, P. J. & COSSART, P. 1999. A comparative study of the actin-based motilities of the pathogenic bacteria *Listeria monocytogenes*, *Shigella flexneri* and *Rickettsia conorii*. *J Cell Sci*, 112 (Pt 11), 1697-708.
GOUIN, E., EGILE, C., DEHOUX, P., VILLIERS, V., ADAMS, J., GERTLER, F., LI, R. & COSSART, P. 2004. The RickA protein of *Rickettsia conorii* activates the Arp2/3 complex. *Nature*, 427, 457-61.
HAGLUND, C. M., CHOE, J. E., SKAU, C. T., KOVAR, D. R. & WELCH, M. D. 2010. *Rickettsia* Sca2 is a bacterial formin-like mediator of actin-based motility. *Nat Cell Biol*, 12, 1057-63.
HARLEY, V. S., DANCE, D. A., DRASAR, B. S. & TOVEY, G. 1998. Effects of *Burkholderia pseudomallei* and other *Burkholderia* species on eukaryotic cells in tissue culture. *Microbios*, 96, 71-93.
HATCHER, C. L., MURUATO, L. A. & TORRES, A. G. 2015. Recent Advances in *Burkholderia mallei* and *B. pseudomallei* Research. *Curr Trop Med Rep*, 2, 62-69.
HEDMAN, A. C., SMITH, J. M. & SACKS, D. B. 2015. The biology of IQGAP proteins: beyond the cytoskeleton. EMBO Rep, 16, 427-46.
HEINZEN, R. A., GRIESHABER, S. S., VAN KIRK, L. S. & DEVIN, C. J. 1999. Dynamics of actin-based movement by *Rickettsia rickettsii* in vero cells. *Infect Immun*, 67, 4201-7.
HEINZEN, R. A., HAYES, S. F., PEACOCK, M. G. & HACKSTADT, T. 1993. Directional actin polymerization associated with spotted fever group *Rickettsia* infection of Vero cells. *Infect Immun*, 61, 1926-35.
HO, H. Y., ROHATGI, R., LEBENSOHN, A. M., LE, M., LI, J., GYGI, S. P. & KIRSCHNER, M. W. 2004. Toca-1 mediates Cdc42-dependent actin nucleation by activating the N-WASP-WIP complex. *Cell*, 118, 203-16.
HOLDEN, M. T., TITBALL, R. W., PEACOCK, S. J., CERDENO-TARRAGA, A. M., ATKINS, T., CROSSMAN, L. C., PITT, T., CHURCHER, C., MUNGALL, K., BENTLEY, S. D., SEBAIHIA, M., THOMSON, N. R., BASON, N., BEACHAM, I. R., BROOKS, K., BROWN, K. A., BROWN, N. F., CHALLIS, G. L., CHEREVACH, I., CHILLINGWORTH, T., CRONIN, A., CROSSETT, B., DAVIS, P., DESHAZER, D., FELTWELL, T., FRASER, A., HANCE, Z., HAUSER, H., HOLROYD, S., JAGELS, K., KEITH, K. E., MADDISON, M., MOULE, S., PRICE, C., QUAIL, M. A., RABBINOWITSCH, E., RUTHERFORD, K., SANDERS, M., SIMMONDS, M., SONGSIVILAI, S., STEVENS, K., TUMAPA, S., VESARATCHAVEST, M., WHITEHEAD, S., YEATS, C., BARRELL, B. G., OYSTON, P. C. & PARKHILL, J. 2004. Genomic plasticity of the causative agent of melioidosis, *Burkholderia pseudomallei*. *Proc Natl Acad Sci U S A*, 101, 14240-5.
HOLT, M. R. & KOFFER, A. 2001. Cell motility: proline-rich proteins promote protrusions. *Trends Cell Biol*, 11, 38-46.

INGLIS, T. J. & SAGRIPANTI, J. L. 2006. Environmental factors that affect the survival and persistence of *Burkholderia pseudomallei*. *Appl Environ Microbiol*, 72, 6865-75.

JENG, R. L., GOLEY, E. D., D'ALESSIO, J. A., CHAGA, O. Y., SVITKINA, T. M., BORISY, G. G., HEINZEN, R. A. & WELCH, M. D. 2004. A *Rickettsia* WASP-like protein activates the Arp2/3 complex and mediates actin-based motility. *Cell Microbiol*, 6, 761-9.

JITPRASUTWIT, N., ZAINAL-ABIDIN, N., VANDER BROEK, C., KURIAN, D., KORBSRISATE, S., STEVENS, M. P. & STEVENS, J. M. 2016. Identification of Candidate Host Cell Factors Required for Actin-Based Motility of *Burkholderia pseudomallei*. *J Proteome Res*, 15, 4675-4685.

JONES, P. W., COLLINS, P. & AITKEN, M. M. 1988. Passive protection of calves against experimental infection with *Salmonella typhimurium*. *Vet Rec*, 123, 536-41.

JONES, A. L., BEVERIDGE, T. J. & WOODS, D. E. 1996. Intracellular survival of *Burkholderia pseudomallei*. *Infect Immun*, 64, 782-90.

KANOKSIL, M., JATAPAI, A., PEACOCK, S. J. & LIMMATHUROTSAKUL, D. 2013. Epidemiology, microbiology and mortality associated with community-acquired bacteraemia in northeast Thailand: a multicenter surveillance study. *PLoS One*, 8, e54714.

KARLSSON, T., TURKINA, M. V., YAKYMENKO, O., MAGNUSSON, K. E. & VIKSTROM, E. 2012. The *Pseudomonas aeruginosa* N-acylhomoserine lactone quorum sensing molecules target IQGAP1 and modulate epithelial cell migration. *PLoS Pathog*, 8, e1002953.

KASANTIKUL, T., SOMMANUSTWEECHAI, A., POLSRILA, K., KONGKHAM, W., CHAISONGKRAM, C., SANANNU, S., KONGMAKEE, P., NARONGWANICHGARN, W., BUSH, M., SERMSWAN, R. W. & BANLUNARA, W. 2016. Retrospective Study on Fatal Melioidosis in Captive Zoo Animals in Thailand. *Transbound Emerg Dis*, 63, e389-94.

KENNEDY, G. M., MORISAKI, J. H. & CHAMPION, P. A. 2012. Conserved mechanisms of *Mycobacterium marinum* pathogenesis within the environmental amoeba *Acanthamoeba castellanii. Appl Environ Microbiol*, 78, 2049-52.

KESPICHAYAWATTANA, W., RATTANACHETKUL, S., WANUN, T., UTAISINCHAROEN, P. & SIRISINHA, S. 2000. *Burkholderia pseudomallei* induces cell fusion and actin-associated membrane protrusion: a possible mechanism for cell-to-cell spreading. *Infect Immun*, 68, 5377-84.

KESPICHAYAWATTANA, W., INTACHOTE, P., UTAISINCHAROEN, P. & SIRISINHA, S. 2004. Virulent *Burkholderia pseudomallei* is more efficient than avirulent *Burkholderia thailandensis* in invasion of and adherence to cultured human epithelial cells. *Microb Pathog*, 36, 287-92.

KHAN, I., WIELER, L. H., MELZER, F., ELSCHNER, M. C., MUHAMMAD, G., ALI, S., SPRAGUE, L. D., NEUBAUER, H. & SAQIB, M. 2013. Glanders in animals: a review on epidemiology, clinical presentation, diagnosis and countermeasures. *Transbound Emerg Dis*, 60, 204-21.

KIM, H., WHITE, C. D., LI, Z. & SACKS, D. B. 2011a. *Salmonella enterica* serotype Typhimurium usurps the scaffold protein IQGAP1 to manipulate Rac1 and MAPK signalling. *Biochem J*, 440, 309-18.

KIM, H., WHITE, C. D. & SACKS, D. B. 2011b. IQGAP1 in microbial pathogenesis: Targeting the actin cytoskeleton. *FEBS Lett*, 585, 723-9.

KLEBA, B., CLARK, T. R., LUTTER, E. I., ELLISON, D. W. & HACKSTADT, T. 2010. Disruption of the *Rickettsia rickettsii* Sca2 autotransporter inhibits actin-based motility. *Infect Immun*, 78, 2240-7.

KOCKS, C., GOUIN, E., TABOURET, M., BERCHE, P., OHAYON, H. & COSSART, P. 1992. *L. monocytogenes*-induced actin assembly requires the actA gene product, a surface protein. *Cell*, 68, 521-31.

KOCKS, C., HELLIO, R., GOUNON, P., OHAYON, H. & COSSART, P. 1993. Polarized distribution of *Listeria monocytogenes* surface protein ActA at the site of directional actin assembly. *J Cell Sci*, 105 (Pt 3), 699-710.

KOCKS, C., MARCHAND, J. B., GOUIN, E., D'HAUTEVILLE, H., SANSONETTI, P. J., CARLIER, M. F. & COSSART, P. 1995. The unrelated surface proteins ActA of *Listeria monocytogenes* and IcsA of *Shigella flexneri* are sufficient to confer actin-based motility on *Listeria innocua* and *Escherichia coli* respectively. *Mol Microbiol*, 18, 413-23.

KRAUSE, M., DENT, E. W., BEAR, J. E., LOUREIRO, J. J. & GERTLER, F. B. 2003. Ena/VASP proteins: regulators of the actin cytoskeleton and cell migration. *Annu Rev Cell Dev Biol*, 19, 541-64.

KRISHNAN, S., FERNANDEZ, G. E., SACKS, D. B. & PRASADARAO, N. V. 2012. IQGAP1 mediates the disruption of adherens junctions to promote *Escherichia coli* K1 invasion of brain endothelial cells. *Cell Microbiol*, 14, 1415-33.

KROKOWSKI, S. & MOSTOWY, S. 2016. Interactions between *Shigella flexneri* and the Autophagy Machinery. *Front Cell Infect Microbiol*, 6, 17.

KUEHL, C. J., DRAGOI, A. M., TALMAN, A. & AGAISSE, H. 2015. Bacterial spread from cell to cell: beyond actin-based motility. *Trends Microbiol*, 23, 558-66.

KURODA S, FUKATA M, NAKAGAWA M, FUJII K, NAKAMURA T, OOKUBO T, ET AL. Role of IQGAP1, a target of the small GTPases Cdc42 and Rac1, in regulation of E-cadherin- mediated cell-cell adhesion. *Science*. 1998;281(5378):832-5.

LAMASON, R. L. & WELCH, M. D. 2017. Actin-based motility and cell-to-cell spread of bacterial pathogens. *Current Opinion in Microbiology*, 35, 48-57.

LAW, H. T., BONAZZI, M., JACKSON, J., COSSART, P. & GUTTMAN, J. A. 2012. Nexilin is a dynamic component of *Listeria monocytogenes* and enteropathogenic *Escherichia coli* actin-rich structures. *Cell Microbiol*, 14, 1097-108.

LAZAR ADLER, N. R., STEVENS, J. M., STEVENS, M. P. & GALYOV, E. E. 2011. Autotransporters and Their Role in the Virulence of *Burkholderia pseudomallei* and *Burkholderia mallei*. *Front Microbiol*, 2, 151.

LAZAR ADLER, N. R., STEVENS, M. P., DEAN, R. E., SAINT, R. J., PANKHANIA, D., PRIOR, J. L., ATKINS, T. P., KESSLER, B., NITHICHANON, A., LERTMEMONGKOLCHAI, G. & GALYOV, E. E. 2015. Systematic mutagenesis of genes encoding predicted autotransported proteins of *Burkholderia pseudomallei* identifies factors mediating virulence in mice, net intracellular replication and a novel protein conferring serum resistance. *PLoS One*, 10, e0121271.

LE CLAINCHE, C., SCHLAEPFER, D., FERRARI, A., KLINGAUF, M., GROHMANOVA, K., VELIGODSKIY, A., DIDRY, D., LE, D., EGILE, C., CARLIER, M. F. & KROSCHEWSKI, R. 2007. IQGAP1 stimulates actin assembly through the N-WASP-Arp2/3 pathway. *J Biol Chem*, 282, 426-35.

LEUNG, Y., ALLY, S. & GOLDBERG, M. B. 2008. Bacterial actin assembly requires toca-1 to relieve N-wasp autoinhibition. *Cell Host Microbe*, 3, 39-47.

LI, S., WANG, Q., CHAKLADAR, A., BRONSON, R. T. & BERNARDS, A. 2000. Gastric hyperplasia in mice lacking the putative Cdc42 effector IQGAP1. *Mol Cell Biol*, 20, 697-701.

LIMMATHUROTSAKUL, D., CHAOWAGUL, W., CHIERAKUL, W., STEPNIEWSKA, K., MAHARJAN, B., WUTHIEKANUN, V., WHITE, N. J., DAY, N. P. & PEACOCK, S. J. 2006. Risk factors for recurrent melioidosis in northeast Thailand. *Clin Infect Dis*, 43, 979-86.

LIMMATHUROTSAKUL, D., WONGRATANACHEEWIN, S., TEERAWATTANASOOK, N., WONGSUVAN, G., CHAISUKSANT, S., CHETCHOTISAKD, P., CHAOWAGUL, W., DAY, N. P. & PEACOCK, S. J. 2010. Increasing incidence of human melioidosis in Northeast Thailand. *Am J Trop Med Hyg*, 82, 1113-7.

LIMMATHUROTSAKUL, D., THAMMASART, S., WARRASUTH, N., THAPANAGULSAK, P., JATAPAI, A., PENGREUNGROJANACHAI, V., ANUN, S., JORAKA, W., THONGKAMKOON, P., SAIYEN, P., WONGRATANACHEEWIN, S., DAY, N. P. & PEACOCK, S. J. 2012. Melioidosis in animals, Thailand, 2006-2010. *Emerg Infect Dis*, 18, 325-7.

LIMMATHUROTSAKUL, D., DANCE, D. A., WUTHIEKANUN, V., KAESTLI, M., MAYO, M., WARNER, J., WAGNER, D. M., TUANYOK, A., WERTHEIM, H., YOKE CHENG, T., MUKHOPADHYAY, C., PUTHUCHEARY, S., DAY, N. P., STEINMETZ, I., CURRIE, B. J. & PEACOCK, S. J. 2013. Systematic review and consensus guidelines for environmental sampling of *Burkholderia pseudomallei*. *PLoS Negl Trop Dis*, 7, e2105.

LIMMATHUROTSAKUL, D., GOLDING, N., DANCE, D. A., MESSINA, J. P., PIGOTT, D. M., MOYES, C. L., ROLIM, D. B., BERTHERAT, E., DAY, N. P., PEACOCK, S. J. & HAY, S. I. 2016. Predicted global distribution of *Burkholderia pseudomallei* and burden of melioidosis. *Nat Microbiol*, 1.

LOISEL, T. P., BOUJEMAA, R., PANTALONI, D. & CARLIER, M. F. 1999. Reconstitution of actin-based motility of *Listeria* and *Shigella* using pure proteins. *Nature*, 401, 613-6.

LOMMEL, S., BENESCH, S., ROTTNER, K., FRANZ, T., WEHLAND, J. & KUHN, R. 2001. Actin pedestal formation by enteropathogenic *Escherichia coli* and intracellular motility of *Shigella flexneri* are abolished in N-WASP-defective cells. *EMBO Rep*, 2, 850-7.

LOSADA, L., RONNING, C. M., DESHAZER, D., WOODS, D., FEDOROVA, N., KIM, H. S., SHABALINA, S. A., PEARSON, T. R., BRINKAC, L., TAN, P., NANDI, T., CRABTREE, J., BADGER, J., BECKSTROM-STERNBERG, S., SAQIB, M., SCHUTZER, S. E., KEIM, P. & NIERMAN, W. C. 2010. Continuing evolution of *Burkholderia mallei* through genome reduction and large-scale rearrangements. *Genome Biol Evol*, 2, 102-16.

LU, Q., XU, Y., YAO, Q., NIU, M. & SHAO, F. 2015a. A polar-localized iron-binding protein determines the polar targeting of *Burkholderia* BimA autotransporter and actin tail formation. *Cell Microbiol*, 17, 408-24.

LU, R., HERRERA, B. B., ESHLEMAN, H. D., FU, Y., BLOOM, A., LI, Z., SACKS, D. B. & GOLDBERG, M. B. 2015b. *Shigella* Effector OspB Activates mTORC1 in a Manner That Depends on IQGAP1 and Promotes Cell Proliferation. *PLoS Pathog*, 11, e1005200.

MADASU, Y., SUAREZ, C., KAST, D. J., KOVAR, D. R. & DOMINGUEZ, R. 2013. *Rickettsia* Sca2 has evolved formin-like activity through a different molecular mechanism. *Proc Natl Acad Sci U S A*, 110, E2677-86.

MAEGRAITH, B. G. & LEITHEAD, C. S. 1964. Melioidosis: A Case-Report. *Lancet*, 1, 862-3.

MAKINO, S., SASAKAWA, C., KAMATA, K., KURATA, T. & YOSHIKAWA, M. 1986. A genetic determinant required for continuous reinfection of adjacent cells on large plasmid in *S. flexneri* 2a. *Cell*, 46, 551-5.

MAPLE, J. & MOLLER, S. G. 2007. Yeast two-hybrid screening. Methods Mol Biol, 362, 207-23.

MATARAZA, J. M., BRIGGS, M. W., LI, Z., ENTWISTLE, A., RIDLEY, A. J. & SACKS, D. B. 2003. IQGAP1 promotes cell motility and invasion. *J Biol Chem*, 278, 41237-45.

MATEER, S. C., MCDANIEL, A. E., NICOLAS, V., HABERMACHER, G. M., LIN, M. J., CROMER, D. A., KING, M. E. & BLOOM, G. S. 2002. The mechanism for regulation of the F-actin binding activity of IQGAP1 by calcium/calmodulin. *J Biol Chem*, 277, 12324-33.

MATSUO, Y., ASAKAWA, K., TODA, T. & KATAYAMA, S. 2006. A rapid method for protein extraction from fission yeast. *Biosci Biotechnol Biochem*, 70, 1992-4.
MAURICIO, R. P., JEFFRIES, C. M., SVERGUN, D. I. & DEANE, J. E. 2017. The *Shigella* Virulence Factor IcsA Relieves N-WASP Autoinhibition by Displacing the Verprolin Homology/Cofilin/Acidic (VCA) Domain. *J Biol Chem*, 292, 134-145.
MCLAUGHLIN, L. M., GOVONI, G. R., GERKE, C., GOPINATH, S., PENG, K., LAIDLAW, G., CHIEN, Y. H., JEONG, H. W., LI, Z., BROWN, M. D., SACKS, D. B. & MONACK, D. 2009. The *Salmonella* SPI2 effector SseI mediates long-term systemic infection by modulating host cell migration. *PLoS Pathog*, 5, e1000671.
MEUMANN, E. M., CHENG, A. C., WARD, L. & CURRIE, B. J. 2012. Clinical features and epidemiology of melioidosis pneumonia: results from a 21-year study and review of the literature. *Clin Infect Dis*, 54, 362-9.
MONACK, D. M. & THERIOT, J. A. 2001. Actin-based motility is sufficient for bacterial membrane protrusion formation and host cell uptake. *Cell Microbiol*, 3, 633-47.
MOSTOWY, S., BONAZZI, M., HAMON, M. A., THAM, T. N., MALLET, A., LELEK, M., GOUIN, E., DEMANGEL, C., BROSCH, R., ZIMMER, C., SARTORI, A., KINOSHITA, M., LECUIT, M. & COSSART, P. 2010. Entrapment of intracytosolic bacteria by septin cage-like structures. *Cell Host Microbe*, 8, 433-44.
MOSTOWY, S. & SHENOY, A. R. 2015. The cytoskeleton in cell-autonomous immunity: structural determinants of host defence. *Nat Rev Immunol*, 15, 559-73.
NIERMAN, W. C., DESHAZER, D., KIM, H. S., TETTELIN, H., NELSON, K. E., FELDBLYUM, T., ULRICH, R. L., RONNING, C. M., BRINKAC, L. M., DAUGHERTY, S. C., DAVIDSEN, T. D., DEBOY, R. T., DIMITROV, G., DODSON, R. J., DURKIN, A. S., GWINN, M. L., HAFT, D. H., KHOURI, H., KOLONAY, J. F., MADUPU, R., MOHAMMOUD, Y., NELSON, W. C., RADUNE, D., ROMERO, C. M., SARRIA, S., SELENGUT, J., SHAMBLIN, C., SULLIVAN, S. A., WHITE, O., YU, Y., ZAFAR, N., ZHOU, L. & FRASER, C. M. 2004. Structural flexibility in the *Burkholderia mallei* genome. *Proc Natl Acad Sci U S A*, 101, 14246-51.
NORITAKE J, FUKATA M, SATO K, NAKAGAWA M, WATANABE T, IZUMI N, ET AL. Positive role of IQGAP1, an effector of Rac1, in actin-meshwork formation at sites of cell-cell contact. *Mol Biol Cell*. 2004;15(3):1065-76.
NORITAKE, J., WATANABE, T., SATO, K., WANG, S. & KAIBUCHI, K. 2005. IQGAP1: a key regulator of adhesion and migration. *J Cell Sci*, 118, 2085-92.
OGAWA, M., YOSHIMORI, T., SUZUKI, T., SAGARA, H., MIZUSHIMA, N. & SASAKAWA, C. 2005. Escape of intracellular *Shigella* from autophagy. Science, 307, 727-31.
PATEL, N., CONEJERO, L., DE REYNAL, M., EASTON, A., BANCROFT, G. J. & TITBALL, R. W. 2011. Development of vaccines against *Burkholderia pseudomallei*. *Front Microbiol*, 2, 198.
PAUL, A. S. & POLLARD, T. D. 2009. Review of the mechanism of processive actin filament elongation by formins. *Cell Motil Cytoskeleton*, 66, 606-17.
PELIKAN-CONCHAUDRON, A., LE CLAINCHE, C., DIDRY, D. & CARLIER, M. F. 2011. The IQGAP1 protein is a calmodulin-regulated barbed end capper of actin filaments: possible implications in its function in cell migration. *J Biol Chem*, 286, 35119-28.
PILATZ, S., BREITBACH, K., HEIN, N., FEHLHABER, B., SCHULZE, J., BRENNEKE, B., EBERL, L. & STEINMETZ, I. 2006. Identification of *Burkholderia pseudomallei* genes required for the intracellular life cycle and in vivo virulence. *Infect Immun*, 74, 3576-86.
POLLARD, T. D. 2016. Actin and Actin-Binding Proteins. *Cold Spring Harb Perspect Biol*, 8.
QUALMANN, B. & KESSELS, M. M. 2009. New players in actin polymerization--WH2-domain-containing actin nucleators. *Trends Cell Biol*, 19, 276-85.

RAN, F. A., HSU, P. D., LIN, C. Y., GOOTENBERG, J. S., KONERMANN, S., TREVINO, A. E., SCOTT, D. A., INOUE, A., MATOBA, S., ZHANG, Y. & ZHANG, F. 2013. Double nicking by RNA-guided CRISPR Cas9 for enhanced genome editing specificity. *Cell*, 154, 1380-9.

REED, S. C., LAMASON, R. L., RISCA, V. I., ABERNATHY, E. & WELCH, M. D. 2014. *Rickettsia* actin-based motility occurs in distinct phases mediated by different actin nucleators. *Curr Biol*, 24, 98-103.

REN, J. G., LI, Z., CRIMMINS, D. L. & SACKS, D. B. 2005. Self-association of IQGAP1: characterization and functional sequelae. *J Biol Chem*, 280, 34548-57.

ROTTY, J. D., WU, C. & BEAR, J. E. 2013. New insights into the regulation and cellular functions of the ARP2/3 complex. *Nat Rev Mol Cell Biol*, 14, 7-12.

RUETZ, T., CORNICK, S. & GUTTMAN, J. A. 2011. The spectrin cytoskeleton is crucial for adherent and invasive bacterial pathogenesis. *PLoS One*, 6, e19940.

RUETZ, T. J., LIN, A. E. & GUTTMAN, J. A. 2012. *Shigella flexneri* utilize the spectrin cytoskeleton during invasion and comet tail generation. *BMC Microbiol*, 12, 36.

SANDER, J. D. & JOUNG, J. K. 2014. CRISPR-Cas systems for editing, regulating and targeting genomes. *Nat Biotechnol*, 32, 347-55.

SAROVICH, D. S., PRICE, E. P., WEBB, J. R., WARD, L. M., VOUTSINOS, M. Y., TUANYOK, A., MAYO, M., KAESTLI, M. & CURRIE, B. J. 2014. Variable virulence factors in *Burkholderia pseudomallei* (melioidosis) associated with human disease. *PLoS One*, 9, e91682.

SCHELL, M. A., ULRICH, R. L., RIBOT, W. J., BRUEGGEMANN, E. E., HINES, H. B., CHEN, D., LIPSCOMB, L., KIM, H. S., MRAZEK, J., NIERMAN, W. C. & DESHAZER, D. 2007. Type VI secretion is a major virulence determinant in *Burkholderia mallei*. *Mol Microbiol*, 64, 1466-85.

SCHMIDT, V. A., SCUDDER, L., DEVOE, C. E., BERNARDS, A., CUPIT, L. D. & BAHOU, W. F. 2003. IQGAP2 functions as a GTP-dependent effector protein in thrombin-induced platelet cytoskeletal reorganization. *Blood*, 101, 3021-8.

SCHWARZ, S., SINGH, P., ROBERTSON, J. D., LEROUX, M., SKERRETT, S. J., GOODLETT, D. R., WEST, T. E. & MOUGOUS, J. D. 2014. VgrG-5 is a *Burkholderia* type VI secretion system-exported protein required for multinucleated giant cell formation and virulence. *Infect Immun*, 82, 1445-52.

SCHWEIZER, H. P. 2012. Mechanisms of antibiotic resistance in *Burkholderia pseudomallei*: implications for treatment of melioidosis. *Future Microbiol*, 7, 1389-99.

SECHI, A. S., WEHLAND, J. & SMALL, J. V. 1997. The isolated comet tail pseudopodium of *Listeria monocytogenes*: a tail of two actin filament populations, long and axial and short and random. *J Cell Biol*, 137, 155-67.

SERIO, A. W., JENG, R. L., HAGLUND, C. M., REED, S. C. & WELCH, M. D. 2010. Defining a core set of actin cytoskeletal proteins critical for actin-based motility of *Rickettsia*. *Cell Host Microbe*, 7, 388-98.

SHAN, G. 2010. RNA interference as a gene knockdown technique. *Int J Biochem Cell Biol*, 42, 1243-51.

SHIBATA, T., TAKESHIMA, F., CHEN, F., ALT, F. W. & SNAPPER, S. B. 2002. Cdc42 facilitates invasion but not the actin-based motility of *Shigella*. *Curr Biol*, 12, 341-5.

SIMON, S., SCHELL, U., HEUER, N., HAGER, D., ALBERS, M. F., MATTHIAS, J., FAHRNBAUER, F., TRAUNER, D., EICHINGER, L., HEDBERG, C. & HILBI, H. 2015. Inter-kingdom Signaling by the *Legionella* Quorum Sensing Molecule LAI-1 Modulates Cell Migration through an IQGAP1-Cdc42-ARHGEF9-Dependent Pathway. *PLoS Pathog*, 11, e1005307.

SITON-MENDELSON, O. & BERNHEIM-GROSWASSER, A. 2017. Functional Actin Networks under Construction: The Cooperative Action of Actin Nucleation and Elongation Factors. *Trends Biochem Sci*, 42, 414-430.

SITTHIDET, C., STEVENS, J. M., CHANTRATITA, N., CURRIE, B. J., PEACOCK, S. J., KORBSRISATE, S. & STEVENS, M. P. 2008. Prevalence and sequence diversity of a factor required for actin-based motility in natural populations of *Burkholderia* species. *J Clin Microbiol*, 46, 2418-22.

SITTHIDET, C., STEVENS, J. M., FIELD, T. R., LAYTON, A. N., KORBSRISATE, S. & STEVENS, M. P. 2010. Actin-based motility of *Burkholderia thailandensis* requires a central acidic domain of BimA that recruits and activates the cellular Arp2/3 complex. *J Bacteriol*, 192, 5249-52.

SITTHIDET, C., KORBSRISATE, S., LAYTON, A. N., FIELD, T. R., STEVENS, M. P. & STEVENS, J. M. 2011. Identification of motifs of *Burkholderia pseudomallei* BimA required for intracellular motility, actin binding, and actin polymerization. *J Bacteriol*, 193, 1901-10.

SMITH, G. A., THERIOT, J. A. & PORTNOY, D. A. 1996. The tandem repeat domain in the *Listeria monocytogenes* ActA protein controls the rate of actin-based motility, the percentage of moving bacteria, and the localization of vasodilator-stimulated phosphoprotein and profilin. *J Cell Biol*, 135, 647-60.

SMITH, M. D., ANGUS, B. J., WUTHIEKANUN, V. & WHITE, N. J. 1997. Arabinose assimilation defines a nonvirulent biotype of *Burkholderia pseudomallei*. *Infect Immun*, 65, 4319-21.

SMITH, J., MANORANJAN, J., PAN, M., BOHSALI, A., XU, J., LIU, J., MCDONALD, K. L., SZYK, A., LARONDE-LEBLANC, N. & GAO, L. Y. 2008. Evidence for pore formation in host cell membranes by ESX-1-secreted ESAT-6 and its role in *Mycobacterium marinum* escape from the vacuole. *Infect Immun*, 76, 5478-87.

SPIERING, D. & HODGSON, L. 2011. Dynamics of the Rho-family small GTPases in actin regulation and motility. *Cell Adh Migr*, 5, 170-80.

SPRAGUE, L. D. & NEUBAUER, H. 2004. Melioidosis in animals: a review on epizootiology, diagnosis and clinical presentation. *J Vet Med B Infect Dis Vet Public Health*, 51, 305-20.

STAMM, L. M., MORISAKI, J. H., GAO, L. Y., JENG, R. L., MCDONALD, K. L., ROTH, R., TAKESHITA, S., HEUSER, J., WELCH, M. D. & BROWN, E. J. 2003. *Mycobacterium marinum* escapes from phagosomes and is propelled by actin-based motility. *J Exp Med*, 198, 1361-8.

STAMM, L. M. & BROWN, E. J. 2004. *Mycobacterium marinum*: the generalization and specialization of a pathogenic mycobacterium. *Microbes Infect*, 6, 1418-28.

STAMM, L. M., PAK, M. A., MORISAKI, J. H., SNAPPER, S. B., ROTTNER, K., LOMMEL, S. & BROWN, E. J. 2005. Role of the WASP family proteins for *Mycobacterium marinum* actin tail formation. *Proc Natl Acad Sci U S A*, 102, 14837-42.

STEVENS, M. P., WOOD, M. W., TAYLOR, L. A., MONAGHAN, P., HAWES, P., JONES, P. W., WALLIS, T. S. & GALYOV, E. E. 2002. An Inv/Mxi-Spa-like type III protein secretion system in *Burkholderia pseudomallei* modulates intracellular behaviour of the pathogen. *Mol Microbiol*, 46, 649-59.

STEVENS, M. P., FRIEBEL, A., TAYLOR, L. A., WOOD, M. W., BROWN, P. J., HARDT, W. D. & GALYOV, E. E. 2003. A *Burkholderia pseudomallei* type III secreted protein, BopE, facilitates bacterial invasion of epithelial cells and exhibits guanine nucleotide exchange factor activity. *J Bacteriol*, 185, 4992-6.

STEVENS, M. P., STEVENS, J. M., JENG, R. L., TAYLOR, L. A., WOOD, M. W., HAWES, P., MONAGHAN, P., WELCH, M. D. & GALYOV, E. E. 2005a. Identification of a bacterial factor required for actin-based motility of *Burkholderia pseudomallei*. *Mol Microbiol*, 56, 40-53.

STEVENS, J. M., ULRICH, R. L., TAYLOR, L. A., WOOD, M. W., DESHAZER, D., STEVENS, M. P. & GALYOV, E. E. 2005b. Actin-binding proteins from *Burkholderia mallei* and *Burkholderia thailandensis* can functionally compensate for the actin-based motility defect of a *Burkholderia pseudomallei* bimA mutant. *J Bacteriol*, 187, 7857-62.

STEVENS, J. M., GALYOV, E. E. & STEVENS, M. P. 2006. Actin-dependent movement of bacterial pathogens. *Nat Rev Microbiol*, 4, 91-101.

STRAUSS, W. M. 2001. Preparation of genomic DNA from mammalian tissue. *Curr Protoc Immunol*, Chapter 10, Unit 10 2.

SUAREZ, C. & KOVAR, D. R. 2016. Internetwork competition for monomers governs actin cytoskeleton organization. *Nat Rev Mol Cell Biol*, 17, 799-810.

SUWANNASAEN, D., MAHAWANTUNG, J., CHAOWAGUL, W., LIMMATHUROTSAKUL, D., FELGNER, P. L., DAVIES, H., BANCROFT, G. J., TITBALL, R. W. & LERTMEMONGKOLCHAI, G. 2011. Human immune responses to *Burkholderia pseudomallei* characterized by protein microarray analysis. *J Infect Dis*, 203, 1002-11.

SUZUKI, T., MIKI, H., TAKENAWA, T. & SASAKAWA, C. 1998. Neural Wiskott-Aldrich syndrome protein is implicated in the actin-based motility of *Shigella flexneri*. *EMBO J*, 17, 2767-76.

SUZUKI, T., MIMURO, H., SUETSUGU, S., MIKI, H., TAKENAWA, T. & SASAKAWA, C. 2002. Neural Wiskott-Aldrich syndrome protein (N-WASP) is the specific ligand for *Shigella* VirG among the WASP family and determines the host cell type allowing actin-based spreading. *Cell Microbiol*, 4, 223-33.

TILNEY, L. G. & PORTNOY, D. A. 1989. Actin filaments and the growth, movement, and spread of the intracellular bacterial parasite, *Listeria monocytogenes*. *J Cell Biol*, 109, 1597-608.

TOBIN, D. M. & RAMAKRISHNAN, L. 2008. Comparative pathogenesis of *Mycobacterium marinum* and *Mycobacterium tuberculosis*. *Cell Microbiol*, 10, 1027-39.

TOCKER AM, DUROCHER E, JACOB KD, TRIESCHMAN KE, TALENTO SM, RECHNITZER AA, ET AL. The Scaffolding Protein IQGAP1 Interacts with NLRC3 and Inhibits Type I IFN Production. *J Immunol*. 2017;199(8):2896-909.

TOESCA, I. J., FRENCH, C. T. & MILLER, J. F. 2014. The Type VI secretion system spike protein VgrG5 mediates membrane fusion during intercellular spread by Pseudomallei group *Burkholderia* species. *Infect Immun*, 82, 1436-44.

VAN CRIEKINGE, W. & BEYAERT, R. 1999. Yeast Two-Hybrid: State of the Art. *Biol Proced Online*, 2, 1-38.

VAN KIRK, L. S., HAYES, S. F. & HEINZEN, R. A. 2000. Ultrastructure of *Rickettsia rickettsii* actin tails and localization of cytoskeletal proteins. Infect Immun, 68, 4706-13.

VAN TROYS, M., LAMBRECHTS, A., DAVID, V., DEMOL, H., PUYPE, M., PIZARRO-CERDA, J., GEVAERT, K., COSSART, P. & VANDEKERCKHOVE, J. 2008. The actin propulsive machinery: the proteome of *Listeria monocytogenes* tails. *Biochem Biophys Res Commun*, 375, 194-9.

VAN ZANDT, K. E., GREER, M. T. & GELHAUS, H. C. 2013. Glanders: an overview of infection in humans. *Orphanet J Rare Dis*, 8, 131.

VANDER BROEK, C. W. & STEVENS, J. M. 2017. Type III Secretion in the Melioidosis Pathogen *Burkholderia pseudomallei*. *Front Cell Infect Microbiol*, 7, 255.

VELLASAMY, K. M., MARIAPPAN, V., SHANKAR, E. M. & VADIVELU, J. 2016. *Burkholderia pseudomallei* Differentially Regulates Host Innate Immune Response Genes for Intracellular Survival in Lung Epithelial Cells. *PLoS Negl Trop Dis*, 10, e0004730.

WAGAR, E. 2016. Bioterrorism and the Role of the Clinical Microbiology Laboratory. *Clin Microbiol Rev*, 29, 175-89.

WAND, M. E., MULLER, C. M., TITBALL, R. W. & MICHELL, S. L. 2011. Macrophage and *Galleria mellonella* infection models reflect the virulence of naturally occurring isolates of *B. pseudomallei*, *B. thailandensis* and *B. oklahomensis*. *BMC Microbiol*, 11, 11.

WANG, S., WATANABE, T., NORITAKE, J., FUKATA, M., YOSHIMURA, T., ITOH, N., HARADA, T., NAKAGAWA, M., MATSUURA, Y., ARIMURA, N. & KAIBUCHI, K. 2007. IQGAP3, a novel effector of Rac1 and Cdc42, regulates neurite outgrowth. *J Cell Sci*, 120, 567-77.

WANG, J., KING, J. E., GOLDRICK, M., LOWE, M., GERTLER, F. B. & ROBERTS, I. S. 2015. Lamellipodin Is Important for Cell-to-Cell Spread and Actin-Based Motility in *Listeria monocytogenes*. *Infect Immun*, 83, 3740-8.

WATANABE, T., WANG, S. & KAIBUCHI, K. 2015. IQGAPs as Key Regulators of Actin-cytoskeleton Dynamics. Cell Struct Funct, 40, 69-77.

WELCH, M. D., IWAMATSU, A. & MITCHISON, T. J. 1997. Actin polymerization is induced by Arp2/3 protein complex at the surface of *Listeria monocytogenes*. *Nature*, 385, 265-9.

WELCH, M. D., ROSENBLATT, J., SKOBLE, J., PORTNOY, D. A. & MITCHISON, T. J. 1998. Interaction of human Arp2/3 complex and the *Listeria monocytogenes* ActA protein in actin filament nucleation. *Science*, 281, 105-8.

WELCH, M. D. & WAY, M. 2013. Arp2/3-mediated actin-based motility: a tail of pathogen abuse. *Cell Host Microbe*, 14, 242-55.

WHITE, C. D., BROWN, M. D. & SACKS, D. B. 2009. IQGAPs in cancer: a family of scaffold proteins underlying tumorigenesis. FEBS Lett, 583, 1817-24.

WIERSINGA, W. J., CURRIE, B. J. & PEACOCK, S. J. 2012. Melioidosis. *N Engl J Med*, 367, 1035-44.

WILLCOCKS, S. J., DENMAN, C. C., ATKINS, H. S. & WREN, B. W. 2016. Intracellular replication of the well-armed pathogen *Burkholderia pseudomallei*. *Curr Opin Microbiol*, 29, 94-103.

WHITLOCK, G. C., DEERAKSA, A., QAZI, O., JUDY, B. M., TAYLOR, K., PROPST, K. L., DUFFY, A. J., JOHNSON, K., KITTO, G. B., BROWN, K. A., DOW, S. W., TORRES, A. G. & ESTES, D. M. 2010. Protective response to subunit vaccination against intranasal *Burkholderia mallei* and *B. pseudomallei* challenge. *Procedia Vaccinol*, 2.

WINKELMAN, J. D., BILANCIA, C. G., PEIFER, M. & KOVAR, D. R. 2014. Ena/VASP Enabled is a highly processive actin polymerase tailored to self-assemble parallel-bundled F-actin networks with Fascin. *Proc Natl Acad Sci U S A*, 111, 4121-6.

WOOD, M. W., ROSQVIST, R., MULLAN, P. B., EDWARDS, M. H. & GALYOV, E. E. 1996. SopE, a secreted protein of *Salmonella dublin*, is translocated into the target eukaryotic cell via a sip-dependent mechanism and promotes bacterial entry. *Mol Microbiol*, 22, 327-38.

YOSHIKAWA, Y., OGAWA, M., HAIN, T., YOSHIDA, M., FUKUMATSU, M., KIM, M., MIMURO, H., NAKAGAWA, I., YANAGAWA, T., ISHII, T., KAKIZUKA, A., SZTUL, E., CHAKRABORTY, T. & SASAKAWA, C. 2009. *Listeria monocytogenes* ActA-mediated escape from autophagic recognition. *Nat Cell Biol*, 11, 1233-40.

YU-KEMP, H. C. & BRIEHER, W. M. 2016. Collapsin Response Mediator Protein-1 Regulates Arp2/3-dependent Actin Assembly. *J Biol Chem*, 291, 658-64.

ZHANG, L., LI, X., ZHANG, L., WANG, B., ZHANG, T. & YE, J. 2012. *Chlamydophila (Chlamydia) pneumoniae* infection promotes vascular smooth muscle cell adhesion and migration through IQ domain GTPase-activating protein 1. *Microb Pathog*, 53, 207-13.

TAKEICHI M. Morphogenetic roles of classic cadherins. *Curr Opin Cell Biol*. 1995;7(5):619-27.

Chapter 7
Supplemental Information

7.1 Bacterial strain and yeast strains, plasmids and antibodies used in this study

Table7.1: Bacterial strain, yeast strain used in this study

Strain	Description	Source/Reference
Burkholderia pseudomallei strain 10276 (NCTC 10276)	Isolated from a British seaman suffering from the chronic form of melioidosis	Maegraith and Leithead (1964)
Salmonella enterica serovar Typhimurium 4/74	Nalidixic acid-resistant (Nal^R)	Jones et al. (1988)
***E. coli* Strains**		
E. coli XL-1 blue	cloning	Agilent Technologies
E. coli XL10-gold	Site-directed mutagenesis	Agilent Technologies
E. coli Rosetta 2 (DE3) pLysS,	Protein expression	Novagen
E. coli Rosetta 2 (DE3) pLysS pGEX-4T-1	Strain expresses GST protein	Sitthidet et al. (2010)
E. coli Rosetta 2 (DE3) pLysS pGEX-BimA	Strain expresses residues 54 to 455 of *B. pseudo-mallei* 10276 BimA fused with GST	Sitthidet et al. (2010)
Saccharomyces cerevisiae		
AH109	Ade–, His–, Leu–, Trp–	Clontech
AH109 pGBKT7-53 pGADT7-T	Control for positive interaction	Clontech
AH109 pGBKT7-Lam pGADT7-T	Control for negative interaction	Clontech
***Pichia pastoris* strains**		
GS115	Methanol-utilising strain (Mut^+), His–, Mut+	Invitrogen
GS115/ Albumin	Control for Mut^S phenotype	Invitrogen
GS115/pPICZ/lacZ	control for Zeocin™ resistance in *Pichia* and Mut^+ phenotype, His–	Invitrogen
KM71H	Methanol utilisation slow (Mut^S)	Invitrogen

Table 7.2: Plasmid used in this study

Plasmid	Description	Source/ Reference
pECFP-C1	Mammalian expression vector with cyan fluorescent protein tag, Kan^R	Clontech
Double nickase plasmid (cat no. sc-400597-NIC)	A pair of plasmid encoding a D10A mutated Cas9 nuclease and target human IQGAP1 for knockout gene expression	Santa Cruz Biotechnology
pGEM-T Easy	Cloning vector, Amp^R	Promega
pGEM-T-FL-IQGAP1	pGEM-T containing full-length IQGAP, Amp^R	This study
pGEM-T-N-IQGAP1	pGEM-T containing N-terminal IQGAP, Amp^R	This study
pGEM-T-C-IQGAP1	pGEM-T containing C-terminal IQGAP, Amp^R	This study
pGEM-T-IQGAP1	pGEM-T containing full-length IQGAP, Amp^R	This study
pWhitescript	Control for site-directed mutagenesis	Agilent Technologies
pMAL-p2X	Bacterial expression vector containing an N–terminal MBP, Amp^R	New England Biolabs
pMAL-p2X-FL-IQGAP1	pMAL-p2X encodes full-length IQGAP1 (aa 1-16567) fused with an N–terminal MBP, Amp^R	This study
pMAL-p2X-N-IQGAP1	pMAL-p2X encodes full-length IQGAP1 aa 1-808 fused with an N–terminal MBP, Amp^R	This study
pMAL-p2X-C-IQGAP1	pMAL-p2X encodes full-length IQGAP1 aa 809-1657 fused with an N–terminal MBP, Amp^R	This study
pPICZ B	Pichia expression vectors containing C–terminal 6xHis tag, Zeo^R	Thermo Fisher Scientific
pPICZ B-IQGAP1	pPICZ B encodes full-length IQGAP1 fused with an C–terminal 6xHis tag, Zeo^R	This study
pME6032-BimA	pME6032 contains the intact *bimA* from *B. pseudomallei* 10276, Tet^R	Stevens et al., (2005a)
pET-21b (+)	Bacterial expression vector containing an C–terminal 6xHis, Amp^R	Novagen
pET-21b (+)-$BimA_{54-470}$	pET-21b (+) encodes BimA aa 54-470 fused with C–terminal 6xHis, Amp^R	This study
pMAL-p2X-$BimA_{54-470}$	pMAL-p2X encodes BimA aa 54-470 fused with an N–terminal MBP, Amp^R	This study
pGBKT7 BD	Yeast expression vector encoding an in-frame GAL4 DNA binding domain and c-Myc tag, Trp+, Kan^R	Clontech
pGBKT7-$BimA_{54-455}$	pGBKT7 encodes the Gal4 DNA-BD fused with BimA aa 54-455, and myc tag, Trp+, Kan^R	Terence Field/ Jitprasutwit et al., (2016)

Table 7.2: Plasmid used in this study (continued)

Plasmid	Description	Source/ Reference
pGBKT7-BimA$_{54-455}$	pGBKT7 encodes the Gal4 DNA-BD fused with BimA aa 54-455, and myc tag, Trp+, Kan^R	Terence Field/ Jitprasutwit et al., (2016)
pGADT7 AD	Yeast expression vector encoding an in-frame GAL4 activating domain and HA tag, Leu+, Amp^R	Clontech
pGADT7-IQGAP1	pGBKT7 encodes the GAL4-AD fused with IQGAP1 and HA tag, Leu+, Amp^R	This study
pGADT7-actin	pGBKT7 encodes the GAL4-AD fused with β-actin and HA tag, Leu+, Amp^R	This study

Table 7.3 Primers used in this study

Primer	Sequence (5' - 3')	Description	Source/ Reference
F-IQ-KO	AAAGTTGGGTGGACGTG AGT	Verify human IQGAP1 exon 13	This study
R-IQ-KO	GCCTGCAAAGAAAATCG GAGC	Verify human IQGAP1 exon 13	This study
F-IQ-FL-XbaI	CTCGTCTAGAATGTCCGC CGCAGACGAG	Amplify full-length and N-terminus of IQGAP1	This study
R-IQ-FL-SalI	ATGGGTCGACACGATCA ATTACTTCCCGTAGAACT	Amplify full-length and C-terminus of IQGAP1	This study
R-IQ-N-SalI	TCTTGTCGACTTCATCTT TGTGGGAGCGCA	Amplify N- terminal IQGAP1	This study
F-IQ-C-XbaI	AGATTCTAGATGTAAAG ATTCAGTCCCTGGCA	Amplify C- terminal IQGAP1	This study
F-A602C	GATGCCTGCCTTTAGCAA GATTGGGGGCATCTTG	Site-directed mutagenesis	This study
R-A602C	CAAGATGCCCCCAATCTT GCTAAAGGCAGGCATC	Site-directed mutagenesis	This study
F-A3731G	CAATAAGATGTTTCTGG GAGATAATGCCCACTTA AGCATCA	Site-directed mutagenesis	This study
R-A3731G	TGATGCTTAAGTGGGCA TTATCTCCCAGAAACATC TTATTG	Site-directed mutagenesis	This study
F-IQ1-XhoI	TTCTCGCTCGAGATGTCC GCCGCAGACGAG	Amplify full-length of IQGAP1 for expression in *Pichia*	This study
R-IQ1-XbaI	TTTTTCTAGACCCTTCCC GTAGAACTTTTTGTTGA GA		This study
F-IQ1-NdeI	TTTTCATATGATGTCCGC CGCAGACGAG	Amplify IQGAP1 for Y2H	This study
R-IQ1-XhoI	TTTTCTCGAGTTACTTCC CGTAGAACTTTTTGTTG A	Amplify IQGAP1 for Y2H	This study
F-actin-NdeI	TTTTCATATGATGGATG ATGATATCGCCG	Amplify β-actin for Y2H	This study
R-actin-XhoI	TTTTCTCGAGCTAGAAGC ATTTGCGGTGG	Amplify β-actin for Y2H	This study
BimA54-BamHI	ATCCGCGGATCCATGAAT CCCCCCGAACCGCCGGGC	Amplify $BimA_{54-470}$	This study
BimA470-SacI	ATCCGCGAGCTCGGAATC ATCGTCAGCGCGGTCGC	Amplify $BimA_{54-470}$	This study
F802IQ	GGCTAAGCAGGACAAAA TGACA	IQGAP1 Sequencing	This study

Table 7.3 Primers used in this study (continued)

Primer	Sequence (5' - 3')	Description	Source/ Reference
F2201IQ	GGGGTGACTGCCGCATATAA	IQGAP1 Sequencing	This study
F3323IQ	CAGACAGGAGAGGCAAGCAA	IQGAP1 Sequencing	This study
5′AOX1	GACTGGTTCCAATTGACAAGC	Screening insertion on pPICZ B	Invitrogen
3′AOX1	GCAAATGGCATTCTGACATCC	Screening insertion on pPICZ B	Invitrogen
T7F	TAATACGACTCACTATAGGGC	pGADT7 Sequencing	Clontech
3AD	AGATGGTGCACGATGCACAG	pGADT7 Sequencing	Clontech
M13F	TGTAAAACGACGGCCAGT	pGEM-T sequencing	Source BioScience
M13R	CAGGAAACAGCTATGACC	pGEM-T sequencing	Source BioScience
T7 promoter (F)	TAATACGACTCACTATAGGG	pET-21b(+) Sequencing	Source BioScience
T7 terminator (R)	GCTAGTTATTGCTCAGCGG	pET-21b(+) Sequencing	Source BioScience
malEforward	GGTCGTCAGACTGTCGATGAAGCC	pMAL-p2X sequencing	Source BioScience

Restriction sites are underlined.

Table 7.4: Antibodies used in this study

Antibody (Species)	Specificity	Application (concentration/ dilution used)	Source/Reference (Catalogue no.)
α-IQGAP1 (rabbit polyclonal)	aa 314-422 mapping near the N-terminus of IQGAP1 of human origin	WB (1 µg/ml) IF (2 µg/ml) IP (4 µg per 1 mg of total protein)	Santa Cruz Biotechnology (sc-10792)
α-Actin (goat polyclonal)	C-terminus of actin of human origin	WB (1 µg/ml)	Santa Cruz Biotechnology (sc-1615)
α-GAPDH (mouse monoclonal)	Human GAPDH	WB (0.5 µg/ml)	Thermo Fisher Scientific (MA5-15738)
α-IQGAP2 (mouse monoclonal)	aa 519-727 mapping to an internal region of IQGAP2 of human origin	WB (1:100)	Santa Cruz Biotechnology (sc-17835)
α-IQGAP3 (rabbit polyclonal)	N-terminal region of Human IQGAP3	WB (1: 500)	Abcam (ab136976)
α-MBP (mouse monoclonal)	Maltose binding protein	WB (1 µg/ml)	New England Biolabs (E8032)
α-GST (mouse monoclonal)	Glutathione-S-Transferase	WB (1 µg/ml)	In house
α-6xHis (mouse Monoclonal)	A poly-histidine (His x 6) fusion protein	WB (1:5000)	Alpha Diagnostic (HISP12)
α-BimA (FG11) (mouse polyclonal)	GST-BimA48−384 *B. pseudomallei* 10276	0.5 µg/ml	(Stevens et al., 2005a)
α-*Pseudomonas mallei* LPS (mouse monoclonal)	LPS of *P. mallei* and *B. pseudomallei*	2 µg/ml	Abcam (ab10011)
α-Rabbit 680 (goat)	Rabbit IgG	WB (1:10,000)	Cell signalling (5366)
α-Mouse 680 (goat)	Mouse IgG	WB (1:10,000)	Cell signalling (5470)
α-Mouse 800 (goat)	Mouse IgG	WB (1:10,000)	Cell signalling (5257)
α-Rabbit 568 (goat)	Rabbit IgG	IF (1:200)	Molecular Probes (A10036)
α-Mouse 568 (goat)	Mouse IgG	IF (1:200)	Molecular Probes (A11004)

Table 7.4: Antibodies used in this study (continued)

Antibody (Species)	Specificity	Application (concentration/ dilution used)	Source/Reference (Catalogue no.)
α-Mouse 405 (goat)	Mouse IgG	IF (1:200)	Molecular Probes (A31553)
α-Goat 0.1 mg (donkey)	Goat IgG	WB (1:20,000)	LI-COR (92632214)

WB: Western blotting, IF: Immunofluorescence Staining, IP: Immunoprecipitation

7.2 Determination of optimal working dilution for IQGAP1 staining in HeLa cells

A series of dilutions in a titration experiment was performed using dilutions of 1:50 and 1:100 of primary antibody using a goat polyclonal antibody and a rabbit polyclonal antibody. The secondary antibodies were diluted at 1:500 and 1:200. Using 1:100 of rabbit polyclonal antibody and detected with 1:200 of the anti-rabbit Ig-Alexa Fluor 568 shows the best staining with low background and specific to IQGAP1 in the cytoplasm and the cell membrane where an overlap in the fluorescence signals in yellow was observed (Figure 7.1).

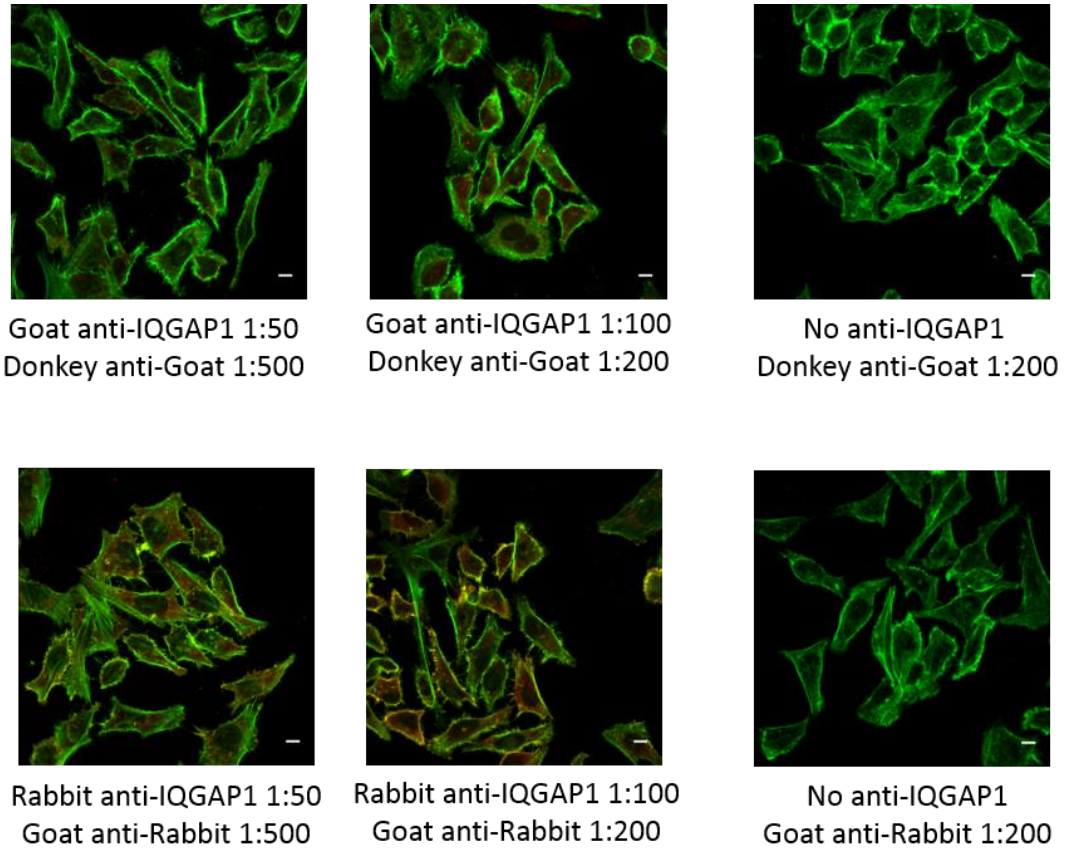

Figure 7.1: IQGAP1 localises with actin tails of *B. pseudomallei*
Representative confocal laser scanning micrographs of uninfected HeLa cells. F-actin (green) was stained with Alexa Fluor 488-conjugated phalloidin. IQGAP1 (red) was stained with a goat polyclonal antibody or a rabbit polyclonal antibody and detected with anti-goat or anti-rabbit Ig-Alexa Fluor 568. Scale bar = 10 μm

7.3 *B. pseudomallei* displayed actin tails in HeLa cells at different points after infection

To study actin tail formation by *B. pseudomallei*, HeLa cells were infected with *B. pseudomallei* for 8, 16, 24 and 32 hours and cell staining to examine the number of bacteria formed actin tail using confocal microscopy. Figure 7.2 shows at 16 hours post-infection, the number of bacteria that displayed actin tails in HeLa cells was largest compared to another time points. From this observation, *B. pseudomallei* actin tail formation was examined after infection for 16 hours.

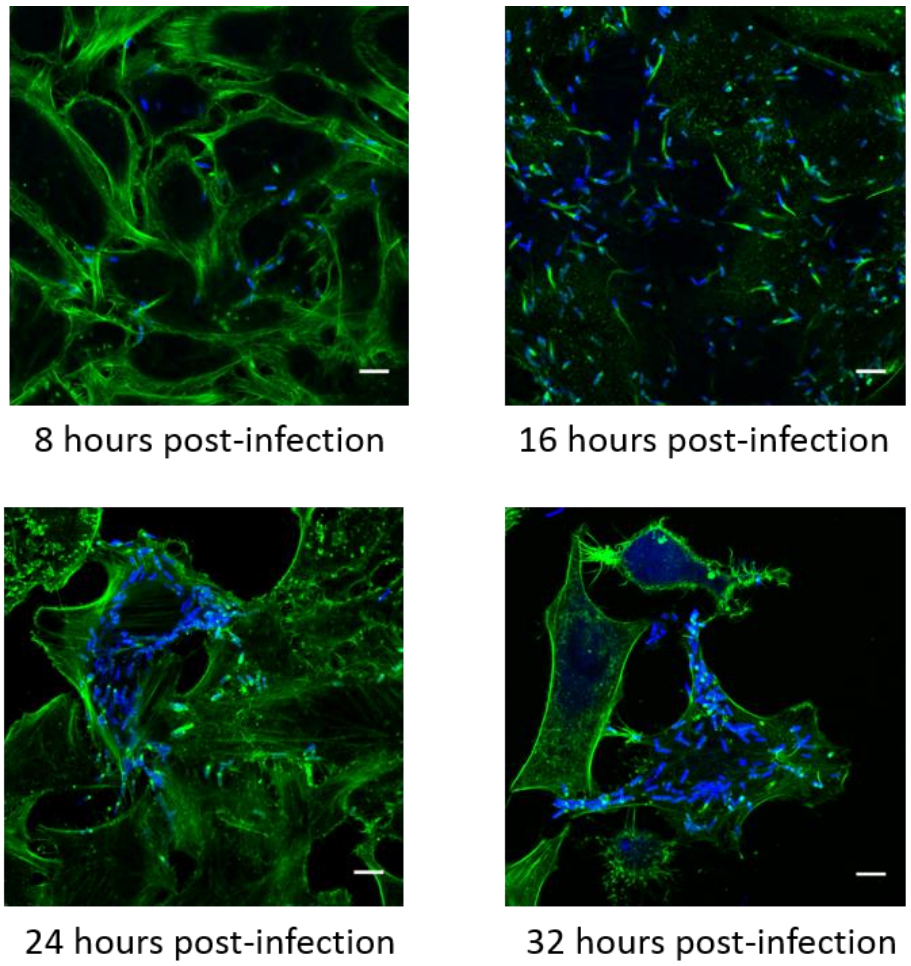

Figure 7.2: Actin tail formation by *B. pseudomallei* in control cells at 8, 16, 24 and 32 hours post-infection
Confocal micrographs of HeLa cells infected with wild-type *B. pseudomallei* 10276. Bacteria were stained with anti-LPS antibody in blue and actin was stained in green. Scale bar = 10 μm

7.4 Expression level of IQGAP isoforms

To inspect expression level of IQGAP2 and IQGAP3 in HeLa cells, the Human Protein Atlas program (https://www.proteinatlas.org/) was utilised. From the information provided, HeLa cell at the early passages was extracted for total RNA has been analysed by RNA-seq to estimate the transcript abundance of each protein-coding gene reported as values of TPM (Transcript Per Million). Figure 7.3 shows RNA expression overview generated by the Human Protein Atlas program. Transcripts for IQGAP1, IQGAP2 and IQGAP3 in HeLa cell show TPM values are 102.7, 4.8 and 36.4 respectively.

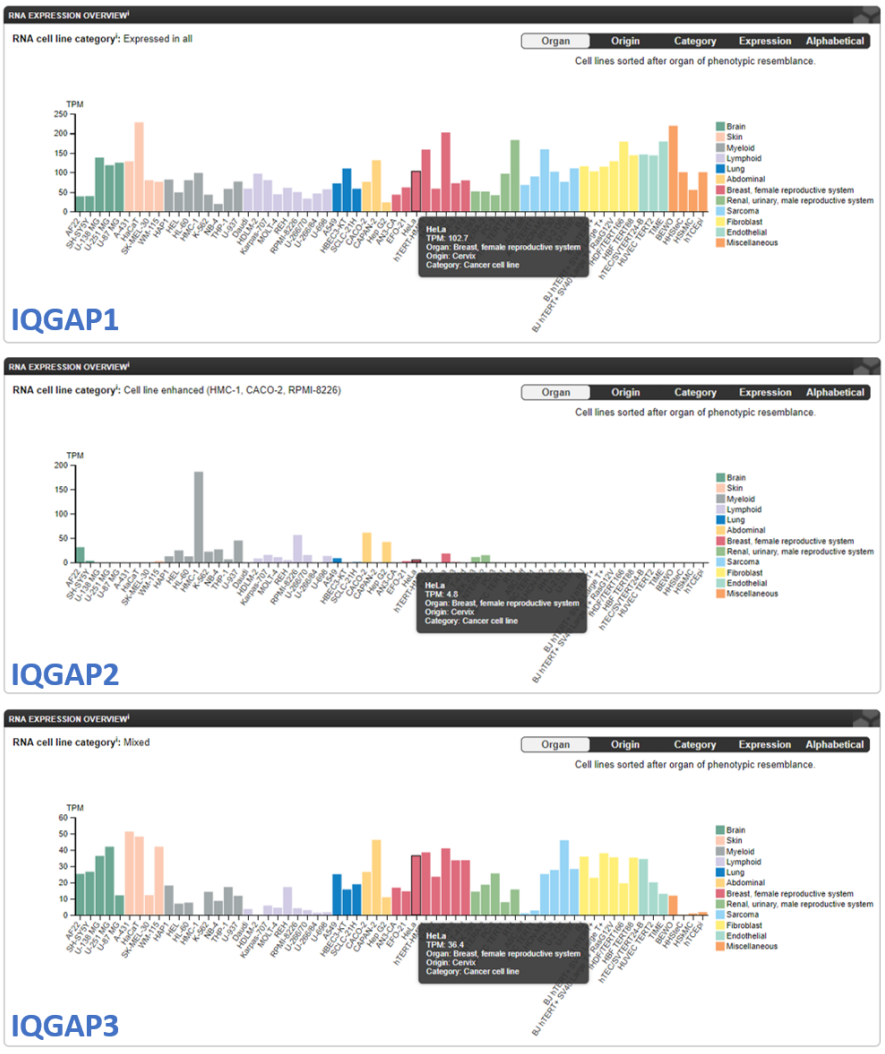

Figure 7.3: RNA expression overview with cell lines sorted generated by the Human Protein Atlas program.
TPM values of IQGAP1, IQGAP2 and IQGAP3 in HeLa cells shown in black boxes.

7.5 Invasion and intracellular survival of *B. pseudomallei* in siIQGAP1 knockdown cells

HeLa cells and siIQGAP1 knockdown cells were infected with *B. pseudomallei* at MOI of 130. At 2 hours post-infection, the infected cells were lysed to examine the invasion efficiency of *B. pseudomallei*. At 24 hours post-infection, the intracellular bacteria were recovered to investigate the number of viable bacteria inside the cells. Figure 7.4 shows percentage of invasion and intracellular survival of *B. pseudomallei* in siIQGAP1 cells were not statistically significant difference, compared to control cells.

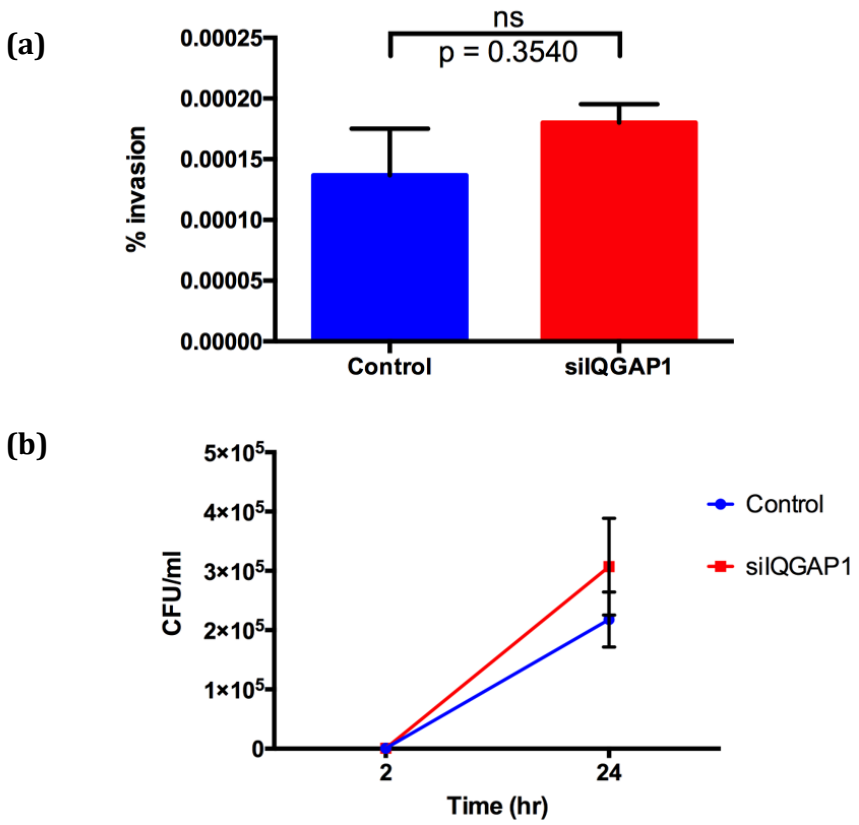

Figure 7.4: Percentage of invasion by *B. pseudomallei* and the number of bacteria in control HeLa cells and siIQGAP1 knockdown cells

(a) At 2 hours post-infection, infected cells were lysed, and the number of intracellular bacteria quantified. Data are expressed as the percentage of invasion calculated as follows: (the number of recovered bacteria/the number of bacterial inoculum) x 100 showing mean ± SEM from three separated experiments (n=3).

(b) Intracellular bacteria were counted after lysing infected cells at 6 and 24 hours post-infection. The data of the number of recovered bacteria at 2 hours post-infection from figure 7.4a is also included. Error bars represent standard errors of the mean for experiments performed in triplicate (n=3).

7.6 Sequencing result of PCR product from control HeLa cells

Genomic DNA extract from WT HeLa cells was subjected to PCR amplification using a pair of primers designed for the region flanking exon 13 of the human IQGAP1 gene. One band of PCR product at the expected size was extracted from the gel for sequencing using the primers used for amplification. Figure 7.5 shows high quality of Sanger sequencing chromatogram of the amplicons and the sequencing result that was blasted against the human genome using *Homo sapiens* (human) Nucleotide BLAST (https://blast.ncbi.nlm.nih.gov/Blast.cgi). From BLAST analysis, it demonstrated that the product share 100% identity with human IQGAP1 gene.

(a)

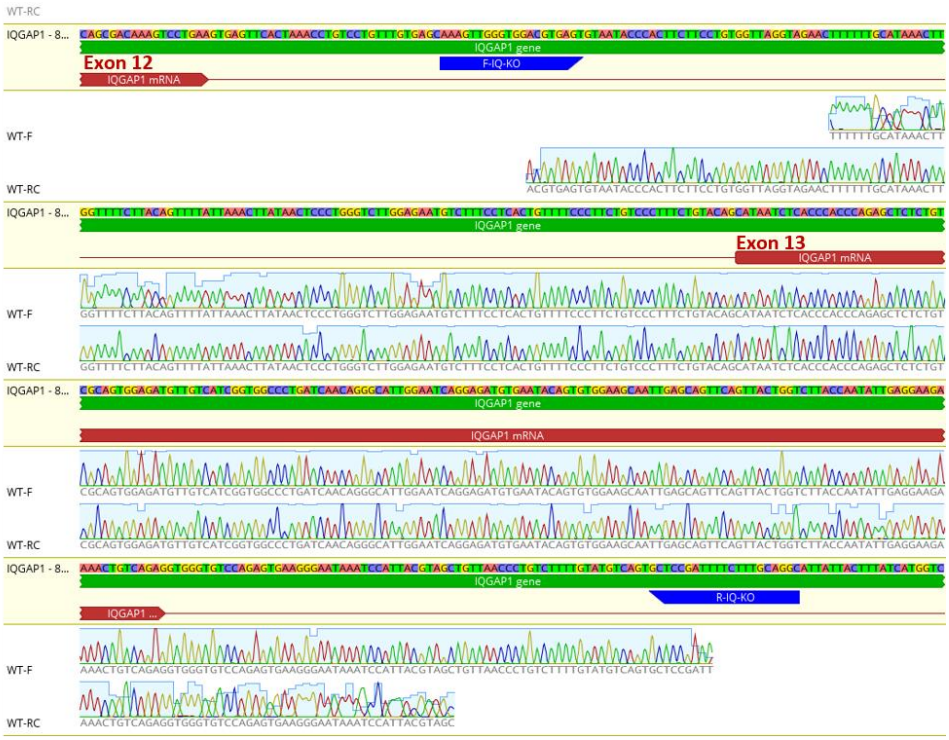

(b)

Homo sapiens chromosome 15, GRCh38.p12 Primary Assembly

Sequence ID: NC_000015.10 Length: 101991189 Number of Matches: 1

Range 1: 90452983 to 90453368 GenBank Graphics ▼ Next Match ▲ Previous Match

Score	Expect	Identities	Gaps	Strand
713 bits(386)	0.0	386/386(100%)	0/386(0%)	Plus/Plus

Features: ras GTPase-activating-like protein IQGAP1

Figure 7.5: Nucleotide sequencing result of PCR product from genomic DNA of HeLa cells (WT) aligned to *Homo sapiens* IQGAP1 gene

(a) Sanger sequencing chromatogram of purified PCR products from genomic DNA of HeLa WT control cells around the sgRNA binding site at exon 13 (red) showing nucleotide alignment with *Homo sapiens* IQGAP1 database (yellow box). The product was sequenced using two primers indicated in blue boxes to cover the editing sites.

(b) The sequencing result was blasted against to *Homo sapiens* nucleotide.

7.7 Sequencing result of PCR product from clone C3

Genomic DNA extract from clone C3 editing cells was subjected to PCR amplification using a pair of primers designed for the region flanking exon 13 of the human IQGAP1 gene. A large band of PCR product at the smaller size than those from WT cells was shown. An extended time of agarose gel electrophoresis was performed to separate the product with similar size. Two smaller bands were revealed and extracted for sequencing. Sequencing result in Figure 7.6 indicated this clone was mixed and two of them showed the deletion mutation when alignment with the wild-type sequence.

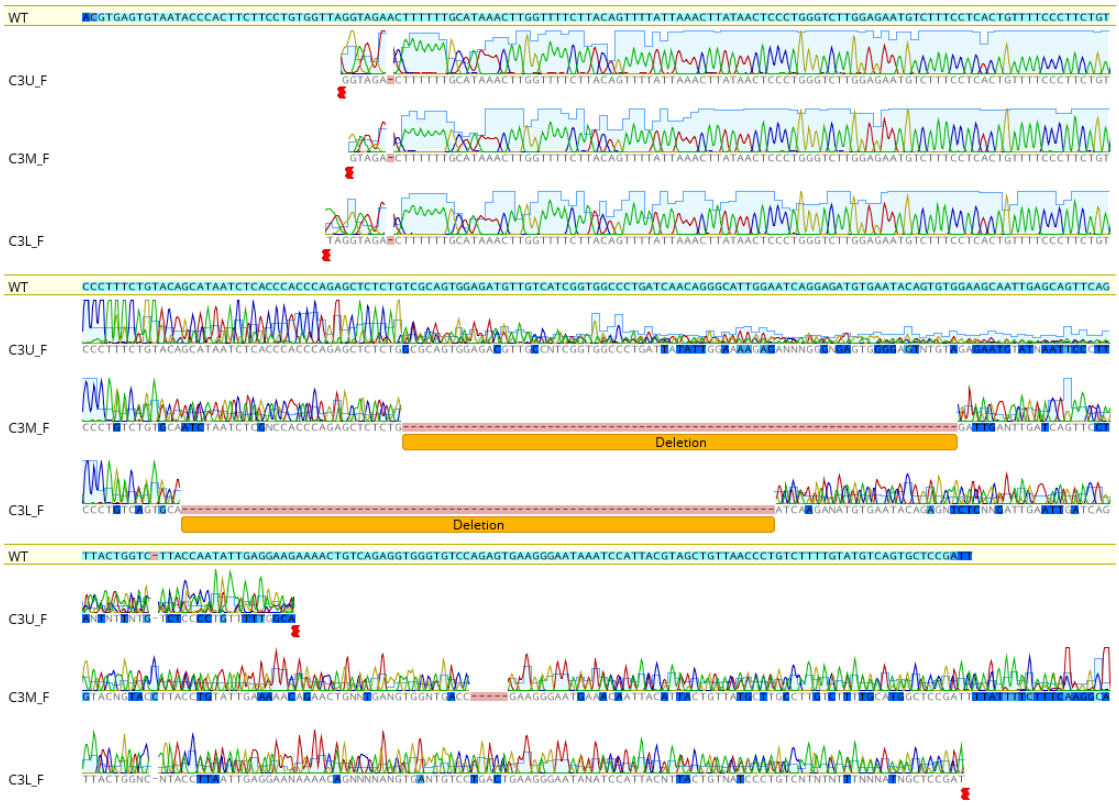

Figure 7.6: Nucleotide sequencing result of PCR product from genomic DNA of clone C3 aligned to *Homo sapiens* IQGAP1 gene
Sanger sequencing chromatogram of purified PCR products from genomic DNA of clone C3 around the sgRNA binding site. C3U, C3M and C3L was the separated bands. Orange boxes indicated deletion mutations, aligned with wild-type sequence (WT).

7.8 Sequencing result of PCR product from clone G12

PCR product from genomic DNA of clone G12 using a pair of primers designed to flank the targeted region on the human IQGAP1 gene showed three distinct PCR bands. Each band was excised from the gel and purified for sequencing. Figure 7.7 shows mutation had occurred either by insertion (G12U) or deletion (G12M and G12L) when alignment with wild-type sequence.

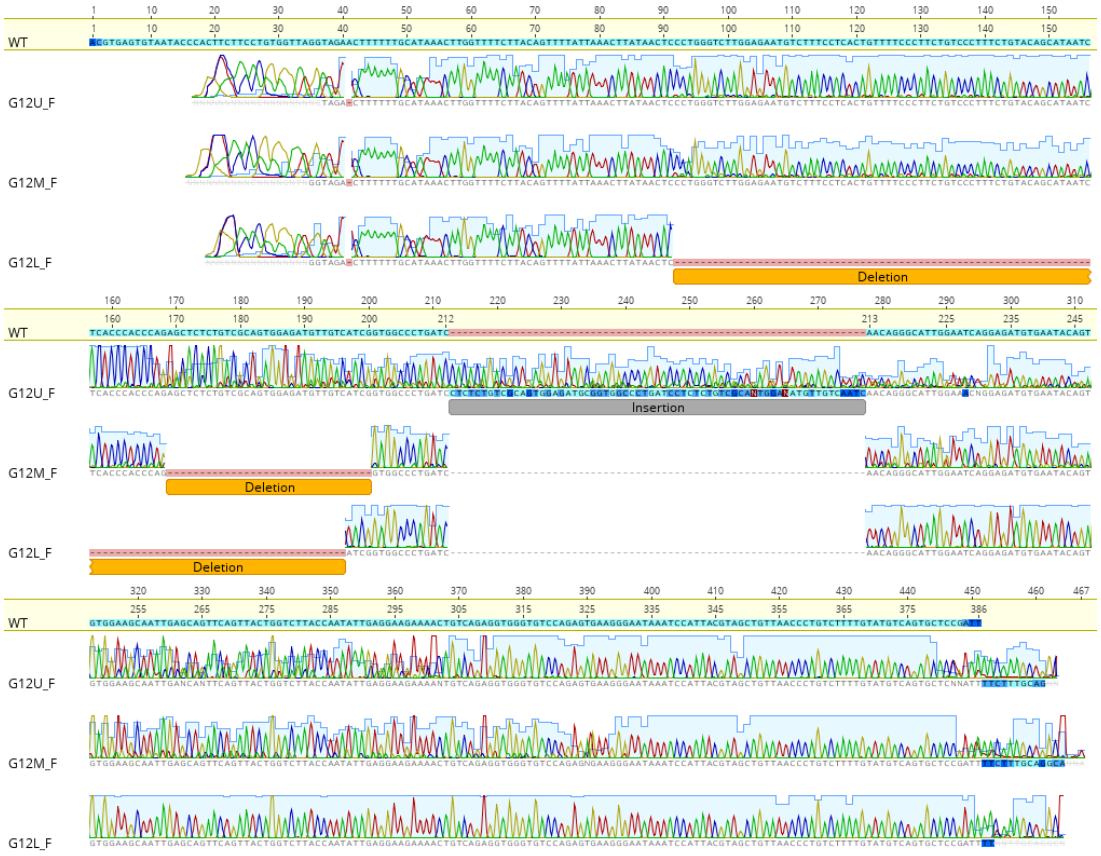

Figure 7.7: Nucleotide sequencing result of PCR product from genomic DNA of clone G12 aligned to *Homo sapiens* IQGAP1 gene
Sanger sequencing chromatogram of purified PCR products from genomic DNA of clone G12 around the sgRNA binding site. G12U, G12M and G12L were separated by agarose gel electrophoresis. Alignment with wild-type (WT) sequence of IQGAP1 gene shows error-prone mutations. Grey box indicates insertion and orange boxes indicates deletion mutations, aligned with wild-type sequence (WT).

7.9 Immunoprecipitation confirms lacking IQGAP1 in Clone H5 knockout cells

Ten-fold increase of total cell lysate extracted from clone H5 IQGAP1 knockout cells, compared to those from wild-type cell, was used for immunoprecipitation to confirm the absence of IQGAP1 in this clone. After precipitation, Western blot analysis using antibody specific to IQGAP1 was unable to detect any distinct protein band in this knockout cell line, compared to the negative controls. This suggested that expression of IQGAP1 in clone H5 was lacked completely.

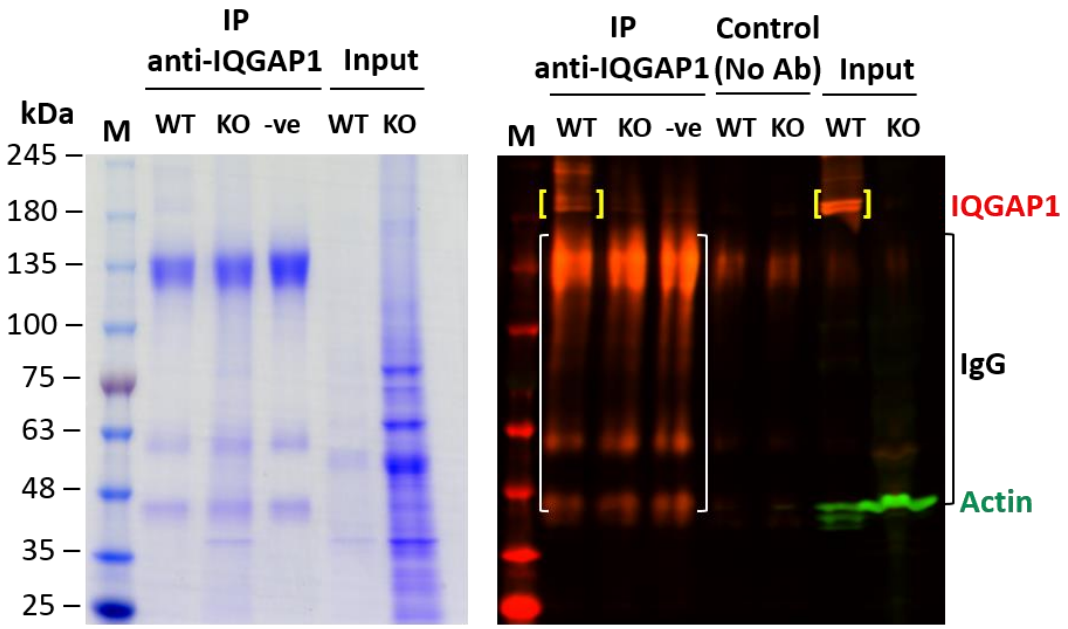

Figure 7.8: Immunoprecipitation of IQGAP1 from control and clone 5 knock-out cells

Precleared HeLa cells lysates were incubated with anti-IQGAP1 antibody and immunoprecipitated with protein A-Sepharose beads. After washing, the proteins were separated and immunoprecipitates were analysed by Coomassie blue staining and immunoblotting. WT: Lysate of control HeLa cells; KO: Lysate of knockout cells (clone H5). Right panel shows Coomassie blue staining and left panel shows Western blot analysis with anti-IQGAP1 and anti-actin (as a loading control)

7.10 Invasion and intracellular survival of *B. pseudomallei* in HeLa control cells and IQGAP1 knockout cells using a high MOI

To study the effect of lacking IQGAP1 in HeLa cells in *B. pseudomallei* invasion and intracellular survival, a high MOI at 260 was used to infect the cells. Despite of a high MOI, percentage of *B. pseudomallei* invasion into both cells, control and IQGAP1 knockout cells was similar (Figure 7.9a). However, the decrease number of bacteria was found in the IQGAP1 knockout cell at 24 hours post-infection with a similar trend in the experiment using MOI at 130, compared those in control cell (Figure 7.9b). Although, the number of bacteria at 24 hours post-infection when using MOI at 260 was lower than those at 6 hours post-infection, the similar number of bacteria was recovered at 6 and 24 hours post-infection when using MOI at 130. A higher number of bacteria infected to cells could cause cell cytotoxicity and caused cell death. This could be challenging to determine the actual number of viable bacteria at the later time point. Together, it implied that IQGAP1 was involved in intracellular life of *B. pseudomallei*.

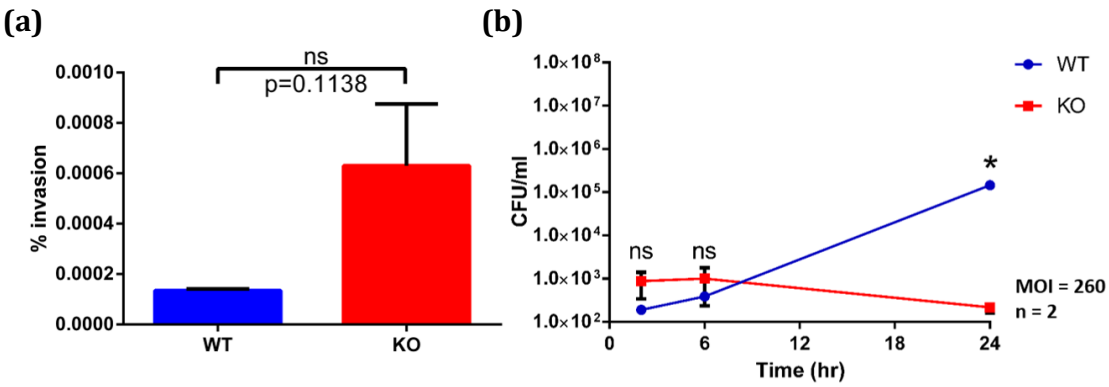

Figure 7.9: Percentage of invasion by *B. pseudomallei* and the number of bacteria in control HeLa cells (WT) and IQGAP1 knockout cells (KO) using MOI at 260

(a) At 2 hours post-infection, infected cells were lysed and the number of intracellular bacteria quantified. Data are expressed as the percentage of invasion showing mean ± SEM from two experiments (n=2, p =0.01138).

(b) Intracellular bacteria were counted after lysing infected cells at 6 and 24 hours post-infection. The data of the number of recovered bacteria at 2 hours post-infection from figure 7.9a is also included. Data are expressed as the percentage of invasion showing mean ± SEM from two experiments (n=2, p = 0.3757 at 6 hours post infection and p = 0.0144 at 6 hours post infection).

7.11 Cell cytotoxicity after *B. pseudomallei* infection

Investigation of intracellular survival of this bacterium was studies at 48 hours post-infection. At this time point the number of bacteria decresed and fluctuated wildly between experiments in both wild-type control cell and IQGAP1 knockout cells (data not shown). LDH release assay was utilised to investigate cell cytotoxicity. Figure 7.10 shows percentage of cytotoxicity increased at 48 hours post-infection. This implied that the cells were leaked, and the intracellular bacteria were released which would be killed in culture media containing the antibiotics. This could be a reason why the number of recovered bacteria was varied and low in the infected cells at the later time points.

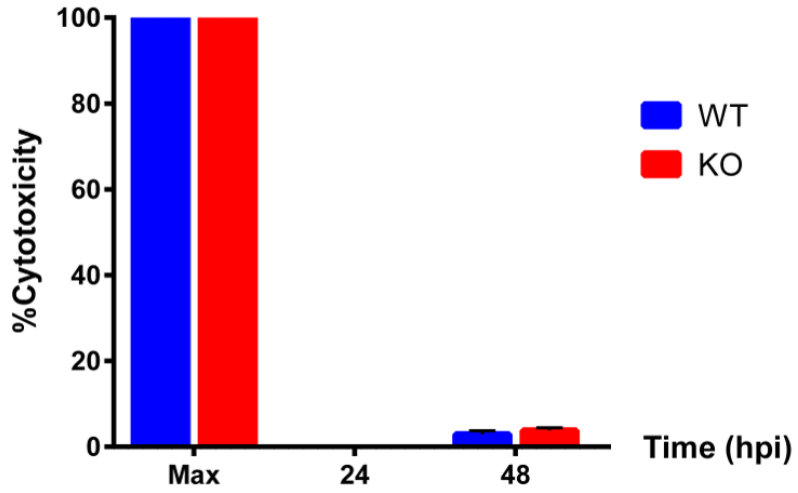

Figure 7.10: Cytotoxic effect of *B. pseudomallei* infection
Cytotoxic effect of *B. pseudomallei* infected HeLa cells at 24 hours and 48 hours post infection. The percentage of cytotoxicity was calculated from OD 490 nm measuring LDH release from cells into the supernatant. The value of maximum LDH released from uninfected cells (Max) taken as 100%. Data shown are mean ± SD representative of triplicate replicated in one experiment.

7.12 Low numbers of bacteria in IQGAP1 knockout cells at later time points

At the later time points of infection, the actual number of bacteria in infected cells could not be obtained because of cell cytotoxicity. It is presumed that the number of intracellular bacteria decreased following the trend observed at 24 hours post-infection. To confirm this, intracellular bacteria in *B. pseudomallei* infected IQGAP1 knockout cells were observed under a microscope. Figure 7.11 shows a very low number of bacteria that were stained in red at 48- and 72- hours post-infection. Whereas a higher number of bacteria in control cells was noticeable. Some bacteria were also localised with actin, which was stained in green, could be seen in yellow in the infected wild-type control cells.

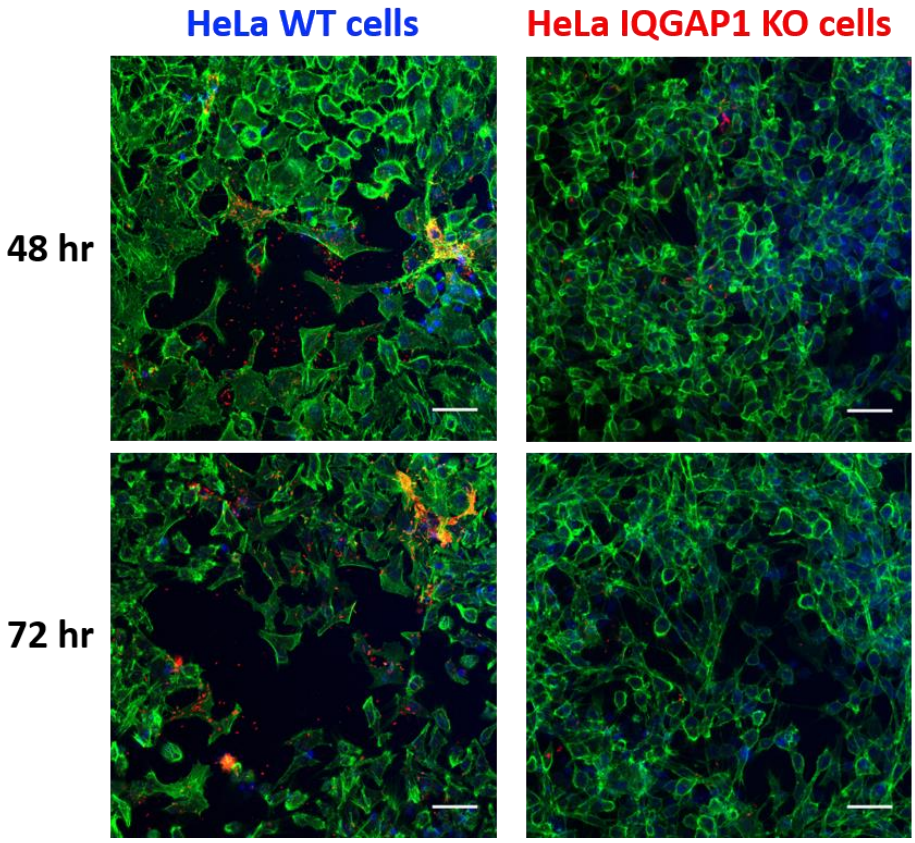

Figure 7.11: Number of *B. pseudomallei* in HeLa wild-type control cells and IQGAP1 knockout cells at 48 and 72 hours post-infection.
Confocal micrographs of HeLa cells infected with wild-type *B. pseudomallei* 10276. Bacteria were stained with anti-LPS antibody in red, nuclei were stained with DAPI in blue and actin was stained in green. Scale bar = 50 μm

7.13 Optimisation of MBP-IQGAP1 expression

From a small-scale production of MBP-IQGAP1, it showed a low level of protein expression. Additionally, the induced proteins were formed in insoluble fractions accumulated in inclusion bodies. To improve this, optimisation of the culture and induction conditions were performed. Figure 7.12 and 7.13 show the conditions used for expression of the full-length, and N-terminus and C-terminus of IQGAP1, respectively, to obtain a high level of protein expression in soluble form. The overnight culture was induced by IPTG directly or was sub-culture before induction. Concentrations of IPTG and temperature of induction were also optimised.

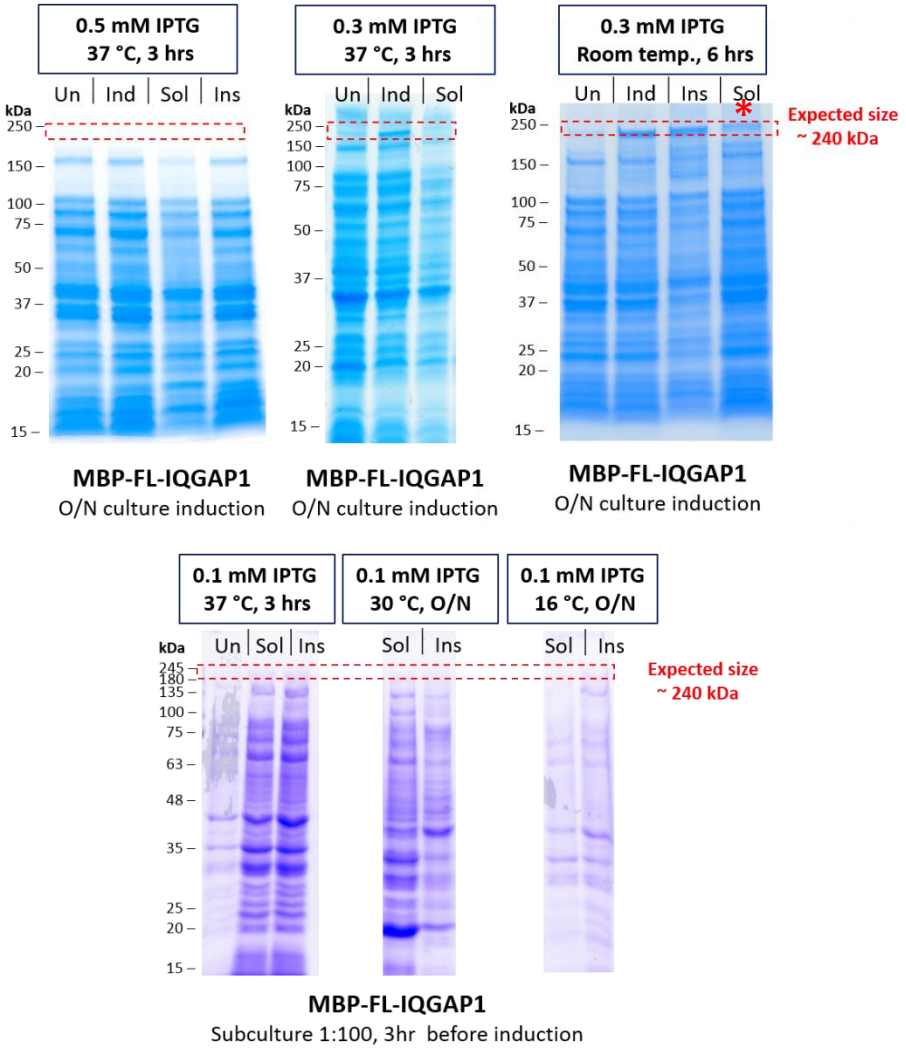

Figure 7.12: SDS–PAGE showing expression of MBP-FL-IQGAP1 recombinant proteins expressed in *E. coli* Rosetta 2 (DE3) pLysS after IPTG induction
Asterisk indicates the best condition for expression the soluble protein used in this study. Un: Uninduced cell, Ind: Induced cell, S: Soluble proteins and Ins: Insoluble proteins.

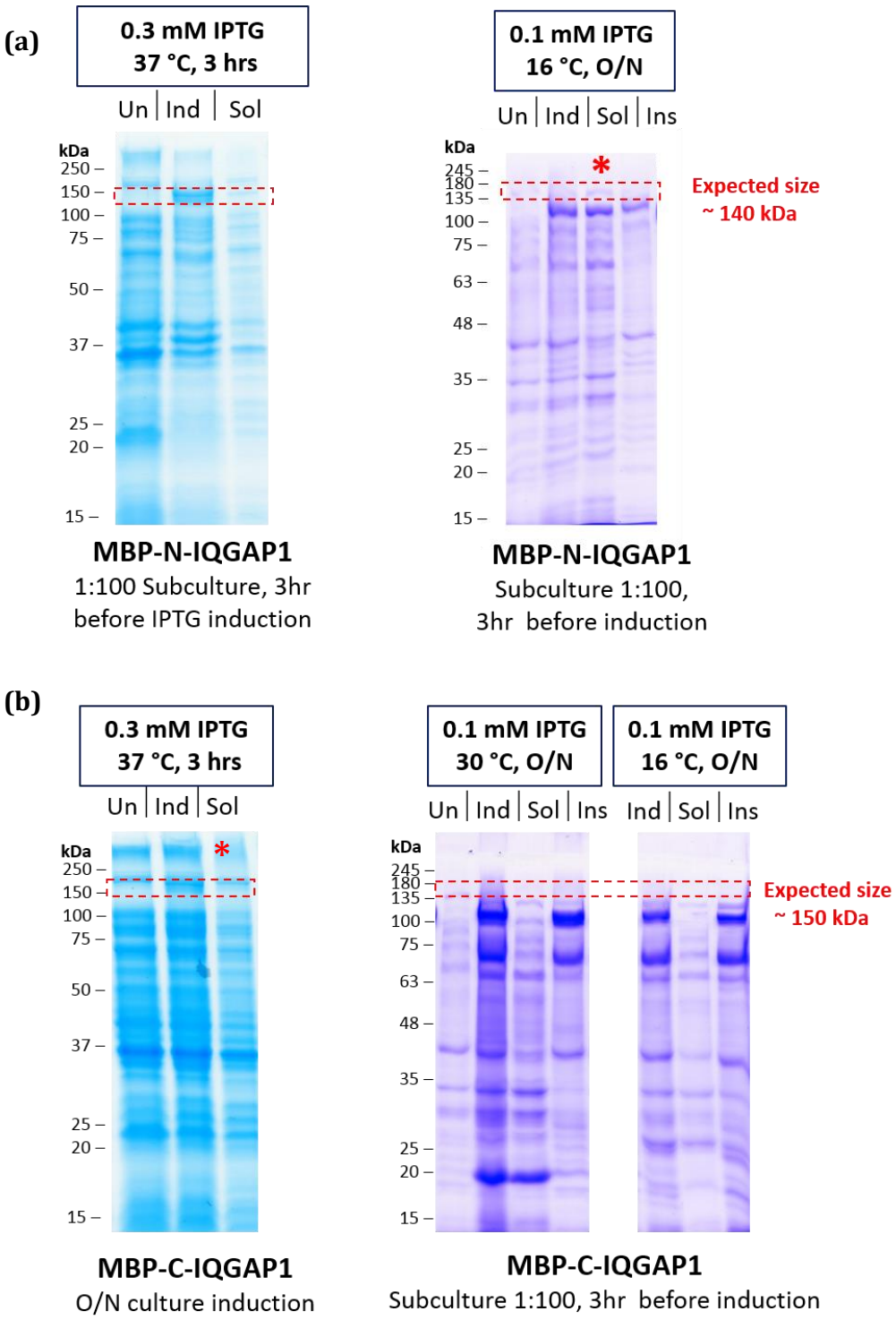

Figure 7.13: SDS–PAGE showing expression of MBP-IQGAP1 recombinant proteins expressed in *E. coli* Rosetta 2 (DE3) pLysS after IPTG induction
Un: Uninduced cell, Ind: Induced cell, S: Soluble proteins and Ins: Insoluble proteins
Asterisk indicates the best condition for expression the soluble protein used in this study.
(a) Expression of MBP-N-IQGAP1 recombinant protein.
(b) Expression of MBP-C-IQGAP1 recombinant protein.

7.14 Degradation of MBP-IQGAP proteins

Yields of MBP-IQGAP1 produced by *E. coli* were poor. It was hypothesie that the proteins were expressed but were degraded by bacterial proteases or protein folding improperly. Western blotting with antibodies specific to MBP was performed to prove this. Figure 7.14 shows protein bands specific to anti-MBP from the expected molecular weight of the fusion protein, indicated in the square brackets, to the size of MBP (42.5 kDa). This result supports the induced MBP-IQGAP1 proteins by *E. coli* were degraded.

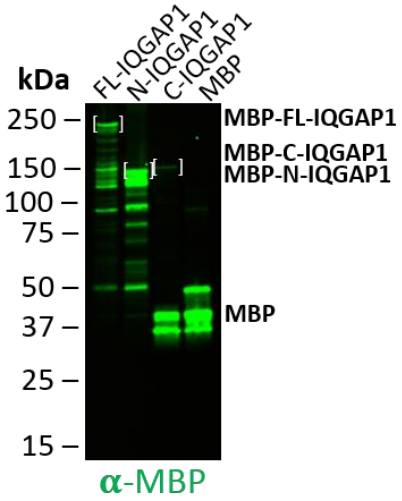

Figure 7.14: MBP-IQGAP1 proteins was degraded during production.
After IPTG induction, protein was expressed by *E. coli* Rosetta 2 (DE3) pLysS. Total cell lysate from *E. coli* carrying MBP- full length IQGAP1, N-terminal IQGAP1, C-terminal IQGAP1 and MBP were subjected to SDS-PAGE and immunoblotting using anti-MBP.

7.15 IQGAP1 expression in *E. coli* strains

Due to a low yield of MBP-FL-IQGAP1in *E. coli* strain Rosetta 2 (DE3) pLysS was concerned, the plasmid encoding MBP-FL-IQGAP1 was transformed into *E. coli* Rosetta-gami B for enhancing the quantity and quality of the fusion protein. Figure 7.15 shows there was no induced proteins after IPTG induction from *E. coli* Rosetta-gami B and derivatives, compared to those from *E. coli* strain Rosetta 2 (DE3) pLysS. Whereas the induced protein band could be detected from the expression in the *E. coli* strain Rosetta 2 (DE3) pLysS, MBP-FL-IQGAP1 was not detected from the induced cells of *E. coli* Rosetta-gami B.

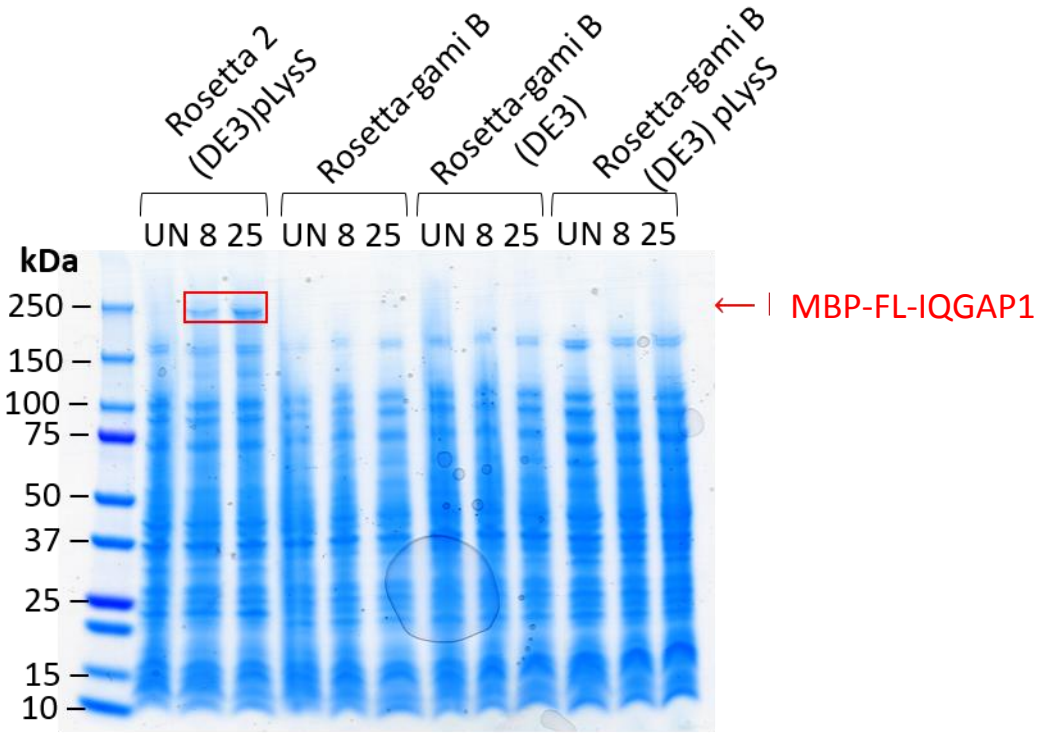

Figure 7.15: SDS–PAGE showing the expression of MBP-FP-IQGAP1 recombinant proteins expressed in *E. coli* Rosetta 2 (DE3) pLysS, *E. coli* Rosetta-gami B and derivatives after IPTG induction
Protein marker was load in the first lane, UN: Uninduced cell, 8: IPTG induced at room temperature for 8 hours, and 25: IPTG induced at room temperature for 25 hours.

7.16 Sequencing result of IQGAP1 and actin on pGADT7

To test the interaction between IQGAP1 and BimA, IQGAP1 gene was cloned into pGADT7 and expressed as a prey protein. Also, β-actin gene was amplified and cloned into the same plasmid. Actin was used as a positive control for the interaction with BimA. The insertion of IQGAP1 and actin need to be in-frame with the GAL4-AD for testing the interaction. Figure 7.16a shows the sequence of pGADT7. With the same frame of the GAL4-AD for construction of a fusion protein, a hemagglutinin (HA) epitope tag was also expressed as a fusion. Using the T7 sequencing primer, the insertion of IQGAP1 and actin were expressed in-frame with HA tag in the correct direction and in-frame with the GAL4-AD as shown in Figure 7.16b and 7.15c, respectively.

Figure 7.16: Alignment of amino acids encoding IQGAP1 and actin on pGADT7

(a) Sequence of pGADT7 showing GAL4-AD and a hemagglutinin (HA) epitope tag were expressed in-frame.

(b) Sanger sequencing chromatogram of the PCR products from pGADT7-IQGAP1. The red lines indicate reading frame number were in-frame with the HA tag shown in the cyan arrow.

(c) Sanger sequencing chromatogram of the PCR products from pGADT7-actin. The red lines indicate reading frame number were in-frame with the HA tag shown in the cyan arrow.

7.17 High concentration of 3-AT

S. cerevisiae AH109 pGBKT7-BimA with the empty prey vector was capable of growing on a SD/-His plate indicated that the expression the HIS3 reporter gene was activated by BimA. To a lesser extent of this activity, 3-amino-1,2,4-triazole (3-AT) was supplemented to SD/-His plates using concentration from 2.5 – 15 mM. Yeast cells containing pGBKT7-BimA was diluted and plated on the media using the same dilution. Figure 7.17 shows growth of AH109 pGBKT7-BimA pGADT7 on the negative control plate (SD/-His without 3-AT) was similar to those on plates containing 3-AT, despite use of a high concentration. Although 3-AT could not reduce the background growth of AH109 pGBKT7-BimA pGADT7 on a SD/-His plate, the interaction of BimA was able to be tested on media lacking adenine.

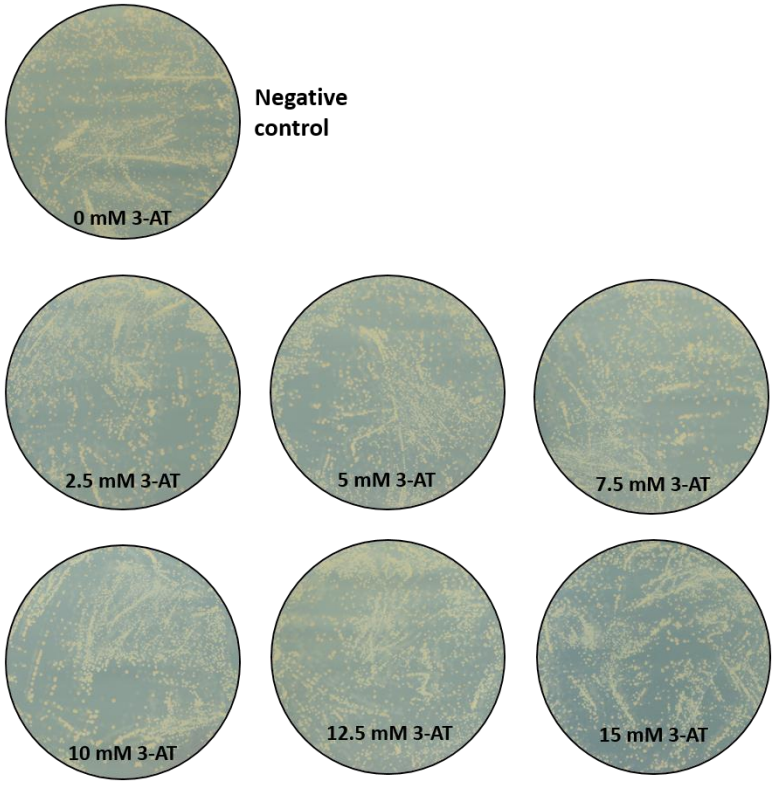

Figure 7.17: Yeast strain AH109 pGBKT7-BimA pGADT7 phenotype on minimal media (SD) lacking histidine supplemented with 3-AT
S. cerevisiae AH109 was transformed with pGBKT7-BimA pGADT7 and cultured. A serial dilution was made and plated on the SD/-His medium with/without 3-AT and incubated at 30°C for 24 hours.

7.18 Yeast two-hybrid assay after 2-days incubation

Yeast two-hybrid assay was utilised in this study to examine the interaction between BimA and IQGAP1. Growth on selective media lacking tryptophan and leucine (DDO) showed that yeasts harbouring both bait and prey proteins. Blue colour of yeast colonies on selective media in the absence of tryptophan, leucine, histidine, adenine supplemented with X-α-Gal (QDO/X-α-Gal) indicates the direct interaction between proteins. AH109 pGBKT7-BimA pGADT7-actin was able to grow and turned the colonies to blue on QDO/X-α-Gal plates demonstrating the direct interaction between BimA and actin, agreed with the previous finding (Stevens et al., 2005a). On the other hand, white colonies of AH109 pGBKT7-BimA pGADT7-IQGAP1 with the slow growth on QDO/X-α-Gal medium implied that IQGAP1 and BimA did not interact with each other directly. This observation was guaranteed by extending incubation of up to 3 days. Figure 7.18 shows the yeast colonies expressing BimA and IQGAP1 were still white after incubation for 2 and 3 days.

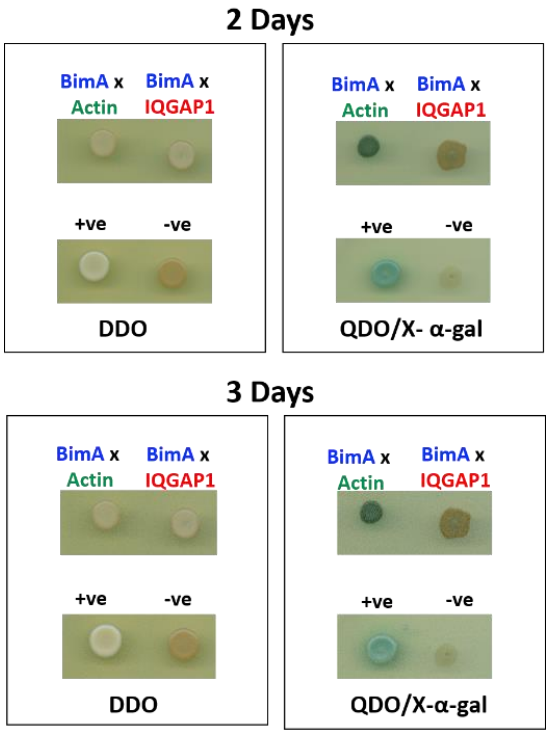

Figure 7.18: Yeast two-hybrid interactions
The pray plasmid expressing actin (pGADT7-actin) or IQGAP1 (pGADT7-IQGAP1) was transformed into *S. cerevisiae* AH109 containing pGBKT7-BimA$_{54–455.}$ Cell suspensions were inoculated onto DDO and QDO/X-α-Gal plates and incubated for 2 and 3 days. The interaction controls were *S. cerevisiae* AH109 harbouring pGBKT7-53 and pGADT7-T (positive interaction control; +ve) and pGBKT7-Lam and pGADT7-T (negative interaction control; -ve).

7.19 Validation of IQGAP1 expression by pGADT7

Studying of protein-protein interaction using yeast two-hybrid system, IQGAP1 was cloned into pGADT7 to express with HA epitope tag under the ADH1 promoter. The protein expression was validated using Western blot analysis. Figure 7.19 shows the immunoblotting using anti-HA and anti-GADPH that used as a loading control. Due to accumulation of ethanol during logarithmic growth of the yeast host cells, the full-length ADH1 promoter in pGADT7 may be repressed. To minimise this effect, the total protein from the yeast strains was extracted by either scrapping the yeast colonies directly from plates or sub-culturing the yeast strains before harvesting. Colonies from plates after incubation for 24 hours were collected for total protein extraction. Alternatively, the overnight culture was transferred into fresh medium to an OD600 = 0.5 and incubated at 30°C for 3 hours with shaking before harvesting. Despite this, only a faint band of actin was shown but IQGAP1 expression could not be detected by this technique (Figure 7.19).

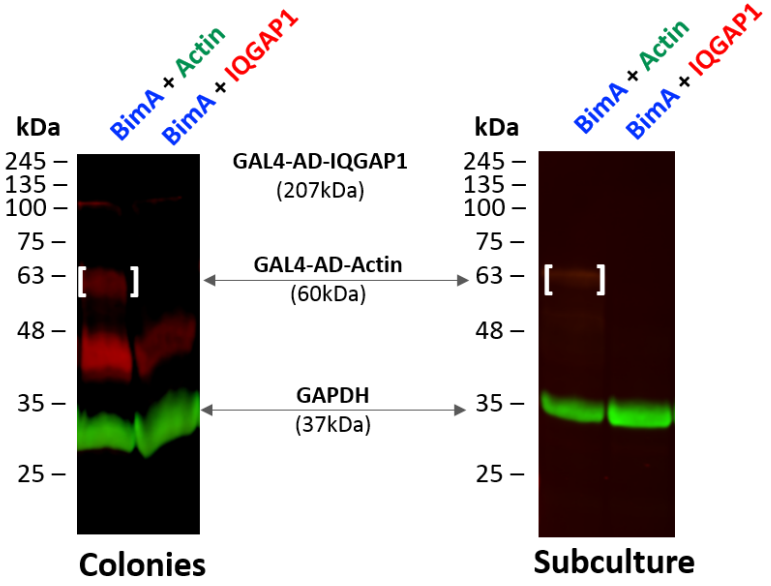

Figure 7.19: Western blot analysis showing expression of yeast fusion proteins in *S. cerevisiae* AH109

S. cerevisiae AH109 strains containing pGBKT7-BimA pGADT7-Actin (BimA+Actin) and pGBKT7-BimA pGADT7-IQGAP1 (BimA+IQGAP1) were harvested. The whole cell lysates were visualised by SDS-PAGE and probed by Western blotting using anti-HA and anti-GAPDH.

7.20 Plasmid instability and toxicity of the IQGAP1 to *E. coli*

Although MBP-IQGAP1 was expressed by the expression vector pMAL-p2X, a low expression levels or no expression at all was encountered, especially in a large-scale production. This could be caused by toxicity of the target protein. To investigate this, the *E. coli* containing pMAL-p2X-FL-IQGAP1 cells were plated on LB agar plates before IPTG induction. Figure 7.20 shows the number of *E. coli* colonies on LB plates indicating the number of all viable cells and *E. coli* cells carrying the plasmid could able to form colonies on LB plates with antibiotics. However, the lower numbers of *E. coli* with a small size on LB plates supplemented with IPTG only (without antibiotics) may imply that *E. coli* had lost the plasmid, or the plasmid may be unstable during the expression. Also, there was no colony of the *E. coli* strain on LB agar supplemented with antibiotics and IPTG. This indicated that the target protein may be toxic to the *E. coli* causing cells death after protein expression.

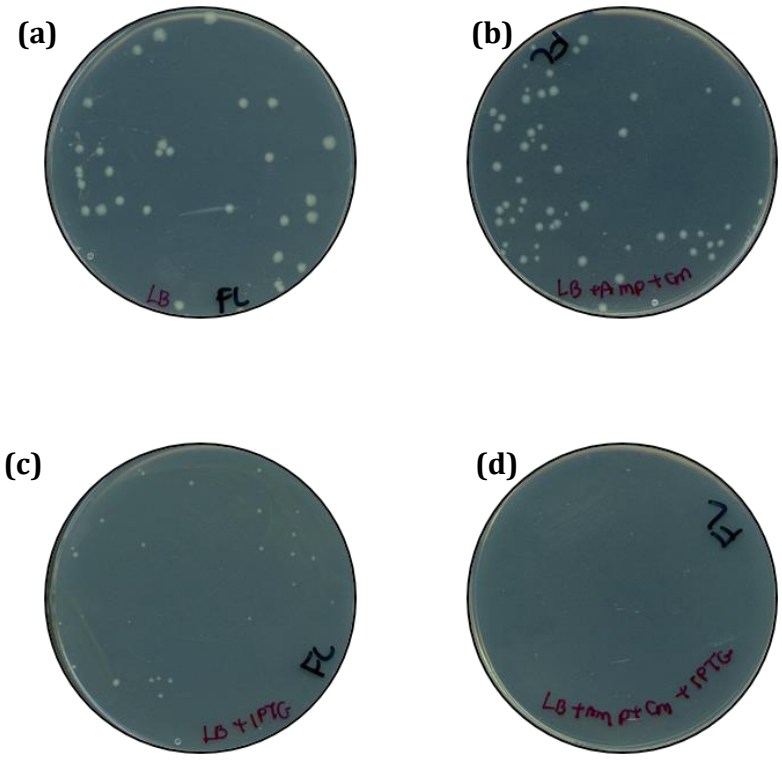

Figure 7.20: Growth of *E. coli* on LB agar plates supplemented with or without antibiotics and IPTG.
A cultures of *E. coli* Rosetta 2 (DE3) pLysS containing pMAL-p2X-FL-IQGAP1 was diluted and plated on a LB agar plate (a), LB agar plate supplemented with 100 µg/ml ampicillin and 34 µg/ml chloramphenicol (b), LB agar plate supplemented with 1mM IPTG without antibiotics (c), and LB agar plate supplemented with antibiotics and 1mM IPTG (d).

7.21 Cloning of IQGAP1 with C-terminal 6xHiS-tag in-frame fusion

The entire coding sequence of the human IQGAP1 was cloned into the yeast expression vector pPICZ B. To express the full-length of IQGAP1 fused with His-tag in *P. pastoris*, the insert was sequenced. A sequencing primer targeting on 3′AOX1 site was used to confirm the correct in-frame sequence with a His-tag (Figure 7.21a). Figure 7.21b showed the sequencing result at the 3′-end of the IQGAP1 insertion were in-frame with the fusion protein.

(a)

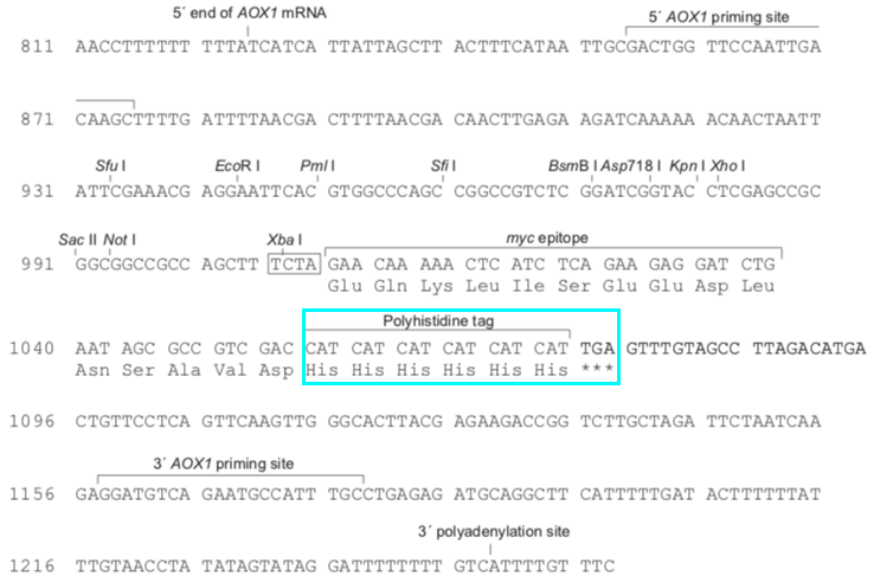

(b)

Figure 7.21: Comparison of the amino acid sequence of IQGAP1 expressed by pPICZ B in *P. pastoris*

(a) Sequence of pPICZ B for expression in *P. pastoris* indicating a His-tag in the cyan rectangle at the 3′-end from the multi-cloning sites.

(b) Sanger sequencing chromatogram of the PCR products at the 3′-end of pPICZ B-IQGAP1. The amino acid sequence translated from the sequencing result was aligned with the IQGAP1 gene showing the correct in-frame sequence with a His-tag indicated in cyan arrow.

7.22 Validation of BimA expression by Western blot analysis

To express and purify BimA, $BimA_{54-470}$ was cloned into the expression vector pET-21b(+). BimAwith His-tag fusion was produced in *E. coli* Rosetta 2 (DE3) pLysS and tested by immunoblotting using antibody specific to $BimA_{48–384}$ (Stevens et al., 2005a). Figure 7.22 shows the protein band specific to anti-BimA was induced, compared to those from negative controls.

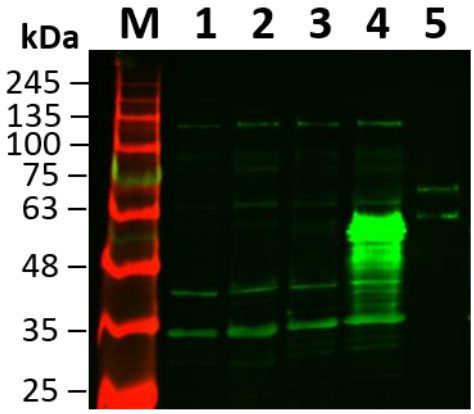

Figure 7.22: Western blot analysis showing expression of BimA in *E. coli* Rosetta 2 (DE3) pLysS

Total proteins from *E. coli* Rosetta 2 (DE3) pLysS strains with and without IPTG induction were subjected to Western blotting. detected using antibody specific $BimA_{48–384}$ for protein expression.

M: Protein molecular weight marker

1: Total cell lysate of uninduced cell of *E.coli* Rosetta2 (DE3) pLysS containing pET21b (+)

2: Total cell lysate of induced cell of *E.coli* Rosetta2 (DE3) pLysS containing pET21b (+)

3: Total cell lysate of induced cell of *E.coli* Rosetta2 (DE3) pLysS containing pET21b (+)-$BimA_{54-470}$

4: Total cell lysate of induced cell of *E.coli* Rosetta2 (DE3) pLysS containing pET21b (+)-$BimA_{54-470}$

5: GST-$BimA_{54-455}$ (Positive control for anti-BimA)

7.23 MBP shows a baseline of nucleation activity

To study the ability of IQGAP1 to stimulate actin polymerisation. Purification of IQGAP1 fused to maltose-binding protein (MBP) was performed. A preliminary experiment of pyrene-actin polymerisation assay supplemented with MBP was tested. Figure 7.23 shows the purified MBP increased actin polymerisation rate dramatically, compared to the GST protein which showed a similar rate with actin alone. With a high level of background nucleation activity of MBP, this fusion protein should be removed by FactorXa.

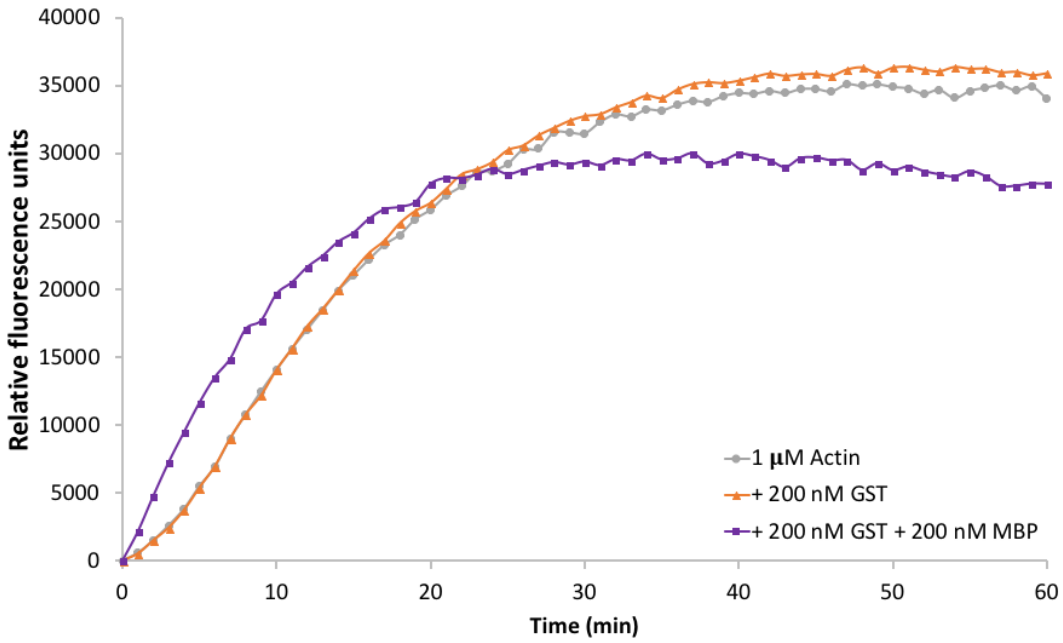

Figure 7.23: MBP shows a baseline of nucleation activity
Emission of fluorescence due to polymerisation of pyrene-labelled actin monomers by MBP (purple line) was increased compared with the reaction containing GST (orange line) or actin alone. The graph shows the emission levels of fluorescence over time from one experiment.

7.24 Rate of actin polymerisation of G-actin alone

Pyrene assay is a biochemical kinetic assay for measuring the changes in fluorescence intensity when pyrene-labelled monomeric actin is polymerised or depolymerise. This assay is very sensitive to small differences in concentration of actin filaments presented in the reaction. Thus, the reaction containing only actin alone was run on the same day when performing the experiments to ensure there is not extensive of actin filament. Working stock of actin was prepare freshly and tested before initiating test with proteins of interest. Due to the reaction with actin alone was perform independently from the test reactions, the data was not included in the Figure 5.16. Fluorescence data was collected every minute for up to 1 hour. During the linear phase of polymerisation, rates of fluorescence units per second were calculated (Figure 7.24). Rate of actin polymerisation of G-actin alone in the polymerisation buffer was similar to those with the GST or N-IQGAP1 alone as shown in the Chapter 5.

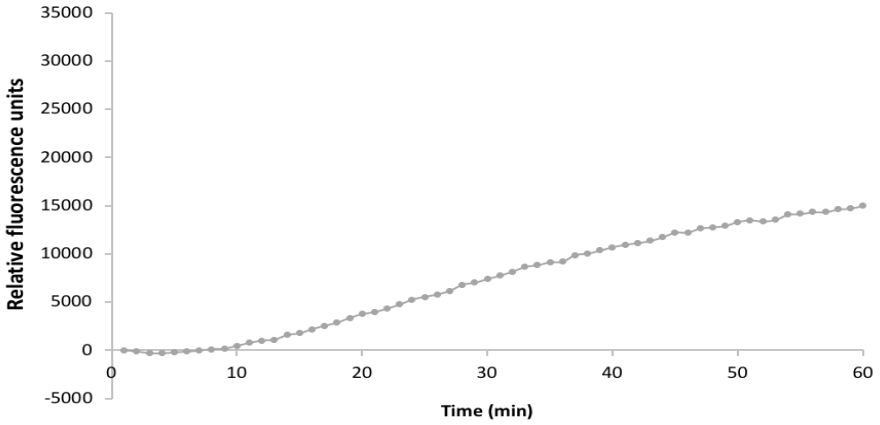

***p* value compared to the reaction of actin alone** Polymerisation rate of actin = 6.41 ± 0.14 units/sec (n= 3)				
N-IQGAP1	**GST**	**GST + N-IQGAP1**	**GST-BimA**	**GST-BimA + N-IQGAP1**
0.7387173	0.6009689	0.9639274	0.0000043*	0.0000002*

Figure 7.24: Rate of actin polymerization using actin alone
Emission of fluorescence due to polymerisation of pyrene-labelled actin monomers by actin alone. Three independent replicates were tested in one experiments and the graphs show the mean emission levels of fluorescence over time. The rise in fluorescence units per second during the linear phase of polymerisation was calculated as rates of polymerisation showing the mean rates of fluorescence units per second ± SEM in the table. Asterisks denote a significant difference in the rate of polymerisation compared to actin alone ($p \leq 0.05$).

7.25 Publication

Identification of Candidate Host Cell Factors Required for Actin-Based Motility of *Burkholderia pseudomallei

Niramol Jitprasutwit, Nurhamimah Zainal-Abidin, Charles Vander Broek, Dominic Kurian, Sunee Korbsrisate, Mark P. Stevens, and Joanne M. Stevens

Journal of Proteome Research **2016** *15* (12), 4675-4685

DOI: 10.1021/acs.jproteome.6b00760

*Publication attached below.

Journal of proteome research

Article

pubs.acs.org/jpr

Identification of Candidate Host Cell Factors Required for Actin-Based Motility of *Burkholderia pseudomallei*

Niramol Jitprasutwit,[†,‡] Nurhamimah Zainal-Abidin,[†] Charles Vander Broek,[†] Dominic Kurian,[†] Sunee Korbsrisate,[‡] Mark P. Stevens,[†] and Joanne M. Stevens*[,†]

[†]The Roslin Institute and Royal (Dick) School of Veterinary Studies, University of Edinburgh, Easter Bush, Midlothian, EH25 9RG, United Kingdom

[‡]Department of Immunology, Faculty of Medicine Siriraj Hospital, Mahidol University Bangkok, 73170 Thailand

ABSTRACT: Intracellular actin-based motility of the melioidosis pathogen *Burkholderia pseudomallei* requires the bacterial factor BimA. Located at one pole of the bacterium, BimA recruits and polymerizes cellular actin to promote bacterial motility within and between cells. Here, we describe an affinity approach coupled with mass spectrometry to identify cellular proteins recruited to BimA-expressing bacteria under conditions that promote actin polymerization. We identified a group of cellular proteins that are recruited to the *B. pseudomallei* surface in a BimA-dependent manner, a subset of which were independently validated with specific antisera including the ubiquitous scaffold protein Ras GTPase-activating-like protein (IQGAP1). IQGAP1 integrates several key cellular signaling pathways including those involved in actin dynamics and has been shown to be involved in the adhesion of attaching and effacing *Escherichia coli* to infected cells and invasion of host cells by *Salmonella enterica* serovar Typhimurium. Although a direct interaction between BimA and IQGAP1 could not be detected using either conventional pulldown or yeast two hybrid techniques, confocal microscopy revealed that IQGAP1 is recruited to *B. pseudomallei* actin tails in infected cells, and siRNA-mediated knockdown highlighted a role for this protein in controlling the length and actin density of *B. pseudomallei* actin tails.

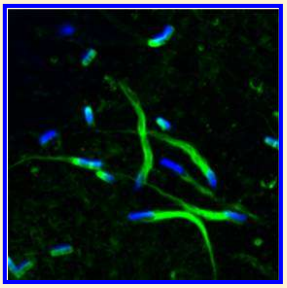

KEYWORDS: *Burkholderia pseudomallei, melioidosis, intracellular bacterial pathogen, actin-based motility, BimA, IQGAP1*

INTRODUCTION

Burkholderia pseudomallei causes melioidosis, a severe invasive disease of humans and animals endemic in Southeast Asia and Northern Australia. Human infections are acquired by inhalation, ingestion, or via abraded skin and may produce a spectrum of diseases ranging from rapidly fatal septicemia and acute pneumonia through chronic or localized abscess formation to subacute infections (reviewed in Wiersinga et al.[1]). Relapse and latency are common in melioidosis, and it is believed that this reflects the ability of *B. pseudomallei* to persist in an intracellular niche and its intrinsic resistance to many classes of antibiotic.

Facultative intracellular pathogens of several bacterial genera have evolved mechanisms to enter and exit eukaryotic cells by harnessing the power of actin polymerization. Some species of *Burkholderia*, *Listeria*, *Mycobacterium*, *Rickettsia*, and *Shigella* are propelled in the cytosol and into adjacent cells by polar nucleation of actin, a process termed actin-based motility. These bacteria use distinct mechanisms for actin-based motility, converging on activation of the cellular Arp2/3 complex by mimicry or recruitment of its regulators (reviewed in Stevens et al.[2]) or by mimicking Arp2/3-independent actin nucleators such as cellular formins or WH2-domain-containing proteins (reviewed in Qualmann and Kessels[3]). In the case of *Burkholderia*, we discovered that this process requires BimA,[4] a putative Type V secreted protein that is conserved among *B. pseudomallei* isolates in the endemic area.[5] *B. pseudomallei* BimA influences intracellular survival, intercellular spread,[6] and virulence in mice;[7] however, the mechanism by which it recruits and activates cellular factors to assemble actin is not fully understood. BimA homologues of divergent N-terminal amino acid sequence exist in the closely related species *B. mallei* and *B. thailandensis*.[8] These proteins vary in their composition and number of actin-binding WH2 domains, the presence of proline-rich motifs, PDAST repeats, and Arp2/3-binding CA domains, implying that different *Burkholderia* species have evolved distinct strategies of actin-based motility.[6,8,9] For example, only *B. thailandensis* BimA sequesters Arp3, consistent with the presence of a unique CA domain.[9a] Despite the variation in sequence, both *B. mallei* and *B. thailandensis* BimA proteins can functionally substitute for the actin-based motility defect of a *B. pseudomallei bimA* mutant.[8] Similarly, BimA proteins from *B. pseudomallei* and *B. mallei* can restore actin-based motility to a *B. thailandensis bimA* mutant.[9b,10] In *B. mallei* and *B. pseudomallei*, *bimA* gene expression is coregulated with the virulence-associated Type VI secretion system cluster through a two-component sensor-regulator VirAG, which senses host cytosolic glutathione levels.[11]

Received: August 19, 2016
Published: November 14, 2016

DOI: 10.1021/acs.jproteome.6b00760
J. Proteome Res. 2016, 15, 4675−4685

In common with other bacterial pathogens capable of actin-based motility, the Arp2/3 complex can be detected in *B. pseudomallei* actin-rich tails.[12] However, we have previously shown that *B. pseudomallei* BimA does not require the Arp2/3 complex to promote actin polymerization in vitro,[4,9a] a finding confirmed recently by Benanti et al.[9b] and supported by observations by Lu and colleagues in which Arp2/3 depletion failed to inhibit *B. pseudomallei* actin-based motility.[10] Taken together with the findings that N(neural)-WASP and the vasodilator-stimulated phosphoprotein (VASP) are not required for actin-based motility of *B. pseudomallei*,[12] and that actin-based motility is insensitive to overexpression of the WA fragment of Scar1 (which inhibits actin-based motility of *L. monocytogenes*, *S. flexneri* and *R. conorii*),[12] it may be inferred that *B. pseudomallei* employs a distinct mechanism for intracellular motility to other pathogens. Indeed, it has recently been suggested that BimA mimics cellular Ena/VASP proteins promoting the polymerization and elongation of actin tails.[9b]

In a similar manner described for the characterization of host cell proteins in the actin tails of *Listeria monocytogenes*,[13] we have utilized an affinity purification approach to identify the cellular proteins recruited to *B. pseudomallei* under conditions that promote actin assembly in vitro. This relied on overexpression of VirAG to drive surface expression of BimA in *B. pseudomallei* and pulldown of host proteins from a murine splenic extract. Using this approach, we have identified a number of proteins common to both the actin-rich tails of *L. monocytogenes* and *B. pseudomallei*, together with a number of proteins uniquely associated with the actin tails of *B. pseudomallei*. Association of a subset of these proteins with BimA-expressing bacteria was validated by immunoblotting. Confocal microscopy confirmed the recruitment of the cellular cytoskeletal scaffold protein Ras GTPase-activating-like protein (IQGAP1) to the actin tails of *B. pseudomallei* in infected cells. Using siRNA-mediated knockdown, we also demonstrate that IQGAP1 plays a role in regulating the actin density and tail length of *B. pseudomallei* actin tails in infected cells.

MATERIALS AND METHODS

Bacterial Strains

Burkholderia pseudomallei strain 10276 (NCTC 10276) was isolated from a British seaman suffering from the chronic form of melioidosis after likely exposure in Bangladesh.[14] Strain 10276 and our *bimA* insertion mutant[4] were transformed with pBHR2-*virAG*[11b] (a kind gift from Paul Brett and Mary Burtnick, University of South Alabama, US) by electroporation[15] to give strains 10276 pBHR2-*virAG* and 10276 *bimA*::pDM4 pBHR2-*virAG*. Bacteria were cultured in Luria–Bertani broth supplemented with appropriate antibiotics at 37 °C with shaking for ∼16 h.

For a *bimA* deletion mutant to be generated, approximately 400 base pairs immediately upstream of the *bimA* gene (annotated as BPSS1492 in the reference *B. pseudomallei* K96243 genome) was amplified using primers P1 (ATATATCTCGAGACCCGACACGCCGTGGACAGAA) and P2 (ATATATGGGCCCCATATCGATTGGCAGTGCCGT) using GC advantage polymerase (Takara Biotech Europe, Saint-German-en-Laye, France) following the manufacturer's instructions. Genomic DNA from strain NCTC 10276 was used as template. The PCR product was digested with *Xho*I and *Apa*I and ligated into similarly digested pDM4, an oriR6K *sacB* positive-selection suicide replicon.[16] The resulting plasmid was designated pDM4-*bimA*1. Next, approximately 540 base pairs downstream of the *bimA* gene was amplified from 10276 genomic DNA by PCR using primers P3 (ATATATGGGCCCTAAGCACCCGCAAACCCCCCCGGGCATC) and P4 (ATATATAGATCTCAGGCTGCAGAACGCAGGCT). The PCR product was restricted with *Apa*I and *Bgl*II prior to ligation with similarly digested pDM4-*bimA*1. The resulting plasmid was designated pDM4-Δ*bimA*.

Construction of the *B. pseudomallei* mutant was performed according to the method described by Logue et al.[17] Briefly, pDM4-Δ*bimA* was introduced into *B. pseudomallei* strain NCTC 10276 by conjugation from *E. coli* S17.1λpir. Colonies were selected on LB agar plates containing 50 μg/mL of kanamycin and 50 μg/mL of chloramphenicol. Colonies were screened by PCR with P1 and P4 primers to detect integration of the plasmid. A *B. pseudomallei* 10276 pDM4-Δ*bimA* merodiploid was next cultured in the absence of selection for the integrated plasmid and then plated on LA plates lacking NaCl and containing 15% (w/v) sucrose to positively select for a second recombination event involving excision of pDM4 and the *bimA* allele. Resulting colonies were then screened by PCR using flanking primers BimA screen 1 (GATGTCGCCGACGAAAGCAG) and BimA screen 2 (AGTGGGCGCGATTCTCGCGGCT) for the presence of a truncated *bimA* gene (of around 1 Kb) instead of the full length gene (of around 2.5 Kb). The resulting *bimA* deletion mutant was designated 10276 Δ*bimA*.

Preparation of Murine Splenic Lysates

Spleens were harvested from BALB/c or VM mice at post mortem. Spleens were rinsed in ice-cold polymerization buffer (10 mM Tris pH 7.5, 50 mM KCl, 2 mM $MgCl_2$). Then, 1 mL of ice-cold polymerization buffer supplemented with protease and phosphatase inhibitors (1 mM phenylmethanesulfonyl fluoride (PMSF), 2 mM Na_2VO_3, 2 mM NaF, 2 mM Na pyrophosphate, 1 μg/mL aprotinin, 10 μg/mL leupeptin, 1 μg/mL pepstatin A) was added per spleen, and the tissues were homogenized. Supernatants were clarified by ultracentrifugation at 100,000*g* for 2 h at 4 °C. The clarified supernatants were carefully pipetted and stored at −70 °C between assays. The protein concentration of the murine splenic lysate was determined to be ∼7 mg/mL using a bicinchoninic acid protein assay kit (Thermo Fisher Scientific, Cramlington, UK).

Affinity Purification of *Burkholderia*-Associated Proteins

Interacting proteins were isolated essentially as described by David et al.[13a] with some modifications. Approximately 1×10^9 bacteria were pelleted and suspended in 1.5 mL of murine splenic lysate supplemented with 5 mM ATP and 30 mM creatine phosphate. Bacteria were incubated for 1 h at 37 °C with gentle agitation. Bacteria were washed gently with 1 mL of ice-cold 10 mM PIPES pH 7.25 containing 40 mM KCl, 5 mM ATP, and 5 mM $MgCl_2$. Interacting proteins were eluted from the bacterial surface using 0.5 mL of 10 mM PIPES pH 7.25 containing 1 M KCl, 5 mM ATP, and 5 mM $MgCl_2$. After repeating the elution, the eluate was filter-sterilized by passing through a 0.2 μm membrane filter before concentrating the proteins using 30 μL of StrataClean resin (Agilent Technologies UK Ltd., Stockport, UK). Resin was suspended in Laemmli sample treatment buffer containing 2% (v/v) β-mercaptoethanol. After incubation at 95 °C for 10 min, samples were separated by SDS-PAGE using a 4–15% gradient gel. After electrophoresis, bands were stained using a SilverSnap kit following the manufacturer's instructions (Thermo Fisher

DOI: 10.1021/acs.jproteome.6b00760
J. Proteome Res. 2016, 15, 4675–4685

Scientific, Cramlington, UK). Bands were excised and subjected to LC–MS/MS.

LC–MS/MS

Gel slices were destained with 15 mM potassium ferricyanide/50 mM sodium thiosulfate for 5 min, reduced with 10 mM DTT/100 mM ammonium bicarbonate for 30 min, and alkylated with 55 mM iodoacetamide/100 mM ammonium bicarbonate for 20 min. Gel slices were washed with 100 mM ammonium bicarbonate and dehydrated with 100% (v/v) acetonitrile. Proteins were digested with 6 ng/mL of trypsin/50 mM ammonium bicarbonate for 5 h at 37 °C, and peptides were extracted in 1% (v/v) formic acid/2% (v/v) acetonitrile followed by 50% (v/v) acetonitrile. LC–MS/MS analysis of peptides was performed on a nanoAcquity UPLC system coupled to Q-Tof Premier mass spectrometer (Waters Corporation, Milford, Massachusetts, USA). Tryptic peptides were desalted and concentrated on a C_{18} TRAP column (180 μm × 20 mm, 5 μm symmetry; Waters) for 3 min at 10 μL/min and resolved on a 1.7 μm BEH 130 C_{18} column (100 μm × 100 mm; Waters Corporation) using a Waters Corporation nanoAcquity UPLC. Peptides were eluted at 400 nL/min with a linear gradient of 0–50% (v/v) acetonitrile/0.1% (v/v) formic acid over 30 min, followed by 85% (v/v) acetonitrile/0.1% (v/v) formic acid for 7 min. Eluted peptides were analyzed on a Q-Tof mass spectrometer in "data directed" acquisition mode, where an MS survey scan was used to automatically select double and multiple charged peptides for further MS/MS fragmentation. From each survey scan, up to three of the most intense peptides were selected for fragmentation. MS/MS collision energy was dependent on precursor ion mass and charge state. A reference spectrum was collected every 30 s from the Glu-fibrinopeptide B (785.8426 m/z) introduced via a reference sprayer.

The raw mass spectral data was processed with ProteinLynx Global Server 2.3 (Waters Corporation) to generate peaklist files. The mass accuracy of the spectra was further corrected using the reference spectra from Glu-fibrinopeptide B. The resulting peaklist files were searched against a locally installed protein sequence database (5855 entries) of the *B. pseudomallei* reference strain K96243 and mouse International Protein Index (IPI) database[18] using Mascot ver. 2.3 (Matrix Science, London, UK). Precursor and fragment ion mass tolerance were set to ±100 ppm and ±0.1 Da, respectively. Trypsin specificity was used for allowing up to one missed cleavage. Carbamidomethylation of cysteines and oxidation of methionines were selected as fixed and variable modifications, respectively. The interpretation and presentation of MS/MS data was performed according to published guidelines.[19]

Immunoblotting of Bacterial and Affinity-Purified Host Proteins

Protein samples were denatured by heating to 95 °C for 5 min in Laemmli buffer containing a final concentration of 1% (v/v) β-mercaptoethanol. Proteins were resolved by SDS-PAGE and transferred to PVDF or nitrocellulose membranes using a semidry transfer system (Bio-Rad, Hemel Hempstead, UK). Membranes were then blocked and incubated sequentially with primary antibodies at a concentration of 0.5–1 μg/mL followed by species-specific antibodies conjugated with horseradish peroxidase (for standard ECL detection; GE Healthcare, Chalfont St. James, UK) or fluorescently labeled secondary antibodies (α-rabbit IgG DyLight^{800}; Cell Signaling Technology, Leiden, The Netherlands), followed by detection using a Biosciences Odyssey infrared imaging system (LI-COR Biosciences, Cambridge, UK). Primary antibodies used in immunoblotting were mouse anti-BimA monoclonals AF8, FB5, and FG11,[4] rabbit anti-BopE,[20] mouse anti-*B. pseudomallei* capsule (a kind gift from Dstl, Porton Down, UK[21]), goat anti-actin (Source Bioscience, Nottingham, UK), goat anti-IQGAP1 (Abcam, Cambridge, UK), rabbit anti-IQGAP1 (Insight Biotechnology, Wembley, UK), rabbit anti-vinculin (Source Bioscience, Nottingham, UK), rabbit anti-HSP90 (Source Bioscience, Nottingham, UK), and rabbit anti-L-Plastin (Source Bioscience, Nottingham, UK).

Cell Infection, siRNA Knockdown, and Fluorescence Microscopy

HeLa cells were cultured on sterile glass coverslips and infected at a multiplicity of infection (MOI) of ∼100 essentially as described in Sitthidet et al.[6] At the indicated time points postinfection, coverslips were rinsed with phosphate-buffered saline (PBS) and incubated for a minimum of 16 h in PBS containing 4% (w/v) paraformaldehyde before staining for confocal microscopy. Coverslips were treated with 0.5% (v/v) Triton-X100 in PBS for 15 min to permeabilize infected cells, blocked for 30 min in 0.5% (w/v) BSA in PBS, and then sequentially incubated in 0.5 μg/mL of primary and fluorescently labeled secondary antibodies or cell stains as indicated in the figure legends. Primary antibodies used in fluorescence microscopy were mouse anti-BimA AF8, FB5, and FG11,[4] mouse anti-*B. pseudomallei* lipopolysaccharide (LPS) (Camlab, Cambridge, UK), and rabbit anti-IQGAP1 (Insight Biotechnology, Wembley, UK). Actin filaments were stained with Phalloidin Alexa Fluor^{488} (Life Technologies Ltd., Paisley, UK). Images were captured using a Leica Microsystems (Milton Keynes, UK) LSM710 confocal scanning microscope and Zen 2011 software (Carl Zeiss Ltd., Cambridge, UK).

For reducing the expression of IQGAP1 in HeLa cells, approximately 30,000 cells plated per well of a 24-well tissue culture plate were transfected with 6 pmol Silencer Select IQGAP1 siRNA duplex (Life Technologies Ltd., Paisley, UK) using Lipofectamine RNAiMax (Life Technologies Ltd., Paisley, UK) essentially as described by the manufacturer's instructions. Cells were lysed at 72 h post-transfection to detect IQGAP1 knockdown by immunoblotting. While optimizing conditions for IQGAP1 knockdown, cells transfected with MISSION negative control siRNA (Sigma-Aldrich, Dorset, UK) were used for reference. For infection experiments, IQGAP1 siRNA-transfected cells were incubated for 56 h prior to infection with *B. pseudomallei* strain 10276. Cells were infected at an MOI of ∼100 for a further 16 h before fixation and staining for confocal microscopy analysis.

Images representing maximal projection z-stacks were captured using identical laser settings from three independent experiments and analyzed using ImageJ software (http://imagej/nih.gov/ij/). The maximal calliper function was used to calculate the length of tails and the corrected total cell fluorescence (CTCF) formula to determine the intensity of actin staining throughout each tail. Data from a total of 100 tails from each condition were collated and analyzed using a student t test in GraphPad Prism.

Yeast Two-Hybrid

A fragment of the *bimA* gene encoding amino acids 54–455 of the BimA protein (capable of binding and polymerizing actin in vitro) was cloned into pGBKT7 (Clontech, Saint-Germain-en-Laye, France) to express an in-frame fusion protein with the

DOI: 10.1021/acs.jproteome.6b00760
J. Proteome Res. 2016, 15, 4675–4685

GAL4 DNA-binding domain. The *bimA* gene was amplified by PCR from 10276 genomic DNA using primers F-BimA (GCGCGCCATATGAATCCCCCCGAACCGCCGGGC) and R-BimA (GCGCGCGAATTCTTAGCGCGCGGTGTC-GGTG). The product was purified, digested with *Nde*I and *Eco*RI, and ligated into a similarly digested vector to give pGBKT7-*bimA*. This plasmid was introduced into *Saccharomyces cerevisiae* strain AH109 using a standard lithium acetate-mediated transformation protocol outlined in the Matchmaker GAL4 Yeast Two Hybrid System 3 handbook (Clontech, Saint-Germain-en-Laye, France) with selection on SD media lacking tryptophan (Clontech, Saint-Germain-en-Laye, France) to give strain AH109 pGBKT7-*bimA*. The *iqgap1* gene was amplified by PCR from HeLa cell cDNA (AMS Biotechnology Ltd., Abingdon, UK) using primers F-IQGAP1 (TTTTCATATGA-TGTCCGCCGCAGACGAG) and R-IQGAP1 (TTTTCTC-GAGTTACTTCCCGTAGAACTTTTTGTTGA). Similarly the *actb* gene was amplified by PCR from HeLa cell cDNA using primers F-actin (TTTTCATATGATGGATGATGATA-TCGCCG) and R-actin (TTTTCTCGAGCTAGAAGCATT-TGCGGTGG). PCR products were purified, digested with *Nde*I and *Xho*I, and ligated into similarly digested pGADT7 (Clontech, Saint-Germain-en-Laye, France) to create pGADT7-*iqgap1* and pGADT7-*actin* encoding in-frame fusion proteins with the GAL4 activation domain. All plasmids were verified by sequencing prior to transformation into AH109 strains and selection on SD media lacking leucine. The pGADT7-*iqgap1* and pGADT7-*actb* plasmids were separately introduced into AH109 pGBKT7-*bimA* by lithium acetate with selection on SD media lacking leucine and tryptophan (double drop out (DDO) media; Clontech, Saint-Germain-en-Laye, France) to give strains AH109 pGBKT7-*bimA* pGADT7-*iqgap1* and AH109 pGBKT7-*bimA* pGADT7-*actin*.

For protein−protein interactions to be identified, single yeast colonies from DDO agar plates were suspended in 20 μL of water, and 5 μL was dotted onto SD agar plates lacking leucine, tryptophan, adenine, and histidine (quadruple drop out (QDO)) supplemented with 20 μg/mL of X-α-galactosidase. Plates were incubated at 30 °C for 24 h before observing the appearance of the colonies. The strains AH109 pGBKT7-*bimA* pGADT7-*iqgap1* and AH109 pGBKT7-*bimA* pGADT7-*actin* were tested alongside yeast strains transformed with positive and negative control vectors (pGADT7-T antigen pGBKT7-p53 and pGADT7-T antigen pGADT7-Lamin C, respectively) supplied with the Matchmaker GAL4 Y2H System 3 (Clontech, Saint-Germain-en-Laye, France).

RESULTS

Engineering a *Burkholderia pseudomallei* Strain that Constitutively Expresses BimA in vitro

BimA (BPSS1492), a predicted Type V autotransporter protein of *Burkholderia pseudomallei*, is required for actin-based motility of the bacterium in the cytosol of infected cells.[4,6] We have found that BimA expression is below the limit of detection in bacteria cultured in common laboratory media (Figure 1a) but detectable from 6 h postinfection by immunoblotting infected cell lysates with antibodies specific to BimA[4] (Figure 1b). The presence of intracellular bacteria in all samples was confirmed by immunoblotting with antibody reactive to the *B. pseudomallei* capsule.[21] In the closely related species *B. mallei*, *bimA* gene transcription and BimA protein expression are positively regulated by a two-component system, VirAG,

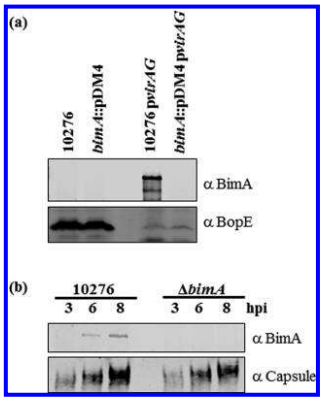

Figure 1. *Burkholderia pseudomallei* BimA expression is not constitutive and can be induced by expression of VirAG in trans. (a) Western blot analysis of BimA expression in whole cell lysates of bacteria cultured in LB overnight at 37 °C. Bacterial lysates were probed for BimA and BopE (as a protein loading control) using specific antibodies and show that BimA is not expressed by wild-type *B. pseudomallei* under standard culture conditions. Expression in trans of the two component regulator VirAG results in BimA expression. Note that approximately 10-fold more 10276 and *bimA*::pDM4 bacteria (than their p*virAG*-containing counterparts) were loaded onto the protein gel for analysis. (b) Western blot analysis of RAW cells infected with wild-type *B. pseudomallei* and a *bimA* mutant at an MOI of 100 at 3, 6, and 8 h postinfection. Lysates were probed for BimA and *Burkholderia* capsule (as a protein loading control) using specific antibodies and indicate detection of BimA in lysates at the later time points postinfection.

encoded adjacent to the *bimA-E* genes on chromosome 2.[11b] To induce BimA expression in LB-cultured bacteria, we therefore introduced the pBHR2-*virAG* plasmid constitutively expressing the *B. mallei virAG* genes[11b] into strain NCTC 10276[14] or our *bimA* insertion mutant giving strains 10276 pBHR2-*virAG* and 10276 *bimA*::pDM4 pBHR2-*virAG*. The VirA and VirG proteins of *B. mallei* and *B. pseudomallei* share 99.4 and 99.6% identity, respectively, and introduction of the pBHR2-*virAG* plasmid into these strains resulted in expression of BimA protein in wild-type bacteria cultured in laboratory medium (Figure 1a). Protein loading was confirmed using an antibody against the *B. pseudomallei* Bsa Type III secretion system effector protein BopE.[20] Localization of BimA on the surface of the 10276 pBHR2-*virAG* strain was confirmed by confocal microscopy of intact bacteria (data not shown).

Isolation of Candidate Host Cell Proteins Involved in Actin-Based Motility of *B. pseudomallei*

Having established an in vitro system in which *B. pseudomallei* bacteria were expressing BimA, we set out to identify host cell proteins that associated with 10276 pBHR2-*virAG* (BimA-expressing bacteria) and common bacterial proteins released from the bacterial surface following elution from 10276 pBHR2-*virAG* and 10276 *bimA*::pDM4 pBHR2-*virAG*. Bacteria were incubated with murine splenic lysates under conditions that promote BimA:actin binding and actin polymerization,[4] and interacting proteins were eluted and concentrated for SDS-PAGE. Following silver staining, gel slices were excised and subjected to in-gel trypsin digestion, extraction, and LC−MS/MS analysis. A representative silver stained gel is shown in

DOI: 10.1021/acs.jproteome.6b00760
J. Proteome Res. 2016, 15, 4675−4685

Figure 2. Spectra were then separately searched against the mouse International Protein Index (IPI) database[18] and an "in-

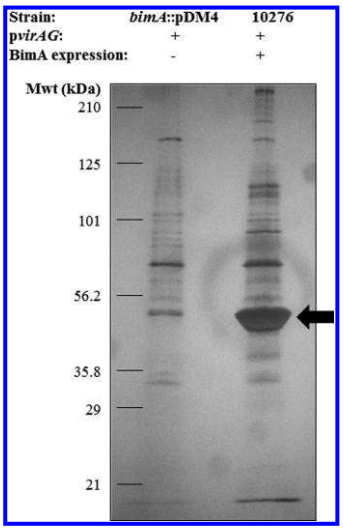

Figure 2. Host cell and bacterial proteins are eluted from the surface of *B. pseudomallei* strains incubated with murine splenic lysate. A representative silver-stained SDS-polyacrylamide gel showing the profile of proteins eluted from 10276 pBHR2-*virAG* and 10276 *bimA*::pDM4 pBHR2-*virAG* bacteria incubated with murine splenic lysates. The abundant presence of actin in the 10276 pBHR2-*virAG* sample is indicated by the arrow. Protein bands from samples from three independent experiments were processed for LC–MS/MS analysis.

house" *B. pseudomallei* K96243 protein database to obtain protein identifications. Data were collected for three independent experiments with both bacterial and host cell proteins identified in the eluted proteins.

We sought to identify host cell proteins that were solely associated with, or identified at a higher frequency with, the BimA-expressing bacteria 10276 pBHR2-*virAG* compared to the *bimA* mutant strain 10276 *bimA*::pDM4 pBHR2-*virAG*. Spectra were screened against the mouse IPI database,[18] and protein identifications were assigned when the proteins were identified in at least two of the three biological replicates. From this analysis, a set of 30 host proteins were isolated (Table 1). In contrast to a previous study on the proteome of *L. monocytogenes* actin tails,[13b] there was a notable lack of microtubule components, intermediate filaments, or myosins. The most abundant and commonly isolated proteins recruited in a VirAG-dependent manner were those of the actin family, consistent with the known actin-binding activity of BimA.[4] Several of the proteins are associated with areas of dynamic actin assembly, such as membrane ruffles and cell junctions, or act as scaffolds to integrate signaling complexes. A selection of host cell proteins recruited by BimA-expressing bacteria contained FERM domains, which are known to localize at the interface between the cytoskeleton and the plasma membrane. The scaffold proteins Talin, 14–3–3 protein zeta/delta, and IQGAP1 were identified, as were components of the Arp2/3 complex (specifically subunits 1b, 2, and 4) previously described as being in the actin tails of *B. pseudomallei*.[12] In addition to actin, we identified several F-actin binding proteins implicated in stabilizing F-actin networks through bundling and cross-linking activities (α-actinins 1 and 4, Filamin A, Spectrin/fodrin, Vinculin, Tropomyosin, Plastin-2/L-Plastin, Transgelin), several F-actin capping proteins (Spectrin/fodrin, ERM proteins, Macrophage capping protein, CapZ), and an actin-depolymerizing factor (ADF) in the form of cofilin. We also identified the proteins WD repeat-containing protein 1 (AIP1) and serine/threonine phosphatase 2A, known regulators of cofilin activity.

Several *B. pseudomallei* proteins were consistently identified in eluates from both wild-type and *bimA* mutant bacteria (Table 2), including the Type VI secreted protein Hcp (BPSS1498) and a number of chaperone proteins and proteases. A number of the *B. pseudomallei* proteins identified in this study have previously been identified in the *B. pseudomallei* outer membrane proteome,[22] the total secretome,[23] or as surface proteins by surface labeling approaches,[24] including the molecular chaperones GroEL (BPSL2697 and BPSS0477), GroES (BPSL2698), DnaK (BPSL2827), and the transcription/translation factors Tuf (BPSL3215) (labeled OM in Table 2). Several have also been shown to be recognized by the sera of convalescent melioidosis patients (labeled I in Table 2).[24,25] The remainder of proteins ranged in function from metabolic enzymes involved in glycolysis, amino acid metabolism, and the TCA cycle to RNA polymerase subunits. These may represent particularly abundant proteins of the bacteria released upon cell lysis or proteins contained within outer membrane vesicles (OMVs). OMVs have recently been reported to have protective efficacy against pulmonary melioidosis and *B. pseudomallei*-induced sepsis;[26] however, a proteomic analysis of the contents of such OMVs has yet to be described.

Validation of the Data Set

The data set described in Table 1 was validated by immunoblotting of independently generated samples for a subset of host cell proteins. An equal volume of eluted protein generated from identical treatment of similar numbers of bacteria was probed in each instance. Proteins that were identified in all three experiments with high MASCOT scores and that were novel when compared to proteins involved in *Listeria* or *Shigella* actin-based motility were confirmed (HSP90 and IQGAP1) (Figure 3). We also chose to validate one of the proteins identified in only two experiments with a moderate MASCOT score (vinculin) or identified in all three experiments with a low MASCOT score (L-Plastin) (Figure 3). As a positive control, the recruitment of actin to BimA-expressing bacteria was also verified (Figure 3). All chosen targets were detected in murine splenic lysate and samples derived from bacteria expressing BimA in vitro (10276 pBHR2-*virAG*) that were absent from those samples lacking BimA (10276 *bimA*::pDM4 pBHR2-*virAG*).

IQGAP1 is Present in Actin Tails Formed by Intracellular *B. pseudomallei*

The Ras GTPase-activating-like protein IQGAP1 is a ubiquitously expressed scaffold protein that integrates multiple host signaling pathways including actin cytoskeleton dynamics, cell cycle, and cell adhesion. To date, this protein has not been shown to be involved in the actin-based motility of intracellular bacteria, although it has been shown to be involved in entry of *Salmonella* into host cells and for actin pedestal formation of

DOI: 10.1021/acs.jproteome.6b00760
J. Proteome Res. 2016, 15, 4675–4685

Table 1. Host Cell Proteins Isolated from BimA-Expressing *Burkholderia pseudomallei*[a]

gene ID	gene name	description	protein accession no.	protein score	# unique peptides	notes
IPI00131138	***flna***	**Filamin A**	**Q8BTM8**	**104**	**32**	**Lm**
IPI00753793	*spna2*	Spectrin alpha chain/fodrin alpha chain	P16546	176	50	Lm
IPI00319830	*spnb2*	Spectrin beta chain/fodrin beta chain	Q62261	79	8	Lm
IPI00465786	*tln1*	Talin 1	P26039	91	8	Lm
IPI00467447	***iqgap1***	**IQ motif containing GTPase activating protein 1, IQGAP1**	**Q9JKF1**	**107**	**49**	
IPI00405227	*vcl*	Vinculin	Q64727	67	12	Lm
IPI00118899	***actn4***	**Alpha-actinin-4**	**P57780**	**109**	**31**	**Lm**
IPI00380436	*actn1*	Alpha-actinin-1	Q7TPR4	116	38	Lm
IPI00229080	*hsp90ab1*	Heat shock protein 90 kDa alpha	Q71LX8	79	17	
IPI00169731	*fermt3*	Fermitin family homologue 3/kindlin 3	Q8K1B8	55	1	
IPI00118892	***lcp1***	**Lymphocyte cytosolic protein 1/plastin −2/L-plastin**	**Q61233**	**58**	**3**	**Lm (T-plastin)**
IPI00338302	*pgm2*	Phosphoglucomutase-2	Q7TSV4	43	2	
b	***ezr/msn/rdx***	**Ezrin/Radixin/Moesin**[b]	*b*	**61**	**4**	**Lm (Ezrin)**
IPI00314748	*wdr1*	WD repeat-containing protein 1/AIP1	O88342	61	2	Lm
IPI00110827	***acta1***	**Alpha actin**	**P68134**	**98**	**34**	**Lm**
IPI00125143	*arpc1b*	Actin-related protein 2/3 complex subunit 1b	Q91Z25	58	2	
IPI00473320	***actb***	**Beta actin-like protein**	**Q3U804**	**140**	**117**	**Lm**
IPI00874482	***actg1***	**Gamma actin**	**P63260**	**140**	**121**	**Lm**
IPI00110850	***actb***	**Beta actin**	**P60710**	**103**	**34**	**Lm**
IPI00277930	*capg*	Macrophage-capping protein	Q99LB4	96	6	
IPI00830701	*tpm1*	Tropomyosin 1	P58771	102	11	Lm
IPI00111556	*ppp2cb*	Serine/threonine phosphatase 2A catalytic subunit	P62715	62	1	
IPI00111265	*capza2*	F-actin-capping protein subunit alpha-2	P47754	77	1	Lm
IPI00874728	*tpm2*	Tropomyosin 2	P58774	102	13	Lm
IPI00775844	*arpc2*	Actin-related protein 2/3 complex subunit 2	Q9CVB6	71	3	Lm
IPI00230044	*tpm3*	Tropomyosin 3	Q58E70	88	7	Lm
IPI00116498	*ywhaz*	14−3−3 protein zeta/delta	P63101	71	6	Lm
IPI00125778	***tagln2***	**Transgelin 2**	**Q9WVA4**	**69**	**2**	**Lm**
IPI00138691	***arpc4***	**Actin-related protein 2/3 complex subunit 4**	**P59999**	**51**	**5**	**Lm**
IPI00890117	*cfl1*	Cofilin-1	P18760	100	3	Lm

[a]List of murine proteins isolated either solely or at a higher frequency from eluates from BimA-expressing bacteria 10276 pBHR2-*virAG* compared to the *bimA* mutant strain 10276 *bimA*::pDM4 pBHR2-*virAG*. Proteins were assigned when peptides were isolated in at least two experiments with a MASCOT score of at least 30, at least one rank 1 peptide where the predicted mass of the protein matched the observed mass, and where the reported cellular localization was listed as cytoplasm or plasma membrane. Proteins shown in bold were isolated in all three experiments. Proteins are listed in order of molecular weight (highest to lowest) with "Lm" in the notes column denoting the identification of this protein in similar proteomic studies of *Listeria monocytogenes* tails. [b]Peptides matched ezrin (IPI00330862, P26040), moesin (IPI00110588, P26041), and radixin (IPI00308324, P26043).

attaching and effacing *E. coli* pathotypes to the apical surface of cells (reviewed by Kim et al.[27]). Our data implied that, in contrast to *Listeria* and other pathogens that display actin-based motility, IQGAP1 may be a component of *B. pseudomallei* actin tails. Indeed, this was supported by immunocytochemistry and confocal microscopy, which revealed the presence of IQGAP1 throughout the tails of *B. pseudomallei* 10276 at 16 h postinfection of HeLa cells (Figure 4a−c). In agreement with a recent report by Benanti et al.,[9b] we could also elucidate the architecture of the *B. pseudomallei* actin tail by fluorescent actin staining coupled with confocal microscopy, albeit at low resolution (Figure 4d). The tails consisted of loosely bundled F-actin filaments reminiscent of those described for certain *Rickettsia* species that rely on the formin-like Sca2 autotransporter for actin polymerization.[28]

Yeast Two-Hybrid Analysis Detects a Direct Interaction between BimA and Actin but not IQGAP1

Although IQGAP1 could readily be detected in the actin tails of all bacteria displaying actin-based motility in infected cells, we sought to determine if this is through direct interaction with the BimA protein using a yeast two-hybrid approach. The yeast two-hybrid assay is a widely utilized and sensitive molecular genetic approach to detect even weak or transient protein:-protein interactions in vivo. It relies on the modular nature of transcriptional *trans*-activators where the DNA-binding and activation domains can be physically separated and expressed as fusions with proteins of interest. If the proteins interact, they bring the DNA-binding and activation domains into close proximity, thereby resulting in transcription of certain reporter genes. In our yeast two-hybrid system, the reporter genes for histidine and adenine biosynthesis (which allow growth on media lacking these two amino acids) and α-galactosidase (which produces blue colonies on media containing X-α-Gal substrate) are utilized. We have expressed amino acid residues 54−455 of the BimA protein as a DNA-binding protein fusion protein in the reporter yeast strain AH109 pGBKT7-BimA. When β-actin is also expressed in this strain as an activation domain fusion protein (AH109 pGBKT7-BimA pGADT7-actin), the yeast generates blue colonies on media containing X-α-Gal substrate but lacking leucine, tryptophan, adenine, and histidine (QDO) (Figure 5), indicating an interaction between these two proteins as we have previously described.[4]

DOI: 10.1021/acs.jproteome.6b00760
J. Proteome Res. 2016, 15, 4675−4685

Table 2. *Burkholderia pseudomallei* Proteins Identified in the Samples[a]

gene ID	gene name	description	protein accession no.	protein score	# unique peptides	notes
bpsl0779	*sucC*	Succinyl-CoA synthetase subunit beta	YP_107404.1	88	2	
bpsl1013	*ppc*	Phosphoenolpyruvate carboxylase	YP_107641.1	67	4	
bpsl1087	*htpG*	Heat shock protein 90	YP_107709.1	103	4	
bpsl1402	***tig***	**Trigger factor**	**YP_108024.1**	**69**	**6**	
bpsl1405	***lon***	**ATP-dependent protease**	**YP_108027.1**	**96**	**6**	
bpsl2192	*aceB*	Malate synthase	YP_108787.1	80	4	
bpsl2270	*eno*	Phosphopyruvate hydratase	YP_108866.1	128	3	
bpsl2305		Oligopeptidase A	YP_108901.1	117	2	
bpsl2697	***groEL***	**Chaperonin GroEL**	**YP_109293.1**	**157**	**38**	**OM, I**
bpsl2698	***groES***	**Co-chaperonin GroES**	**YP_109294.1**	**169**	**8**	**I**
bpsl2827	*dnaK*	Molecular chaperone DnaK	YP_109422.1	107	6	OM, I
bpsl2953	*tktA*	Transketolase	YP_109547.1	101	8	
bpsl3004	*rpmA*	50S ribosomal protein L27	YP_109599.1	109	2	
bpsl3196	*rpsE*	30S ribosomal protein S5	YP_109790.1	78	5	
bpsl3215	***tuf***	**Elongation factor Tu**	**YP_109809.1**	**104**	**9**	
bpsl3220	***rpoC***	**DNA-directed RNA polymerase subunit beta′**	**YP_109814.1**	**102**	**23**	
bpsl3221	***rpoB***	**DNA-directed RNA polymerase subunit beta**	**YP_109815.1**	**117**	**22**	
bpss0421	*rfbH*	Lipopolysaccharide biosynthesis protein (O-antigen-related)	YP_110445.1	45	1	I
bpss0879		Porin protein	YP_110888.1	83	2	OM, I
bpss0913		Methionine gamma-lyase	YP_110922.1	104	4	
bpss1356		hypothetical protein	YP_111366.1	133	22	OM
bpss1498	*hcp*	hypothetical protein (Type VI secretion system secreted protein Hcp)	YP_111505.1	112	14	
bpss1715	*gltA*	Type II citrate synthase	YP_111721.1	81	7	
bpss1722	*mdh*	Malate dehydrogenase	YP_111728.1	107	5	I
bpss1726	***acnA***	**Aconitate hydratase**	**YP_111732.1**	**118**	**20**	

[a]List of *Burkholderia pseudomallei* proteins isolated from eluates of both 10276 pBHR2-*virAG* and 10276 *bimA*::pDM4 pBHR2-*virAG* bacteria. Proteins were assigned when peptides were isolated from both samples in at least two experiments with a MASCOT score of at least 30 and at least one rank 1 peptide where the predicted mass of the protein matched the observed mass. Proteins in bold were isolated in all three experiments. In the notes column, "OM" indicates that the protein has previously been described as surface associated or a component of the *B. pseudomallei* outer membrane proteome,[22,24] and "I" indicates the protein is recognized by recovering human melioidosis patient sera.[24,25] Proteins are listed in order of *B. pseudomallei* gene number with chromosome 1 encoded proteins (BPSLxxxx) listed first.

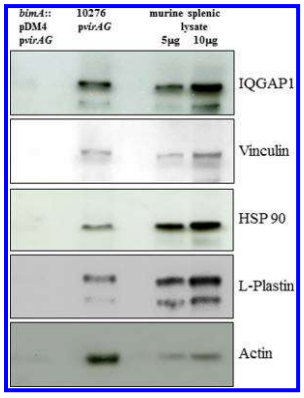

Figure 3. Independent validation confirms the presence of a subset of host cell proteins in eluates from *B. pseudomallei* strains incubated with murine splenic lysate. Independent protein eluates from 10276 pBHR2-*virAG* and 10276 *bimA*::pDM4 pBHR2-*virAG* bacteria incubated with murine splenic lysates were prepared and immunoblotted to confirm the specific presence of IQGAP1, vinculin, HSP90, and L-plastin in the 10276 pBHR2-*virAG* samples. As positive controls for the antibodies, 5 and 10 μg of total splenic lysate were loaded.

Conversely, introduction of a vector expressing IQGAP1 as an activation domain fusion protein into the BimA yeast strain (AH109 pGBKT7-BimA pGADT7-IQGAP1) resulted in growth of the yeast strain on QDO media; however, the colonies remained white even after extended incubation times (Figure 5). Growth on selective media in the absence of detectable α-galactosidase activity indicates that these two proteins do not directly interact with each other. Growth under these circumstances can be attributed to a low level of intrinsic *trans*-activation in yeast strains harboring the pGBKT7-BimA plasmid as shown in Figure 5.

Consistent with the yeast two-hybrid data presented in Figure 5, we were unable to detect a direct interaction between BimA and IQGAP1 by conventional pulldown assay using affinity-purified glutathione S-transferase (GST)-$BimA_{54-455}$ and maltose-binding protein (MBP)-IQGAP1 fusion proteins expressed by *E. coli* under conditions previously used to detect the direct interaction of actin with BimA[4] (data not shown).

Effect of IQGAP1 Knockdown on Actin Density and Length of BimA-Induced Actin Tails

Given the presence of IQGAP1 in the tails of *B. pseudomallei* in infected cells, we next utilized an IQGAP1 siRNA approach to determine the functional relevance of this host cell protein in *B. pseudomallei* actin-based motility. Transfection of Silencer Select siRNA against IQGAP1 into HeLa cells consistently resulted in efficient knockdown of around 70% as assessed by IQGAP1 immunoblotting (Figure 6a and b). Following

DOI: 10.1021/acs.jproteome.6b00760
J. Proteome Res. 2016, 15, 4675−4685

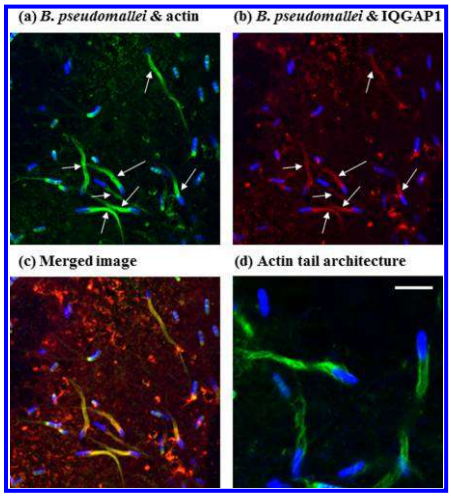

Figure 4. IQGAP1 is recruited to *B. pseudomallei* actin tails in infected HeLa cells. HeLa cells were infected with *B. pseudomallei* at an MOI of 100 and fixed at 16 h postinfection for visualization of actin tails by immunohistochemistry and confocal microscopy. Representative images of (a) bacteria (blue) and actin (green) and (b) bacteria (blue) and IQGAP1 (red). White arrows indicate areas of colocalization of actin and IQGAP1 in bacterial tails. (c) Merged image of panels a and b. (d) Architecture of the actin tails in which the scale bar is 5 μm.

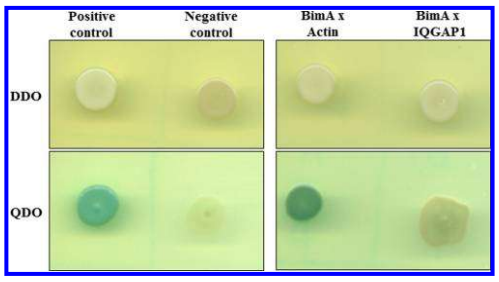

Figure 5. BimA and IQGAP1 do not interact in a yeast two-hybrid assay. For protein:protein interactions to be identified, single yeast colonies from SD agar plates lacking leucine and tryptophan (DDO) were suspended in 20 μL of water, and 5 μL was dotted onto SD agar plates lacking leucine, tryptophan, adenine, and histidine (QDO) supplemented with 20 μg/mL of X-α-galactosidase. Plates were incubated at 30 °C for 24 h before observing the appearance of the colonies. The strains AH109 pGBKT7-*bimA* pGADT7-*iqgap1* (BimA X IQGAP1) and AH109 pGBKT7-*bimA* pGADT7-*actin* (BimA X actin) were tested alongside yeast strains transformed with positive and negative control vectors (pGADT7-T antigen pGBKT7-p53 and pGADT7-T antigen pGADT7-Lamin C, respectively). The blue coloration of the yeast indicates a direct interaction between the two proteins, as demonstrated by the positive control and BimA X actin strains. White coloration indicates a lack of interaction between the two proteins, as demonstrated by the negative control and BimA X IQGAP1 strains.

infection of siRNA knockdown cells and control nontransfected cells, over 2000 bacteria were imaged from each infected cell type across three biological replicates. There was no significant difference in the proportion of tailing bacteria in either cell type under the assay conditions used (~42%). It was evident that bacteria could still form actin tails in the knockdown cells; however, this may be a result of the residual IQGAP1 expression in the cells or compensation by the related IQGAP proteins IQGAP2 or IQGAP3, which are also expressed in this cell type.

Using Image J software, we next measured the length and actin density of tails as described in the Materials and Methods; 100 tails from control and siRNA-transfected HeLa cells across three biological replicates were analyzed. The data showed a statistically significant increase in overall tail length (p = 0.0033) with a concomitant decrease in actin density (p = 0.0001) in IQGAP1 knockdown cells compared with control cells (Figure 6c and d). In cells with reduced levels of IQGAP1, tails were significantly longer with a mean length of 20.5 μm compared to a mean length of 14.8 μm in control cells (Figure 6c). Although longer in length, the actin density of tails generated in IQGAP1 knockdown cells was lower with a mean signal of 1036.0 au compared to a mean signal of 2522.4 au measured for tails in control cells.

DISCUSSION

Burkholderia pseudomallei is a facultative intracellular bacterium capable of escape from the endocytic vacuole into the cytosol of host cells. In common with several other bacteria, namely *Listeria monocytogenes*, *Shigella flexneri*, *Mycobacterium marinum*, and several *Rickettsia* spp., it is capable of harnessing cellular actin to promote its movement within and between host cells by actin-based motility. It is clear that these bacteria have evolved several independent mechanisms to utilize cellular actin and accessory proteins for actin-based motility. For example, *L. monocytogenes* expresses ActA, a protein that recruits the host cell Arp2/3 complex to its surface where it directly interacts with actin and stimulates its polymerization.[29] Conversely, certain rickettsial species express Sca2, a protein that acts through functional mimicry of eukaryotic formins.[28] We have previously characterized the *B. pseudomallei*-encoded protein required for actin-based motility. Known as BimA, this predicted Type V autotransporter protein is expressed on a single pole of the bacterium where it recruits cellular actin and stimulates its polymerization to mediate intracellular movement.[4,6] We and others have shown that this protein can stimulate actin polymerization in vitro in a manner that is independent of other host cell factors such as the Arp2/3 complex.[4,9] Despite localization of Arp2/3 components to the actin-rich tails of *B. pseudomallei* in infected cells,[12] tail formation does not require the activity of this cellular actin nucleation complex because it can be observed in cells depleted of Arp2/3.[10] Although it is known that actin-based motility of *B. pseudomallei* does not require Arp2/3, the potential involvement of other cellular factors is unclear.

Here, we have used an in vitro affinity approach to identify cellular factors recruited to BimA overexpressing bacteria under actin polymerizing conditions. We report the identification of 30 cellular proteins, including actin, actin-depolymerizing factor, and capping protein, the minimal requirement for polymerization in the presence of a bacterial actin polymerization factor in vitro.[30] The identification of vinculin and α-actinin is corroborated by the work of Breitbach et al., who demonstrated the presence of these proteins in *B. pseudomallei* actin tails by immunofluorescence microscopy.[12] Although α-

DOI: 10.1021/acs.jproteome.6b00760
J. Proteome Res. 2016, 15, 4675−4685

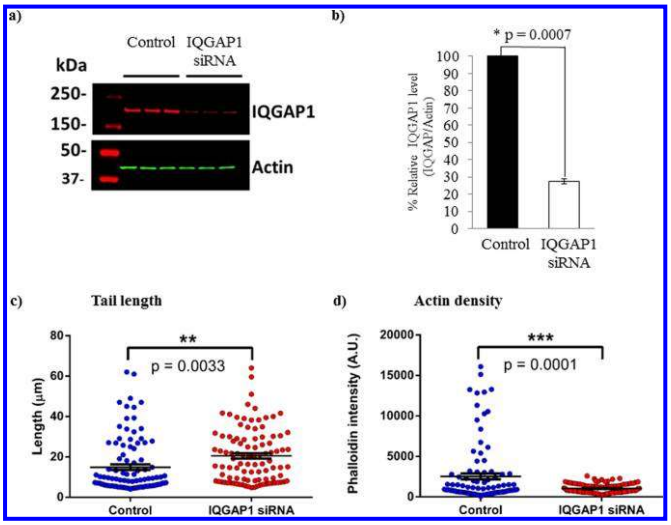

Figure 6. siRNA-mediated knockdown of IQGAP1 in HeLa cells affects *B. pseudomallei* tail morphology. (a) Western blot analysis of HeLa cell lysates from three independent experiments. IQGAP1 and actin (as a protein loading control) were detected in lysates prepared from cells treated only with transfection reagent (control) and cells transfected with 6 pmol siIQGAP1 for 72 h (IQGAP1 siRNA). (b) Quantitation of IQGAP1 protein levels in control and IQGAP1 siRNA cells indicates that IQGAP1 expression is reduced by ∼70% in siRNA-treated cells. Control and IQGAP1 siRNA cells were infected with *B. pseudomallei* at an MOI of 100 and fixed at 16 h postinfection for visualization of actin tails by immunohistochemistry and confocal microscopy. Images were collected from three independent experiments, and tail length in μm (c) and actin density in au of phalloidin intensity (d) were assessed using ImageJ software.

actinin is commonly detected in the tails of bacteria that display actin-based motility, vinculin has been reported to be absent from *R. rickettsii* tails.[31]

In comparison to previous studies, it was notable that our data set lacked any microtubules, intermediate filaments, or myosins that were shown to be present in *Listeria* tails,[13b] or VASP or profilin, which have been shown to be components of *R. rickettsia* actin tails.[31] Two proteins that have not previously been associated with actin-based motility of intracellular pathogens, HSP90 and IQGAP1, were identified in this analysis, and the presence of IQGAP1 was detected in actin-rich tails formed by *B. pseudomallei* in HeLa cells. IQGAP1 is a ubiquitously expressed scaffold protein that integrates numerous signaling pathways and regulates multiple cellular processes. Involved in *Salmonella* Typhimurium host cell invasion and *Chlamydophila pneumoniae*-induced vascular smooth cell migration, IQGAP1 has also been implicated in the adhesion of EPEC to the cell surface and viral trafficking and replication of Mu-MuLV (reviewed in Kim et al.[27]). IQGAP1 has been shown to interact directly with the EPEC Ibe and Tir proteins and *Salmonella* T3SS effector protein SseI, although the yeast two-hybrid and pulldown results are not consistent with a direct interaction between IQGAP1 and BimA. Indeed, the finding that the protein localizes along the length of the actin-rich tail in *B. pseudomallei* infected tails together with reports that IQGAP1 is an actin-binding protein, suggests it is recruited indirectly through its interaction with actin filaments.[32] Furthermore, we demonstrate that IQGAP1 plays a functional role in organizing the architecture of the actin tails formed by *B. pseudomallei*. Indeed, siRNA-mediated knockdown resulted in a significant lengthening of the tails concomitant with a reduction in the actin density. This warrants further investigation, as does the role of the other validated and candidate host cell proteins in actin-based motility of this fascinating bacterial pathogen.

■ CONCLUSIONS

We have demonstrated a hitherto unknown role for the cellular protein IQGAP1 in modulating the length and actin density of actin tails induced by the intracellular bacterial pathogen *Burkholderia pseudomallei*.

■ AUTHOR INFORMATION

Corresponding Author

*Tel. +44 131 651 9100. Fax. +44 131 651 9105. E-mail jo.stevens@roslin.ed.ac.uk.

ORCID

Joanne M. Stevens: 0000-0001-9992-2854

Notes

The authors declare no competing financial interest.

■ ACKNOWLEDGMENTS

This work was supported by the BBSRC (Grant BBSRC BB/E 021212/1) and Institute Strategic Grant funding from the BBSRC (J.M.S., M.P.S., C.V.B., D.K.). N.J. was supported by a Siriraj Development Scholarship (Bangkok, Thailand). N.Z.-A. was supported by a scholarship awarded by Majlis Amanah Rakyat (MARA) (Council of Trust for the People, Malaysia). We thank Joann Prior and Andrew Scott at Dstl, Porton Down, UK for supplying the capsule-specific antibody. We also thank Paul Brett and Mary Burtnick at the University of South Alabama, US for providing the pBHR2-*virAG* plasmid used in

DOI: 10.1021/acs.jproteome.6b00760
J. Proteome Res. 2016, 15, 4675−4685

this study. The work described in this manuscript was undertaken in the United Kingdom through funding obtained from UK sources and in strict accordance with UK Health and Safety Executive (HSE) guidance. Our work in relation to genetic modification has been extensively reviewed both by our own University of Edinburgh Biosafety Unit, the HSE, and by the UK Counter Terrorism and Security Agency. The genetically modified *B. pseudomallei* strains described in this paper do not constitute a US Government Dual Use of Research Concern because these modifications do not enhance the pathogenicity of the microorganism, do not interfere with immunity or immunization strategies, do not confer resistance to useful prophylactic or therapeutic agents, and do not alter the transmissibility, host range, or tropism of the pathogen.

REFERENCES

(1) Wiersinga, W. J.; van der Poll, T.; White, N. J.; Day, N. P.; Peacock, S. J. Melioidosis: insights into the pathogenicity of *Burkholderia pseudomallei*. *Nat. Rev. Microbiol.* **2006**, *4* (4), 272−82.

(2) Stevens, J. M.; Galyov, E. E.; Stevens, M. P. Actin-dependent movement of bacterial pathogens. *Nat. Rev. Microbiol.* **2006**, *4* (2), 91−101.

(3) Qualmann, B.; Kessels, M. M. New players in actin polymerization−WH2-domain-containing actin nucleators. *Trends Cell Biol.* **2009**, *19* (6), 276−85.

(4) Stevens, M. P.; Stevens, J. M.; Jeng, R. L.; Taylor, L. A.; Wood, M. W.; Hawes, P.; Monaghan, P.; Welch, M. D.; Galyov, E. E. Identification of a bacterial factor required for actin-based motility of *Burkholderia pseudomallei*. *Mol. Microbiol.* **2005**, *56* (1), 40−53.

(5) Sitthidet, C.; Stevens, J. M.; Chantratita, N.; Currie, B. J.; Peacock, S. J.; Korbsrisate, S.; Stevens, M. P. Prevalence and sequence diversity of a factor required for actin-based motility in natural populations of *Burkholderia* species. *Journal of clinical microbiology* **2008**, *46* (7), 2418−22.

(6) Sitthidet, C.; Korbsrisate, S.; Layton, A. N.; Field, T. R.; Stevens, M. P.; Stevens, J. M. Identification of motifs of *Burkholderia pseudomallei* BimA required for intracellular motility, actin binding, and actin polymerization. *Journal of bacteriology* **2011**, *193* (8), 1901−10.

(7) Lazar Adler, N. R.; Stevens, M. P.; Dean, R. E.; Saint, R. J.; Pankhania, D.; Prior, J. L.; Atkins, T. P.; Kessler, B.; Nithichanon, A.; Lertmemongkolchai, G.; Galyov, E. E. Systematic Mutagenesis of Genes Encoding Predicted Autotransported Proteins of *Burkholderia pseudomallei* Identifies Factors Mediating Virulence in Mice, Net Intracellular Replication and a Novel Protein Conferring Serum Resistance. *PLoS One* **2015**, *10* (4), e0121271.

(8) Stevens, J. M.; Ulrich, R. L.; Taylor, L. A.; Wood, M. W.; Deshazer, D.; Stevens, M. P.; Galyov, E. E. Actin-binding proteins from *Burkholderia mallei* and *Burkholderia thailandensis* can functionally compensate for the actin-based motility defect of a *Burkholderia pseudomallei bimA* mutant. *Journal of bacteriology* **2005**, *187* (22), 7857−62.

(9) (a) Sitthidet, C.; Stevens, J. M.; Field, T. R.; Layton, A. N.; Korbsrisate, S.; Stevens, M. P. Actin-based motility of *Burkholderia thailandensis* requires a central acidic domain of BimA that recruits and activates the cellular Arp2/3 complex. *Journal of bacteriology* **2010**, *192* (19), 5249−52. (b) Benanti, E. L.; Nguyen, C. M.; Welch, M. D. Virulent *Burkholderia* species mimic host actin polymerases to drive actin-based motility. *Cell* **2015**, *161* (2), 348−60.

(10) Lu, Q.; Xu, Y.; Yao, Q.; Niu, M.; Shao, F. A polar-localized iron-binding protein determines the polar targeting of *Burkholderia BimA* autotransporter and actin tail formation. *Cell. Microbiol.* **2015**, *17* (3), 408−24.

(11) (a) Wong, J.; Chen, Y.; Gan, Y. H. Host Cytosolic Glutathione Sensing by a Membrane Histidine Kinase Activates the Type VI Secretion System in an Intracellular Bacterium. *Cell Host Microbe* **2015**, *18* (1), 38−48. (b) Schell, M. A.; Ulrich, R. L.; Ribot, W. J.; Brueggemann, E. E.; Hines, H. B.; Chen, D.; Lipscomb, L.; Kim, H. S.; Mrazek, J.; Nierman, W. C.; Deshazer, D. Type VI secretion is a major virulence determinant in *Burkholderia mallei*. *Mol. Microbiol.* **2007**, *64* (6), 1466−85.

(12) Breitbach, K.; Rottner, K.; Klocke, S.; Rohde, M.; Jenzora, A.; Wehland, J.; Steinmetz, I. Actin-based motility of *Burkholderia pseudomallei* involves the Arp 2/3 complex, but not N-WASP and Ena/VASP proteins. *Cell. Microbiol.* **2003**, *5* (6), 385−93.

(13) (a) David, V.; Gouin, E.; Troys, M. V.; Grogan, A.; Segal, A. W.; Ampe, C.; Cossart, P. Identification of cofilin, coronin, Rac and capZ in actin tails using a *Listeria* affinity approach. *Journal of cell science* **1998**, *111* (Pt 19), 2877−84. (b) Van Troys, M.; Lambrechts, A.; David, V.; Demol, H.; Puype, M.; Pizarro-Cerda, J.; Gevaert, K.; Cossart, P.; Vandekerckhove, J. The actin propulsive machinery: the proteome of *Listeria monocytogenes* tails. *Biochem. Biophys. Res. Commun.* **2008**, *375* (2), 194−9.

(14) Maegraith, B. G.; Leithead, C. S. Melioidosis: A Case-Report. *Lancet* **1964**, *1* (7338), 862−3.

(15) Choi, K. H.; Kumar, A.; Schweizer, H. P. A 10-min method for preparation of highly electrocompetent *Pseudomonas aeruginosa* cells: application for DNA fragment transfer between chromosomes and plasmid transformation. *J. Microbiol. Methods* **2006**, *64* (3), 391−7.

(16) Milton, D. L.; O'Toole, R.; Horstedt, P.; Wolf-Watz, H. Flagellin A is essential for the virulence of *Vibrio anguillarum*. *J. Bacteriol.* **1996**, *178* (5), 1310−9.

(17) Logue, C. A.; Peak, I. R.; Beacham, I. R. Facile construction of unmarked deletion mutants in *Burkholderia pseudomallei* using *sacB* counter-selection in sucrose-resistant and sucrose-sensitive isolates. *J. Microbiol. Methods* **2009**, *76* (3), 320−3.

(18) Kersey, P. J.; Duarte, J.; Williams, A.; Karavidopoulou, Y.; Birney, E.; Apweiler, R. The International Protein Index: an integrated database for proteomics experiments. *Proteomics* **2004**, *4* (7), 1985−8.

(19) Taylor, G. K.; Goodlett, D. R. Rules governing protein identification by mass spectrometry. *Rapid Commun. Mass Spectrom.* **2005**, *19* (23), 3420.

(20) Stevens, M. P.; Friebel, A.; Taylor, L. A.; Wood, M. W.; Brown, P. J.; Hardt, W. D.; Galyov, E. E. A *Burkholderia pseudomallei* type III secreted protein, BopE, facilitates bacterial invasion of epithelial cells and exhibits guanine nucleotide exchange factor activity. *Journal of bacteriology* **2003**, *185* (16), 4992−6.

(21) Cuccui, J.; Milne, T. S.; Harmer, N.; George, A. J.; Harding, S. V.; Dean, R. E.; Scott, A. E.; Sarkar-Tyson, M.; Wren, B. W.; Titball, R. W.; Prior, J. L. Characterization of the *Burkholderia pseudomallei* K96243 capsular polysaccharide I coding region. *Infection and immunity* **2012**, *80* (3), 1209−21.

(22) Schell, M. A.; Zhao, P.; Wells, L. Outer membrane proteome of *Burkholderia pseudomallei* and *Burkholderia mallei* from diverse growth conditions. *J. Proteome Res.* **2011**, *10* (5), 2417−24.

(23) Vander Broek, C. W.; Chalmers, K. J.; Stevens, M. P.; Stevens, J. M. Quantitative Proteomic Analysis of *Burkholderia pseudomallei* Bsa Type III Secretion System Effectors Using Hypersecreting Mutants. *Mol. Cell. Proteomics* **2015**, *14* (4), 905−16.

(24) Harding, S. V.; Sarkar-Tyson, M.; Smither, S. J.; Atkins, T. P.; Oyston, P. C.; Brown, K. A.; Liu, Y.; Wait, R.; Titball, R. W. The identification of surface proteins of *Burkholderia pseudomallei*. *Vaccine* **2007**, *25* (14), 2664−72.

(25) (a) Su, Y. C.; Wan, K. L.; Mohamed, R.; Nathan, S. A genome level survey of *Burkholderia pseudomallei* immunome expressed during human infection. *Microbes Infect.* **2008**, *10* (12−13), 1335−45. (b) Felgner, P. L.; Kayala, M. A.; Vigil, A.; Burk, C.; Nakajima-Sasaki, R.; Pablo, J.; Molina, D. M.; Hirst, S.; Chew, J. S.; Wang, D.; Tan, G.; Duffield, M.; Yang, R.; Neel, J.; Chantratita, N.; Bancroft, G.; Lertmemongkolchai, G.; Davies, D. H.; Baldi, P.; Peacock, S.; Titball, R. W. A *Burkholderia pseudomallei* protein microarray reveals serodiagnostic and cross-reactive antigens. *Proc. Natl. Acad. Sci. U. S. A.* **2009**, *106* (32), 13499−504.

(26) (a) Nieves, W.; Asakrah, S.; Qazi, O.; Brown, K. A.; Kurtz, J.; Aucoin, D. P.; McLachlan, J. B.; Roy, C. J.; Morici, L. A. A naturally derived outer-membrane vesicle vaccine protects against lethal

DOI: 10.1021/acs.jproteome.6b00760
J. Proteome Res. 2016, 15, 4675−4685

pulmonary *Burkholderia pseudomallei* infection. *Vaccine* **2011**, *29* (46), 8381−9. (b) Nieves, W.; Petersen, H.; Judy, B. M.; Blumentritt, C. A.; Russell-Lodrigue, K.; Roy, C. J.; Torres, A. G.; Morici, L. A. A *Burkholderia pseudomallei* outer membrane vesicle vaccine provides protection against lethal sepsis. *Clinical and vaccine immunology: CVI* **2014**, *21* (5), 747−54.

(27) Kim, H.; White, C. D.; Sacks, D. B. IQGAP1 in microbial pathogenesis: Targeting the actin cytoskeleton. *FEBS Lett.* **2011**, *585* (5), 723−9.

(28) Haglund, C. M.; Choe, J. E.; Skau, C. T.; Kovar, D. R.; Welch, M. D. *Rickettsia* Sca2 is a bacterial formin-like mediator of actin-based motility. *Nat. Cell Biol.* **2010**, *12* (11), 1057−63.

(29) (a) Welch, M. D.; Iwamatsu, A.; Mitchison, T. J. Actin polymerization is induced by Arp2/3 protein complex at the surface of *Listeria monocytogenes*. *Nature* **1997**, *385* (6613), 265−9. (b) Welch, M. D.; Rosenblatt, J.; Skoble, J.; Portnoy, D. A.; Mitchison, T. J. Interaction of human Arp2/3 complex and the *Listeria monocytogenes* ActA protein in actin filament nucleation. *Science* **1998**, *281* (5373), 105−108.

(30) Loisel, T. P.; Boujemaa, R.; Pantaloni, D.; Carlier, M. F. Reconstitution of actin-based motility of *Listeria* and *Shigella* using pure proteins. *Nature* **1999**, *401* (6753), 613−616.

(31) Van Kirk, L. S.; Hayes, S. F.; Heinzen, R. A. Ultrastructure of *Rickettsia rickettsii* actin tails and localization of cytoskeletal proteins. *Infection and immunity* **2000**, *68* (8), 4706−13.

(32) (a) Mateer, S. C.; Morris, L. E.; Cromer, D. A.; Bensenor, L. B.; Bloom, G. S. Actin filament binding by a monomeric IQGAP1 fragment with a single calponin homology domain. *Cell Motil. Cytoskeleton* **2004**, *58* (4), 231−41. (b) Erickson, J. W.; Cerione, R. A.; Hart, M. J. Identification of an actin cytoskeletal complex that includes IQGAP and the Cdc42 GTPase. *J. Biol. Chem.* **1997**, *272* (39), 24443−7.

DOI: 10.1021/acs.jproteome.6b00760
J. Proteome Res. 2016, 15, 4675−4685